Gastrointestinal microbial diversity and diagenetic alteration of bone from the American alligator (*Alligator mississippiensis*)

A Dissertation Presented for the

Doctor of Philosophy

Degree

The University of Tennessee, Knoxville

Sarah Wheeler Keenan

May 2014

Dedication

This dissertation is dedicated to all of the teachers I have had over the course of my education, from elementary school through my graduate degrees. I would particularly like to dedicate this work to the public school teachers at Samuel Staples Elementary School and Helen Keller Middle School in Easton, Connecticut. From a young age I was supported in my quest for knowledge, from science to the humanities, largely by the educators I with whom interacted on a daily basis. The teachers who that influenced my early education were pivotal in laying the groundwork for my future educational successes, and without their devotion and commitment to foster learning, I would not be where I am today.

I would also like to dedicate this dissertation to my late grandfather, Eugene Keenan. As an arborist, naturalist, and outdoorsman, Grampie taught me as a small child the importance of nature, the wonder and splendor that exists in the woods, lakes, rivers, and rocks of Vermont, and instilled in me a sense of curiosity for natural science. Through his training, I became an expert at catching insects, reptiles, and amphibians, notably frogs. For anyone who has successfully caught or tried to catch a frog, it requires patience, practice, finesse, trial and error, perseverance, and when successful, instills a sense of pride. The same skill set that I developed catching frogs as a child has been invaluable in all aspects of my life, and I attribute this largely to my grandfather.

Acknowledgements

None of this would have been possible without the support of my friends and family. I owe much of who I am today to my parents and sisters. My parents gave me my first microscope, which stimulated a life-long fascination with nature. They supported me throughout my varied scientific endeavors, including my mycology adventures, which involved storing specimens (some of them poisonous) in our freezer. Without their full emotional and financial support of my passion for natural and geological sciences, I would not be where I am today. My sisters, Charlotte and Annabel, have always been there for me, listening (or pretending to listen) while I describe the geology of Connecticut, Vermont, England, Scotland, and Italy, staring at rocks or fossils in museums for hours, exploring the woods of New England with me, and most importantly, supporting my "nerdy" pursuits. I would also like to thank my father for helping me move, twice, in the balmy Louisiana summer—sorry I have so many rocks and books.

I am indebted to Audrey Paterson for field and lab assistance, for listening to my ramblings, for keeping the lab organized and efficient, and for being an amazing friend. Brendan "El Brendone" Headd was the best officemate at LSU and UTK, providing feedback and insight on topics ranging from bioinformatics to college football. Kathleen Brannen helped with several field sampling adventures and has been a good friend, first at LSU and then UTK.

Without the support and encouragement of my friends, both new and old, and too many to list, none of this work would have been possible. In particular, I would like to thank Scott Engel for being a sane outside observer, concocting amazing homebrew, and for teaching me about caving. I thank my fellow graduate students, including (in alphabetical order): Will Atwood, Latisha Brengman, Tim Diedish, Brendan Donnelley, Timmon Drumm, Kate Griener, Geoff Guilleaudeau, Remy Leger, Mike Lucas, Chad Novack, Blake Roberts, Arya Udry, Celina

Will, and Kyle White, as well as the exceptional undergraduate students I had the opportunity to interact with, including Mattie Friday, Dalia Harmon, Alissa Phillips, Scott Beeler, and Shane Cone. I also thank my caving friends from the Wittenberg University Speleological Society, the East Tennessee Grotto, the Smoky Mountain Grotto, and others for the always welcome subterranean adventures. Melody Branch, Angie Staley, and Teresa Parrott are graciously acknowledged for all their help with everything university related.

My advisor, Annette S. Engel, has served as an inspiration to me on numerous levels of my academic and non-academic life. Even before starting my Ph.D. with Annette I was inspired by her research as an interdisciplinary and transformative geologist, and after spending five years as her student and collaborator, she continues to inspire me. She serves as a model academician and an exemplar scientist. Annette and Scott introduced me to the world of caves and taught me everything I know about exploring the subsurface. For their passion for caving, science, exploring the unknown, and life, I am indescribably grateful.

Additionally, I would like to thank my committee members—Chris Fedo, Linda Kah, Mark Radosevich—for their feedback, insight, constructive criticism, and encouragement over the course of my doctoral research at UTK. Throughout my academic journey at both LSU and UTK I have had the pleasure of interacting with numerous other faculty members who inspired me in various aspects of my research and life. In particular, I thank Brooks Ellwood for teaching me to persevere in the face of not so kind reviewers, Laurie Anderson for the insightful discussions on paleobiology, and Larry Taylor for being a mentor, having an open door, and serving as an inspiration to “always stay curious.”

Chapter 2: This work required the help of numerous individuals, and each is gratefully acknowledged. Phillip “Scooter” Trosclair, III supplied salvaged alligator tissues. Celina Will, Brendan Headd, Brooke Hopkins, Michelle Osborne, Jason Hicks, Brendan Donnelly, Ryo Teruyama assisted with sample collection. Laurie Anderson, Javier Nevarez, Gary Byerly, Valentine Lance, Colin Sumrall, Chris Fedo, Linda Kah, and Mark Radosevich provided feedback to the manuscript. Shane Cone assisted with data analysis. David Hines provided feed samples and discussion of feed manufacturing. Marisa Tellez provided identifications of crocodylian parasites. Mark Merchant provided discussion on crocodylian biochemistry.

Chapter 3: Modern alligator bones were provided by Louisiana Department of Wildlife and Fisheries through the Louisiana National Heritage Program (permit LNHP-10-009) and obtained from salvaged animals. Ruth Elsey assisted with field logistics and provided access to sampling locations at the Rockefeller Wildlife Refuge. Kathleen Brannen assisted with fluorescence analyses and data processing.

Chapter 4: Logistical support was provided by the CAMD support staff and technicians. Cretaceous fossil samples were provided by Jack Horner and the Museum of the Rockies, Montana, and Gray Fossil Site specimens from Tennessee were obtained through the McClung Museum of Natural History and Culture, University of Tennessee, Knoxville. Financial support was provided by the Jones Endowment fund.

Chapter 5: Samples used for analyses were provided by the McClung Museum of Natural History and Culture, University of Tennessee, Knoxville. Larry Taylor is graciously

acknowledged for access to the electron microprobe and for enlightening discussions. Allan Patchen assisted with EMP analyses. We also thank Chris Fedo for microscope access.

Financial support: I have been fortunate over the course of my doctoral research to receive funding from several sources. At LSU, funding came from the Marathon Oil Corporation Geoscience Diversity Enrichment Program (GeoDE), the Department of Geology and Geophysics, a Geological Society of America Student Research Award, the Farouk El Baz student research grant. At UTK, funding came from the Jones Endowment fund and the Department of Earth & Planetary Sciences.

Logistical support: The Rockefeller Wildlife Refuge, Grand Chenier, Louisiana, and the Louisiana Department of Wildlife and Fisheries provided lodging, field assistance, airboat access, access to sampling locations at the Refuge, permission to bury salvaged alligators at the Refuge, watching my back when sampling alligator nests, and permitting. I would particularly like to thank Ruth Elsey, with whom I have had the pleasure of collaborating since 2009.

Abstract

One of the most challenging questions in paleobiology is how bone transforms from a living tissue into a fossil. In life, the gastrointestinal tract microbiome of an animal promotes host health. But, in death, these microbial communities, as well as soil communities, begin to degrade tissue, including bones. Using the American alligator from coastal wetland habitats as a model system, the gastrointestinal tract microbiome was found to contain microbial communities consisting of Fusobacteria, Proteobacteria, Bacteroidetes, and Firmicutes, with variations based on tissue type along the length of the digestive tract. The overall dominance of Fusobacteria is distinct from any other tetrapod studied to date and is suggestive of a retained ancestral condition that may be controlled by conservative host morphology, behavior, and niche occupation. Alligators are crown archosaurs that have occupied similar wetland habitats since their divergence in the Late Triassic, with an accompanying crocodylian fossil record that is replete with bones preserved in wetland environments. Following alligator death, structural and chemical changes to alligator bone, including transformations into more thermodynamically stable mineral phases, occur within days to weeks when bone is exposed to indigenous soil and water microbial communities, as well as from abiotic processes controlled by habitat geochemistry. Direct exposure to indigenous microbial communities slows alteration, which may be critical for stability of bone over geologic time. Despite different compositional chemistries, experimentally treated and fossil bones of varying ages converge on a common mineral lattice arrangement at the atomic-level that may facilitate bone preservation.

Table of Contents

List of Tables

List of Figures

Chapter 1: Introduction

Portions of this chapter were previously published as an encyclopedia chapter. Additional background material, references, and an overview section were added.

Keenan, S.W., 2013. Freshwater vertebrate animal metagenomics, alligatorinae, in: *The Encyclopedia of Metagenomics*, Neslon, K. (ed.), Springer-Verlag, Heidelberg.

Both physical and chemical processes alter the remains of living and dead organisms. Soft tissue preservation is exceedingly rare in the rock record (e.g., Schweitzer et al., 1997), and this has restricted our understanding of cardiovascular, digestive, and other physiological traits in extinct taxa. However, the nature of the fossil record fundamentally changed following bone formation in early fishes from a cartilaginous ancestor (Ruben and Bennett, 1987; Smith and Hall, 1990; Arnason et al., 2001). The rise of aquatic, then terrestrial, vertebrates that biomineralize bone, and subsequent fossilization provided a mechanism to record extinct taxa compared to soft tissues. However, because of their chemistry, bones can also be susceptible to taphonomic alteration, which introduces biases in the vertebrate fossil record from every point in the 'taphonomic window,' from deposition and burial to subsequent surface exposure.

Taphonomic alteration of fossils, whether vertebrate bones or shelly remains of invertebrates, has been caused by microorganisms. The majority of life on Earth at present and in the geologic past is prokaryotic and inhabits a diversity of ecological niches from deep-sea hydrothermal vents (e.g., Brazelton et al., 2010) to metazoan digestive tracts (e.g., Eckburg et al., 2005). The vertebrate gut represents a 'world within worlds' (*sensu stricto* Ley et al., 2008b) because of complex co-evolutionary relationships between the vertebrate host and the resident symbiotic, and occasionally pathogenic, microbial communities. The microbial diversity of

vertebrate guts is only beginning to be explored (Eckburg et al., 2005; Turnbaugh et al., 2007; Walter and Ley, 2011). The advent of molecular genetic approaches in the mid 1990's made it possible to explore microbial diversity and to examine microbial genes directly from the environment (e.g., Woese et al., 1990; Pace, 1997). These advances removed biases that were imparted by culture-based approaches and provided an evaluation of previously underestimated microbial diversity associated with biogeochemical processes and with animals. Within the past decade, next-generation sequencing methods have revolutionized studies of microbial diversity, and the number of metagenomic studies aimed at characterizing the composite microbial genome within environmental samples, including gut tissues and feces, have exponentially increased, particularly for humans (Xu and Gordon, 2003; Eckburg et al., 2005; Ley et al., 2007; Costello et al., 2009; Goodman et al., 2009; Arumugam et al., 2011). By applying molecular-based methods to evaluate microbial communities associated with a range of vertebrate systems, metagenomics of microbes inhabiting the gastrointestinal tract has emerged as a thriving frontier in microbial ecology, biogeochemistry, and geomicrobiology.

The acquisition and maintenance of a resident microbial community within the gastrointestinal tract of a vertebrate is crucial for the host's health and survival. This resident community, or microbiome, plays numerous symbiotic roles in the host animal, such as promoting the uptake of nutrients that would be inaccessible to the host otherwise (Hooper et al., 2002; Zoetendal et al., 2008), and providing the first line of defense against invading pathogens (Karasov and Carey, 2009). There is some indication that, in addition to providing a critical role in regulating host health, the breakdown of the symbiotic relationship, or dysbiosis, can be detrimental to the host and may potentially contribute to disorders like obesity and Chron's disease (Cho and Blaser, 2012).

For microbial ecologists, evolutionary biologists, and biogeochemists, the microbial community composition of a vertebrate gastrointestinal microbiome can provide broader information than simply host health or disease. For microbial ecologists, the GI tract microbial diversity and community composition is a direct reflection of host diet, environment, and the co-evolution of the host with its resident symbiotic communities (Ley et al., 2008a; Walter and Ley, 2011). For evolutionary biologists, GI tract microbiome composition can be used to reconstruct host phylogenetics, such as in the great apes (Ochman et al., 2010; Moeller et al., 2012) and other mammalian taxa (Ley et al., 2008a). An evaluation of non-mammalian taxa phylogenetics has not been attempted using a similar approach. For biogeochemists, after the death of an animal and deposition into an environmental system, the gut microbiome that promoted host health in life is believed to be involved in the breakdown of the host organic tissues. The introduction of a carcass into the environment provides a newly available supply of degradable organic carbon (e.g., from the organs and tissues, including bone) for endogenous (i.e. gut-derived) and exogenous (i.e. soil-derived) microbial communities, as well as soil meio- and macrofauna (Campobasso et al., 2001; Jans et al., 2004; Amendt et al., 2010; Pacheco et al., 2012).

Carcass introduction to an environment, and the degradation processes associated with carcass decay, have been intensely studied, particularly in the forensic sciences (Boddington et al., 1987; Collins et al., 2002; Dent et al., 2004; Carter et al., 2007). Processes affecting bone, however, are less well studied. It is unclear whether bones from an animal's newly introduced carcass will become preserved in the depositional setting, which is determined by overall site geochemistry including soil mineralogy, organics, porewater dissolved ions, pH, redox, and temperature, etc. After removal of soft tissues (e.g., skin, muscles, adipose), bone alteration from

abiotic and biotic processes, particularly within hours to weeks to years of exposure, are not well constrained. Clearly, changes to the chemistry and structure of the primary mineral in bone, hydroxyapatite (HAP), during early diagenesis results in mineral recrystallization because thermodynamically more stable apatite phases, such as fluorapatite (FAP) or carbonated fluorapatite, are identified in fossil bones (Van Cappellen and Berner, 1988; Berna et al., 2004).

Consequently, the main goal of this research has been to bridge the gaps in our understanding regarding how early stages of bone decomposition and diagenesis are influenced by biotic and abiotic processes, and the impact of these processes on long-term preservation as a fossil bone. To frame the overall research with the interdisciplinary context it is, a review of the literature pertaining to bone structure and diagenesis in modern depositional systems and previous research done to investigate bone taphonomy in wetland settings is included. Justification for why I chose to use the American alligator as a model system to study microbiome acquisition and evolution, as well as bone preservation, is also presented. I conclude this chapter with a summary of research objectives and hypotheses for each dissertation chapter.

Bone structure and diagenesis

Bone is a biomineral comprised of interlayered organic materials (i.e. collagen, lipids) and a hydroxyapatite (HAP) mineral fraction ($Ca_{10}(PO_4)_6(OH)_2$) (Fig. 1.1A). The *in vivo* process of bone biomineralization still eludes biologists and materials scientists. Current questions include the initial formation phases (e.g., nucleation on collagen and apatite growth, or mineral development from an amorphous precursor phase) (Nudelman et al., 2010), and the classification of bone as a composite material (e.g., a “fiber-reinforced ceramic-matrix” or “nanoparticle-reinforced polymer-matrix” composite) (Olszta et al., 2007). In life, the presence of collagen

serves several functions for a vertebrate, including nucleation sites for HAP or sites for the formation of an amorphous precursor calcium phosphate phase that develops into HAP (Olszta et al., 2007). The composition of fresh, unaltered bone generally consists of 20-30% collagen, non-collagenous proteins, and water, with the remaining 70-80% consisting of non-stoichiometric HAP or carbonated apatite (Table 1.2). The intimate association of organic material with HAP, predominantly type I collagen, imparts bone with characteristic strength and a certain degree of flexibility in life (Burr, 2002; Viguet-Carrin et al., 2006). Type I collagen is a ubiquitous protein found in bone, as well as vertebrate skin, tendon, and muscles. In bone, collagen fibers are arrayed parallel and staggered, which results in a series of regularly-spaced gaps or grooves between collagen molecules (Fratzl et al., 2004). The spaces between collagen fibrils provide the sites for subsequent apatite mineral development, which ultimately form an inter-layered organic and mineral phase (Fig. 1.2). HAP crystallite orientation in bone can be uncertain, although recent data suggest that not all HAP crystallites are arranged in parallel; some crystallites may be oriented as much as 15° from the principle *c*-axis (Olszta et al., 2007).

Despite uncertainty in the biomineralization process, the presence of collagen, as well as other non-collagenous proteins, is critical for the growth and development of bone *in vivo* (Viguet-Carrin et al., 2006) and for bone stability in an environmental system after death and removal from the relative homogeneity and homeostasis the bone experienced within the living vertebrate. After bone deposition in a natural environment, collagen is removed through autolytic (Pfretzschner, 2004) and/or biologic activity (White and Hannus, 1983; Hubert et al., 1996). Exposure of collagen to varying temperatures can cause denaturation (Leikina et al., 2002), which relaxes the triple helix structure and opens the bone or tissue up to decomposition. Open pore spaces and canals in bone, caused by collagen removal, enhance the movement of fluids,

dissolved ions, and microorganisms (Fig. 1.1B), and expose mineral surfaces to ionic substitutions (Fig. 1.2). There is no consensus regarding whether biologic or abiotic (i.e. autolytic) processes control collagen degradation during different stages of decomposition (e.g., Pfretzschner, 2004), or the timing of the two processes, and whether or not they operate in isolation or together. One study suggests that there is no microbial activity acting on collagen after 6 to 12 months (Pfretzschner, 2004), but another study suggests that microbial activity may not act on collagen until as much as 15 years post burial (Yoshino et al., 1991). Additionally, expansion, swelling, and hydrolysis of collagen can result from exposure to aqueous solutions (Trueman et al., 2008). This process has been used to explain fracturing observed in bones that were deposited in aqueous environments (Pfretzschner, 2004).

Changes in HAP geochemical conditions *in vivo* to conditions in a natural environment directly influence the thermodynamic stability of HAP, which can lead to diagenetic alteration of bone. Bone diagenesis is broadly divided into two periods: early and late. Early diagenesis refers to the processes that alter the organic components (i.e. collagen, lipids) and the mineralized fraction (i.e. HAP) of bone immediately following its introduction into a geochemical or depositional system (e.g., Pfretzschner, 2004). In general, late diagenesis is regarded as the point at which HAP recrystallization is complete (Kohn, 2008; Trueman et al., 2008). The timing and duration of early diagenesis, and the subsequent transition to "late" diagenesis, are not well-defined and are likely to vary as a function of depositional environment, or even the type of vertebrate or the bone type (i.e. phalange, tibia, femur, etc.) or the tissue microstructure (i.e. fibrolamellar, woven).

Defining the mechanisms, processes, rates, and depositional conditions responsible for the formation of a fossil bone over geologic time has presented paleobiologists with a long-

standing and formidable challenge. Approaches that integrate geochemistry, mineralogy, physics, hydrology, sedimentology, and taphonomy have all furthered our understanding of fossilization, but there are still several fundamental gaps. Notably, we do not understand the timing of diagenesis (e.g., early or late), and the transformation rate(s) of original HAP into a thermodynamically more stable phase, such as FAP or a carbonated-fluorapatite. We also do not understand the parameters imparted by the depositional environment for bone dissolution or preservation. Perhaps most importantly, we are still unable to define the structural and chemical changes that occur to bone during early diagenesis, or to explain how rapid, early changes to bone composition helps to establish long-term preservation and potential fossilization.

Modern systems as windows to evaluate the geologic past

Wetlands are distinct depositional environments characterized by strong geochemical gradients, sediment with high organic carbon content, and clay to silt-sized, water-saturated sediment. In general, the fossil record is replete with taxa preserved in floodplain or overbank deposits (e.g., Nadon, 1993; Keenan and Scannella, 2014), with 66% of all bonebed deposits (i.e. accumulations of more than one individual of the same species) ascribed to this depositional setting. Nearly 50% of these deposits are also considered to be former wetlands (Eberth et al., 2007). For taxa inhabiting wetlands, the assumption is that following death, exposure, tissue and bone degradation, and potential burial, the bones and teeth are likely to occur in the same type of environment that the host lived within (Fig. 1.3).

For crocodylians, in particular, the fossil record is biased towards wetland depositional environments (Greb et al., 2006; Vasconcellos and Carvalho, 2010), which provide support for the significance of essentially *in situ* preservation in the habitats occupied in life. A number of

extinct crocodylians are thought to have occupied similar niches as top predators to their modern counterparts, including *Postosuchus* (Chatterjee, 1985) and *Theriosuchus* (Schwarz and Salisbury, 2005) (Fig. 1.4). Members of Crocodylomorpha have occupied wetland environments since their divergence in the Late Triassic and have dominated similar geochemical systems to their modern counterparts (Schwarz and Salisbury, 2005). Therefore, evaluating the physical, chemical, and biological processes associated with the burial of an extant crocodylian, such as an alligator, in a modern wetland system can be used to reconstruct diagenetic conditions that likely operated in the geologic past to preserve (or degrade) bone.

Actualistic taphonomy is the study of decay, disarticulation, and diagenesis of modern bone, and results provide a window into the geologic past. This field of study has been embraced by forensic scientists, as well as paleobiologists, to better understand the initial processes involved in soft and hard tissue alteration (e.g., Beherensmeyer, 1988; Weigelt, 1989; Amendt et al., 2010). Despite the potential for thorough assessment of early diagenesis in modern systems to inform processes in the geologic past, there have been relatively few taphonomic studies that approach diagenesis from a holistic view (Nielsen-Marsh and Hedges, 2000; Lee-Thorp, 2002). A landmark study by Berna (2004) evaluated the 'recrystallization window' of bone in archaeological sites by focusing on variable aqueous geochemistry of buffered solutions within a narrow pH range (6.2 to 7.8). Despite the fact that the experiments in that study did not exactly replicate water geochemistry expected under natural conditions and only focused on a single variable (i.e. pH), the results suggest a link between bone preservation and pH that is controlled by the solubility of the inorganic fraction of bone. Controlled experiments evaluating bone stability under a wider range of pH conditions, using aqueous media designed to replicate conditions observed in nature, are notably absent. As such, there continues to be significant gaps

in our understanding of the role of geochemistry and (micro)biology in facilitating or preventing bone preservation. Questions to be answered include, how do varying concentrations of dissolved chemical species, such as phosphate or calcium, affect HAP stability? What roles do biology, particularly microorganisms, play in bone alteration? How long do initial transformations of bone take to occur, once a bone is introduced into an environmental system with or without soft tissue?

The American alligator: a model organism

American alligators (*Alligator mississippiensis*) are semi-aquatic vertebrates endemic to wetlands, ponds, rivers, and other freshwater environments in the southeastern United States (Joanen and McNease, 1989; Elsey and Woodward, 2010; Saalfeld et al., 2011) (Fig. 1.5). After being threatened with extinction in the 1960's, successful conservation efforts throughout the 1970's and 1980's bolstered alligator populations in Louisiana (e.g., Joanen and McNease, 1979) and paved the way for extensive research on alligator diet and biochemistry (Merchant et al., 2003; Merchant et al., 2006; Merchant et al., 2011), as well as seasonally-driven changes in their physiology (Schachner et al., 2011), growth (Tsai and Holliday, 2012), behavior (Lance et al., 2009), development (Ferguson and Joanen, 1982), and gut microbiomes (Keenan et al., 2013). Alligators have been widely studied because of their phylogenetic position as crown archosaurs (Brochu, 2003; Pol et al., 2009; Nesbitt, 2011). Crocodylian serum has the unique capacity of being an antibacterial medium that provides a level of protection from potential environmentally-derived pathogens. The protective ability of alligator blood following injury (Merchant et al., 2003) is distinct among vertebrate taxa, and may reflect an ancestral trait (Merchant et al., 2006;

Keenan et al., 2013). Alligator host biochemistry and physiology may impact symbiotic gastrointestinal tract microbial community acquisition and maintenance over geologic time.

Overview of dissertation research

Chapter 2: The alligator gut microbiome and implications for archosaur symbioses

Guided by the hypothesis that a vertebrate's GI tract microbiome reflects a basal ancestral state, this chapter aims to characterize the modern gut microbiome of the American alligator as a window into ancestral archosaur symbioses. Although previous studies of the vertebrate microbiome rely on feces as a representative sampling of the entire gastrointestinal tract, we tested the hypothesis that each region of the GI tract serves as a distinct ecosystem with the potential of shaping microbial community composition and diversity. As a result of physiologically distinct roles in nutrient uptake, each tissue or organ along the GI tract was expected to contain a characteristic and specific microbiome. Ultimately, the results of this work reveal a distinct microbial community from alligator GI tracts compared to previous gut microbiome research. The findings also provide insight into how gut microbes may impact early degradation of a buried alligator, and how *in vivo* communities differ from microorganisms associated with an environment, such as wetland soil.

Chapter 3: Visualizing early diagenesis of bone

The objective of Chapter 3 is to evaluate the early diagenetic (i.e. structural and chemical) changes that bones may experience when directly and indirectly exposed to microbial cells in a natural wetland environment. Experimental batch reactions simulated bone exposure to shallow burial conditions for one month, as well as to variable pH solutions. A three-year burial

experiment was also done. Bones were examined using a combination of analytical techniques, including electron microprobe analyses, Fourier transform infrared spectroscopy, and X-ray diffraction. The results highlight that quantifiable changes to bone chemistry occur over days to weeks. These early transformations are likely critical for preservation. As such, the results have implications for our understanding of the fossilization process and rates of early diagenetic changes.

Chapter 4: Evaluating bone diagenesis and fossilization with X-ray absorption spectroscopy

This chapter focuses on using applied synchrotron-based approaches, specifically X-ray absorption near edge structure (XANES) spectroscopy, to evaluate the atomic-level structural composition of modern and fossil bones. XANES spectroscopy has not been well integrated into fossil bone paleontological or paleobiological research. Mineral lattice configurations at the P K-edge and Ca K-edge were examined from a range of fossil bones of varying ages and distinct depositional environments. Despite each of the analyzed bones originating from highly variable geochemical systems and different depositional settings, the results indicate that the fossil apatite structure converges on a common lattice arrangement, and that bone structure, perhaps to a greater extent than geochemistry, dictates bone preservation over geologic time.

Chapter 5: Reconstructing site diagenetic conditions from fossil bone geochemistry

Fossil bone major and trace element geochemistry has the potential to reveal valuable information regarding the conditions that facilitated bone preservation in the geologic past (e.g., Pate et al., 1989; Budd et al., 2000; Trueman and Tuross, 2002; Trueman, 2013). The well-preserved bones from the Gray Fossil Site, in Gray, Tennessee, are distinctive because they lack

secondary minerals infilling pore spaces. The Late Miocene to Early Pliocene (4.5 to 7.0 Ma) lacustrine deposits are well-known for abundant and diverse floral and faunal assemblages that provide a perspective into Late Neogene North American paleoclimate (Cerling et al., 1997). Despite previous studies evaluating site sedimentology (Shunk et al., 2006; Shunk et al., 2009; Zobaa et al., 2011), bone isotopic composition (DeSantis and Wallace, 2008), as well as fossil descriptions (Wallace and Wang, 2004; Mead et al., 2012), the conditions that facilitated bone preservation has not been explored. The aim of this study was to reconstruct diagenetic conditions from the geochemistry of alligator phalange bones (*Alligator* sp., currently belonging to an unnamed species). The hypothesis tested was that conditions were suboxic to anoxic, as well as reducing and acidic, in order to preserve Fe^{2+}-enriched bones.

Chapter 6: Conclusions

There were several goals of this dissertation, all focused on using a modern taxon, the American alligator, as a window into the geologic past. The first goal was to test hypotheses related to gut microbial symbioses and microbial community compositions. The results highlight that the vertebrate microbiome is understudied, particularly for non-mammalian taxa, thereby impacting our understanding of metazoan symbiotic acquisition and evolution over time. The second goal of this dissertation was to evaluate processes affecting bone preservation in modern wetland systems as a way to understand preservation (or destruction) of extinct archosaur bone. Diagenetic alteration of bone was observed on timescales from days to weeks, which are crucial for chemical and structural changes. This has the potential to fundamentally alter our perception of fossilization processes and rates.

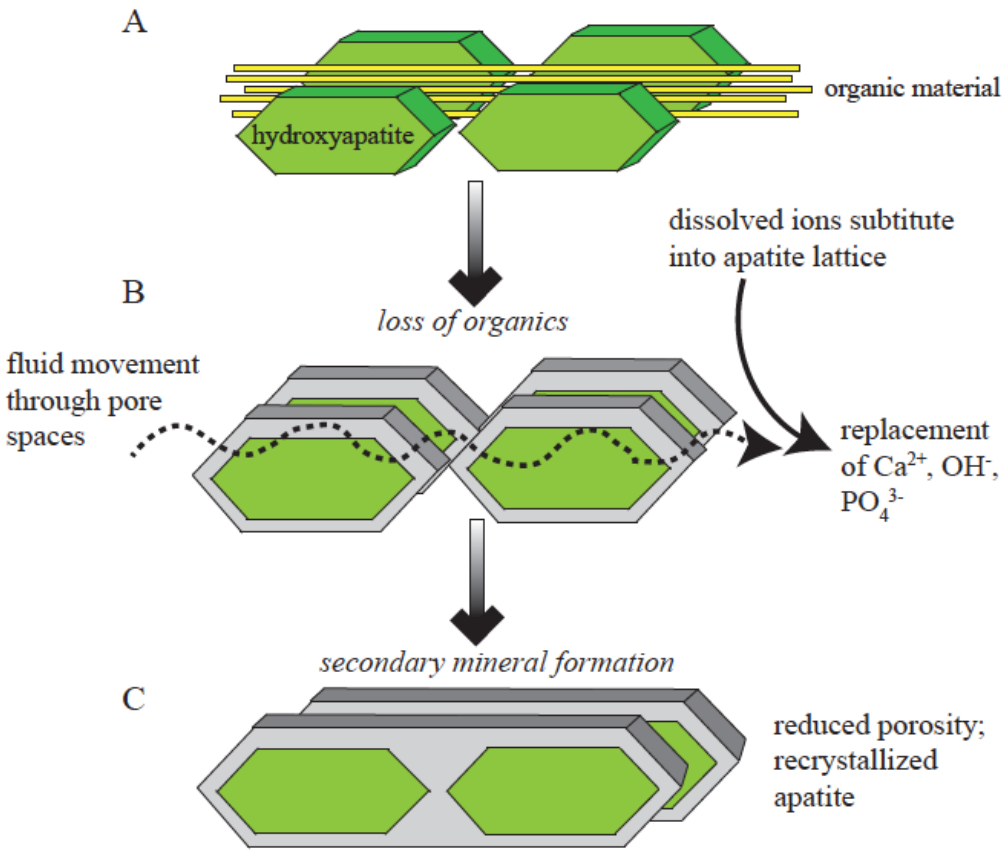

Fig. 1.1: Schematic view of changes to bone microstructure during diagenesis. (A) Interlayered mineral (hydroxyapatite) and organic material (collagen) in fresh bone rapidly undergo degradation, as shown in (B), which opens pore spaces for fluid movement. (B-C) Movement of dissolved ions into bone provides an opportunity for recrystallization of hydroxyapatite, or other apatite mineral phases, to occur. (C) This results in the formation of a thermodynamically more stable form, such as fluorapatite.

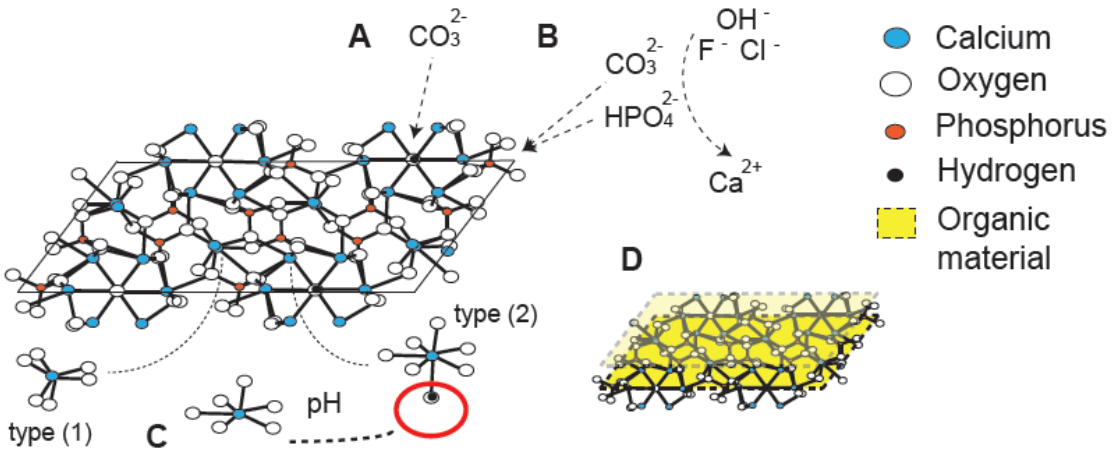

Fig. 1.2: Schematic view of the apatite mineral lattice. Potential substitution sites are noted by arrows and dashed lines. (B) Disruption at the phosphate sites in the lattice, through protonation or substitution with carbonate ions, may open the lattice to further alteration. (C) Replacement or substitution of calcium may occur at the Ca(1) and Ca(2) sites in the lattice, which can form a complex that is difficult to predict but would potentially be driven by the flexible lattice structure. (D) In life, the presence of collagen forms sheet-like layers between mineral crystallites, which protects the mineral from dissolution or recrystallization.

Fig. 1.3: Idealized view of crocodylian bone preservation and survival over geologic time. (A-B) Following the death of an animal, like an alligator, the bones may be deposited within the same system occupied in life. (C) The activity of scavengers, microorganisms, or physical processes may remove some of the bones, which will cause a fragmented and incomplete fossil record for that animal. Burial and diagenesis, which transform the original bone into fossil apatite, enhance preservation potential. (D) Subsequent erosion of overlying sediments may bring the fossilized bone back to the surface

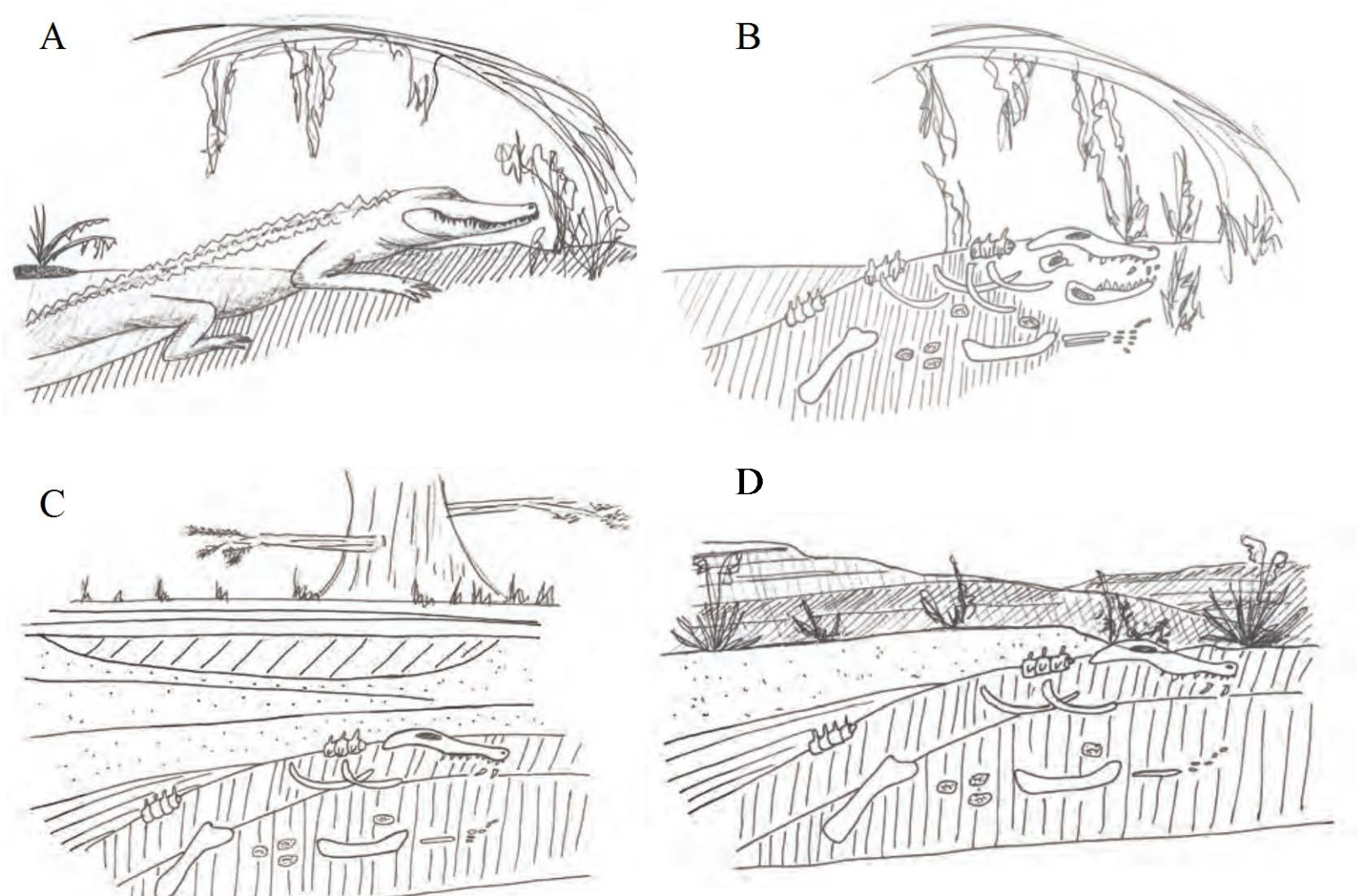
A
B
C
D

Fig. 1.4: Schematic time-calibrated phylogeny of select archosaur lineages with inferred dietary and niche occupation. Solid black rectangles correspond to known fossil occurrences, solid triangles indicate merged clades, white triangles reflect polyphyletic clades, and the dashed triangle refers to Avemetatarsalia, which includes extant taxa. Inferences regarding diet and niche occupation, based on functional analyses of select fossil taxa (in parenthesis) and associated niches (from interpretations of depositional environment) were gathered from the published literature (Table 1.1). The presence of carnivorous and/or semi-aquatic lifestyle is not necessarily reflective of entire clades. Timescale and divergences compiled from Brochu (2003), Pol et al. (2009), and Nesbitt (2011).

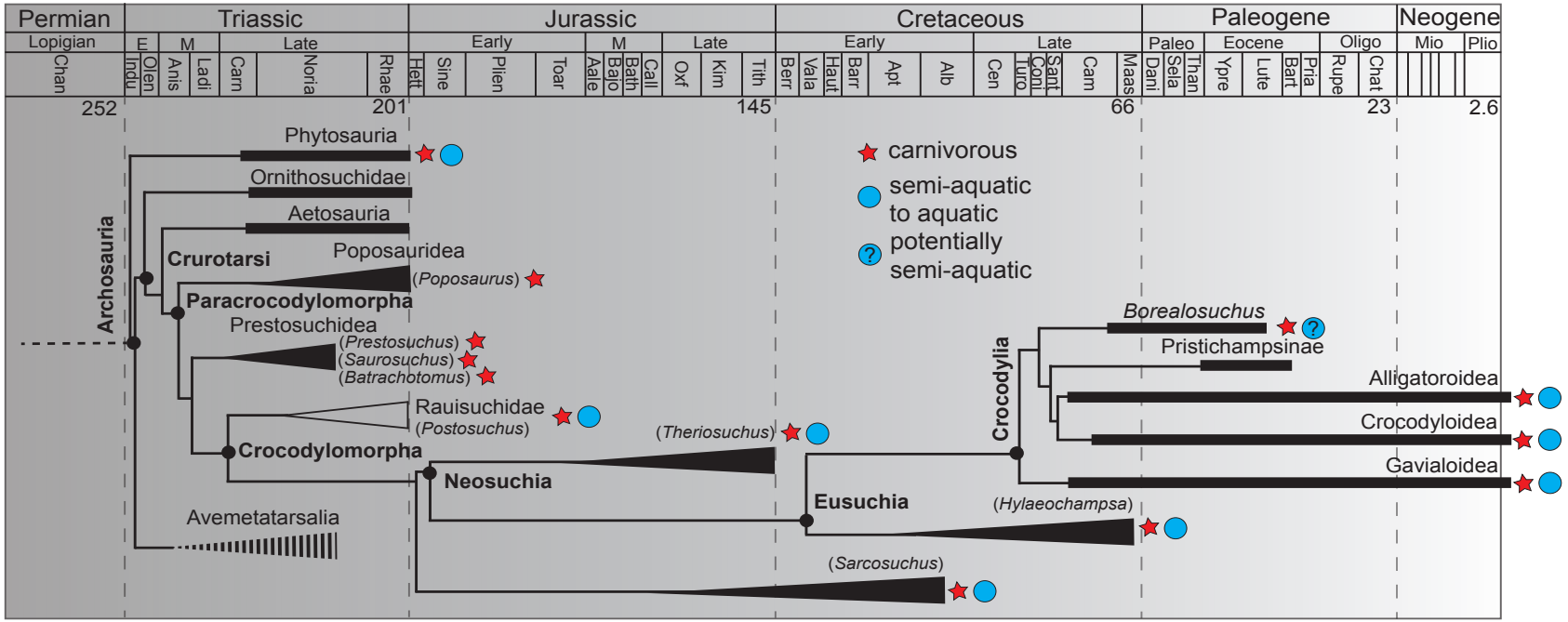
Permian
Triassic
Jurassic
Cretaceous
Paleogene
Neogene
Lopigian
Early
M
Late
Paleo
Eocene
Oligo
Mio
Plio
Chan
Indu
Olen
Anis
Ladi
Carn
Noria
Rhae
Hett
Sine
Plien
Toar
Aale
Baio
Bath
Call
Oxf
Kim
Tith
Berr
Vala
Haut
Barr
Apt
Alb
Cen
Turo
Coni
Sant
Cam
Maas
Dani
Sela
Than
Ypre
Lute
Bart
Pria
Rupe
Chat
252
201
145
66
23
2.6
Phytosauria
Ornithosuchidae
Aetosauria
Archosauria
Crurotarsi
Poposauridea
(Poposaurus)
Paracrocodylomorpha
Prestosuchidea
(Prestosuchus)
(Saurosuchus)
(Batrachotomus)
Rauisuchidae
(Postosuchus)
Crocodylomorpha
Neosuchia
Avemetatarsalia
(Theriosuchus)
Eusuchia
(Sarcosuchus)
carnivorous
semi-aquatic to aquatic
potentially semi-aquatic
Borealosuchus
Pristichampsinae
Crocodylia
Alligatoroidea
Crocodyloidea
Gavialoidea
(Hylaeochampsa)

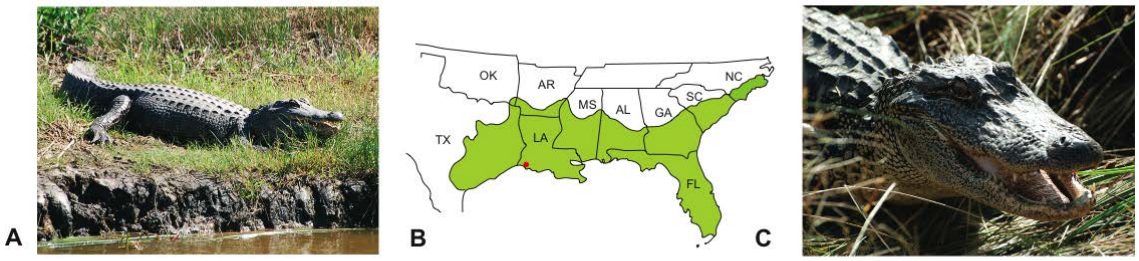

Fig. 1.5: Alligators are semi-aquatic, ectothermic vertebrates that inhabit habitats adjacent to waterways throughout the southeast of North America. (A) Alligators rely on ambient conditions to raise body temperature, and are frequently observed basking adjacent to water throughout this region. (B) The present day range of alligators extends from eastern portions of Texas to as far north as coastal regions of North Carolina. The red dot indicates the location of Rockefeller Wildlife Refuge, Grand Chenier, Louisiana, where research for this dissertation was completed. (C) Alligators are exposed to an array of environmentally microorganisms, and are frequently observed with sediment and organic debris in their mouth (A, used with permission of Ruth Elsey; C, used with permission of Phillip L. Trosclair, III) (Figure from Keenan, 2013).

Table 1.1: Selected archosaur taxa used to assess the evolution of gut symbioses.

Fossil Taxa	Formation, Age, and Location	Functional or Morphological Support	Depositional Environment and Inferred Niche	References
Phytosauridae indet. (possibly *Nicrosaurus* sp., *Mystriosuchus planirostris*, or an unnamed species)	Stubensandstein (Upper Triassic, Norian), Germany	compressed, serrated teeth	fluvial, floodplain	Hungerbuhler (1998)
Poposaurus gracilis	Chinle Formation (Late Triassic, Norian) Utah, USA	cranial, post-cranial morphology, teeth	inferred terrestrial, bipedal, cursorial	Gauthier et al. (2011)
Saurosuchus galilei	Ischigualasto Formation (Late Triassic) Argentina	cranial morphology, teeth	inferred terrestrial	Alcober (2000)
Batrachotomus kupferzellensis		cranial morphology, teeth	inferred terrestrial	Henderson and Weishampel (2002)
	Erfurt Formation, (Middle Triassic, Lanidian) Germany	post-cranial morphology	inferred terrestrial, quadrupedal	Gower and Schoch (2009)
Postosuchus	Dockum Group (Late Triassic), Texas, USA	cranial, pelvic, hind limb, and vertebral morphology	fluvial, lacustrine, floodplain	Chatterjee (1985)
Hylaeochampsa vectiana	Vectis Formation (Early Cretaceous, Barremian), Isle of Wight	cranial morphology, tooth shape	fluvial, floodplain	Clark and Norell (1992)
Sarcosuchus imperator	El Rhaz Formation (Lower Cretaceous, Aptian-Albian), Niger	comparative morphology (cranial) to modern taxa	fluvial, marginal floodplains	Sereno et al. (2001)
Theriosuchus guimarotae	Abadia Formation (Late Jurassic, Kimmeridgian), Portugal	comparative morphology to fossil and modern taxa, overall body size	wetland, swamp	Schwarz and Salisbury (2005)
Alligatoridea	modern	observations of behavior	wetlands, floodplains, lacustrine, fluvial	Elsey et al. (1992)
Crocodyloidea	modern	observations of behavior	wetlands, floodplains, lacustrine, fluvial, fresh and saline water	
Gavaloidea	modern	observations of behavior	wetlands, floodplains, lacustrine, fluvial	

References

Alcober, O., 2000. Redescription of the skull of *Saurosuchus galilei* (Archosauria: Rauisuchidae). J Vertebr Paleontol 20, 302-316.

Amendt, J., Goff, M.L., Campobasso, C.P., Grasserbger, M., 2010. Current concepts in forensic entomology. Springer, Dordrecht, p. 376.

Arnason, U., Gullberg, A., Janke, A., 2001. Molecular phylogenetics of gnathostomous (jawed) fishes: old bones, new cartilage. Zool Scr 30, 249-255.

Arumugam, M., Raes, J., Pelletier, E., Le Paslier, D., Yamada, T., Mende, D.R., Fernandes, G.R., Tap, J., Bruls, T., Batto, J.M., Bertalan, M., Borruel, N., Casellas, F., Fernandez, L., Gautier, L., Hansen, T., Hattori, M., Hayashi, T., Kleerebezem, M., Kurokawa, K., Leclerc, M., Levenez, F., Manichanh, C., Nielsen, H.B., Nielsen, T., Pons, N., Poulain, J., Qin, J.J., Sicheritz-Ponten, T., Tims, S., Torrents, D., Ugarte, E., Zoetendal, E.G., Wang, J., Guarner, F., Pedersen, O., de Vos, W.M., Brunak, S., Dore, J., Weissenbach, J., Ehrlich, S.D., Bork, P., Consortium, M., 2011. Enterotypes of the human gut microbiome. Nature 473, 174-180.

Behrensmeyer, A.K., 1988. Vertebrate preservation in fluvial channels. Palaeogeogr Palaeocl 63, 183-199.

Berna, F., Matthews, A., Weiner, S., 2004. Solubilities of bone mineral from archaeological sites: the recrystallization window. J Archaeol Sci 31, 867-882.

Boddington, A., Garland, A.N., Janaway, R.C., 1987. Death, decay, and reconstruction : approaches to archaeology and forensic science. Manchester University Press, Manchester, UK ; Wolfeboro, NH, USA.

Brazelton, W.J., Ludwig, K.A., Sogin, M.L., Andreishcheva, E.N., Kelley, D.S., Shen, C.C., Edwards, R.L., Baross, J.A., 2010. Archaea and bacteria with surprising microdiversity show shifts in dominance over 1,000-year time scales in hydrothermal chimneys. Proc Natl Acad Sci U S A 107, 1612-1617.

Brochu, C.A., 2003. Phylogenetic approaches toward crocodylian history. Annu Rev Earth Pl Sc 31, 357-397.

Budd, P., Montgomery, J., Barreiro, B., Thomas, R.G., 2000. Differential diagenesis of strontium in archaeological human dental tissues. Appl Geochem 15, 687-694.

Burr, D.B., 2002. The contribution of the organic matrix to bone's material properties. Bone 31, 8-11.

Campobasso, C.P., Di Vella, G., Introna, F., 2001. Factors affecting decomposition and Diptera colonization. Forensic Sci Int 120, 18-27.

Carter, D.O., Yellowlees, D., Tibbett, M., 2007. Cadaver decomposition in terrestrial ecosystems. Naturwissenschaften 94, 12-24.

Cerling, T.E., Harris, J.M., MacFadden, B.J., Leakey, M.G., Quade, J., Eisenmann, V., Ehleringer, J.R., 1997. Global vegetation change through the Miocene/Pliocene boundary. Nature 389, 153-158.

Chatterjee, S., 1985. Postosuchus, a new thecodontian reptile from the Triassic of Texas and the origin of Tyrannosaurs. Philos T Roy Soc B 309, 395-460.

Cho, I., Blaser, M.J., 2012. Applications of Next-Generation Sequencing the human microbiome: At the interface of health and disease. Nat Rev Genet 13, 260-270.

Clark, J.M., Norell, M., 1992. The Early Cretaceous crocodylomorph *Hylaeochampsa vectiana* from the Wealden of the Isle of Wight. Am Mus Novit 3032, 1-19.

Collins, M.J., Nielsen-Marsh, C.M., Hiller, J., Smith, C.I., Roberts, J.P., Prigodich, R.V., Wess, T.J., Csapò, J., Millard, A.R., Turner-Walker, G., 2002. The survival of organic matter in bone: a review. Archaeometry 44, 383-394.

Costello, E.K., Lauber, C.L., Hamady, M., Fierer, N., Gordon, J.I., Knight, R., 2009. Bacterial community variation in human body habitats across space and time. Science 326, 1694-1697.

DeSantis, L.R.G., Wallace, S.C., 2008. Neogene forests from the Appalachians of Tennessee, USA: Geochemical evidence from fossil mammal teeth. Palaeogeogr Palaeocl 266, 59-68.

Eberth, D.A., Shannon, M., Noland, B.G., 2007. A bonebeds database: Classification, biases, and patterns of occurrence, in: Rogers, R.R., Eberth, D.A., Fiorillo, A.R. (Eds.), Bonebeds: Genesis, analysis, and paleobiological significance. University of Chicago Press, Chicago, pp. 103-131.

Eckburg, P.B., Bik, E.M., Bernstein, C.N., Purdom, E., Dethlefsen, L., Sargent, M., Gill, S.R., Nelson, K.E., Relman, D.A., 2005. Diversity of the human intestinal microbial flora. Science 308, 1635-1638.

Elsey, R.M., McNease, L., Joanen, T., Kinler, N., 1992. Food habits of native wild and farm-released juvenile alligators. Proc Annu Conf SEAFWA 46, 57-66.

Elsey, R.M., Woodward, A.R., 2010. American alligator *Alligator mississippiensis*, in: Manolis, S.C., Stevenson, C. (Eds.), Crocodiles: status, survey, and conservation action plan, Third ed. Crocodile Specialist Group, Darwin, pp. 1-4.

Ferguson, M.W.J., Joanen, T., 1982. Temperature of egg incubation determines sex in *Alligator mississippiensis*. Nature 296, 850-853.

Fratzl, P., Gupta, H.S., Paschalis, E.P., Roschger, P., 2004. Structure and mechanical quality of the collagen-mineral nano-composite in bone. J Mater Chem 14, 2115-2123.

Gauthier, J.A., Nesbitt, S.J., Schachner, E.R., Bever, G.S., Joyce, W.G., 2011. The bipedal stem crocodilian *Popsaurus gracilis*: inferring function in fossils and innovation in archosaur locomotion. Bull Peabody Mus Nat Hist 52, 107-126.

Goodman, A.L., McNulty, N.P., Zhao, Y., Leip, D., Mitra, R.D., Lozupone, C.A., Knight, R., Gordon, J.I., 2009. Identifying genetic determinants needed to establish a human gut symbiont in its habitat. Cell Host Microbe 6, 279-289.

Gower, D.J., Schoch, R.R., 2009. Postcranial anatomy of the rauisuchian archosaur *Batrachotomus kupferzellensis*. J Vertebr Paleontol 29, 103-122.

Greb, S.F., DiMichele, W.A., Gastaldo, R.A., 2006. Evolution and importance of wetlands in earth history. Geol Soc Am Spec Pap 399, 1-40.

Henderson, D.M., Weishampel, D.B., 2002. Convergent evolution of the maxilla-dental complex among carnivorous archosaurs. Senckenb lethaea 82, 77-91.

Hooper, L.V., Midtvedt, T., Gordon, J.I., 2002. How host-microbial interactions shape the nutrient environment of the mammalian intestine. Annu Rev Nutr 22, 283-307.

Hubert, J.F., Panish, P.T., Chure, D.J., Prostak, K.S., 1996. Chemistry, microstructure, petrology, and diagenetic model of Jurassic dinosaur bones, Dinosaur National Monument, Utah. J Sediment Res 66, 531-547.

Hungerbuhler, A., 1998. Taphonomy of the prosauropod dinosaur *Sellosaurus*, and its implications for carnivore faunas and feeding habits in the Late Triassic. Palaeogeogr Palaeocl 143, 1-29.

Jans, M.M.E., Nielsen-Marsh, C.M., Smith, C.I., Collins, M.J., Kars, H., 2004. Characterisation of microbial attack on archaeological bone. J Archaeol Sci 31, 87-95.

Joanen, T.E.D., McNease, L., 1979. Culture of the American alligator. International Zoo Yearbook 19, 61-66.

Joanen, T., McNease, L.L., 1989. Ecology and physiology of nesting and early development of the American alligator. Am Zool 29, 987-998.

Karasov, W.H., Carey, H.V., 2009. Metabolic teamwork between gut microbes and hosts. Microbe 4, 323-328.

Keenan, S.W., 2013. Freshwater vertebrate animal metagenomics, alligatorinae, in: Nelson, K. (Ed.), Encyclopedia of Metagenomics. Springer-Verlag, Berlin Heidelberg.

Keenan, S.W., Engel, A.S., Elsey, R.M., 2013. The alligator gut microbiome and implications for archosaur symbioses. Scientific Reports 3, DOI:10.1038/srep02877.

Keenan, S.W., Scannella, J.B., 2014. Paleobiological implications of a *Triceratops* bonebed from the Hell Creek Formation, Garfield County, northeastern Montana, in: Hartman, J., Wilson, G., Horner, J.R., Clemens, W. (Eds.), Through the end of the Cretaceous in the type locality of the Hell Creek Formation in Montana and adjacent areas. Geol S Am S 503, 349-364.

Kohn, M.J., 2008. Models of diffusion-limited uptake of trace elements in fossils and rates of fossilization. Geochim Cosmochim Acta 72, 3758-3770.

Lance, S.L., Tuberville, T.D., Dueck, L., Holz-Schietinger, C., Trosclair, P.L., Elsey, R.M., Glenn, T.C., 2009. Multiyear multiple paternity and mate fidelity in the American alligator, Alligator mississippiensis. Mol Ecol 18, 4508-4520.

Lance, V.A., Elsey, R.M., Butterstein, G., Trosclair, P.L., Merchant, M., 2010. The effects of Hurricane Rita and subsequent drought on alligators in southwest Louisiana. J Exp Zoo Part A 313, 106-113.

Lee-Thorp, J., 2002. Two decades of progress towards understanding fossilization processes and isotopic signals in calcified tissue minerals. Archaeometry 44, 435-446.

Leikina, E., Mertts, M.V., Kuznetsova, N., Leikin, S., 2002. Type I collagen is thermally unstable at body temperature. Proc Natl Acad Sci U S A 99, 1314-1318.

Ley, R.E., Hamady, M., Lozupone, C., Turnbaugh, P.J., Ramey, R.R., Bircher, J.S., Schlegel, M.L., Tucker, T.A., Schrenzel, M.D., Knight, R., Gordon, J.I., 2008a. Evolution of mammals and their gut microbes. Science 320, 1647-1651.

Ley, R.E., Knight, R., Gordon, J.I., 2007. The human microbiome: eliminating the biomedical/environmental dichotomy in microbial ecology. Environ Microbiol 9, 3-4.

Ley, R.E., Lozupone, C.A., Hamady, M., Knight, R., Gordon, J.I., 2008b. Worlds within worlds: evolution of the vertebrate gut microbiota. Nat Rev Microbiol 6, 776-788.

Mead, J.I., Schubert, B.W., Wallace, S.C., Swift, S.L., 2012. Helodermatid lizard from the Mio-Pliocene oak-hickory forest of Tennessee, eastern USA, and a review of monstersaurian osteoderms. Acta Palaeontol Pol 57, 111-121.

Merchant, M., Royer, A., Broussard, Q., Gilbert, S., Falconi, R., Shirley, M.H., 2011. Characterization of serum dipeptidyl peptidase IV activity in three diverse species of West African crocodilians. Herpetol J 21, 153-159.

Merchant, M.E., Mills, K., Leger, N., Jenkins, E., Vliet, K.A., McDaniel, N., 2006. Comparisons of innate immune activity of all known living crocodylian species. Comp Biochem Phys B 143, 133-137.

Merchant, M.E., Roche, C., Elsey, R.M., Prudhomme, J., 2003. Antibacterial properties of serum from the American alligator (*Alligator mississippiensis*). Comp Biochem Phys B 136, 505-513.

Moeller, A.H., Degnan, P.H., Pusey, A.E., Wilson, M.L., Hahn, B.H., Ochman, H., 2012. Chimpanzees and humans harbour compositionally similar gut enterotypes. Nat Comm 3, DOI:10.1038/ncomms2159.

Nadon, G.C., 1993. The association of anastomosed fluvial deposits and dinosaur tracks, eggs, and nests - implications for the interpretation of floodplain environments and a possible survival strategy for Ornithopods. Palaios 8, 31-44.

Nesbitt, S.J., 2011. The early evolution of archosaurs: relationships and the origin of major clades. B Am Mus Nat Hist, 1-288.

Nielsen-Marsh, C.M., Hedges, R.E.M., 2000. Patterns of diagenesis in bone I: The effects of site environments. J Archaeol Sci 27, 1139-1150.

Nudelman, F., Pieterse, K., George, A., Bomans, P.H.H., Friedrich, H., Brylka, L.J., Hilbers, P.A.J., de With, G., Sommerdijk, N.A.J.M., 2010. The role of collagen in bone apatite formation in the presence of hydroxyapatite nucleation inhibitors. Nat Mater 9, 1004-1009.

Ochman, H., Worobey, M., Kuo, C.H., Ndjango, J.B., Peeters, M., Hahn, B.H., Hugenholtz, P., 2010. Evolutionary relationships of wild hominids recapitulated by gut microbial communities. PLoS Biol 8, DOI:10.1371/journal.pbio.1000546.

Olszta, M.J., Cheng, X.G., Jee, S.S., Kumar, R., Kim, Y.Y., Kaufman, M.J., Douglas, E.P., Gower, L.B., 2007. Bone structure and formation: a new perspective. Mat Sci Eng R 58, 77-116.

Pace, N.R., 1997. A molecular view of microbial diversity and the biosphere. Science 276, 734-740.

Pacheco, M.L.A.F., Villagran, X.S., Martins, G.R., 2012. Macroscopic and microbiological alterations of bird and small mammal bones buried in a Cerrado biome (south western Brazil). J Archaeol Sci 39, 1394-1400.

Pate, F.D., Hutton, J.T., Norrish, K., 1989. Ionic exchange between soil solution and bone - toward a predictive model. Appl Geochem 4, 303-316.

Pfretzschner, H.U., 2004. Fossilization of Haversian bone in aquatic environments. Cr Palevol 3, 605-616.

Pol, D., Turner, A.H., Norell, M.A., 2009. Morphology of the Late Cretaceous crocodylomorph *Shamosuchus djadochtaensis* and a discussion of neosuchian phylogeny as related to the origin of Eusuchia. B Am Mus Nat Hist, 1-103.

Ruben, J.A., Bennett, A.A., 1987. The evolution of bone. Evolution 41, 1187-1197.

Saalfeld, D.T., Conway, W.C., Calkins, G.E., 2011. Food habits of American alligators (*Alligator mississippiensis*) in East Texas. Southeast Nat 10, 659-672.

Schachner, E.R., Farmer, C.G., McDonald, A.T., Dodson, P., 2011. Evolution of the dinosauriform respiratory apparatus: new evidence from the postcranial axial skeleton. Anat Rec294, 1532-1547.

Schwarz, D., Salisbury, S.W., 2005. A new species of Theriosuchus (Atoposauridae, Crocodylomorpha) from the Late Jurassic (Kimmeridgian) of Guimarota, Portugal. Geobios 38, 779-802.

Schweitzer, M.H., Johnson, C., Zocco, T.G., Horner, J.R., Starkey, J.R., 1997. Preservation of biomolecules in cancellous bone of *Tyrannosaurus rex*. J Vertebr Paleontol 17, 349-359.

Sereno, P.C., Larsson, H.C.E., Sidor, C.A., Gado, B., 2001. The giant crocodyliform *Sarcosuchus* from the Cretaceous of Africa. Science 294, 1516-1519.

Shunk, A.J., Driese, S.G., Clark, G.M., 2006. Late Miocene to earliest Pliocene sedimentation and climate record derived from paleosinkhole fill deposits, Gray Fossil Site, northeastern Tennessee, U.S.A. Palaeogeogr Palaeocl 231, 265-278.

Shunk, A.J., Driese, S.G., Dunbar, J.A., 2009. Late Tertiary paleoclimatic interpretation from lacustrine rhythmites in the Gray Fossil Site, northeastern Tennessee, USA. J Paleolimnol 42, 11-24.

Smith, M.M., Hall, B.K., 1990. Development and evolutionary origins of vertebrate skeletogenic and odontogenic tissues. Biol Rev Camb Philos Soc 65, 277-373.

Trueman, C.N., 2013. Chemical taphonomy of biomineralized tissues. Palaeontology 56, 475-486.

Trueman, C.N., Palmer, M.R., Field, J., Privat, K., Ludgate, N., Chavagnac, V., Eberth, D.A., Cifelli, R., Rogers, R.R., 2008. Comparing rates of recrystallisation and the potential for preservation of biomolecules from the distribution of trace elements in fossil bones. Cr Palevol 7, 145-158.

Trueman, C.N., Tuross, N., 2002. Trace elements in recent and fossil bone apatite, in: Kohn, M.J., Rakovan, J., Hughes, J.M. (Eds.), Rev Mineral Geochem. Mineralogical Society of America, Washington, D.C., pp. 489-521.

Tsai, H.P., Holliday, C.M., 2012. Ontogeny of the alligator cartilago transiliens and its significance for sauropsid jaw muscle evolution. Integr Comp Biol 52, E177-E177.

Turnbaugh, P.J., Ley, R.E., Hamady, M., Fraser-Liggett, C.M., Knight, R., Gordon, J.I., 2007. The human microbiome project. Nature 449, 804-810.

Van Cappellen, P., Berner, R.A., 1988. A mathematical model for the early diagenesis of phosphorus and fluorine in marine sediments: apatite precipitation. Am J Sci 288, 289-333.

Vasconcellos, F.M., Carvalho, I.D.S., 2010. Paleoichnological assemblage associated with Baurusuchus salgadoensis remains, a Baurusuchidae mesoeucrocodylia from the Bauru Basin, Brazil (Late Cretaceous), in: Milan, J., Lucas, S.G., Lockley, M.G., Spielman, J.A. (Eds.), Crocodyle tracks and traces. New Mexico Museum of Natural History and Science, pp. 227-238.

Viguet-Carrin, S., Garnero, P., Delmas, P.D., 2006. The role of collagen in bone strength. Osteoporosis Int 17, 319-336.

Wallace, S.C., Wang, X.M., 2004. Two new carnivores from an unusual late Tertiary forest biota in eastern North America. Nature 431, 556-559.

Walter, J., Ley, R., 2011. The human gut microbiome: ecology and recent evolutionary changes. Annu Rev Microbiol 65, 411-429.

Weigelt, J., 1989. Recent vertebrate carcasses and their paleobiological implications. University of Chicago Press, Chicago, p. 188.

White, E.M., Hannus, L.A., 1983. Chemical-weathering of bone in archaeological soils. Am Antiquity 48, 316-322.

Woese, C.R., Kandler, O., Wheelis, M.L., 1990. Towards a natural system of organisms: proposal for the domains Archaea, Bacteria, and Eucarya. Proc Natl Acad Sci U S A 87, 4576-4579.

Xu, J., Gordon, J.I., 2003. Honor thy symbionts. Proc Natl Acad Sci U S A 100, 10452-10459.

Yoshino, M., Kimijima, T., Miyasaka, S., Sato, H., Seta, S., 1991. Microscopic study on estimation of time since death in skeletal remains. Forensic Sci Int 49, 143-158.

Zobaa, M.K., Zavada, M.S., Whitelaw, M.J., Shunk, A.J., Oboh-Lkuenobe, F.E., 2011. Palynology and palynofacies analyses of the Gray Fossil Site, eastern Tennessee: their role in understanding the basin-fill history. Palaeogeogr Palaeocl 308, 433-444.

Zoetendal, E.G., Rajilic-Stojanovic, M., de Vos, W.M., 2008. High-throughput diversity and functionality analysis of the gastrointestinal tract microbiota. Gut 57, 1605-1615.

Chapter 2: The alligator gut microbiome and implications for archosaur symbioses

This chapter is a reformatted version of a paper published in Scientific Reports under the same name. Additional results incorporating published data on amphibians was incorporated into this dissertation chapter.

Keenan, S.W., Engel, A.S., and Elsey, R.M., 2013. The alligator gut microbiome and implications for archosaur symbioses. Scientific Reports, DOI:10.1038/srep02877.

SWK and ASE designed the sampling protocol, collected samples, analyzed and interpreted the data, and wrote the paper. RME assisted with sample collection and contributed to the text.

Abstract

Among vertebrate gastrointestinal microbiome studies, complete representation of taxa is limited, particularly among reptiles. Here, we provide evidence for previously unrecognized host-microbiome associations along the gastrointestinal tract from the American alligator, a crown archosaur with shared ancestry to extinct taxa, including dinosaurs. Microbiome compositional variations reveal that the digestive system consists of multiple, longitudinally heterogeneous microbiomes that strongly correlate to specific gastrointestinal tract organs, regardless of rearing histories or feeding status. A core alligator gut microbiome comprised of Fusobacteria, but depleted in Bacteroidetes and Proteobacteria common to mammalians, is compositionally unique from other vertebrate gut microbiomes, including other reptiles, fish, and herbivorous and carnivorous mammals. As such, modern alligator gut microbiomes advance our understanding of archosaur gut microbiome evolution, particularly if conserved host ecology has retained archosaur-specific symbioses over geologic time.

Introduction and background

Vertebrate gastrointestinal (GI) tracts are distinct microenvironments formed by conserved ecological interactions and ancient evolutionary processes between a host and resident microbial flora. Interest in unraveling the ecologies and evolutionary histories of host-microbe symbiotic associations has surged following the advent of next-generation sequencing and '-omics' approaches (Eckburg et al., 2005; Ley et al., 2008b; Qu et al., 2008; Matsui et al., 2010). However, reconstruction of vertebrate-microbe evolutionary histories has been limited because some host groups are underrepresented among microbiome studies. Specifically, despite mammals representing only ~10% of known vertebrate taxa (Barnosky et al., 2011), the majority of GI tract microbiome studies to date focus on mammalian, predominately human, health and disease (e.g. obesity) (Ley, 2010) or microbiome acquisition (Buddington et al., 2010). In contrast, reptilian taxa (e.g. crocodylians, tuatara, turtles, squamates) (Costello et al., 2010; Hong et al., 2011; Keenan, 2013) represent ~17% of known, extant vertebrate species (Barnosky et al., 2011). Except for evaluation of fecal coliform bacteria (Johnston et al., 2010), which typically do not reflect the actual GI tract microbial diversity (Zoetendal et al., 2004), and from culture-based studies focusing on *Salmonella* spp. (Obwolo and Zwart, 1993), almost nothing is known about modern crocodylian GI tract microbiome diversity and ecology, despite its importance (Zanno and Makovicky, 2011) to advance respiratory and cardiovascular system development studies Barboza et al., 2010).

Non-mammalian GI tract microbiome acquisition and diversification

The estimated number of microbes residing within each vertebrate outnumber the host cells 10:1 (Hattori and Taylor, 2009), predominately due to a combination of environmental and evolutionary processes that influence normal flora maintenance and selection (Ley et al., 2006).

The origin of metazoans is believed to have occurred within aquatic environments (McFall-Ngai, 2002), and subsequent diversification and radiation paved the way for the origin of tetrapods in the Devonian (Fig. 2.1A) and subsequent colonization of land. The transition from an aquatic environment to a terrestrial system resulted not only in a diversification of vertebrate taxa and occupation of a new range of terrestrial niches, but also likely in the diversification of GI tract microbiome composition, which would have been largely driven by major shifts in diet (Ley et al., 2008a). Unfortunately, testing this hypothesis through comparative analysis of gut microbiomes from aquatic and terrestrial amphibian or reptilian taxa is greatly limited by the paucity of microbiome studies involving non-terrestrial, non-mammalian taxa. To date, there are only five studies of amphibian and reptilian gut microbiome ecology based on 11 species (Table 2.1), despite this group accounting for over 25% of estimated extant vertebrate species (15,140 of 55,701 species total), their rapidly declining global populations (Barnosky et al., 2011), and potential role as indicators of ecosystem health (Beebee and Griffiths, 2005). The overwhelming majority of gut microbiome studies focus on humans, which biases our understanding of GI tract microbial community acquisition, evolution, maintenance, diversity, and function.

Here, we expand the current knowledge of GI tract microbiomes from the semi-aquatic, predominantly freshwater American alligator (*Alligator mississippiensis*), indigenous to the southeastern United States. From wild and farm-raised alligators from fasting and feeding seasons, we identify distinct bacterial communities partitioned as a function of organ type along the length of the GI tract and the presence of a shared or "core" bacterial community. Because the modern alligator has been used as an analogue to understand and infer physiological (Schachner et al., 2011) and biomechanical (Rayfield, 2007) traits of extinct aquatic and terrestrial forms, including carnivorous theropod dinosaurs (Rayfield, 2007), as well as to

characterize extinct archosaur thermoregulation (Seymour et al., 2004), feeding (Farmer et al., 2008), respiration (Schachner et al., 2011), and mobility (Rayfield, 2007), we propose that the alligator microbiome also provides insight into the evolutionary history of predator digestive systems (Varricchio, 2001; Zanno and Makovicky, 2011; Hone et al., 2012) and archosaur microbiome symbioses (Farlow, 1987) based on conserved ecological niche and extant symbiotic associations (Ley et al., 2008a, b; Moeller et al., 2012).

Methods

Sample and dataset acquisition

Organs and tissues sampled along the length of the gastrointestinal tract (Fig. 2.3) from eight salvaged *A. mississippiensis* juveniles (114-180 cm, snout to tail lengths) were acquired within hours of death from individuals sacrificed for other studies in December 2009, May/April, August, and December 2010 at the Rockefeller Wildlife Refuge, Louisiana, USA (under the Louisiana Natural Heritage Program, permit LNHP-10-009). In the winter, two farm-raised but fasted (140 and 160 cm, snout to tail length; fasted 6 weeks) and two wild fasting (114 and 180 cm) alligators were used. In the spring, two fed farm-raised (130 and 131 cm) and two presumed feeding (which was later confirmed from the presence of prey items in the stomachs) wild alligators (132 and 140 cm) were used. As the alligators were salvaged, not all tissues were available for sampling every time (e.g. esophageal tissue was collected from a wild and a farmed animal during the spring because tongue tissue was unavailable due to skull removal by a different researcher). Within hours of death, several grams of epithelial tissue were aseptically excised or scraped from along the digestive tract with sterile scalpel blades and stored in 100% molecular grade ethanol at -20º C. Tissue scrapings ensured complete evaluation of the biofilms

lining the GI tract, as well as any microbes adhering to or within the mucosa. Gastric fluid was collected by making a small (6-10 cm length) incision into the stomach with sterile scalpel blades to provide direct access to the contents. Liquids were collected using sterile pipettes and solid material was collected using sterilized forceps. Stomach contents were then transferred to sterile 50 mL Falcon tubes. Following the collection of gastric contents, tissue scrapings were collected. Fecal samples were collected directly from the colon aseptically with sterile scalpel blades by making a small (6-10 cm) incision into the colon. As with gastric tissue samples, colon scrapings were collected following collection and removal of fecal material. In triplicate, tissue (~1 cm^3), gastric fluids (200 μl), and fecal material (~1 cm^3 when present) were homogenized in 150 to 200 μl 1x TE buffer using a hand-held Kontes pellet pestle, and total nucleic acids were extracted using the Qiagen DNeasy kit, following manufacturer instructions.

Purified DNA from each gastrointestinal sample (n = 48) was sent to the Research and Testing Laboratories in Lubbock, TX (USA), for 454 tag-encoded FLX titanium amplicon pyrosequencing of the V1-V3 region of bacterial 16S rRNA genes from nucleic acids extracted from gastric fluids, fecal material, and epithelial lining from along the digestive tract. Samples from two individuals (SKA_09D_W and SKA_09D_F) were sequenced in January 2010 and the remaining samples from six additional individuals were sequenced in January/February 2011. After purification of DNA using previously described methods (Dowd et al., 2008), amplicon pyrosequencing was done using the forward primer 28f (5'-GAGTTTGATCNTGGCTCAG-3') and the reverse primer 519r (5'-GTNTTACNGCGGCKGCTC-3') (Dowd et al., 2008).

Data obtained in this study for the American alligator were compared with data available in the published literature for other reptilian taxa and amphibians (Table 2.1). Datasets were deemed adequate for comparative purposes if the goal of the prior study was to evaluate

microbiome composition, and if bacterial phylum-level compositions were displayed visually or in tables, and if details on sample type (e.g., gut or skin) were provided in the publication. The resulting dataset incorporated six reptilian and six amphibian taxa, which includes all microbiome studies for these two groups to our knowledge.

Dataset processing and statistical analysis

Amplicon trimming, removal of primers, barcodes, and low quality reads, screening for chimera, alignments, taxonomic assignments, assessment of α- and β-diversity, and statistical analyses were consistent with previous studies (Schloss et al., 2009; Zhang et al., 2009; Matsui et al., 2010; Schloss et al., 2011). Additional screening, OTU definitions at 96% sequence identity, average-neighbor cluster analysis, rarefaction curves, and statistical calculations were run with MOTHUR, version 1.28.0 (Schloss et al., 2009). The datasets were used to calculate rarefaction curves (Fig. A.1), revealing high to moderate sample coverage, as well as bacterial diversity indices (Fig. A.2) and richness values (Fig. A.2). The Ribosomal Database Project (RDP) was utilized for sequence trimming, alignment, and taxonomic assignment (Zhang et al., 2009; Matsui et al., 2010). Processing included screening to trim reads less than 150 bp in length, removing primers, barcodes, and low quality reads ($Q < 20$) using RDP. Following alignment in RDP, potentially chimeric reads were identified using the UCHIME command in MOTHUR (Schloss et al., 2009). Reads identified as potentially chimeric were visually examined, compared to known reads using BLAST, and removed. Additional screening following chimera removal using MOTHUR included removing sequences with homopolymeric regions (> 8 bp), removing ambiguous reads, and ensuring uniform start positions for all reads and a minimum length of 150 bp (Schloss et al., 2011). After filtering, reads were uploaded to RDP for taxonomic assignment.

Subsequent average-neighbor clustering, rarefaction curve generation, and statistical analyses were performed using MOTHUR. A core microbiome was obtained by clustering reads using variable OTU cut-offs (96%, 95%, 91% sequence similarity). Raw pyrosequence files were deposited in the GenBank Short Read Archive (accession numbers SRA023831 and SRA062824). Student's *t*-tests and NPMANOVA were performed in PAST (Hammer et al., 2001) to test the significance of bacterial community composition, number of recovered OTUs, and percentages of OTUs ($\alpha = 0.05$). NPMANOVA based on Euclidean distances of log-transformed data was utilized to evaluate the environmental variable(s) that accounted for the observed variations in bacterial community composition. For microbiome comparisons across reptile and amphibian host taxonomic groups, the compiled bacterial phylum-level compositions were analyzed using PAST. Cluster analyses based on Bray-Curtis dissimilarity, and Euclidean-based NMDS were also utilized.

Results

Wild *A. mississippiensis* generally fast from October to March (Joanen and McNease, 1987). We hypothesized that protracted fasting would yield the composition of the indigenous symbiotic gut microflora, based on findings from the Burmese python that captured postprandial remodeling in microbiome composition (Costello et al., 2010). During fasting (Joanen and McNease, 1987), the wild alligator stomach contents (< 15 mL) consisted of viscous, semi-opaque yellow gastric juices with pH 2.1 to 3.0 (average 2.6; n = 5) and that were occasionally mixed with green, fluid-like material reminiscent of vegetation. Alligators routinely ingest vegetation as a consequence of capturing prey along shorelines, and prey for wild alligators includes small mammals, birds, crustaceans, fish, amphibians, and other reptiles (Elsey et al.,

1992). During feeding, wild alligator stomach contents consisted of residual plant material, cutaneous fragments of partially digested crawfish, and whole crawfish, with a stomach pH 1.6 to 3.7 (average 2.8; n = 10). From animal "N", there were 17 whole, 2.5 cm long crawfish recovered, and from animal "D", nematodes, common in wild alligators, were recovered. In contrast, the farm-raised animals were fed a commercially available, dry, pelleted alligator ration (manufactured by Cargill) that consisted primarily of crude protein (45-56%), fat (9-12%), and fiber (3-4%) derived from animal protein products (dried blood meal, meat, and bone), wheat, soy, corn, and animal fat. Stomach contents from farm-raised individuals were viscous, opaque, brown to yellow fluids, and stomach pH ranged from 1.7 to 6.6 (average 3.3; n = 5) during fasting and from 3.0 to 5.9 (average 4.4; n = 5) while feeding.

General patterns of bacterial phylum-level and proteobacterial class-level relative abundances for each alligator microbiome correlated to seasonal fasting or feeding based on nonparametric multivariate analysis of variation (NPMANOVA) (Fig. 2.2; Tables A.1 and A.2). Wild fasting (winter) microbiome compositions shifted from communities dominated by Proteobacteria to Firmicutes- and Fusobacteria-dominated communities after renewed feeding in the spring (NPMANOVA $P = 0.001$, $F = 8.17$). *Gammaproteobacteria* comprised ~30% of all wild (fasting) tissue communities, whereas Firmicutes and Fusobacteria comprised 67% and 25%, respectively, for wild spring-collected tissues. Firmicutes represented 17.6% of the winter wild microbiome amplicons, but 66.9% upon renewed feeding and active fat deposition (Wang et al., 2006) (NPMANOVA $P < 0.001$, $F = 16.75$). In contrast, Firmicutes comprised a significant portion of both winter farm-raised (35.5% of recovered amplicons) and spring farm-raised (48.5% of recovered amplicons) gut communities (NPMANOVA $P = 0.002$, $F = 3.66$). Animal rearing history (i.e. wild or farmed), sex, and overall length (as a proxy for age and size) did not

significantly explain the observed bacterial variability (NPMANOVA $P > 0.05$). Similarly, non-metric multidimensional scaling (NMDS) plots showed that wild and farm-raised bacterial communities responded similarly to scaling dimensions in NMDS space (Fig. A.3). Among all the alligators, seasonal feeding / fasting status explained the significant differences in bacterial compositions (NPMANOVA $P < 0.001$, $F = 6.09$).

But, for each alligator, significant changes in bacterial community compositions were attributed to specific organ or tissue type (i.e. in reference to changes in epithelial tissue along the alimentary canal) (NPMANOVA $P < 0.001$, $F = 2.42$; Fig. 2.2). The mouths had the richest α-diversity based on the number of operational taxonomic units (OTUs). As alligators frequently open their mouths for thermoregulation (Spotila et al., 1977), rich α-diversity potentially reflects frequent inoculation with transient environmental bacteria. The upper GI tract communities (e.g., stomach tissue, fluids, duodenum) had the lowest richness and diversity (Fig. A.2), likely as a consequence of low pH. Intermediate richness and α-diversity values were obtained for the lower GI tract tissues (colon and feces; Fig. A.3). From the oral and upper GI tract only (i.e. stomach, duodenum), 94% of the amplicons were affiliated with Proteobacteria (*Betaproteobacteria* and *Gammaproteobacteria*), Bacteroidetes, and Firmicutes, whereas 73% of the amplicons from the lower GI tract (i.e. ileum, colon, and feces when present) were affiliated with Fusobacteria, Firmicutes, and Bacteroidetes. In general, Fusobacteria dominated the lower GI tract, particularly feces (NPMANOVA $P = <0.001$, $F = 23.5$), but were a minor group (4%) when present in the rest of the GI system. Unique community ordination according to tissue type in NMDS space (Fig. 2.3) showed that communities retrieved from the colon and ileum occupied the largest NMDS ordination space compared to other tissue communities that did not overlap (i.e. feces and tongue). This was supported by β-diversity analyses of shared bacterial OTUs that also

revealed a potentially high level of endemism to each organ. The greatest similarity levels in community composition were only among physiologically adjacent organs or from samples derived from the same organ (i.e. stomach and gastric juices; Table A.3).

We used average-neighbor cluster analyses of amplicons recovered from each organ or tissue type to assess the potential for a core microbiome. Defining a host-specific or environment-specific core microbial community can be used to develop a screening tool that could identify host health, immunity, and disease (Zhang et al., 2009; Roeselers et al., 2011) and to deduce symbiotic evolutionary relationships through time (Ochman et al., 2010). The number of unique OTUs were not significantly different between feeding and fasting in wild (two-tailed, paired *t*-test $P = 0.17$) and farmed ($P = 0.25$) animals. More unique OTUs were recovered from oral samples; however, for individuals where tongue tissues were unavailable and esophageal tissues were utilized, the greatest number of unique OTUs was from the lower GI (colon or feces; Table A.4). The number of unique OTUs specific to wild and farm-raised organ or tissue type ranged from 2.7% up to 86.6% of all recovered OTUs from that sample type (average of 26.2% unique OTUs per organ or tissue; Table A.3). The largest number of shared OTUs based on average-neighbor cluster analysis was observed in individuals from the same season (e.g., winter vs. spring; Table A.4). A maximum of 13 OTUs were shared among all wild individuals (Fig. 2.5; Table A.5). Although it may be too stringent given potential error incurred with pyrosequencing (Kunin et al., 2010), a 96% sequence similarity cutoff was used to denote species- to genus-level associations (Huse et al., 2012) among the OTUs. One OTU from the GI tracts of all wild and farmed individuals was assigned to the *Enterobacteriales*. The number of shared OTUs increased by lowering the sequence similarity cut-offs to 95% and 91%, which represented higher taxonomic associations (Kunin et al., 2010; Huse et al., 2012) (Table 2.2).

Resulting OTUs identified at this level included representatives of Bacteroidetes (*Bacteroidales*), Firmicutes (*Clostridia, Clostridiaceae, Clostridiales*), Fusobacteria (*Fusobacteriaceae*), and *Gammaproteobacteria* (*Enterobacteriales*).

Patterns of microbiome composition emerge after focusing on the available microbiome data for reptiles and amphibians (Table 2.1). In general, the microbiome of reptiles from fecal samples was dominated by Firmicutes (or Fusobacteria in the American alligator), while amphibians contained a greater proportion of Proteobacteria (Figs. 2.5, 2.6). Cluster analyses of the taxa based on microbiome composition grouped amphibians and reptiles separately, which suggested that microbiome composition may reflect dietary, evolutionary, and genetic differences between the hosts. However, host class-level taxonomic assignments (Fig. 2.6A) and sample type (Fig. 2.6B) equally explained the distinct groups that form in NMDS space. These results revealed potential pitfalls of trying to reconstruct a maintained, derived microbiome composition for ancestral taxa.

Discussion

Microbiome acquisition occurs over evolutionary time and reflects complex feedbacks between the host (Zoetendal et al., 2001), environment (Wu et al., 2012), diet (Wu et al., 2011), immune response, and microbe-microbe community interactions (Faust and Raes, 2012) that change as new lineages invade new ecological niches. However, reptilian taxa are currently underrepresented among gut microbiome studies, thereby resulting in limited potential to reconstruct the evolutionary history of vertebrate-microbe symbioses. Based on previous studies that emphasize host feeding status controls microbiome composition (Costello et al., 2010), and because alligators have distinctive physiological and biochemical differences compared to other

animal hosts, particularly with respect to seasonal fasting (Lance et al., 2001), we expected that alligator GI tract microbiomes would differ as a function of rearing history. Our results reveal longitudinally heterogeneous microbiomes along the alligator GI tract, with compositional differences significantly correlating to organ or tissue and also to the farm-raised versus wild alligator diets.

The dissimilarity between our alligator microbiome compositional findings and the conclusions drawn in earlier GI tract studies is striking. This is likely because the previous work, including from mammalian hosts, relies predominately on colonic biopsies (Zoetendal et al., 2004; Zhang et al., 2009; Ochman et al., 2010; Roeselers et al., 2011), feces (Ley et al., 2008a; Lu et al., 2008; Ochman et al., 2010; Hong et al., 2011), gastric fluids (Pei et al., 2010), cecal contents (Matsui et al., 2010), or intestines (Eckburg et al., 2005; Roeslers et al., 2011; Wu et al., 2012) to define host microbiomes. However, these limited samples may not provide the insight intended (Zoetendal et al., 2004). From our analyses, distinct microbial communities were detected between the alligator mucosa and lumenal contents, as has also been observed in mice (Nava et al., 2011). Also, the fecal microbial community composition did not represent the composite alligator GI tract microbiome. Representatives from the Fusobacteria phylum were most abundant from farm-raised and wild feces, but were minor members of GI tract communities (Table A.1). In contrast, other undetected phyla in the feces (e.g. Actinobacteria) had significant representation in other regions of the GI tract. If alligator feces alone were used to represent the gut microbiome, or at least the lower GI tract, then Bacteroidetes would be considered the most prevalent microbial group in the alligator microbiome. But, four OTUs total were affiliated with Bacteroidetes, which comprised only 10% of the composite microbiome from all of the digestive organs (Table 2.2). The relative abundances of Bacteroidetes were

considerably lower than what has been reported in other vertebrate microbiome studies (Ley et al., 2005; Pei et al., 2010), which again may be due to the use of fecal, cecal, or intestinal samples alone. Additionally, it is possible that increasing the number of individual hosts in a study could alter interpretations of inferred composite microbiomes. However, at least from our results, the observed pattern of microbial community variation along the length of the alimentary canal should remain because of the underlying function of each organ for digestion and the significant correlation between community composition and organ or tissue type. Future studies should utilize representative samples of the entire gut if the GI tract is considered to be a heterogeneous ecosystem with organ-specific microbiomes.

Significant differences in the alligator GI tract microbiome community composition according to organ or tissue type may be due to the host's metabolism and physiology (e.g., carnivore, herbivore, or omnivore) and metabolic capabilities of members of the gut microbiome. But, differences between farm-raised and wild alligator gut bacterial community compositions could also be attributed to host diet. Firmicutes dominated the farm-raised alligator GI tract microbiomes throughout the year, comparable to microbiomes of other captive-bred and raised reptiles (Costello et al., 2010; Hong et al., 2011). However, Firmicutes only dominated wild alligator microbiomes during seasonal feeding. The farm-raised alligators had significantly greater fat deposits compared to their wild counterparts. Obesity in farm-raised alligators has been observed previously (Elsey et al., 1992) due to a diet high in carbohydrates and saturated fats (Lance et al., 2001) to increase animal size for commercial meat and skin production. Obesity and excess fatty tissue have been correlated to shifts in microbiome composition in humans (Ley et al., 2005; Ley, 2010). In other mammalian taxa, including mice (Ley, 2010), Firmicutes are also prevalent members of microbiome communities from obese individuals. The

intriguing association between increased fat deposition and the predominance of Firmicutes in gut microbiomes from feeding alligators, as well as from obese vertebrates, suggests that diet has the potential to modify gut microbiome physiology when the ecological niche occupied by the wild counterpart changes.

From the alligator GI tract microbiomes, a core community of Fusobacteria, Bacteroidetes, Firmicutes, and Proteobacteria is strikingly different from the core microbiomes inferred for other vertebrates, including mammals (Ley et al., 2008a; Costello et al., 2009), birds (Lu et al., 2008; Qu et al., 2008; Matsui et al., 2010), and even other reptiles (Costello et al., 2010; Hong et al., 2011; Keenan, 2013) (Fig. 2.5, Tables A.7 and A.8). As all other vertebrates sampled to date possess representatives of Bacteroidetes, Firmicutes, and Proteobacteria, regardless of host taxonomy, the presence of Fusobacteria in all alligators sampled makes the alligator gut microbiome unique. Fusobacteria represented ~12% of the OTUs in the core alligator microbiome, and dominated the lower GI tract tissue bacterial communities and fecal material (Table 2.2). In contrast, Fusobacteria have been retrieved in low abundances from composite gut microbiomes from human (<10% of all oral sequences) (Costello et al., 2009), fish (<13% of sequences) (Wu et al., 2012), and chicken (<3.0% of sequences) (Qu et al., 2008) hosts, with Fusobacteria recovered from human oral cavities playing a critical role in initial biofilm development (Mira et al., 2004). In these other hosts, Firmicutes and Bacteroidetes represent the overwhelming majority of recovered microbiome OTUs.

Our results raise a fundamental question: why are Fusobacteria prevalent in the American alligator GI tract? Fusobacteria are a poorly-studied phylum comprised of approximately 32 described species, with an overall uncertain phylogenetic history. Some researchers place the phylum at a basal position (Battistuzzi and Hedges, 2008) based on both rRNA and core protein

analyses with the hyperthermophilic Aquificae and Thermotogae phyla, but others consider Fusobacteria to have closer phylogenetic affiliation with Bacteroidetes and Firmicutes (Mira et al., 2004). Placement as a basal phylum has led to an inferred divergence ~3.5 billion years ago (Battistuzzi and Hedges, 2008). However, because of high horizontal gene transfer within Firmicutes, and because Fusobacteria are frequently recovered with Firmicutes, a divergence no earlier than 400 Myr is also proposed, which coincides with the origin of the vertebrate digestive tract (Mira et al., 2004). The almost complete lack of environmental studies that describe the presence, diversity, and functional role of Fusobacteria (Battistuzzi and Hedges, 2008) in microbiomes confounds the uncertain phylogenetic position. Although Fusobacteria are associated with oral diseases in humans (Mira et al., 2004), their prevalence in alligators can be interpreted as specialized, perhaps critical to host health or nutrient acquisition, because alligators possess innate immune compatibility not present in mammalians. Fusobacteria are also known to play a role in biofilm development (Mira et al., 2004), so their presence in the GI tract could affect lumen biofilm development. This would explain the dominance of Fusobacteria in alligator feces. As other vertebrate microbiome studies rarely sample epithelial tissue (although see Zoetendal et al., 2002, and Wang et al., 2003, for exceptions), it is possible that Fusobacteria have been undersampled in microbiome studies until now. Nevertheless, based on what data are available, we speculate that Fusobacteria in the lower GI tract of alligators may occupy a functional role in digestion organ development and nutrient acquisition that precedes a similar ecological niche that is now occupied by Firmicutes and Bacteroidetes in mammals based on a combination of strong selective pressures driven by host genetics, a conserved diet, niche occupation, and unique biochemical adaptations (Merchant et al., 2006).

Reconstructing an ancestral microbiome

Compared to the other reptilian and amphibian taxa studied to date, alligators have a distinct microbiome composition dominated by Fusobacteria (Fig. 2.5B). In other reptiles, Fusobacteria is only observed in the python and land iguana (Fig. 2.1B), forming a small (<1 %) part of the community composition. Although alligators and pythons, which diverged ~285 million years ago (Mya) (Shen et al., 2011) are both carnivores, community composition between the two animals is distinct implying that carnivory is not the driving force behind resident bacteria. The giant tortoise and alligator, which diverged approximately 240 Mya (Shen et al., 2011), have remarkably dissimilar gut communities, implying that subsequent host divergence, changes in diet (herbivory vs. carnivory), and occupation of distinct ecological niches may have all shaped microbial community composition. Previous studies on the role diet type (herbivorous, carnivorous or omnivorous) on gut composition in mammals indicate that, in general, herbivores and omnivores contain similar gut communities (Ley et al., 2008a). Carnivores, however, do not have similar communities, implying that for at least carnivores, diet is not the defining characteristic that controls gut microbial composition (Ley et al., 2008a). Additionally, the presence of Fusobacteria in appreciable numbers in both alligators and chicken (Aves) (Fig. 2.1) hints at a shared functional role that may have been present in their last common ancestor before the lineages diverged in the Permian.

Conclusions

Microbiomes have the potential to provide a window into an ancestral condition that has been retained over geologic time. Others postulate that vertebrate gut microbiome evolution may correlate to tetrapod evolution (Ley et al., 2008a, b). But, the diversity of bacterial communities

residing in vertebrate guts is far from explored, as evidenced from our study that reveals a distinct alligator gut microbiome. An analysis of current microbiome data, albeit based on feces that likely represent biased microbiome compositional information (Fig. 2.7), still shows that microbiome compositions do not reflect host phylogenetic affiliations for all Vertebrata. Placement of sister taxa based on microbiome composition alone may lead to non-biologically meaningful information (i.e. placement of gorillas as sister taxa to zebrafish rather than to other hominids included in the dataset). Consequently, what is known from mammals is likely not representative of tetrapods as a whole, although successful attempts have been made to reconstruct the evolutionary history of mammalian digestive systems (Ley et al., 2008a, b; Moeller et al., 2012).

With a similar approach, the alligator microbiomes can be used conservatively to reconstruct the ecology and evolutionary history of crocodylian, and perhaps even archosaur, digestive systems (Hone et al., 2012). Pseudosuchia and Avemetatarsalia, lineages within Archosauria, diverged in the Early Triassic (approx. 250 Myr ago), giving rise to modern crocodylians and avians, respectively (Nesbitt, 2011). The order Crocodylia is comprised of 23 extant species of caiman, alligators, crocodiles, and gharials within the Alligatoridea, Crocodyloidea, and Gavialoidea families (Brochu, 2003). Recent phylogenetic reconstructions from extant taxa and the robust crocodylian fossil record, which extends from the Late Cretaceous (70-84 Myr ago), highlight that modern crocodylians have had extensive, dynamic evolutionary histories that inform us about the ecology, physiology, and biochemistry of the ancient lineages (Brochu, 2003; Seymour et al., 2004). For instance, the biochemically unique crocodylian blood serum with its antibacterial properties was likely an ancestral trait that originated in response to aggressive behavior associated with frequent injuries and occupation of

potentially pathogen-rich wetlands (Merchant et al., 2006). Fossil evidence indicates that numerous crocodylian taxa had similar trophic statuses and occupied comparable ecological niches to the modern (Noto et al., 2012), generally functioning as top predators and scavengers within a narrow aquatic to semi-aquatic niche (e.g., wetlands and floodplains). We do not know when modern archosaur symbioses became established in the geologic past, and what the ancestral condition may have been. However, it is possible that ancestral crocodylian and extinct archosaur GI tract microbiomes would have been more similar to modern alligators than to other vertebrates studied to date, assuming comparable trophic status, diet, and niche occupation through time. Future research should include a robust evaluation of the ecological status (i.e. aquatic, semi-aquatic or terrestrial), feeding habits, and phylogenetic position of archosaurs (Pol et al., 2009; Nesbitt, 2011) to test this hypothesis. Nevertheless, the implications from the modern alligator gut microbiome comprised of Bacteroidetes, Firmicutes, Proteobacteria, and Fusobacteria, the dominance of which is unique among vertebrates, advance our understanding of archosaur gut microbiome evolution and host-microbe symbioses.

Fig. 2.1: Schematic phylogeny showing major clades and diversification events through geologic time. (A) Tetrapoda originated in the late Devonian with the evolution of semi-aquatic and terrestrial vertebrates. The number of average microbiomes above each taxon reflects what is currently known for the phylum-level gut composition in each animal host (data presented in Table 2.2; *n* = number of animals sampled in each study). (B) Expanded reptile phylogeny with dates indicating the placement of nodes for major diversification events. Pie charts reflect fecal metagenomes from reptiles (dates compiled from Shen et al., 2011). Figure from Keenan (2013).

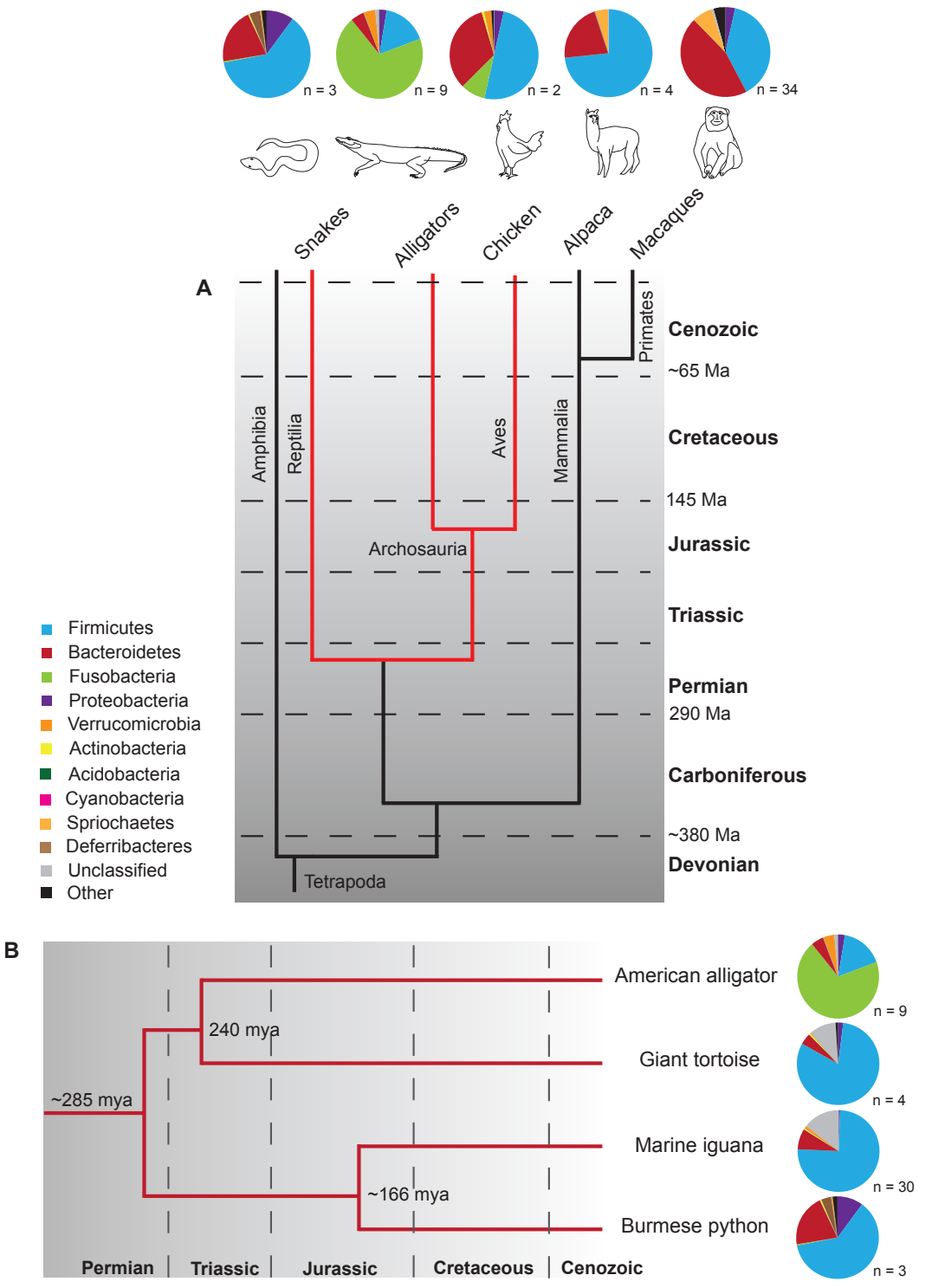
n = 3
n = 9
n = 2
n = 4
n = 34
Snakes
Alligators
Chicken
Alpaca
Macaques
A
Amphibia
Reptilia
Aves
Mammalia
Primates
Archosauria
Tetrapoda
Cenozoic
~65 Ma
Cretaceous
145 Ma
Jurassic
Triassic
Permian
290 Ma
Carboniferous
~380 Ma
Devonian
Firmicutes
Bacteroidetes
Fusobacteria
Proteobacteria
Verrucomicrobia
Actinobacteria
Acidobacteria
Cyanobacteria
Spriochaetes
Deferribacteres
Unclassified
Other
B
American alligator
Giant tortoise
Marine iguana
Burmese python
240 mya
~285 mya
~166 mya
Permian
Triassic
Jurassic
Cretaceous
Cenozoic
n = 9
n = 4
n = 30
n = 3

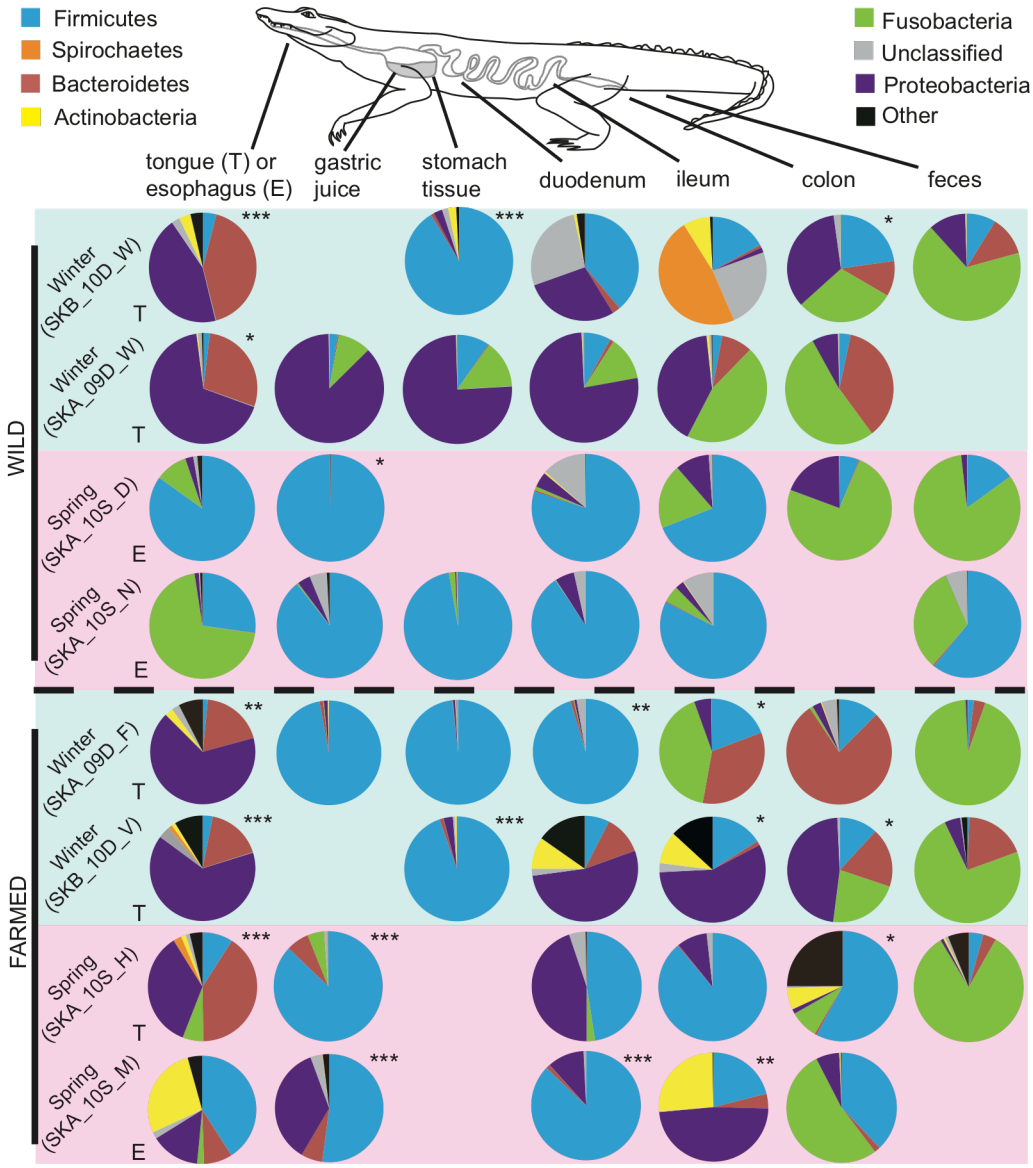

Fig. 2.2: Phylum-level, gastrointestinal bacterial community representation (>2% of retrieved amplicons) from wild and farm-raised, winter and spring, *A. mississippiensis* individuals and schematic sample locations. Data are divided based on rearing history (wild vs. farmed), and subdivided based on season (winter and spring, blue and pink backgrounds, respectively) (Appendix Table B.1). Significant differences in bacterial composition between downstream tissues or organs (paired Student's *t*-test) are denoted by asterisks: $P = 0.05 – 0.01$ (*), 0.01-0.001 (**), and $P < 0.001$ (***) (full *t*-tests in Table B.7).

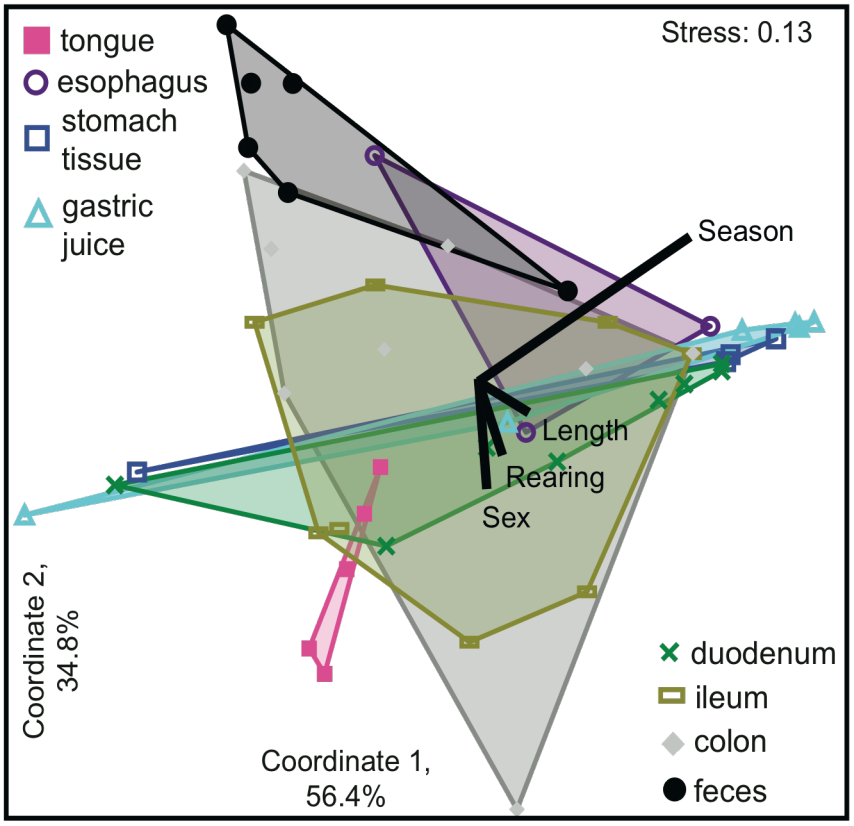

Fig. 2.3: Euclidean-based NMDS plot of bacterial diversity as a function of tissue type from all individuals, regardless of rearing history or feeding status. Gastrointestinal samples proximal to each other had more similar bacterial communities. The plot was constructed using normalized log abundances, and the parameters season (spring or winter), animal length, rearing history (farmed or wild), and sex (male or female). Lines denote vector overlays on NMDS ordination, indicating the directionality and strength of change (line length) for a specific parameter.

Fig. 2.4: Schematic average neighbor cluster analyses for shared bacterial OTUs retrieved from wild and farm-raised alligators. OTU taxonomy was based on BLAST results (Table A.5), and the value shown in brackets refers to the number of OTUs at phylum- or class-level. Cluster analysis at 96% sequence similarity (solid black lines) resulted in 63 shared OTUs, one of which was recovered from all wild and farmed individuals (*Enterobacteriales*). Reducing the similarity threshold to 95% (dashed lines), and 91% (grey lines), reduced the number of OTUs to 59 and 41, respectively. At 95%, two shared OTUs among all animals formed.

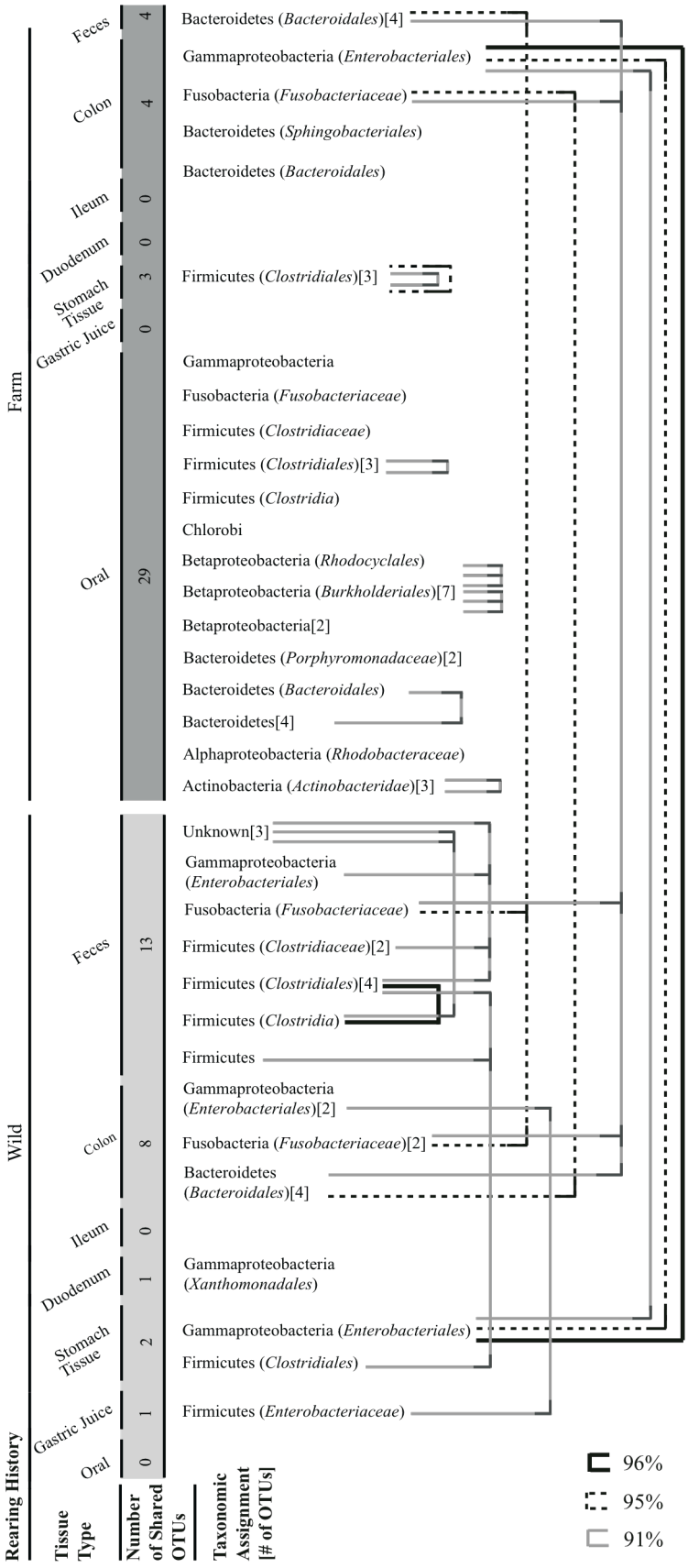
Rearing History
Tissue Type
Number of Shared OTUs
Taxonomic Assignment [# of OTUs]
Farm
Wild
Feces
Colon
Ileum
Duodenum
Stomach Tissue
Gastric Juice
Oral
4
4
0
0
3
0
29
13
8
0
1
2
1
0
Bacteroidetes (Bacteroidales)[4]
Gammaproteobacteria (Enterobacteriales)
Fusobacteria (Fusobacteriaceae)
Bacteroidetes (Sphingobacteriales)
Bacteroidetes (Bacteroidales)
Firmicutes (Clostridiales)[3]
Gammaproteobacteria
Fusobacteria (Fusobacteriaceae)
Firmicutes (Clostridiaceae)
Firmicutes (Clostridiales)[3]
Firmicutes (Clostridia)
Chlorobi
Betaproteobacteria (Rhodocyclales)
Betaproteobacteria (Burkholderiales)[7]
Betaproteobacteria[2]
Bacteroidetes (Porphyromonadaceae)[2]
Bacteroidetes (Bacteroidales)
Bacteroidetes[4]
Alphaproteobacteria (Rhodobacteraceae)
Actinobacteria (Actinobacteridae)[3]
Unknown[3]
Gammaproteobacteria (Enterobacteriales)
Fusobacteria (Fusobacteriaceae)
Firmicutes (Clostridiaceae)[2]
Firmicutes (Clostridiales)[4]
Firmicutes (Clostridia)
Firmicutes
Gammaproteobacteria (Enterobacteriales)[2]
Fusobacteria (Fusobacteriaceae)[2]
Bacteroidetes (Bacteroidales)[4]
Gammaproteobacteria (Xanthomonadales)
Gammaproteobacteria (Enterobacteriales)
Firmicutes (Clostridiales)
Firmicutes (Enterobacteriaceae)
96%
95%
91%

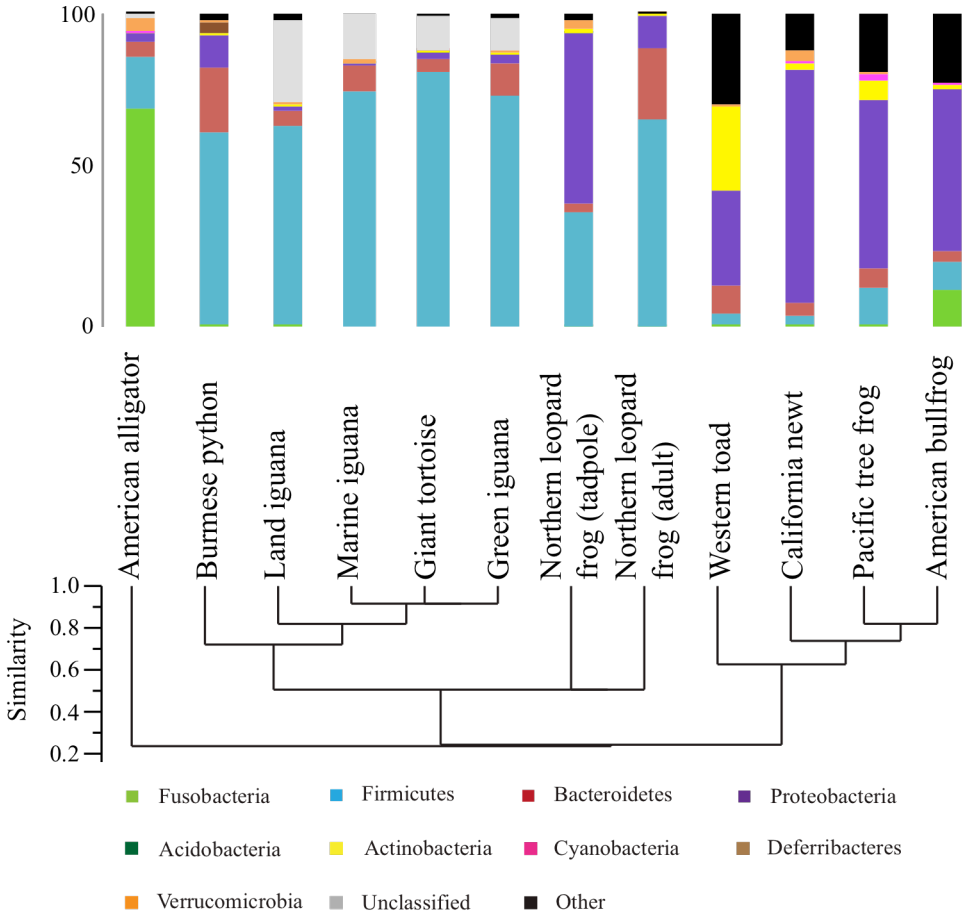

Fig. 2.5: Constrained cluster analysis of bacterial phylum-level microbiome composition of reptiles and amphibians based on unpaired groups and Bray-Curtis dissimilarity. Normalized bacterial phyla are presented above the dendogram, highlighting the species-specific variability in microbiome composition (Table 2.1 for references).

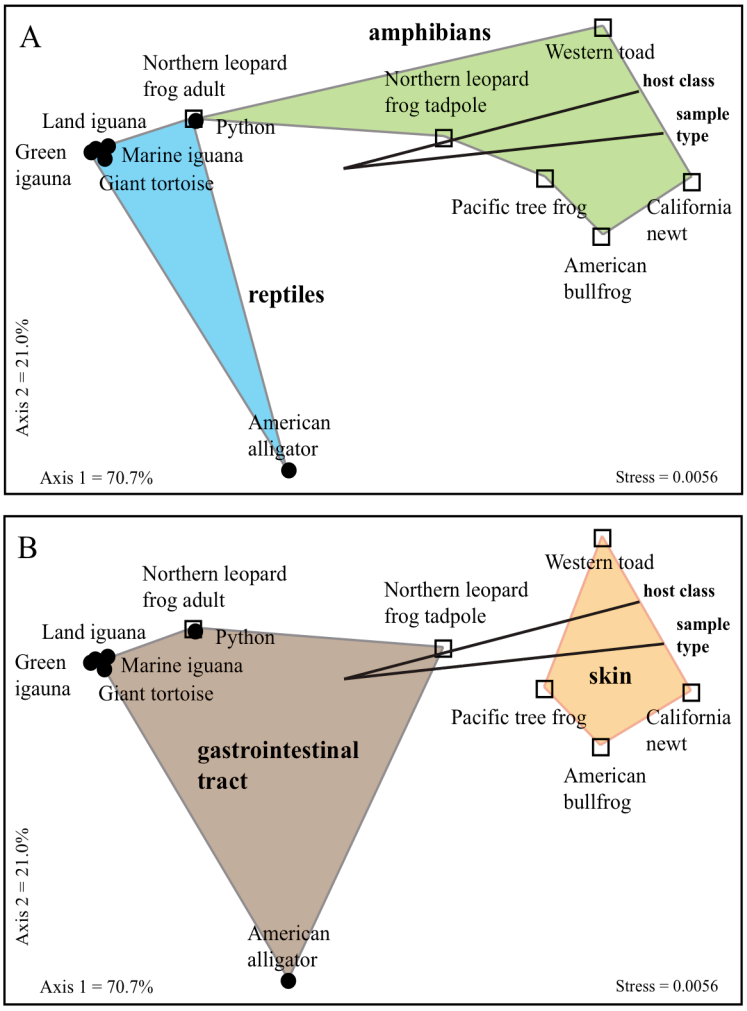

Fig. 2.6: Non-metric multidimensional scaling (NMDS) plots of bacterial phylum-level microbiome composition for reptiles and amphibians based on Euclidean distances (data in Table 2.1). (A) Grouping vertebrate taxa by class-level reveals two distinct clusters, reptiles and amphibians indicate that there are host-specific differences in microbiome composition. (B) Grouping host taxa by the type of sample examined also reveals distinct groups (e.g., gastrointestinal vs. skin microbiome), which suggests potentially tissue or organ-specific microbiomes. These findings highlight limitations with respect to grouping microbiomes by sample type and that attempts to infer an evolutionary or ecological control on microbiome composition may be inaccurate.

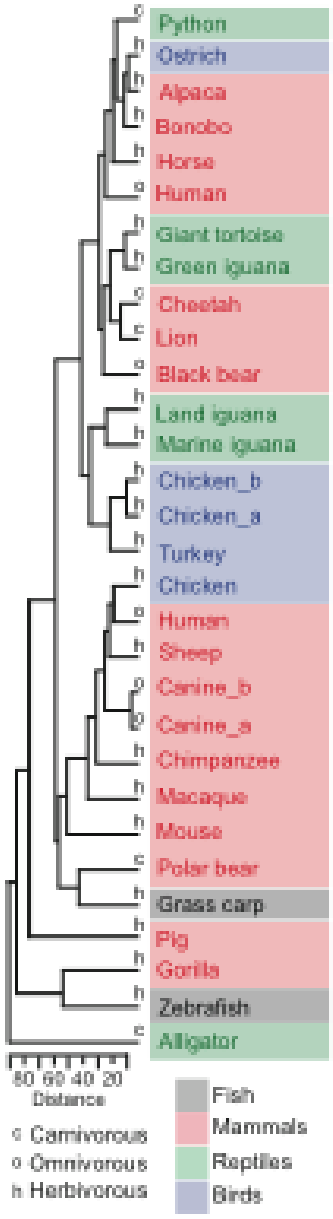

Fig. 2.7: Euclidean-based cluster analysis of phylum-level bacterial diversity of representative vertebrate taxa. Colors correspond to major divisions of host phylogenetic affiliation (mammals, reptiles, birds, and fish) and letters reflect diet. Data used for alligator are based on average feces bacterial composition (Table A.8). Feces were selected as the majority of microbiome studies utilize fecal material. Phylum-level bacterial assignments were selected as the published data generally did not include lower taxonomic assignments.

Table 2.1: Phylum-level microbiome composition for reptiles and amphibians determined using molecular approaches.

	Vertebrate Host (sample location)	Source of Data	No. animals	Fusobacteria	Firmicutes	Bacteroidetes	Proteobacteria	Acidobacteria	Actinobacteria	Cyanobacteria	Deferribacteres	Verrucomicrobia	Unclassified	Other
Reptilia	Alligator, *Alligator mississippiensis* (feces)	Keenan (2013)	n = 9	69.6	16.7	5	2.7	0.002	0.08	0.1	0	4.3	1.4	0.12
	Burmese python (fasted, pooled GI tract)	Costello et al. (2010)	n = 3	0.5	61.8	20.6	10.1	0	0.6	0	3.9	0.6	0	1.90
	Land iguana (feces)	Hong et al. (2011)	n = 16	0.6	63.9	4.2	1.4	0	1.3	0	0	0.2	26.6	1.80
	Marine iguana (feces)	Hong et al. (2011)	n = 30	0	75.1	8.2	0.6	0	0.6	0	0	1	14.5	0.00
	Giant tortoise (feces)	Hong et al. (2011)	n = 4	0	81.1	4.4	2	0.1	0.8	0.1	0	0.1	10.4	1.00
	Green iguana (feces)	Hong et al. (2011)	n = 2	0	74	10.1	3.1	0	0.1	0	0	1	10.1	1.60
Amphibia	Northern leopard frog tadpole, *Lithobates pipiens* (intestine)	Kohl et al. (2013)	n = 7	0.01	36.61	2.43	54.86	0.09	1.13	0	0	2.66	0	2.21
	Northern leopard frog adult, *Lithobates pipiens* (intestine)	Kohl et al. (2013)	n = 8	0.32	66.05	22.82	10.43	0	0.08	0	0	0.03	0	0.27
	Western toad, *Anaxyrus boreas* (skin)	Kueneman et al. (2013)	n = 47	0.7	3.7	8.9	30.3	0	26.6	0	0	0.8	0	29.00
	California newt, *Taricha torosa* (skin)	Kueneman et al. (2013)	n = 16	0.8	3.0	3.7	74.7	0	2.2	0.7	0	3.0	0	11.90
	Pacific tree frog, *Pseudacris regilla* (skin)	Kueneman et al. (2013)	n = 30	0.8	11.8	5.9	53.7	0	6.3	2.0	0	0.8	0	18.70
	American bullfrog, *Lithobates catesbeianus* (skin)	Kueneman et al. (2013)	n = 11	11.8	8.9	3.7	51.3	0	1.9	0.5	0	0.2	0	21.70

Table 2.2: Taxonomic assignments of shared OTUs.

Wild	No. of OTUs (% of total)	Farmed	No. of OTUs (% of total)
Bacteroidetes	4 (16)	Actinobacteria	3 (7.5)
Bacteroidales	4	*Actinobacteridae*	3
Firmicutes	10 (40)	Alphaproteobacteria	1 (2.5)
Clostridia	1	*Rhodobacteraceae*	1
Clostridiaceae	2	Bacteroidetes	13 (32.5)
Clostridiales	4	*Bacteroidales*	6
Enterobacteriaceae	1	*Porphyromonadaceae*	1
Fusobacteria	3 (12)	*Sphingobacteriales*	1
Fusobacteriaceae	3	Betaproteobacteria	10 (25)
Gammaproteobacteria	5 (20)	*Burkholderiales*	7
Enterobacteriales	4	*Rhodocyclales*	1
Xanthomonadales	1	Chlorobi	1 (2.5)
Unknown	3 (12)	Firmicutes	8 (20)
		Clostridia	1
		Clostridiaceae	1
		Clostridiales	6
		Fuosbacteria	2 (5)
		Fusobacteriaceae	2
		Gammaproteobacteria	2 (5)
		Enteroabcteriales	1

The numbers of OTUs refer to the total number of OTUs recovered in wild or farm-raised individuals and assigned to the phyla or class, where assignment was possible according to BLAST (Table A.5). Values in parentheses refer to the percentage of the shared community represented by each phylum.

References

Barboza, P.S., Bennett, A., Lignot, J.H., Mackie, R.I., McWhorter, T.J., Secor, S.M., Skovgaard, N., Sundset, M.A., Wang, T., 2010. Digestive challenges for vertebrate animals: microbial diversity, cardiorespiratory coupling, and dietary specialization. Physiol Biochem Zool 83, 764-774.

Barnosky, A.D., Matzke, N., Tomiya, S., Wogan, G.O.U., Swartz, B., Quental, T.B., Marshall, C., McGuire, J.L., Lindsey, E.L., Maguire, K.C., Mersey, B., Ferrer, E.A., 2011. Has the Earth's sixth mass extinction already arrived? Nature 471, 51-57.

Battistuzzi, F.U., Hedges, S.B., 2008. A major clade of prokaryotes with ancient adaptations to life on land. Mol Biol Evol 26, 335-343.

Beebee, T.J.C., Griffiths, R.A., 2005. The amphibian decline crisis: A watershed for conservation biology? Biol Conserv 125, 271-285.

Bjerrum, L., Engberg, R.M., Leser, T.D., Jensen, B.B., Finster, K., Pedersen, K., 2006. Microbial community composition of the ileum and cecum of broiler chickens as revealed by molecular and culture-based techniques. Poult Sci 85, 1151-1164.

Brazaitis, P., Watanabe, M.E., 2011. Crocodilian behaviour: a window to dinosaur behaviour? Hist Biol 23, 73-90.

Brochu, C.A., 2003. Phylogenetic approaches toward crocodylian history. Annu Rev Earth Pl Sc 31, 357-397.

Buddington, R.K., Williams, C.H., Kostek, B.M., Buddington, K.K., Kullen, M.J., 2010. Maternal-to-infant transmission of probiotics: concept validation in mice, rats, and pigs. Neonatology 97, 250-256.

Costello, E.K., Gordon, J.I., Secor, S.M., Knight, R., 2010. Postprandial remodeling of the gut microbiota in Burmese pythons. ISME J 4, 1375-1385.

Costello, E.K., Lauber, C.L., Hamady, M., Fierer, N., Gordon, J.I., Knight, R., 2009. Bacterial community variation in human body habitats across space and time. Science 326, 1694-1697.

Daly, K., Stewart, C.S., Flint, H.J., Shirazi-Beechey, S.P., 2001. Bacterial diversity within the equine large intestine as revealed by molecular analysis of cloned 16S rRNA genes. FEMS Microbiol Ecol 38, 141-151.

Dodson, P., 2003. Allure of el lagarto: why do dinosaur paleontologists love alligators, crocodiles, and their kin? Anat Rec Part A 274A, 887-890.

Dowd, S.E., Callaway, T.R., Wolcott, R.D., Sun, Y., McKeehan, T., Hagevoort, R.G., Edrington, T.S., 2008. Evaluation of the bacterial diversity in the feces of cattle using 16S rDNA bacterial tag-encoded FLX amplicon pyrosequencing (bTEFAP). BMC Microbiol 8, DOI:10.1186/1471-2180-8-125.

Eckburg, P.B., Bik, E.M., Bernstein, C.N., Purdom, E., Dethlefsen, L., Sargent, M., Gill, S.R., Nelson, K.E., Relman, D.A., 2005. Diversity of the human intestinal microbial flora. Science 308, 1635-1638.

Elsey, R.M., McNease, L., Joanen, T., Kinler, N., 1992. Food habits of native wild and farm-released juvenile alligators. Proc Annu Conf SEAFWA 46, 57-66.

Farlow, J.O., 1987. Speculations About the diet and digestive physiology of herbivorous dinosaurs. Paleobiology 13, 60-72.

Farmer, C.G., Uriona, T.J., Olsen, B.D., Steenblik, M., Sanders, K., 2008. The right-to-left shunt of crocodilians serves digestion. Physiol Biochem Zool 81, 125-137.

Faust, K., Raes, J., 2012. Microbial interactions: from networks to models. Nat Rev Microbiol 10, 538-550.

Hammer, Ø., Harper, D.A.T., Ryan, P.D., 2001. PAST: paleontological statistics software pacakge for education and data analysis. Palaeontologia Electronica 4, 1-9.

Hattori, M., Taylor, T.D., 2009. The human intestinal microbiome: a new frontier of human biology. DNA Res 16, 1-12.

Hill, D.A., Hoffmann, C., Abt, M.C., Du, Y., Kobuley, D., Kirn, T.J., Bushman, F.D., Artis, D., 2010. Metagenomic analyses reveal antibiotic-induced temporal and spatial changes in intestinal microbiota with associated alterations in immune cell homeostasis. Mucosal Immunol 3, 148-158.

Hone, D., Tsuihiji, T., Watabe, M., Tsogtbaatr, K., 2012. Pterosaurs as a food source for small dromaeosaurs. Palaeogeogr Palaeocl 331, 27-30.

Hong, P.Y., Wheeler, E., Cann, I.K.O., Mackie, R.I., 2011. Phylogenetic analysis of the fecal microbial community in herbivorous land and marine iguanas of the Galápagos Islands using 16S rRNA-based pyrosequencing. ISME J 5, 1461-1470.

Huse, S.M., Ye, Y., Zhou, Y., Fodor, A.A., 2012. A core human microbiome as viewed through 16S rRNA sequence clusters. PLoS One 7, DOI:10.1371/journal.pone.0034242.

Joanen, T., McNease, L., 1987. Alligator farming research in Louisiana, USA, in: Webb, G.J.W., Manolis, S.C., Whitehead, P.J. (Eds.), Wildlife Management: Crocodiles and Alligators. Surrey Beatty & Sons, Australia, pp. 329-340.

Johnston, M.A., Porter, D.E., Scott, G.I., Rhodes, W.E., Webster, L.F., 2010. Isolation of faecal coliform bacteria from the American alligator (*Alligator mississippiensis*). J Appl Microbiol 108, 965-973.

Keenan, S.W., 2013. Freshwater vertebrate animal metagenomics, Alligatorinae, in: Nelson, K. (Ed.), Encyclopedia of Metagenomics. Springer-Verlag Berlin Heidelberg.

Kunin, V., Engelbrektson, A., Ochman, H., Hugenholtz, P., 2010. Wrinkles in the rare biosphere: pyrosequencing errors can lead to artificial inflation of diversity estimates. Environ Microbiol 12, 118-123.

Lance, V.A., Morici, L.A., Elsey, R.M., Lund, E.D., Place, A.R., 2001. Hyperlipidemia and reproductive failure in captive-reared alligators: vitamin E, vitamin A, plasma lipids, fatty acids, and steroid hormones. Comp Biochem Phys B 128, 285-294.

Lance, V.A., Elsey, R.M., Butterstein, G., Trosclair, P.L., Merchant, M., 2010. The effects of Hurricane Rita and subsequent drought on alligators in southwest Louisiana. J Exp Zoo Part A 313A, 106-113.

Ley, R.E., 2010. Obesity and the human microbiome. Curr Opin Gastroenterol 26, 5-11.

Ley, R.E., Backhed, F., Turnbaugh, P., Lozupone, C.A., Knight, R.D., Gordon, J.I., 2005. Obesity alters gut microbial ecology. Proc Natl Acad Sci U S A 102, 11070-11075.

Ley, R.E., Peterson, D.A., Gordon, J.I., 2006. Ecological and evolutionary forces shaping microbial diversity in the human intestine. Cell 124, 837-848.

Ley, R.E., Hamady, M., Lozupone, C., Turnbaugh, P.J., Ramey, R.R., Bircher, J.S., Schlegel, M.L., Tucker, T.A., Schrenzel, M.D., Knight, R., Gordon, J.I., 2008a. Evolution of mammals and their gut microbes. Science 320, 1647-1651.

Ley, R.E., Lozupone, C.A., Hamady, M., Knight, R., Gordon, J.I., 2008b. Worlds within worlds: evolution of the vertebrate gut microbiota. Nat Rev Microbiol 6, 776-788.

Lu, J.R., Domingo, J.S., 2008. Turkey fecal microbial community structure and functional gene diversity revealed by 16S rRNA gene and metagenomic sequences. J Microbiol 46, 469-477.

Matsui, H., Kato, Y., Chikaraishi, T., Moritani, M., Ban-Tokuda, T., Wakita, M., 2010. Microbial diversity in ostrich ceca as revealed by 16S ribosomal RNA gene clone library and detection of novel Fibrobacter species. Anaerobe 16, 83-93.

McFall-Ngai, M.J., 2002. Unseen forces: The influence of bacteria on animal development. Dev Biol 242, 1-14.

McKenna, P., Hoffmann, C., Minkah, N., Aye, P.P., Lackner, A., Liu, Z., Lozupone, C.A., Hamady, M., Knight, R., Bushman, F.D., 2008. The macaque gut microbiome in health, lentiviral infection, and chronic enterocolitis. PLoS Pathog 4, DOI:10.1371/journal.ppat.0040020.

Merchant, M.E., Mills, K., Leger, N., Jenkins, E., Vliet, K.A., McDaniel, N., 2006. Comparisons of innate immune activity of all known living crocodylian species. Comp Biochem Phys B 143, 133-137.

Mira, A., Pushker, R., Legault, B.A., Moreira, D., Rodriques-Valera, F., 2004. Evolutionary relationships of *Fusobacterium nucleatum* based on phylogenetic analysis and comparative genomics. BMC Evol Biol 4, DOI:10.1186/1471-2148-4-50 .

Moeller, A.H., Degnan, P.H., Pusey, A.E., Wilson, M.L., Hahn, B.H., Ochman, H., 2012. Chimpanzees and humans harbour compositionally similar gut enterotypes. Nat Commun 3, DOI:10.1038/ncomms2159.

Nava, G.M., Friedrichsen, H.J., Stappenbeck, T.S., 2011. Spatial organization of intestinal microbiota in the mouse ascending colon. ISME J 5, 627-638.

Nesbitt, S.J., 2011. The early evolution of archosaurs: relationships and the origin of major clades. B Am Mus Nat Hist, 1-288.

Noto, C.R., Main, D.J., Drumheller, S.K., 2012. Feeding traces and paleobiology of a Cretaceous (Cenomanian) crocodyliform: example from the Woodbine Formation of Texas. Palaios 27, 105-115.

Obwolo, M.J., Zwart, P., 1993. Prevalence of *Salmonella* in the intestinal tracts of farm-reared crocodiles (*Crocodylus niloticus*) in Zimbabwe. J Zoo Wildlife Med 24, 175-176.

Ochman, H., Worobey, M., Kuo, C.H., Ndjango, J.B., Peeters, M., Hahn, B.H., Hugenholtz, P., 2010. Evolutionary relationships of wild hominids recapitulated by gut microbial communities. PLoS Biol 8, DOI:10.1371/journal.pbio.1000546.

Pei, C.X., Liu, Q., Dong, C.S., Li, H., Jiang, J.B., Gao, W.J., 2010. Diversity and abundance of the bacterial 16S rRNA gene sequences in forestomach of alpacas (*Lama pacos*) and sheep (*Ovis aries*). Anaerobe 16, 426-432.

Pol, D., Turner, A.H., Norell, M.A., 2009. Morphology of the Late Cretaceous crocodylomorph *Shamosuchus djadochtaensis* and a discussion of neosuchian phylogeny as related to the origin of Eusuchia. B Am Mus Nat Hist, 1-103.

Pryde, S.E., Richardson, A.J., Stewart, C.S., Flint, H.J., 1999. Molecular analysis of the microbial diversity present in the colonic wall, colonic lumen, and cecal lumen of a pig. Appl Environ Microbiol 65, 5372-5377.

Qu, A., Brulc, J.M., Wilson, M.K., Law, B.F., Theoret, J.R., Joens, L.A., Konkel, M.E., Angly, F., Dinsdale, E.A., Edwards, R.A., Nelson, K.E., White, B.A., 2008. Comparative metagenomics reveals host specific metavirulomes and horizontal gene transfer elements in the chicken cecum microbiome. PLoS One 3, DOI:10.1371/journal.pone.0002945.

Rayfield, E.J., 2007. Finite element analysis and understanding the biomechanics and evolution of living and fossil organisms. Annu Rev Earth Pl Sc 35, 541-576.

Roeselers, G., Mittge, E.K., Stephens, W.Z., Parichy, D.M., Cavanaugh, C.M., Guillemin, K., Rawls, J.F., 2011. Evidence for a core gut microbiota in the zebrafish. ISME J 5, 1595-1608.

Saalfeld, D.T., Conway, W.C., Calkins, G.E., 2011. Food habits of American alligators (*Alligator mississippiensis*) in East Texas. Southeast Nat 10, 659-672.

Schachner, E.R., Farmer, C.G., McDonald, A.T., Dodson, P., 2011. Evolution of the dinosauriform respiratory apparatus: new evidence from the postcranial axial skeleton. Anat Rec 294, 1532-1547.

Schloss, P.D., Gevers, D., Westcott, S.L., 2011. Reducing the effects of PCR amplification and sequencing artifacts on 16S rRNA-based studies. PLoS One 6, DOI:10.1371/journal.pone.0027310.

Schloss, P.D., Westcott, S.L., Ryabin, T., Hall, J.R., Hartmann, M., Hollister, E.B., Lesniewski, R.A., Oakley, B.B., Parks, D.H., Robinson, C.J., Sahl, J.W., Stres, B., Thallinger, G.G., Van Horn, D.J., Weber, C.F., 2009. Introducing mothur: open-source, platform-independent, community-supported software for describing and comparing microbial communities. Appl Environ Microbiol 75, 7537-7541.

Seymour, R.S., Bennett-Stamper, C.L., Johnston, S.D., Carrier, D.R., Grigg, G.C., 2004. Evidence for endothermic ancestors of crocodiles at the stem of archosaur evolution. Physiol Biochem Zool 77, 1051-1067.

Shirley, M.H., Vliet, K.A., Carr, A.N., Austin, J.D., 2013. Rigorous approaches to species delimitation have significant implications for African crocodilian systematics and conservation. P Roy Soc B-Biol Sci 281, DOI:10.1098/rspb.2013.2483.

Spotila, J.R., Terpin, K.M., Dodson, P., 1977. Mouth gaping as an effective thermoregulatory device in alligators. Nature 265, 235-236.

Subalusky, A.L., Fitzgerald, L.A., Smith, L.L., 2009. Ontogenetic niche shifts in the American Alligator establish functional connectivity between aquatic systems. Biol Conserv 142, 1507-1514.

Swanson, K.S., Dowd, S.E., Suchodolski, J.S., Middelbos, I.S., Vester, B.M., Barry, K.A., Nelson, K.E., Torralba, M., Henrissat, B., Coutinho, P.M., Cann, I.K.O., White, B.A., Fahey, G.C., 2011. Phylogenetic and gene-centric metagenomics of the canine intestinal microbiome reveals similarities with humans and mice. ISME J 5, 639-649.

Varricchio, D.J., 2001. Gut contents from a Cretaceous Tyrannosaurid: implications for theropod dinosaur digestive tracts. J Paleontol 75, 401-406.

Wang, T., Hung, C.C.Y., Randall, D.J., 2006. The comparative physiology of food deprivation: from feast to famine. Annu Rev Physiol 68, 223-251.

Wang, X., Heazlewood, S.P., Krause, D.O., Florin, T.H.J., 2003. Molecular characterization of the microbial species that colonize human ileal and colonic mucosa by using 16S rDNA sequence analysis. J Appl Microbiol 95, 508-520.

Wu, G.D., Chen, J., Hoffmann, C., Bittinger, K., Chen, Y.Y., Keilbaugh, S.A., Bewtra, M., Knights, D., Walters, W.A., Knight, R., Sinha, R., Gilroy, E., Gupta, K., Baldassano, R., Nessel, L., Li, H.Z., Bushman, F.D., Lewis, J.D., 2011. Linking long-term dietary patterns with gut microbial enterotypes. Science 333, 105-108.

Wu, S.G., Wang, G.T., Angert, E.R., Wang, W.W., Li, W.X., Zou, H., 2012. Composition, diversity, and origin of the bacterial community in grass carp intestine. PLoS One 7, DOI: 10.1371/journal.pone.0030440.

Zanno, L.E., Makovicky, P.J., 2011. Herbivorous ecomorphology and specialization patterns in theropod dinosaur evolution. Proc Natl Acad Sci U S A 108, 232-237.

Zhang, H.S., DiBaise, J.K., Zuccolo, A., Kudrna, D., Braidotti, M., Yu, Y.S., Parameswaran, P., Crowell, M.D., Wing, R., Rittmann, B.E., Krajmalnik-Brown, R., 2009. Human gut microbiota in obesity and after gastric bypass. Proc Natl Acad Sci U S A 106, 2365-2370.

Zoetendal, E., Akkermans, A.D., Akkermans-van, V., de Visser, J.A.G.M., De Vos, W.M., 2001. The host genotype affects the bacterial community in the human gastrointestinal tract. Microbial Ecol Health D 13, 129-134.

Zoetendal, E.G., Cheng, B., Koike, S., Mackie, R.I., 2004. Molecular microbial ecology of the gastrointestinal tract: from phylogeny to function. Curr Issues Intest Microbiol 5, 31-47.

Zoetendal, E.G., von Wright, A., Vilpponen-Salmela, T., Ben-Amor, K., Akkermans, A.D., de Vos, W.M., 2002. Mucosa-associated bacteria in the human gastrointestinal tract are uniformly distributed along the colon and differ from the community recovered from feces. Appl Environ Microbiol 68, 3401-3407.

Chapter 3: Visualizing early diagenesis of bone

Some of the results of this chapter will be submitted for review and potential publication, with a preliminary citation of: Keenan, S.W., Engel, A.S., Bovenkamp, G.L., and Roy, A., Visualizing early diagenesis of bone.

SWK collected and prepared samples, collected data, conducted data analysis, and wrote the manuscript. ASE assisted in data analysis, and helped to write the manuscript. GLB and AR assisted with data collection and analysis, and edited the manuscript.

Abstract

One of the most challenging questions in paleobiology is how bone transforms from a living tissue into a fossil. Although the geologic record is replete with vertebrate fossils preserved from wetland depositional systems, thermodynamic models suggest that bone hydroxyapatite is generally unstable in a range of varying geochemical conditions and should readily dissolve if not altered to a more stable phase, including fluorapatite. We assess early diagenesis of alligator bone, on timescales ranging from days to years, via thermodynamic models, and hypothesize that kinetic controls related to microbial colonization of bone must dictate preservation potential. Experimental mesocosms simulated burial in sediments with strong redox gradients, and bone chemistry and structural alterations were analyzed after one week using electron microprobe analyses and infrared spectroscopy. Hydroxyapatite recrystallization occurred after one month when bone was separated from indigenous microbial colonization, but not in experiments where bones were directly in contact with sediment and microbial cells. Microbial biofilm formation on the bone may have decreased alteration rates, at least initially, by reducing ion substitution sites in the bone mineral lattice. Changes to the hydroxyapatite lattice were primarily at the Ca(II)

site, which corresponds to protonation of the hydroxyl ion that would open the lattice to additional substitutions. These results have implications for understanding diagenetic rates and microbial contributions to bone alteration during early diagenesis, and ultimately highlight the impact of early diagenesis on altering the vertebrate fossil record over geologic time.

Introduction

Bone is a composite material consisting of organic (i.e. collagen, lipids) and inorganic (i.e. mineral) components. The mineralized fraction is a nonstoichiometric apatite phase, usually hydroxyapatite (HAP) [$Ca_{10}(PO_4)_6(OH)_2$] or a carbonated HAP (Elliott, 2002; Olszta et al., 2007). In life, ion replacement and substitution flexibility of the apatite lattice permits bone to serve as a reservoir of Ca, Na, and other trace elements for biosynthesis (Bergstrom and Wallace, 1954; Green and Kleeman, 1991). Once removed from a living organism and deposited in the environment, bone HAP lattice can potentially accommodate substitutions and replacements at all sites (e.g., Ca(I), Ca(II), PO_4^{3-}, OH^-). Such chemical alterations are considered essential for long-term preservation of bone based on trace element enrichment in fossil bones compared to unaltered bone, often by several orders of magnitude, in F, Fe, Mn, Sr, Ba, and rare earth elements (e.g., Hubert et al., 1996). Other parameters for bone fossilization include reducing dissolution rates by changing mineral surface area to volume ratios (i.e. from increased crystallite size or structural ordering) (e.g., Kohn, 2008; Trueman et al., 2008) and degrading and removing organics to enhance ion transport and fluid migration (e.g., Child, 1995; Kohn, 2008).

Despite extensive evaluation of major and trace element composition (e.g., Trueman and Benton, 1997; Koenig et al., 2009), isotopic records (e.g., Kolodny et al., 1996), and structure and development histories of bone through time (e.g., Olszta et al., 2007), significant gaps

remain in our understanding of the earliest stages of bone diagenesis, specifically once bone is introduced into an environment with potentially aggressive geochemical fluids. Several questions motivate this research: What is the timing of bone apatite recrystallization? Are chemical and structural alterations that occur in the first stages of diagenesis maintained in fossil bone, such that geochemical conditions in the depositional environment become recorded in the fossil? To what extent does the (micro)biology within a depositional setting have the potential to influence bone diagenesis? Here, we evaluate structural and compositional changes in alligator bone during early diagenesis, within a wetland environment containing strong redox gradients, and explore the potential role of indigenous sediment microbial communities. Understanding structural and bonding transformations that occur within days to weeks to bone HAP, following exposure to environmental conditions, are critical to determining how fossilization and preservation may have proceeded in the geological past.

Methods and analytical techniques

Aqueous and sediment geochemical parameters used to populate thermodynamic models

Dynamic thermodynamic geochemical models predict mineral stabilities under varying geochemical conditions. Aqueous geochemical data were collected from ~1 km^2 fresh to brackish water wetlands, including sediment pore water, at Rockefeller Wildlife Refuge (RWR), located within the Chenier Plains of southwestern Louisiana, USA (Fig. 3.1, Table 3.1). As a modern depositional system in which alligators thrive (Elsey and Woodward, 2010) and are likely to be buried following death, we could assess geochemical processes affecting *in situ* alligator bone diagenesis. Alligators are crown-group archosaurs that have been used in other studies to assess the physiology (Schachner et al., 2011), biomechanics (Cuff and Rayfield,

2013), and symbioses (Keenan et al., 2013) in extinct taxa. Archosaurs have an extensive fossil record and some have occupied semi-aquatic environments since their divergence with avemetatarsalians (Chatterjee, 1985). As such, experimental use of modern alligator bones provides a good analogue for archosaurian bone preservation.

At RWR, silt to clay-sized sediment accumulated as overbank deposits in relic Mississippi River floodplains, and laterally migrating beach-ridge complexes. Soils locally known as Creole clay are vertisols that consist predominantly of mixed-layer smectite, mica, and quartz (Table 3.2) (Midkiff and Roy, 1995). Organic carbon content was determined in triplicate from loss on ignition (LOI) estimates (Wright et al., 2008; Wang et al., 2011; Wang et al., 2012), and ranged from 52 to 237 g/kg; inorganic carbon content ranged from 5 to 10 g/kg (Table 3.3). Sediment pH ranged from 5.4 to 7.6 based on sediment slurry measurements (1:2, sediment to deionized water) (Robertson et al., 1999).

The phosphorus sorption capacity of RWR clay minerals, up to 112 mg of total phosphorus ($[P_T]$)/100 g of sediment, was determined from several representative sediment samples along a depth profile from 7.5 to 30 cm depth (Table 3.4), following methods modified from Bache and Williams (1971) and Lajtha et al. (1999). In brief, the target wet weight of each sample was calculated based on the ratio of wet to dry mass after drying sediment at 105°C for 24 hours, with target wet weights ranging from 3.3 to 4.3 g. Wet sediment was processed in triplicate. A stock solution of 0.01 M $CaCl_2 \bullet 2H_2O$ was used instead of 0.01 M KCl, and no chloroform was added. A phosphate stock solution with a concentration of 130 mg/L P as PO_4 was added to each sample (25 mL) in a 50 mL centrifuge tube (Falcon), and placed on a shaking platform (120 rpm) for 24 hours. $[P_T]$ was measured using ion chromatography (Dionex ICS-2100) of solutions gravimetrically filtered (Whatman 42) into acid-washed 50 mL syringes.

Solutions were then filtered to 0.45 μm (Whatman) into glass IC sample vials and analyzed within 1-2 hours of filtration.

Temperature, pH, and conductivity were measured in the field using standard electrode methods (APHA, 2005). Ion measurements utilized water samples filtered with 0.2 μm-PDVF filers (Millipore) in the field into pre-cleaned HDPE bottles, followed by analysis using ion chromatography (Dionex ICS-2100) (APHA, 2005). Cation sample bottles were HCl-washed and filtered samples were preserved with trace metal grade HNO_3. Dissolved oxygen, ferrous, ferric and total iron, sulfide, and ammonia were measured in the field using standard colorimetric methods (CHEMetrics, Calverton, Virginia) (APHA, 2005). Alkalinity from filtered samples was determined by titration using 0.1 N H_2SO_4 to pH 4.3 within 24 hours after collection (APHA, 2005). RWR water geochemical analyses were supplemented with United States Geological Survey (USGS) data from local streams (http://waterdata.usgs.gov/nwis), as well as fog data from the published literature (Raja et al., 2008) (Table B.1). Over three years, all waters examined from RWR were classified as Na-K-Cl type waters (Fig. 3.2).

Thermodynamic models were run with PHREEQC-I, version 2.18 (Parkhurst and Appelo, 1999; Appelo and Postma, 2005; USGS, 2011) to determine activity and saturation indices (SI) for mineral phases known to be present based on X-ray diffraction (XRD) analyses or otherwise expected (e.g., calcite, dolomite, hydroxyapatite, fluorinated and carbonated apatite, gypsum, halite, goethite), according to calculated ion activity products (IAP) and the solubility product constant (K_{sp}) for a mineral, as $SI = \log(IAP/K_{sp})$. For ionic strength values ≤ 0.1 M/L, the extended form of the Debye-Hückel equation was used to calculate activity coefficients (USGS, 2011). Models were run iteratively by varying temperatures (5-40°C), pH (6.0-9.0), and $[P_T]$ (0.0006 to 0.0484 mmol/L).

X-ray diffraction (XRD) analyses of air- and oven-dried, coarsely ground sediment (20 to 100 mg) were conducted on a Rigaku Ultima IV X-ray diffractometer under 40 kV and 30 mA operating conditions with a continuous scan speed of 2° per minute. Samples were placed onto a glass sample holder and inserted into the instrument, according to manufacturer instructions, and scanned from 4° to 70° 2θ with Cu Kα radiation. Diffractograms were input into the Rigaku software package PDXL for peak identification, characterization of mineralogy, and calculation of mineral content (as %).

Wetland sediment mesocosms and **in situ** *burial experiments*

Batch mesocosm experiments were conducted using autoclaved ~240 mL glass jars that were partly filled with aseptically collected sediment plugs (75 g) and 100 mL of 0.2 μm-filtered surface water from RWR. Alligator vertebrae salvaged from RWR (under permit LNHP-10-009) were cleaned of soft tissues by dermestid beetles, and any residual debris was removed by brushing, followed by immersion in Milli-Q deionized water by sonication (Branson 2510) for 60 min. Vertebrae surfaces were further cleaned and sterilized using a critical point drying method, starting with 70% reagent grade ethanol and ending with 100% reagent grade ethanol (Hamilton, 1999). Bones were dried overnight at room temperature prior to introduction into the mesocosms. Exclusion treatments were evaluated using bone kept from having direct microbial interaction (through colonization) with microbes in the sediment. This was accomplished by placing vertebrae into dialysis tubing (Spectrapor 3, Spectrum Laboratories Inc., 3.5 kDa molecular-weight cutoff; Gray and Engel, 2013), prepared according to manufacturer instructions. In mesocosms designed to evaluate direct microbial interactions (colonization treatments), pre-sterilized vertebrae were placed directly into jars using sterile forceps.

In addition to mesocosm experiments, two salvaged alligators, complete with soft tissues, were buried intact at RWR in April, 2010, at ~ 0.3 m depth to assess changes to bone and soil microbial communities over several years exposure in the field. Pre-burial sediment was collected prior to the introduction of the salvaged alligators. Annually, sediment samples were collected at the burial site at depths from the surface to ~ 37 cm along a linear transect, marked at 0 (on burial), 7.5, 15, 30, 60, and 120 cm intervals, that radiated outwards from the center of the burial. Each year, a different ordination transect was established (e.g., E-W, S-N, etc.) to minimize re-sampling of previously excavated sediments. At each point along the transect, a narrow trench was excavated to ~ 37 cm using a trowel. Sediment samples (~ 20 g) were collected using aseptic techniques, transferred to sterile whirl pack bags or 50 mL Falcon tubes, and stored on ice until returned to the lab and frozen at ¯20°C until further processing. When thawed for extraction of total nucleic acids, aliquots were also processed for pH, water content, total carbon (TC), total inorganic carbon (TIC), and total organic carbon (TOC) using LOI optimized for wetland sediments (e.g., 475°C and 800°C) (Wang et al., 2011). Most samples were processed in triplicate for LOI and averaged (Table 3.3). Sediment color was determined using wet samples and a Munsell soil color chart (Munsell Color Company Inc., Baltimore, MD). Air-dried sediments were coarsely ground for XRD analyses, as described above.

Molecular analysis of sediment microbial diversity

Extraction of total nucleic acids from sediment before burial experiments was done in triplicate from each sample, following protocols modified from Somerville et al. (1989) and Zhou et al. (1996). From the field, approximately 1.5 g of sediment was weighed into sterile 15 mL Falcon tubes, and 5 mL of freshly made sucrose lysis buffer (SLB) was added to each tube in

a biological safety cabinet using aseptic techniques. The SLB extraction solution consisted of 50 mM Tris-HCl (pH 7), 40 mM Na-EDTA (pH 8), 0.5 M sucrose (filter sterilized with a 0.2 μm Whatman Puradisc PES filter, GE Healthcare Life Sciences, UK) combined with 1 mg/ml fresh lysozyme (Somerville et al., 1989; Zhou et al., 1996). For nucleic acid extractions from the burial experiment, bones that were retrieved with sediment adhering to them were collected and stored in sterile whirl pack bags. In 2010, vertebrae were collected and part of the dentary was found in 2013. Approximately 10 mL of autoclaved deionized water was added to the bags containing the bones and shaken vigorously to remove adhering sediment and microorganisms. From 2 to 3 mL of sediment slurry for each of these samples were transferred to 15 mL Falcon tubes for nucleic acid extraction, following the same protocol used for sediments.

Tubes of sediment with SLB and lysozyme were vortexed harshly for 5-7 min and placed in a 37°C waterbath for 1 hour. After 1 hour, a solution of 20 mg/ml Proteinase K with 1% CTAB and 10% SDS solution with additional SLB were added to each tube (Somerville et al., 1989; Zhou et al., 1999). After gently mixing, tubes were sealed with parafilm and shaken horizontally at 120 rpm at 55°C overnight. After cooling to room temperature, 10 M filter-sterilized ammonium acetate was added to each tube and mixed by inversion prior to centrifugation at 5,000 rpm and 18°C for 15 min. The supernatant was transferred to a fresh tube with additional ammonium acetate, then recentrifuged for an additional 15 min. While avoiding any residual sediment and a potential SDS layer, triplicate supernatant aliquots were transferred to sterile 1.5 mL microcentrifuge tubes containing 100% reagent grade isopropanol. Tubes were mixed by inversion and placed in a freezer at ¯20°C overnight prior to centrifugation at 13,000 x g for 10 min. Pellets were retained after decanting, rinsed twice with cold 100% reagent grade ethanol. Pellets were air-dried before being resuspended with TE Buffer (pH 8). Extraction

efficiency was evaluated by measuring the concentration of recovered nucleic acids with a spectrophotometer (NanoDrop 2000, Thermo Scientific), and evaluating samples with gel electrophoresis prior to sequencing. Extractions were stored at ¯20°C.

Aliquots of DNA extracted in triplicate were pooled and cleaned using the Power Soil DNA Cleanup Kit (MoBio), following manufacturer instructions, prior to FLX Titanium 454 tag-encoded pyrosequencing by MRDNA (Shallowater, TX) of the V1-V3 region of bacterial 16S rRNA genes using the forward primer 28f (5'-GAGTTTGATCNTGGCTCAG-3') and the reverse primer 519r (5'-GTNTTACNGCGGCKGCTC-3') using previously described methods (Dowd et al., 2008; Keenan et al., 2013). All samples for all of the experiments were sequenced together in October 2013.

Amplicon data processing and analysis followed the methods outlined by Keenan et al. (2013). The Ribosomal Database Project (RDP) was utilized for initial sequence trimming, removal of primers and barcodes, alignment, and taxonomic assignment (Zhang et al., 2009; Matsui et al., 2010). Further screening, removal of low quality reads, screening for chimera, rarefaction curves (Fig. B.1), assessment of α- and β-diversity (Fig. B.2), and other statistical analyses were consistent with previous studies and utilized the latest version of MOTHUR (version 1.32.0) (Schloss et al., 2009; Zhang et al., 2009; Matsui et al., 2010; Schloss et al., 2011, Keenan et al., 2013).

Synthetic wetland water development and pH mesocosm experiments

Berna et al. (2004) suggest that pH exerts a significant control on apatite mineral stability. To test HAP alteration and collagen release under variable pH conditions, batch reactions were established with sterile 60 mL glass serum bottles (Wheaton), 1 cm^2 sterilized

bone chips, and synthetic water designed to match the general representative composition of water at RWR (Table 3.1, Table B.2). Synthetic water consisted of 4.76 mmol/L $NaHCO_3$ (Fisher Scientific), 2.53 mmol/L Na_2SO_4 (Fisher), 12.85 mmol/L $MgCO_3$ (Fisher), 0.92 mmol/L KCl (Fisher), 4.47 mmol/L $CaCl_2 \cdot 2H_2O$ (J.T. Baker), and 34.86 mmol/L NaCl (Fisher), which was autoclaved prior to adjusting to experimental pH values, from 6.0 to 11.0, at 1 unit intervals by adding 1 M NaOH or 0.1 M HCl. Once the appropriate pH was reached, sterilized (from ethanol washing) bone chip was added and the serum bottle was capped with a chlorobutyl stopper (Wheaton, Fisher). Collagen release into the solutions was determined spectroscopically using a Horiba Fluoromax-4 Spectrofluorometer and a UV-visible spectrometer (Evolution 201, Thermo Scientific) by measuring dissolved fluorophores after 1, 2, 3, 6, 14, and 30 days. For each analysis, 1 mL of solution was removed using a sterile needle and luer lock syringe, and then filtered to 0.2 μm using a sterile Whatman Puradisc PES filter into a quartz cuvette. Filtered samples were diluted to 3 mL by adding autoclaved deionized water. Collagen fluorescence was visualized by measuring the excitation and emission wavelengths from 240 to 450 nm and 250 to 560 nm, respectively. The characteristic collagen peak occurs at excitation wavelengths between 330-340 nm and an emission wavelength of ~395 nm (Georgakoudi et al., 2002). Fluorescence data were analyzed using MATLAB (Mathworks).

Bone chips were also removed after 1, 2, 3, 6, 14, and 30 days using sterile forceps. Chips were rinsed with autoclaved deionized water, dried at 37°C in sterile petri dishes, and ground using an agate mortar and pestle to a uniform powder that was stored in sterile microcentrifuge tubes until analysis.

Quantitative and qualitative bone geochemical assessment

Bone composition and atomic-level structure were examined from (i) thin sections using electron microprobe (EMP) analyses for unaltered and buried bones from the experiments in this study, as well as from a representative Late Cretaceous fossil, and (ii) from powders using Fourier transform infrared spectroscopy (FTIR). All analytical work was done at the University of Tennessee-Knoxville. EMP and FTIR have been used to determined bone composition previously (e.g., Weiner and Bar-Yosef, 1990; Sponheimer and Lee-Thorp, 1999; Pucéat et al., 2004; Trueman et al., 2008) because the approaches provide insight into bone mineral composition (e.g., CO_3^{2-} and organic material) and structure (e.g., crystallinity). The fossil used in this study was obtained by permission of the Museum of the Rockies (Montana State University, Bozeman). A *Triceratops* limb bone fragment was collected in 2009 from overbank deposits in the Upper Hell Creek Formation. All bone fragments (approximately 1 cm^3) were cleaned of sediment with autoclaved deionized Milli-Q water, followed by 70% ethanol (Hamilton, 1999), and ground using an agate mortar and pestle to a uniform consistency. To avoid contamination, all equipment was rinsed with deionized water, dried, and cleaned further with 100% reagent grade acetone prior to and after sample processing. All powdered bone aliquots were stored in sterile centrifuge tubes until analysis (e.g., Sponheimer and Lee-Thorp, 1999; Reiche et al., 2002).

EMP analysis is a quantitative tool to assess major, minor, and potentially trace element composition of mineral phase(s) (Hubert et al., 1996; Tutken et al., 2004). Bone fragments were cut using a Dremel hand drill and embedded in resin (EpoThin Epoxy Resin, Buehler) under vacuum in a glass desiccation chamber to ensure complete diffusion of resin into pore spaces and to remove any air bubbles. Once set, sections were polished with progressively finer grit sizes

from 240 to 600 by hand using an abrasive belt grinder (Buehler) and with a MiniMet (Buehler) polisher to achieve a final uniform surface of 1 μm using MetaDi (monocrystalline diamond suspension, Buehler). Mosaic maps of the thin sections were made with reflected light to guide EMP analyses, and thin sections were carbon-coated.

The distribution and quantitative analyses of major (P, Ca, Na), minor (Mn, Mg, Fe, S, Si, Al), and trace (i.e. La, Ce, Cl) element chemistry and element mapping were performed on a Cameca SX-100. Prior to the start of analyses, instrument calibration and accuracy were checked by measuring known standards and re-calibrating when an element was less than 98% of the anticipated weight %. Spot analyses were run under standard operating conditions (Pyle et al., 2002) with an electron beam of 10 nA, an accelerating potential of 15 kV, and 10 μm spot size. Elements were analyzed in a fixed order under the same spectrometer conditions (Table B.3). Count times for elements ranged from 20 seconds for major elements to 60 seconds for minor and trace elements (Table B.3). Data were internally corrected using the "PAP" model (e.g., Pouchou and Pichoir, 1991), an approach analogous to ZAF that accounts for the effects of atomic number (Z), absorption (A), and fluorescence (F), with the Cameca software PeakSight. Detection limits (3σ) for each element calculated by PeakSight ranged from ~150 ppm for Al to ~1000 ppm for F (Table B.3). Analytical precision is presented as standard deviations for each element, most of which are less than 20. In modern bone, approximately 30% of the bulk composition consisted of organic carbon, lipids, and water, which resulted in element totals of ~70% (Table 3.5).

Element maps were constructed to visualize potential sub-micron variations in the apatite-phase chemistry and to evaluate potential for chemical heterogeneity of samples, which was expected given the high standard deviations for some elements. Elements for mapping were

selected after examining the spot analysis data and noting that certain compounds (e.g., FeO, P_2O_5) had larger standard deviations than expected (>20). Additional elements selected were Na as NaO, an element expected to be mobile in an aqueous environment given its high mobility in living bone tissue (Bergstrom and Wallace, 1954), and F, an element known to increase in apatite during diagenesis (e.g., Hubert et al., 1996). Several areas of cortical and trabecular bone were mapped to evaluate the variation of selected elements (Fe, P, Na, F, Ca). Resulting maps were false colored using the PeakSight to assess concentration changes, presented as changes to the number of counts measured by the detector; brighter colors represented higher counts or greater concentrations. False color element mixing also provided a way to assess variations in multiple elements (e.g., P and Fe).

Evaluating bone microstructure and composition

FTIR analyses were conducted on an Agilent Cary 660 FTIR using a diffuse reflectance accessory (Pike) to assess diagenetic alteration (e.g., Person et al., 1995; Sponheimer and Lee-Thorp, 1999; Pucéat et al., 2004; Munro et al., 2007; Trueman et al., 2008). Powdered bone samples were mixed in an agate mortar and pestle with KBr at a ratio of 1-5% sample to 99-95 % KBr, and then transferred to the stainless steel sample holder. Each sample was measured at least three times with fresh powders mixed for each analysis. Absorbance spectra were measured with a resolution of 4 cm^{-1} and 32 scans per analysis from 4000 to 400 cm^{-1} wavenumber. The resulting dataset for each sample was averaged using ResolutionsPro software, and averaged spectra were used in subsequent data analysis. Following previously published methods, crystallinity (IRSF) (Weiner and Bar-Yosef, 1990), mean crystal length (nm) (Trueman et al., 2004), amide content (Am/P), organic weight % (Trueman et al., 2008), and carbonate/phosphate

ratio (Pucéat et al., 2004) were calculated using baselines established in ResolutionsPro drawn between 2000 and 500 cm^{-1} wavenumber. Carbonate content was also determined from the ratio of type B carbonate to the primary phosphate peak [BPI], type A carbonate to the primary phosphate peak [API], and the ratio of type B carbonate to type A carbonate [BAI] (Sponheimer and Lee-Thorp, 1999).

Statistical analyses

Non-metric multidimensional scaling (NMDS) based on log-transformed data were used to evaluate the environmental variable(s) that accounted for the observed variations in bacterial community composition. Tests of significance in bacterial community composition were based on pairwise F-tests for equal variance (Tables B.4, B.5). Significance was set at $p < 0.05$. Additional multivariate statistical analyses, including principal components analysis (PCA) with correlation-based matrices were conducted using sediment geochemistry and bacterial community diversity (e.g., Shannon Index) to determine whether these variables exhibited patterns as a function of sampling depth or year. One sample collected at 7.5 cm depth in 2013 (13S_004) was excluded from PCA analyses due to significantly distinct bacterial community membership (Table B.4), which was likely an artifact of low sampling coverage (Fig. B.1). To evaluate changes to bone composition and structure, multivariate statistical analyses were performed, including PCA with correlation-based matrices to evaluate changes to experimentally treated bone, and after combining data obtained through EMP analyses and FTIR. All analyses were performed in PAST (Hammer et al., 2001).

Results

Bone mineral stability

Thermodynamic modeling indicated that HAP (K_{sp} $10^{-111.3}$ at 25° C) is undersaturated throughout the range of pH, temperature, and [P_T] conditions observed at RWR (Fig. 3.3). However, if bone altered through ion substitution(s) and structural rearrangement to either a fluorapatite (K_{sp} $10^{-122.9}$ at 25° C) or a carbonated fluorapatite phase (K_{sp} $10^{-107.5}$ at 25° C, based on maximum substitution of carbonate ions at 6.5 wt. %; Kuo et al., 2009), then bone comprised of those minerals would be stable, even under the slightly acidic (~ pH 6.25) conditions observed at RWR (Fig. 3.3). If less carbonate was incorporated into a carbonated fluorapatite phase, then K_{sp} values decrease.

Short-term changes to bone over days to weeks

Batch mesocosm experiments were performed to test the hypothesis that HAP must undergo early structural and chemical changes to a more stable mineral phase if bone is to be preserved over time. The effects of early changes (i.e. from days to weeks) on bone composition, with and without the influence of microbial colonization to bone, were evaluated. From short-term (days to weeks) mesocosm experiments, EMP and FTIR analyses indicated that bone structure and elemental composition changed after one week for both the types of treatments, with bone in direct contact with sediment and bone separated from the sediment via dialysis tubing (referred to as the colonization exclusion conditions) (Fig. 3.4, Fig. B.3; Tables 3.5 and 3.6). Under exclusion conditions, bone S content decreased, but there was less compositional variation compared to colonization conditions where bone was in direct contact with sediments and indigenous microbes (Table 3.5). Specifically, bones under colonization treatment had lower

Na (0.10 wt. % depleted) and higher F (0.05 wt. % enriched) after 7 days. Additionally in colonization treatments, Mn and Fe, elements below detection or absent in unaltered bones or bones recovered from exclusionary mesocosms, exhibited high standard deviations after 7 days, indicating HAP lattice chemical heterogeneity. From the variable pH experiments, collagen release was evident within 24 hours across all pH ranges (Fig. 3.5). The presence of collagen in solution persisted up to one month. Based on FTIR ratios (Table 3.6), bones from both experimental conditions exhibited increased crystal length, from 41.5 nm in unaltered bone to ~ 43 nm in experimentally treated samples within 7 days. There were also other changes to the carbonate content, with a decrease in carbonate/phosphate ratio, decrease in BPI and API in the colonization exclusion experiments, but an increase in BPI and API for the colonization treatments. Thus, in addition to the S, Na, Fe and Mn changes, bone also lost P and incorporated carbonate after only one week when in direct contact with sediments and indigenous microbes.

After one month, there was continued loss of Na in both experiments, from 0.76 wt. % in unaltered bone to 0.43 and 0.35 wt. % in exclusion and colonization treatments, respectively. Compared to unaltered bone, experimental bone had a slight loss of Ca, as well as P decrease. There was a reduction in the organic content of bone after one month, from ~38 wt. % in unaltered bone to ~ 34 wt. % in both experimental treatments (Table. 3.6). Chemical changes to Ca and P observed with EMP analyses were also observed with FTIR. Ca and P chemical alterations resulted in continued opposite trends for the carbonate/phosphate ratio and BPI for the two experimental treatments.

Ratios used to characterize bone composition from FTIR analysis (Table 3.7) were evaluated according to PCA to assess the role of pH and duration of exposure to an aqueous solution on altering bone composition (Fig. 3.6). PC1 accounted for 75.96 % of observed

variations in bone structure, including all measures of organic and carbonate content. PC2 accounted for 11.3 % of structural variability, and was explained largely by crystal length. Structurally, bones exposed to variable pH conditions exhibited the greatest variability in composition after 7 days (Fig. 3.6A). After 30 days, bones from all pH experiments converged upon a similar structure, which correlated to lower carbonate/phosphate ratios caused by either carbonate loss, increased phosphate, or decreased organic content (Fig. 3.6A). Grouping samples as a function of pH treatment indicated that bones exposed to pH 8 exhibited little change in structure over one month of treatment, although bones under pH 9 and pH 10 treatments underwent more pronounced structural changes.

Long-term changes to burial sediment geochemistry and microbial diversity

At the RWR burial site, soil physical and chemical parameters were evaluated. In general, soil organic content decreased with depth (Fig. B.4C; $R^2 = 0.134$) and inorganic C increased with depth (Fig. B.4A, $R^2 = 0.032$). Soil pH (average = 6.8) did not vary as a function of depth (Fig. B.4D). Water content increased with depth, from 15.8 wt. % at the surface to ~ 48.0 wt. % at 37.5 cm depth (Fig. B.4B). PSI provided information about the capacity of the wetland sediments to sorb phosphate. From samples examined at a single time point along a depth profile, sediments at depth had a greater capacity to sorb phosphate from solution (Table 3.4). Soil mineralogy corresponding to samples with the highest PSI consisted of quartz, magnesioferrite, and a sodium-bearing silicate mineral (Table 3.2). Sediment mineralogy collected at a different sampling time, but from a similar depth, was dominated (up to 96%) by phyllosilicates (paragonite and amesite) with 4-9 % quartz.

Changes in microbial community composition were also evaluated from the long-term (i.e. months to years) burial experiment. The hypothesis was that microbial activity influences bone mineral stabilities through both direct (i.e. colonization) and indirect processes (e.g., Pfretzschner et al., 2004; Daniel and Chin, 2010). Changes to microbial communities were expected over the course of carcass decomposition as the availability of nutrients changed, particularly collagen, which is known to readily degrade in the presence of microorganisms in environmental systems (White and Hannus, 1983; Child, 1995; Leikina et al., 2002). Over the course of three years at the burial site, sediment communities varied as a function of depth below the sediment surface (Fig. 3.7). Overall, Proteobacteria (i.e. *Gammaproteobacteria, Betaproteobacteria, Deltaproteobacteria,* and *Alphaproteobacteria*), Acidobacteria, Actinobacteria, Chloroflexi, Firmicutes, and unclassified phyla dominated the communities. In 2010, a significant ($F = 3.39$, $p = 0.02$) difference was observed in samples obtained at 37.5 cm and 15 cm depth, while in all other samples, bacterial community membership was not significantly different (Table B.4). No statistically significant differences existed in community composition in samples collected in 2012 along the depth transect from 7.5 to 37.5 cm. Sediment bacterial community compositions were significantly different in 2013 in pair-wise comparisons at all sampling depths, except for communities at 7.5 and 37.5 cm depths (Table B.4).

In December 2010, eight months after burial, there was a shift in community composition at 30 cm from pre-burial compositions, which were dominated by *Deltaproteobacteria*, to increased representation of *Alphaproteobacteria* and *Gammaproteobacteria* (Fig. 3.7). Bacterial community composition below the burial closely resembled pre-burial phylum level abundances. Two years after burial, there were no significant changes in community composition from 2010 to 2012 at all sampling depths (Table B.5). Firmicutes comprised a dominant proportion of the

community composition in pre-burial (i.e. surface), two-, and three-year post-burial sediments collected 7.5 cm below the surface. At 30 cm depth, the same level that the alligators were buried at, pre-burial to post-burial bacterial communities had increased proportions of Bacteroidetes, from representing 0.5 % of the community to 14 % of total community abundance, with significant ($F = 3.34$, $p = 0.02$) differences in community membership were observed between 2012 and 2013. Bacterial community composition at 15 cm was significantly different in 2013 compared to communities observed at an equivalent depth in 2010 ($F = 11.98$, $p < 0.01$) and 2012 ($F = 12.17$, $p < 0.01$) (Table B.5).

Overall diversity based on the Shannon Index did not exhibit a predictable pattern with depth (Fig. B.2). Some years, the diversity was greatest in shallower (7.5 cm) sediments (i.e. winter 2010), while at other times (i.e. 2012), diversity broadly increased with depth. By evaluating Shannon Index values for diversity in the context of soil physical and chemical parameters, samples with the highest diversity also corresponded to the lowest organic and inorganic C for each time-series depth transect (Fig. B.6). Applying multivariate statistical analyses to integrate sediment diversity using Shannon Index values and organic geochemical parameters revealed that sediments partitioned as a function of year (Fig. 3.8). Sediment samples in 2010 plotted more closely together, and positively correlated with diversity and negatively correlated with inorganic C content. Sediment samples collected in 2012 and 2013 exhibited an overall shift towards increased inorganic C content, water content, and soil pH.

Long-term changes to buried bone over months to years

After one year of burial, bone exhibited chemical (Fig. 3.9; Table 3.5) and structural (Fig. 3.10) changes, in addition to displaying evidence for morphological alteration to bone surfaces in

the form of pits and tube-like structures (Fig. 3.11). EMP spot analyses from bones collected over three years of burial show non-linear increases in S, Mn, Fe, Ca, and F content compared to unaltered, fresh bone (Table 3.5). There was also a loss of Na and Cl in buried bones compared to unaltered bones. However, element maps suggested that major and trace element chemistry changes, except P, were non-uniform through the bone cortex (Fig. 3.9). This resulted in distinctly zoned regions in the bone after as little as one year of burial. Changes to P content and distribution in the HAP lattice were evident after three years of burial, but difficult to distinguish in samples after one and two years of burial (Appendix Fig. B.4). For bones buried for three years, organic matter content decreased, as did the amide/phosphate ratio (Table 3.6). Additionally, mean crystal length and crystallinity, which were visualized from a narrowing and increasing height of the primary phosphate peak at 1035 cm^{-1} wavenumber, increased (Fig. 3.10). Increased spectral variability between 400 and 500 cm^{-1} indicated increased association of metals (e.g., Fe, Mn), either structurally within the HAP lattice or as surface coatings for bones buried for three years.

Structural information from FTIR spectroscopy, and chemical compositions obtained with EMP analyses, were used for statistical analyses using PCA for experimentally treated (indirect and direct microbial colonization mesocosms) and buried bones after three years. Samples of similar treatment clustered together (Fig. 3.12). Bones experimentally treated for one week, under indirect treatment, were closer to unaltered bone, while bones exposed to direct microbial colonization plot closely with both experimentally treated bones after one month based on major and trace element chemistry (Fig. 3.12A) and structure (Fig. 3.12B). Buried bones are separate from bones treated for one week and one month and positively correlated with PC1, which accounted for 58.43 % of observed variation, and corresponding to increased trace

element concentrations (e.g., F, Sr, Mn, Fe, S). When considering structural variability in experimentally treated bones, samples clustered according to experimental treatment duration (Fig. 3.12B). PC1, which included changes to organic and carbonate content, accounted for 59.96 % of observed variation. As observed based on chemistry, buried bones were more similar structurally than to the other experimentally treated bones from the mesocosms.

Discussion

Chemical changes to bone during early diagenesis as a function of microbial interactions

EMP-based element maps suggest that the association with Fe is through structural incorporation of Fe into the apatite lattice from surrounding pore fluids occurred at the expense of some of the Ca, forming Ca-Fe-phosphate phases preferentially along bone margins (Fig. 3.9). Bone margins were in direct contact with sediment and pore fluids, and these regions would be expected to exhibit the earliest signs of chemical diagenesis following burial. Trace element incorporation in cortical bone as a diffusive front, extending from the outer margin to the inner cortex, is commonly observed in fossilized bone (e.g., Koenig et al., 2009), particularly with respect to the uptake of rare earth elements and uranium. Diffusive uptake of Fe at the expense of Ca in bone after as little as one year highlights the critical role of early diagenetic alteration on influencing subsequent trace element uptake. Early ion exchanges along bone margins may serve as a mechanism to retard ion exchange deeper into the cortex by reducing pore spaces through recrystallization. These early changes may help to explain the complex movement of ions into bone diagenesis (e.g., Koenig et al., 2009; Kohn and Moses, 2012).

Changes to the apatite lattice from the experiments in this study occurred much earlier than has been reported in the literature. Mesocosm experiments confirmed prior studies that

apatite mineralogy is sensitive to pH, which can result in diagenetic changes (e.g., Berna et al., 2004) and may result from protonation of OH^-, which would open the lattice and enhance replacement with F^- to form thermodynamically more stable FAP. The open lattice could also permit alteration to the carbonate type A associated with Ca site II, which is the site bound to OH^- in the HAP lattice. The ratio of type B to type A carbonate (BAI) either had decreased type B and/or increased type A after three years of burial. Type A carbonate is associated with the Ca site II. As such, if carbonate is incorporated into this location, then lattice instability at the Ca(II) site might also serve as a mechanism to allow other metals to substitute for Ca^{2+}. FTIR results also indicated that changes occurred primarily at the Ca(II) site (Table 3.6). These early diagenetic changes in bone on time-scales as short as days, based on the release of collagen and lipids, to years based on significant chemical and structural changes, are likely critical for determining the long-term fate of bone in a natural system.

Microbial contributions to bone diagenesis

The observation of pits, tunnels, or tube-like structures in archaeological and fossil bone is widely attributed to the activity of microorganisms (e.g., "bacteria" and fungi; Child, 1995; Jans et al., 2004; Jans, 2008; Daniel and Chin, 2010). After one year of burial, putative indications of bioerosion in the form of pits and tunnels occurred along the bone margin (Fig. 3.9). Additional surface modification was observed in samples recovered after two and three years of burial. No bioerosion or dissolution features were observed in direct or indirect colonization mesocosm experiments after one week or one month under backscatter imaging of resin-embedded samples. This suggests that dissolution features can be attributed to bone exposure to microbial communities and/or aggressive geochemical conditions for greater than

one month. After one week of exposure to wetland waters under conditions of indirect colonization, limited changes to bone chemistry and structure were observed. However, after one month, bones from both indirect and direct colonization treatments demonstrated altered geochemistry, suggesting that microorganism may not only act as destructive agents (e.g., Child, 1995; Jans et al., 2004), but may also facilitate preservation under specific conditions of direct colonization (e.g., Daniel and Chin, 2010).

Influence of site geochemistry on diagenesis

At RWR, vertisols have a high cation and anion exchange capacity (Midkiff and Roy, 1995). Measurement of the phosphate sorption capacity of RWR soils indicate a high ability for [P] sorption onto clay mineral surfaces, onto metal oxides in the sediment, or onto organic matter (Table 3.3) (e.g., Darke and Walbridge, 2000; Harrell and Wang, 2006). Combining thermodynamic predictions of HAP solubility with the high sorption capacity of wetland sediments for [P], bone preservation in this depositional system is not expected. In a shallow burial system consisting of low porosity and low permeability clay-rich sediments, the system would be expected to reach equilibrium with respect to HAP as dissolution reached a critical threshold. However, the high capacity for ionic sorption of RWR clays, up to 112 mg of [P]/100 g of sediment, may act to maintain undersaturation for a protracted period of time. Rapid and early dissolution of bone by both biotic and abiotic processes would release collagen and [P], resulting in a positive feedback loop where continued dissolution exposes more interior portions of bone to interactions with persistently undersaturated fluids. RWR sediment geochemistry and sorption capacity variability suggest that preservation potential may not only be controlled by overall site conditions but also by very specific (micro)environments on cm-scales. The

geochemical and microbial community heterogeneities observed laterally, vertically, and temporally at RWR emphasize the difficulties inherent in sampling a single system or site. Additionally, site physical and chemical variability in a modern system may help to explain the preservation of geochemically variable bones from a single site in the geologic past (e.g., Trueman et al., 2006).

Conclusions

Once introduced into any environmental system, bone must undergo chemical changes early to achieve a more stable composition. Alternately, the crystallites must be shielded from direct contact with undersaturated fluids through the precipitation of secondary phases on bone surfaces or possibly through the formation of microbial biofilms. Chemical and structural alteration to bone buried in wetland sediments occurred on time-scales ranging from days to years, transforming the original HAP lattice. Within one month, under conditions enabling direct colonization by microbial cells and treatments preventing colonization, alteration to the HAP lattice structure and chemistry were observed. After as little as one year, the incorporation of trace elements, particularly Fe and Mn in buried bones, indicates that ionic substitutions under shallow burial conditions occur early during diagenesis. Alteration of the lattice structure by ionic substitutions transformed a mineral phase predicted to be undersaturated with respect to solution geochemistry, namely HAP, to a new Ca-Fe-PO_4 apatite phase or FAP, thereby enhancing preservation potential.

The role of microorganisms in bone diagenesis may not always be destructive as previously viewed (e.g., Child, 1995; Jans et al., 2004; Jans, 2008), but may also provide stability to the bone that enhances preservation potential by shielding crystallites to bulk solution

chemistry via biofilm development and by establishing distinct microenvironments surrounding mineral surfaces. The dynamic interactions between microorganisms and bone, both the organic and mineral components, are vastly understudied, and results in ambiguity as to the exact nature of biotic interactions with bone. Additionally, the relationship between biology and bone will likely change under variable geochemical conditions or nutrient limitation, although this has yet to be tested. Depositional site-specific conditions, including redox, pH, dissolved ions, and sediment mineralogy, combined with indigenous soil microbial communities, are integral to the alteration of bone. Early diagenesis, and the transformations of bone following introduction into a depositional system, are still vastly understudied, yet hold the potential to be critical for establishing long-term preservation (or destruction) potential of bone over geologic time.

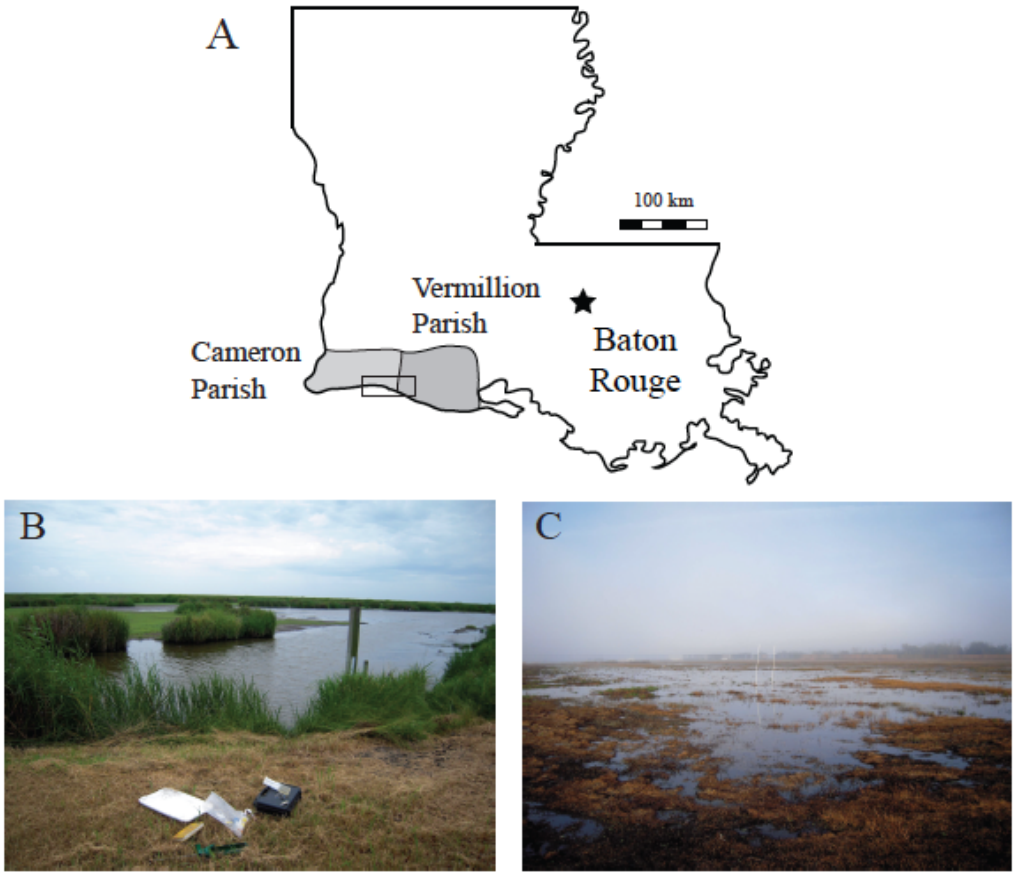

Fig. 3.1: Location of the Rockefeller Wildlife Refuge in southwestern Louisiana. (A) RWR is located in Cameron and Vermillion parishes along the Gulf of Mexico. (B) View of the wetland at one sampling location (Spring 2013). This site contained a dense population of blue crabs, one of the primary food sources for juvenile alligators, and several alligators were observed at the site during sampling. (C) Parts of the wetland are seasonally burned under controlled conditions in the winter and spring to promote vegetation growth. Several sampling locations on the refuge experienced seasonal flooding due to meteoric input. One sampling location (adjacent to the white poles) was saturated during all sampling times, sometimes more than others.

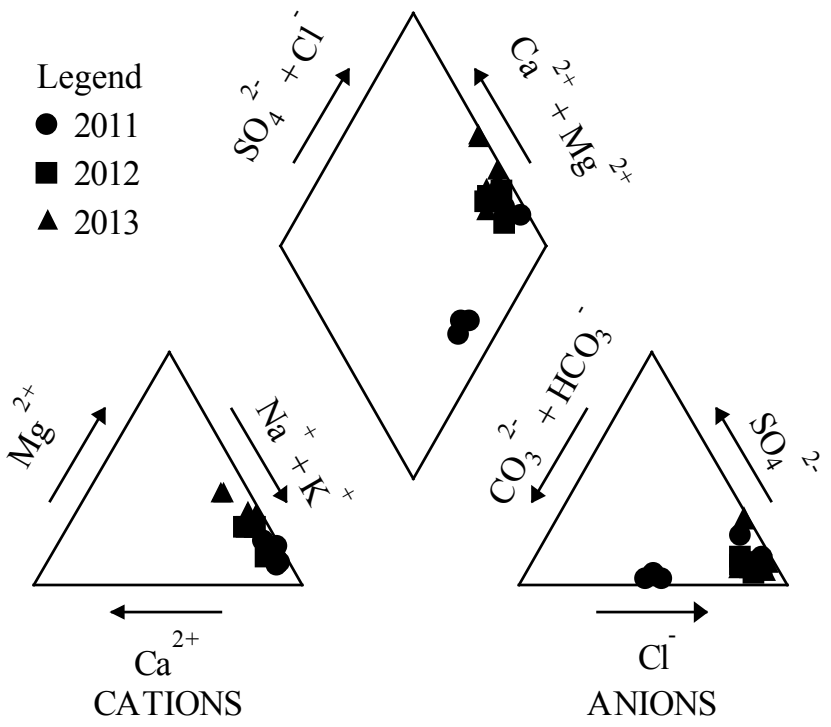

Fig. 3.2: Piper diagram of surface and subsurface water geochemistry from the Rockefeller Wildlife Refuge. In general, waters are Na-K-Cl type, with some samples from 2011 exhibiting a slight increase in HCO_3^-.

Fig. 3.3: Predicted saturation states for apatite minerals under variable pH, temperature, and total [P] at RWR. Under acidic and low [P] conditions typical of RWR, waters are predicted to be undersaturated with respect to HAP (hydroxyapatite) under a range of temperatures. As the [P] increases, stability fields shift from undersaturation towards equilibrium with respect to HAP. In contrast, under a range of temperatures, pH conditions, and [P], carbonated fluorapatite is thermodynamically stable, suggesting mineral stability. Fluorapatite is unstable under low [P] and acidic conditions. However, as [P] increases, the stability field shifts towards saturation.

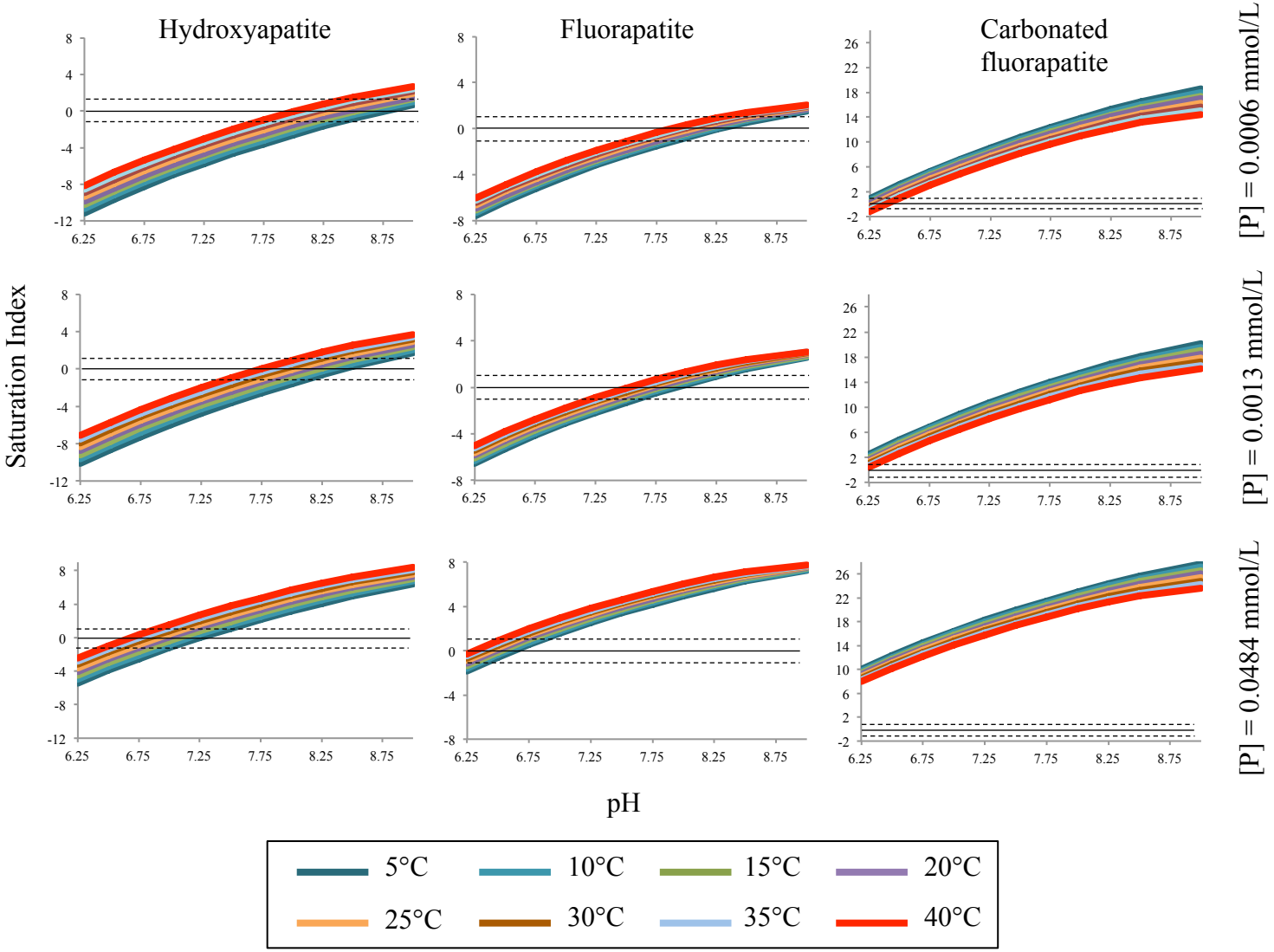
Hydroxyapatite
Fluorapatite
Carbonated fluorapatite
[P] = 0.0006 mmol/L
[P] = 0.0013 mmol/L
[P] = 0.0484 mmol/L
Saturation Index
pH
5°C
10°C
15°C
20°C
25°C
30°C
35°C
40°C

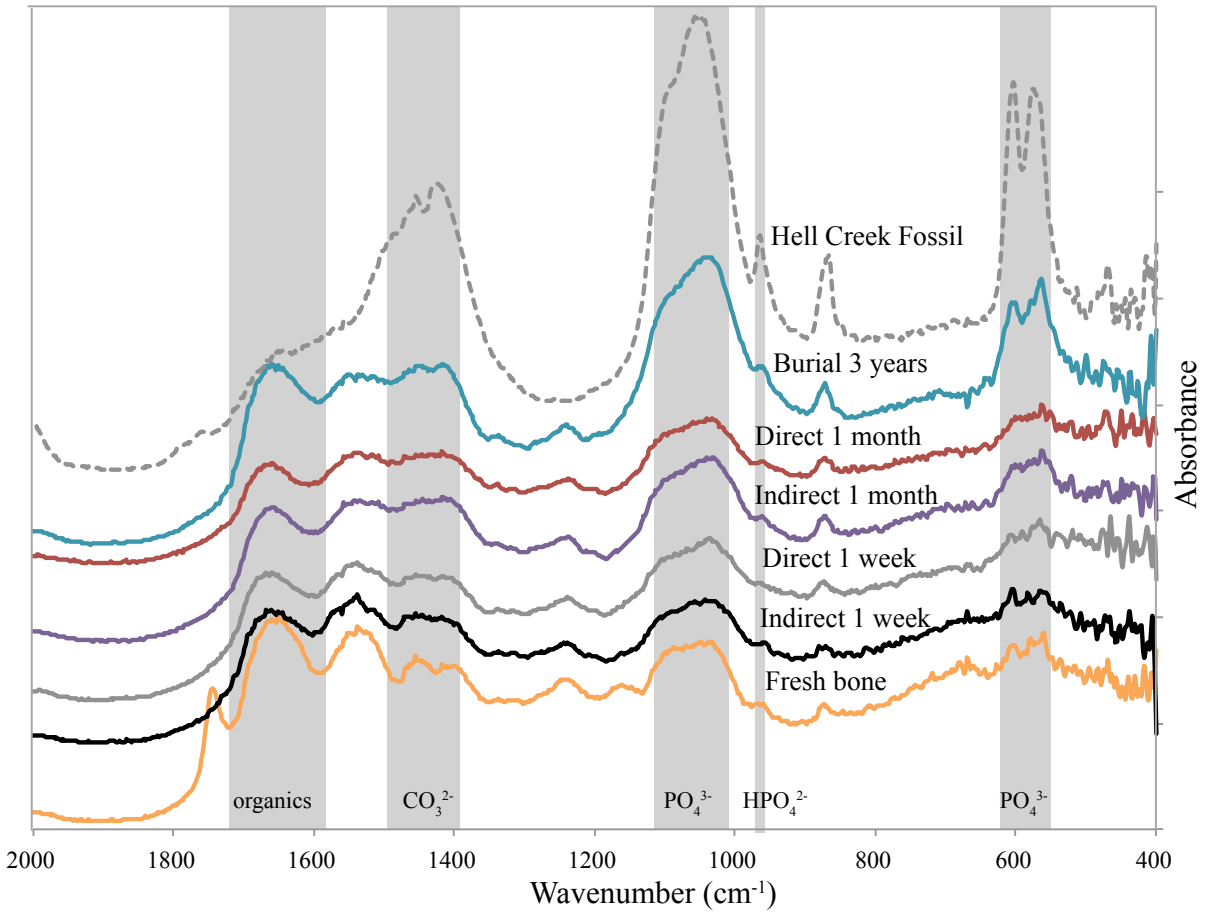

Fig. 3.4: FTIR spectra of indirect and direct colonization of bones, with peak characteristics highlighted in gray. Representative modern and fossil bones are also included to demonstrate the changes that occur during early diagenesis as bone crystallinity increases.

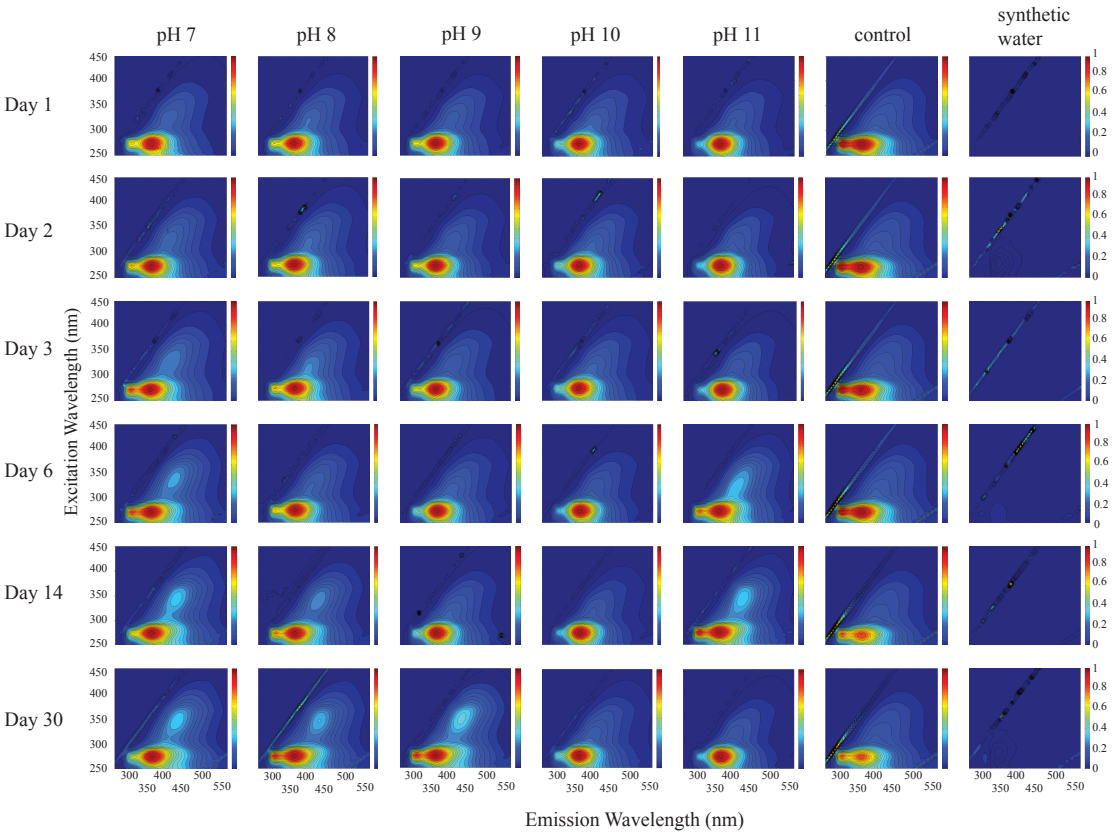

Fig. 3.5: Excitation and emission matrices generated using fluorescence. The release of collagen is evident across all pH ranges within one day as the high intensity, red peak at 350 nm. Control refers to bone in synthetic wetland water without the addition of NaOH or HCl to adjust pH.

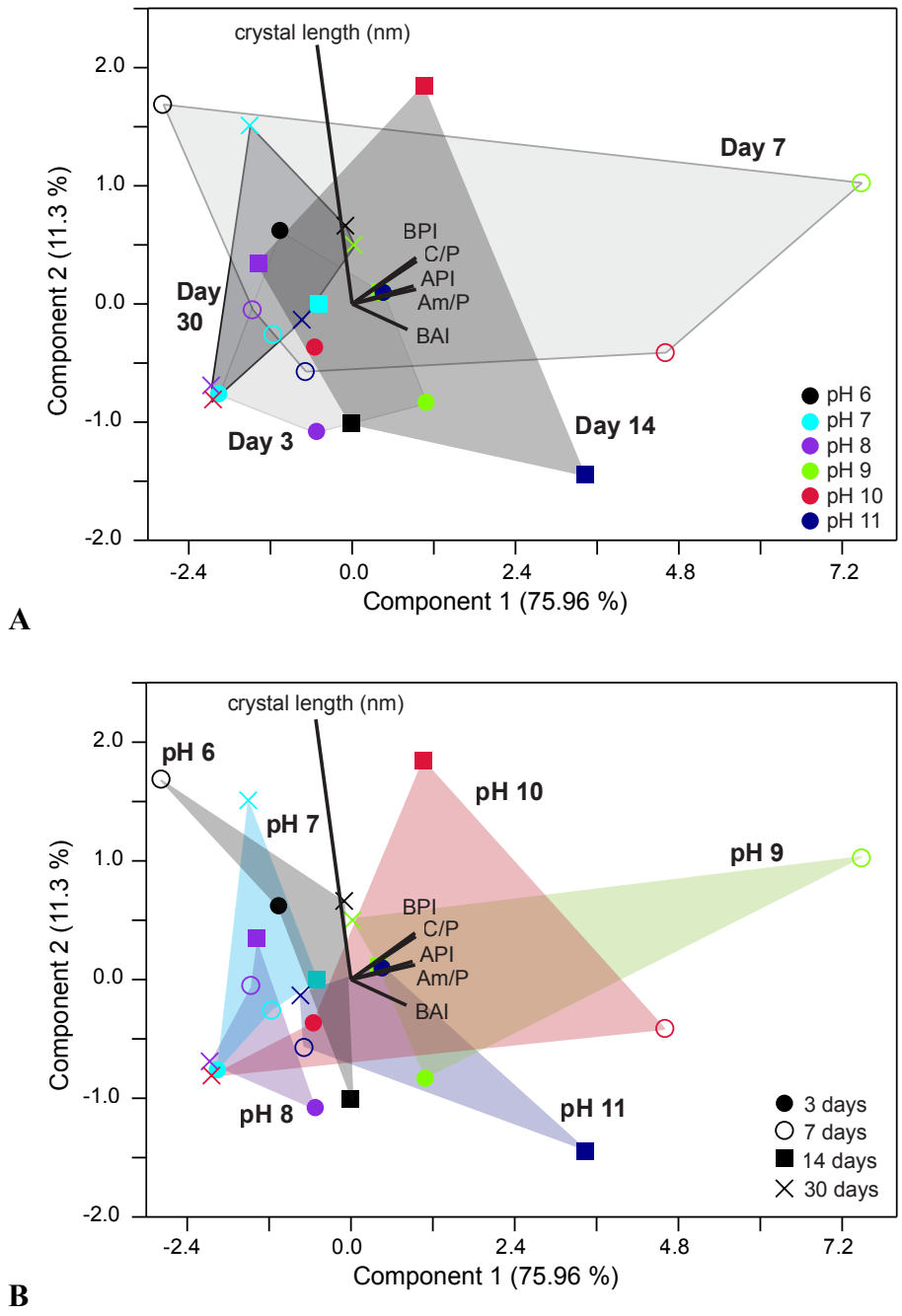

Fig. 3.6: Principle components analysis of FTIR ratios from bones treated under different pH conditions from 1 to 30 days. (A) Samples are grouped according to duration of exposure to variable pH solutions (indicated by different colored symbols). (B) Bones are grouped from each treatment pH, highlighting the structural variability observed under variable solution pH.

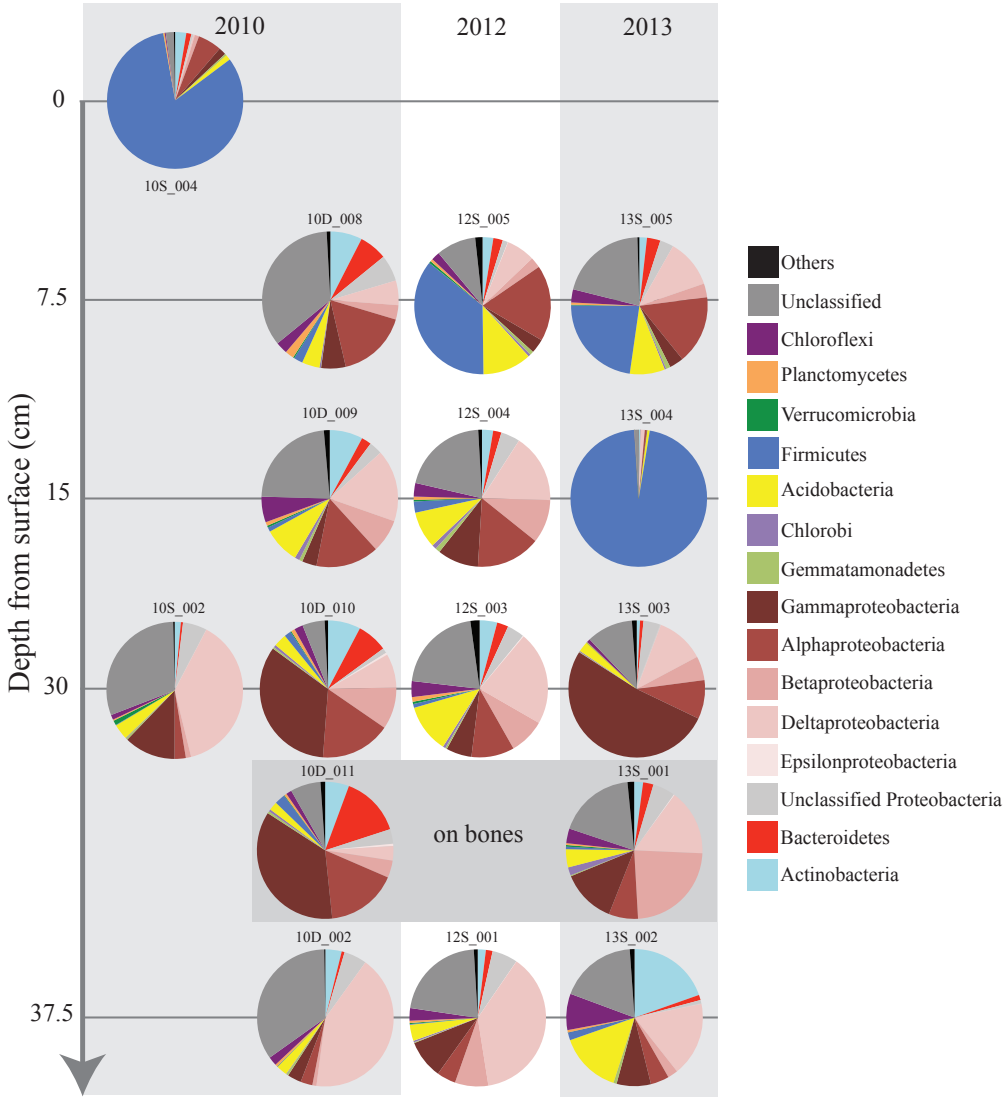

Fig. 3.7: Bacterial phylum-level abundances plotted as a function of depth and time. Pre-burial samples were collected in April 2010, and the first post-burial sediment collection occurred in December 2010. Bacterial abundances associated with bones recovered from the site were collected between 30 and 37.5 cm depth. Vertical axis is not to scale.

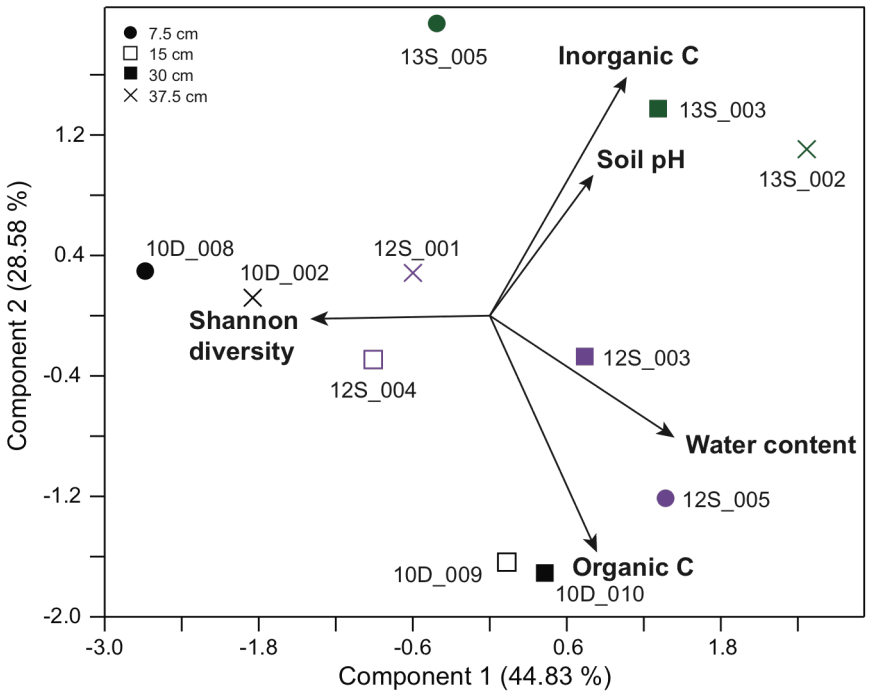

Fig. 3.8: Principal components analysis of wetland sediment bacterial diversity and organic geochemsitry as a function of depth and year along vertical transects above the burial. Samples are labelled to sample year, sample season (D = winter, S = spring), and sample number, corresponding spatially with Fig. 3.7 and Table 3.3. Symbols refer to different sampling depths and different colors reflect sampling years.

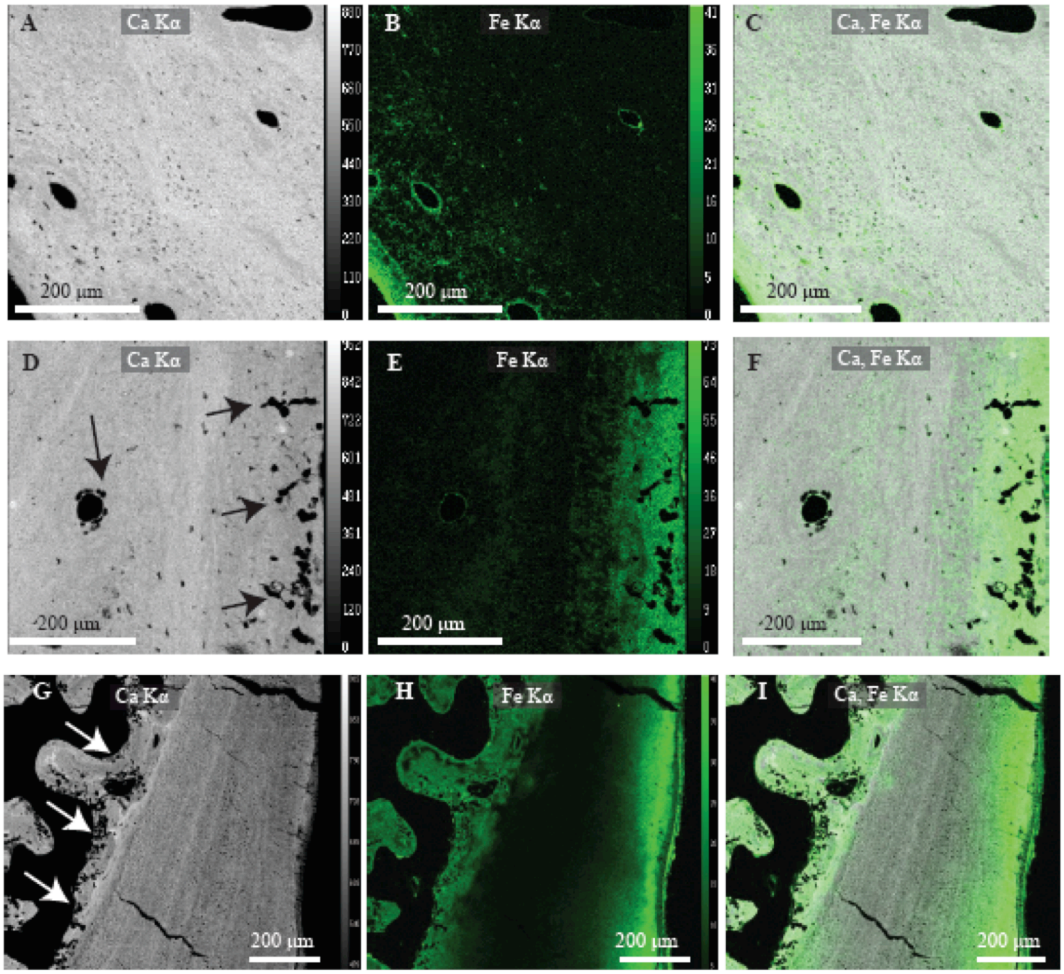

Fig. 3.9: False colored EMP element maps of alligator cortical and trabecular bone over the course of three years of burial. Putative indicators of bioerosion (pits and tunnels) are prominent along the trabecular margin (denoted by arrows). (A-C) After one year of burial, Ca exhibits a narrow zone of depletion (darker grey) along the outermost margin of the cortical bone (bottom left of image). (B) Along the outer cortical margin and lining vascular canals, there is Fe enrichment with the zone of enrichment extending ~ 50 µm from the outer to the inner cortex. (C) Mixed element maps highlight the formation of heterogeneous Fe-Ca-phosphate phases. (D-F) After two years of burial, there is continued Ca depletion extending ~ 150 µm into the cortex accompanied by Fe enriched. (G-I) Three years after burial there is continued loss of Ca accompanied by increased concentrations of Fe. (I) Enrichment of Fe and loss of Ca are evident both along the cortical margin (right side of image) as well as along the trabeculae (left side of image).

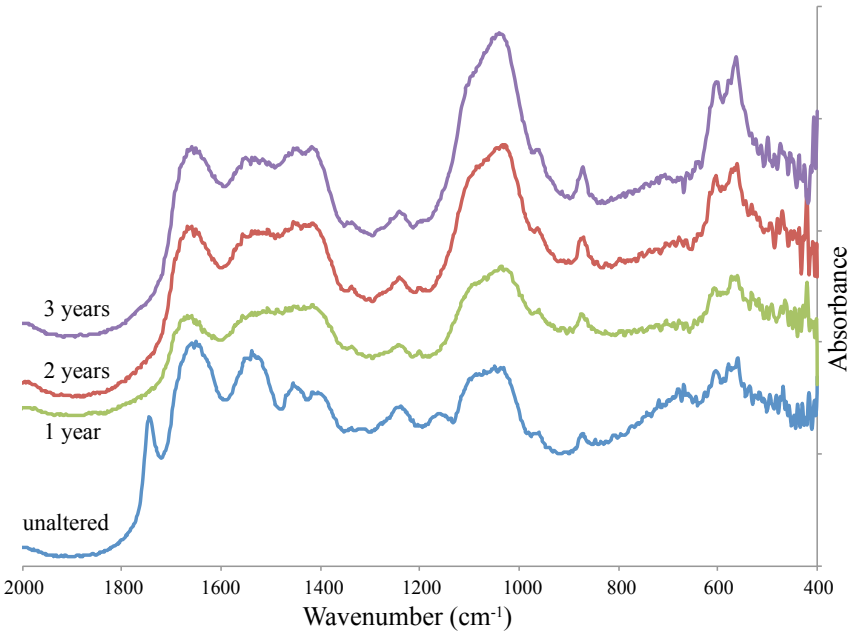

Fig. 3.10: FTIR spectra of bone after three years of burial. Key features to note include increased peak height and narrowing of the main phosphate peak (1035 cm^{-1}), and a loss of organics including amide (~1540 cm^{-1}). Additionally, increased spectral variability between 400 and 500 cm^{-1} indicates increased association of metals (e.g., Fe, Mn), either structurally within the HAP lattice or as surface coatings.

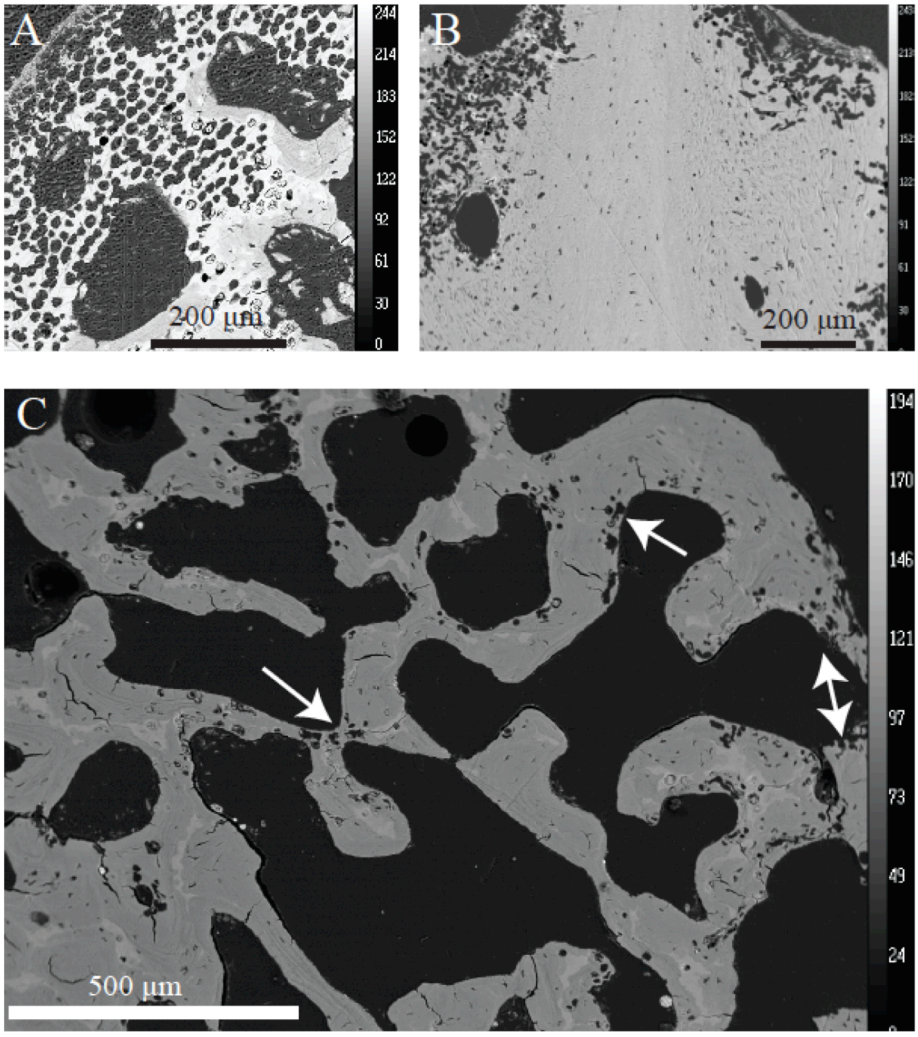

Fig. 3.11: Backscatter images of putative indications of bioerosion in buried bones. (A) After one year, extensive pitting and etching is evident along the outer margin of a centrum, extending ~500 µm into the bone. (B) Additional surface modifications are also observed after two years of burial. (C) Alteration of bone morphology is constrained largely to trabecular bone after three years of burial (denoted by arrows).

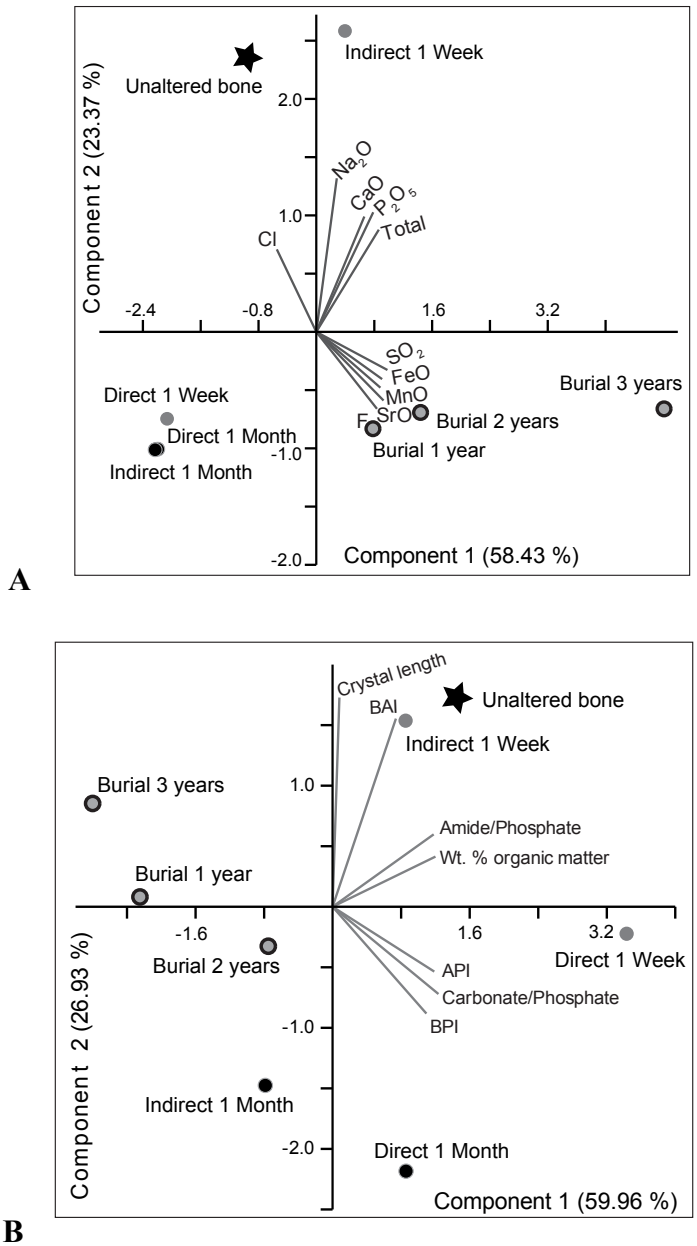

Fig. 3.12: Principal component analysis of experimentally treated bone chemistry and structure. (A) Principal component (PC)1 of changes in bone chemistry was explained by variations in trace element concentrations, including F, Sr, Fe, Mn, and S and accounted for 58.43 % of observed variations. PC2 included the two major elements found in bone, Ca and P as well as Na, a dominant cation in fresh bone. (B) Structural differences in experimentally treated bones were explained by PC1 (59.96 %), which included alteration to organics and carbonate incorporation. PC2 explained 26.93 % of observed variations and included structural alteration to crystal length and carbonate (BAI).

Table 3.1: Water geochemistry of the Rockefeller Wildlife Refuge (2011-2013) from surface, subsurface, and canal waters. BDL = below detection limits; NM = not measured.

					mg/L	mmol/L										μmol/L	
Source Type	Sample Name	Conductivity (mS)	pH	Temp (°C)	TDS	Na^+	K^+	NH^{4+}	Ca^{2+}	Mg^{2+}	Fe^{2+}	Cl^-	HCO_3^-	F^-	SO_4^{2-}	PO_4^{3-}	NO_3^-
Canal	SKM_11S_001	31.8	7.82	25.2	21306	506.22	BDL	47.89	4.95	5.31	NM	593.92	2.54	BDL	36.80	BDL	9.25
Shallow pond	SKM_11S_002	30.9	8.09	25.1	20703	432.45	BDL	39.71	4.39	4.32	NM	499.49	2.93	BDL	28.88	BDL	BDL
Shallow pond	SKM_11S_003	16.6	8.75	27.8	11122	485.00	10.60	BDL	10.70	55.10	NM	566.00	2.40	BDL	29.30	BDL	0.01
Shallow pond	SKM_11S_004	4.86	8.93	27.4	3256.2	42.61	0.36	BDL	1.00	2.07	NM	42.78	6.18	BDL	0.82	BDL	0.51
Shallow pond	SKM_11S_005	4.85	8.96	28.4	3249.5	19.10	0.36	BDL	1.05	1.19	NM	5.67	17.80	0.089	0	BDL	32.00
Shallow pond	SKM_11S_007	5.84	9.11	32	3912.8	47.90	0.15	BDL	0.68	0.79	NM	17.40	14.80	0.356	5.20	BDL	7800.00
Subsurface	SKM_11S_008	13.19	6.44	23.4	8837.3	194.00	4.91	6.16	0.04	0.02	NM	53.90	138.00	6.28	0.15	BDL	11.63
Surface	SKC_12S_001	2.76	7	27.6	1849.2	17.63	0.43	BDL	1.17	3.31	NM	18.21	1.83	BDL	0.99	BDL	BDL
Subsurface	SKC_12S_002	3.03	6.5	25.5	2030.1	19.81	0.49	BDL	1.22	3.71	NM	23.84	3.45	BDL	1.71	BDL	BDL
Open canal	SKC_12S_003	1.87	7.1	25.9	1252.9	12.84	0.38	BDL	0.42	2.32	NM	13.11	0.85	BDL	0.60	BDL	2.58
Shallow pond	SKC_12S_004	2.05	7.2	25.8	1373.5	13.78	0.42	BDL	0.50	2.50	NM	14.49	1.41	BDL	0.44	BDL	0.98
Shallow pond	SKC_12S_005	1.426	8.2	26.5	955.42	BDL	2.26	BDL	2.78	4.21	NM	116.07	2.85	BDL	3.61	BDL	1.39
Shallow pond	SKC_12S_006	8.42	8.6	26	5641.4	58.49	1.31	BDL	2.89	4.28	NM	66.06	2.65	BDL	3.88	BDL	0.39
Surface	SKC_12S_008	2.4	6.8	24.4	1608	16.04	0.46	BDL	1.12	1.51	NM	33.72	0.00	BDL	1.92	BDL	BDL
Canal	SKR_13S_001	4.69	7.81	12.2	3142.3	25.19	1.21	0.16	1.06	6.14	0.36	70.11	2.01	BDL	3.03	2.21	1.61
Shallow pond	SKR_13S_002	3.8	8.9	14.2	2546	16.02	0.99	0.01	0.63	3.03	0.00	49.35	2.37	BDL	1.80	3.95	1.61
Surface	SKR_13S_003	4.178	7.67	18.2	2799.26	16.31	0.81	0.10	0.59	3.09	0.03	43.75	2.43	BDL	2.14	8.74	BDL
Subsurface	SKR_13S_004	9.19	6.08	16	6157.3	36.61	0.69	0.38	3.70	14.12	0.29	115.13	4.25	BDL	22.79	27.59	0.48
Subsurface	SKR_13S_005	9.19	6.06	14.5	6157.3	35.54	0.75	0.38	3.59	13.81	0.29	88.54	3.87	BDL	16.79	27.59	0.48
"crab shack" (shallow pond)	SKR_13S_007	9.3	8.49	21.1	6231	41.97	1.63	0.26	1.05	9.28	0.10	123.29	3.12	BDL	2.89	31.69	19.84
Surface (ditch)	SKR_13S_008	1.44	7.85	19.6	964.8	5.55	0.42	0.01	0.36	1.15	0.00	12.35	1.15	BDL	0.48	3.95	1.61

Table 3.2: X-ray diffraction data for selected RWR wetland sediments.

Sample	Treatment Temperature (°C)	Mineralogy	Formula	Content (%)
12S_001	20	Quartz	SiO_2	50.06
		Muscovite (2M1)	$Al_2H_3NaO_{12}Si_2$	47.52
		Vermiculite (2M)	$Al_{1.3}H_{9.44}Mg_{3.41}O_{15.72}Si_{2.86}$	2.42
12S_001	105	Quartz	SiO_2	100
		Paragonite (2M1)	$Al_3H_2NaO_{12}Si_3$	0.00
13S_012	20	Amesite (6R2)	$Al_{3.7}H_8Mg_{4.15}O_{18}Si_{2.15}$	96.00
		Quartz	SiO_2	4.29
13S_012	105	Muscovite (2M1)	$Al_{3.7}F_{0.8}Fe_{0.04}H_{1.2}K_{0.984}Mg_{0.75}O_{11.2}Si_{3.81}$	91.00
		Quartz	SiO_2	9.30
13S_002	20	Quartz	SiO_2	55.51
		Sodium-bearing silicate	$Al_3NaO_{11}Si_3$	31.36
		Magnesioferrite	Fe_2MgO_4	15.12

Table 3.3: Wetland sediment water content, organic C and inorganic C content. Water content (24 hours at 105°C), organic carbon (3 hours at 475°C), and inorganic carbon (12 hours at 800°C) values based on samples processed in triplicate by loss on ignition (method based on Wright et al., 2008; Wang et al., 2011; Wang et al., 2012), except samples denoted by "*", which were processed in duplicate. Samples without standard deviations are based on single analyses due to limited sediments. Measurements of soil pH based on a slurry of 2:1 water to sediment using deionized water. Distance from burial refers to sampling locations along linear transects from a buried alligator at the sampling location (buried April, 2010).

Sample	Distance from burial (cm)	Depth from surface (cm)	Munsell (10YR)	Water content (%)		Organic C (g/kg)		Inorganic C (g/kg)		Soil pH
10S_003	0	0	3/1	22.26	±1.69*	199.30	±11.75*	5.20	±0.18*	7.03
10S_004	0	0	3/1	15.83	±1.52	95.26	±25.17	6.38	±0.24	5.42
10S_002	0	30	3/1	39.56	±0.14	67.24	±2.00	6.58	±0.11	6.58
10S_001	0	37.5	3/1	42.93	±0.30	57.14	±1.47	5.87	±0.10	6.78
10D_008	0	7.5	2/2	35.89		75.22		5.84		6.76
10D_009	0	15	2/1	49.84	±0.59*	158.50	±0.24*	6.16	±0.11*	6.58
10D_010	0	30	2/1	49.92	±1.90	148.74	±10.52	6.12	±0.18	6.32
10D_012	30	15	2/1	45.19	±0.37*	137.46	±0.06*	7.32	±0.09*	6.48
10D_013	30	30	4/1	43.23	±0.75	69.14	±1.54	6.52	±0.24	6.75
10D_004	51	6	4/1	35.20		64.03		5.85		6.19
10D_005	51	15	2/1	46.40	±0.07*	149.20	±11.78*	6.31	±0.30*	6.02
10D_006	51	30	4/1	40.35		63.28		6.49		6.64
10D_014	60	15	2/1	52.49	±1.71*	198.69	±14.23*	6.75	±0.04*	6.47
10D_015	60	30	3/2	44.15	±0.27*	69.35	±2.92*	7.59	±1.10*	6.26
10D_007	102	30	2/1	45.60		117.41		6.27		
10D_001	366	15	2/2	43.75	±1.78*	78.68	±64.69*	17.37	±16.28*	6.75
10D_003	366	37.5	3/1	40.86		55.62		6.29		6.4
12S_005	0	7.5	2/1	55.02		162.77		6.66		7.23
12S_004	0	15	4/1	47.66	±1.26	82.04	±14.44	6.19	±0.12	6.68
12S_003	0	30	2/2	52.32	±1.26	121.54	±2.42	6.50	±0.23	7.57
12S_001	0	37.5	4/3	50.01	±0.23	58.10	±3.92	6.61	±0.08	6.85
12S_002	0	60	3/2	55.51	±1.40	115.37	±9.75	6.84	±0.15	6.58
12S_015	15	7.5	3/1	41.20	±0.34	66.23	±6.56	7.26	±0.48	7.12
12S_016	15	15	2/1	48.60	±1.12	129.93	±11.05	7.63	±1.02	6.55
12S_017	15	30	4/1	46.75	±1.09	54.54	±0.57	7.90	±0.38	6.99
12S_012	30	7.5	3/1	43.80	±1.18	98.58	±8.48	6.47	±0.22	6.86
12S_013	30	15	2/1	46.68	±0.19	127.31	±3.97	6.75	±0.05	6.79
12S_014	30	30	4/1	44.76	±0.61	58.27	±3.83	6.95	±0.06	6.36
12S_009	60	7.5	2/1	46.33	±0.68*	135.64	±4.65*	6.42	±0.06*	7.16
12S_010	60	15	3/1	44.49	±0.24*	86.99	±0.15*	6.56	±0.11*	6.16
12S_011	60	30	2/1	50.80	±2.40	112.35	±4.04	6.89	±0.08	7.09
13S_005	0	7.5	3/1	39.43	±0.57	80.51	±2.42	8.52	±0.17	7.53
13S_004	0	15	2/2	52.35	±1.35	165.47	±7.83	8.62	±0.10	6.63
13S_003	0	30	4/1	49.15	±1.20	60.65	±2.99	8.90	±0.12	6.8
13S_002	0	37.5	2/1	54.00	±0.29	109.81	±12.47	9.48	±0.20	7.36
13S_008	7.5	7.5	3/1	38.93	±0.69	102.15	±9.62	9.44	±0.35	7.15
13S_007	7.5	15	2/1	45.62	±1.35	129.02	±5.39	9.71	±0.40	6.88
13S_006	7.5	30	3/2	46.60	±0.64	69.72	±1.03	8.86	±0.27	6.73
13S_011	15	7.5	2/2	44.44	±0.83	130.55	±4.98	6.65	±0.15	6.25
13S_010	15	15	2/2	53.02	±1.58	169.12	±1.02	6.43	±0.27	6.96
13S_009	15	30	4/1	50.34	±0.84	88.97	±11.87	5.75	±0.16	6.64
13S_014	30	7.5	2/1	48.01	±0.95	142.37	±5.94	7.37	±0.26	6.89
13S_013	30	15	3/1	43.78	±0.30	72.24	±1.03	7.33	±0.18	7.02
13S_012	30	30	2/2	48.19	±1.12	89.00	±8.76	6.71	±0.09	7.07
13S_017	60	7.5	2/1	46.44	±1.87	80.65	±14.45	6.71	±0.20	6.12
13S_016	60	15	2/1	48.13	±0.71	121.00	±1.40	8.79	±0.13	6.79
13S_015	60	30	4/2	43.11	±0.27	52.48	±3.50	8.17	±0.58	7.34
13S_020	120	7.5	2/2	57.87	±4.06	236.55	±38.72	6.00	±0.05	6.85
13S_019	120	15	2/1	45.98	±0.35	126.55	±7.46	6.50	±0.13	6.66
13S_018	120	30	3/1	43.42	±1.09	81.50	±9.25	6.70	±0.06	6.64

Table 3.4: Carbon content and phosphate sorption indices for selected wetland sediments from RWR.

Sample Name	Sample Season and Year	Depth (cm)	Water content (%)		Organic C (g/kg)		Inorganic C (g/kg)		pH	PO_4 (mg/L)		PSI (mg/100g)	
13S_002	Spring 2013	45	54.00	±0.29	109.81	±12.47	9.48	±0.20	7.36	17.989	±3.04	112.826	±10.08
13S_003	Spring 2013	30	49.15	±1.20	60.65	±2.99	8.90	±0.12	6.8	36.949	±7.04	71.945	±9.99
13S_004	Spring 2013	15	52.35	±1.35	165.47	±7.83	8.62	±0.10	6.63	42.989	±6.99	66.100	±7.48
10S_002	Spring 2010	30	39.56	±0.14	67.24	±2.00	6.58	±0.11	6.58	59.703	±10.12	50.513	±12.10

Table 3.5: Major and trace element chemistry (wt. %) for apatite standards, modern, and representative fossil bone. Values in parentheses reflect standard deviations (1σ).

			Weight % Composition															
	Age	Number of Analyses Per Specimen	P_2O_5	SiO_2	SO_2	Al_2O_3	La_2O_3	Ce_2O_3	CaO	MnO	FeO	SrO	BaO	H_2O	Na_2O	F	Cl	Total
Fluorinated apatite hand sample (Ward's)	Standard	n = 12	38.8 (10)	0.93 (22)	0.47 (32)		0.27 (7)	0.72 (15)	53.6 (3)		0.01 (1)	0.17 (2)	0.32 (37)	0	0.10 (4)	4.13 (15)	0.04 (3)	99.6 (8)
Analytical grade apatite (Ward's)	Standard	n = 16	40.3 (2)	0.51 (4)	0.24 (11)		0.56 (6)	0.76 (5)	53.2 (2)		0.03 (2)	0.03 (1)	0.11 (18)	0.00 (1)	0.29 (2)	3.62 (16)	0.41 (5)	100.1 (4)
Modern mammal	Modern	n = 10	27.8 (31)	0.01 (1)	0.27 (5)	0.00 (1)	0.01 (1)	0.01 (1)	36.6 (39)	0.00 (1)	0.02 (3)	0.00 (0)	0.01 (1)	1.00 (12)	0.34 (15)	0.33 (13)	0.12 (3)	66.7 (72)
Unaltered alligator vertebra	Modern	n = 12	28.8 (11)	0.02 (1)	0.48 (10)	0.00 (1)	0.02 (2)	0.01 (1)	38.2 (15)	0.00 (0)	0.00 (1)	0.02 (1)	0.02 (2)	1.09 (7)	0.76 (17)	0.07 (4)	0.46 (18)	70.0 (28)
Exclusion 1 Week	Modern	n = 10	30.8 (18)	0.03 (2)	0.39 (6)	0.17 (10)	0.01 (1)	0.00 (0)	39.4 (14)	0.01 (1)	0.01 (2)	0.02 (1)	0.00 (1)	1.22 (6)	0.74 (11)	0.08 (4)	0.18 (4)	73.0 (32)
Colonization 1 Week	Modern	n = 13	26.8 (14)	0.03 (3)	0.43 (13)	0.15 (6)	0.01 (1)	0.00 (0)	34.0 (26)	0.10 (29)	0.02 (5)	0.01 (1)	0.01 (2)	1.00 (9)	0.64 (30)	0.12 (5)	0.29 (9)	63.6 (36)
Exclusion 1 Month	Modern	n = 16	26.5 (14)	0.01 (1)	0.32 (7)	0.02 (2)	0.01 (3)	0.01 (2)	36.0 (21)	0.01 (2)	0.01 (1)	0.02 (2)	0.01 (1)	1.05 (7)	0.41 (20)	0.07 (5)	0.24 (7)	64.6 (37)
Colonization 1 Month	Modern	n = 15	26.6 (18)	0.01 (1)	0.28 (6)	0.02 (2)	0.01 (1)	0.01 (2)	36.3 (26)	0.02 (3)	0.02 (2)	0.02 (2)	0.01 (1)	1.05 (10)	0.35 (21)	0.06 (4)	0.26 (12)	65.0 (46)
Alligator vertebra, 1 year post-burial	Modern	n = 15	28.2 (33)	0.01 (1)	0.63 (21)	0.00 (0)	0.00 (1)	0.01 (2)	37.6 (44)	0.06 (4)	0.04 (3)	0.11 (3)	0.05 (3)	1.04 (12)	0.50 (19)	0.29 (17)	0.17 (4)	68.8 (80)
Alligator dentary, 2 years post-burial	Modern	n = 16	28.4 (25)	0.01 (1)	0.80 (13)	0.00 (0)	0.01 (2)	0.01 (2)	37.7 (36)	0.17 (29)	0.20 (36)	0.11 (2)	0.04 (3)	1.10 (7)	0.57 (14)	0.22 (18)	0.11 (6)	69.4 (62)
Alligator vertebra, 3 yrs post-burial	Modern	n = 19	30.3 (30)	0.01 (1)	1.26 (35)	0.00 (1)	0.01 (2)	0.02 (2)	38.5 (42)	0.63 (44)	0.76 (78)	0.15 (4)	0.05 (4)	1.13 (16)	0.60 (16)	0.29 (14)	0.17 (6)	73.8 (71)
Triceratops limb bone, Hell Creek Fm., MT	65 Mya	n = 65	34.5 (9)	0.06 (11)	0.38 (15)			0.18 (19)	49.8 (13)		0.77 (19)	0.24 (3)	0.16 (4)	0.3 6(5)	0.44 (8)	2.38 (10)	0.04 (2)	89.5 (22)

Table 3.6: FTIR ratios for mesocosm samples with direct and indirect exposure to microbial communities and representative modern and fossil bone.

	Age	Crystallinity	Mean crystal length (nm)	Amide/ phosphate	Wt. % organic matter	Carbonate/ phosphate	BPI	API	BAI
Unaltered bone	modern	2.81	41.47	1.60	37.64	2.38	2.13	2.52	1.18
Exclusion 1 week	modern	2.93	43.99	1.71	38.32	2.24	1.97	2.20	1.11
Colonization 1 week	modern	2.89	43.02	1.59	37.51	2.89	3.47	3.90	1.12
Exclusion 1 month	modern	2.03	25.09	1.10	33.48	2.19	2.23	2.25	1.01
Colonization 1 month	modern	1.86	21.58	1.22	34.56	2.78	2.73	2.82	1.03
Burial 1 year	modern	2.48	34.54	0.83	30.34	1.73	1.73	1.83	1.06
Burial 2 years	modern	2.67	38.43	0.92	31.47	2.13	2.36	2.50	1.06
Burial 3 years	3 years	3.04	46.28	0.69	28.34	1.59	1.69	1.78	1.06
Hell Creek	~65 Ma	3.10	47.36	0.23	15.98	1.20	1.13	1.10	0.97

Table 3.7: FTIR ratios from bones under variable pH treatments.

pH	Sampling Day	Crystallinity (IRSF)	Mean crystal length (nm)	Amide/ Phosphate	Weight % organic matter	Carbonate/ Phosphate	BPI	API	BAI
6	1	2.85	42.25	1.41	36.22	1.93	2.08	2.15	1.04
6	3	3.33	52.32	1.18	34.28	1.53	1.53	1.53	1.00
6	7	2.24	29.44	1.66	38.01	2.05	2.00	2.11	1.05
6	30	2.87	42.60	1.37	35.91	2.47	2.23	2.59	1.16
7	1	2.46	34.16	1.07	33.18	1.63	1.77	1.88	1.06
7	3	2.57	36.32	1.26	34.98	1.88	2.08	2.19	1.06
7	7	2.65	38.13	1.53	37.16	1.89	1.90	2.07	1.09
7	30	3.15	48.58	1.18	34.23	2.44	2.23	2.32	1.04
8	1	2.21	28.93	1.31	35.42	2.10	2.39	2.50	1.05
8	3	2.71	39.25	1.20	34.40	1.83	1.74	1.91	1.10
8	7	2.78	40.75	1.19	34.37	2.02	2.13	2.26	1.06
8	30	2.56	36.26	1.00	32.43	1.56	1.50	1.70	1.13
9	1	2.30	30.79	1.67	38.09	2.37	2.27	2.68	1.18
9	3	2.33	31.49	2.35	41.90	4.93	6.00	7.80	1.30
9	7	2.64	37.93	1.50	36.92	2.51	2.26	2.63	1.16
9	30	2.82	41.59	1.36	35.87	2.39	2.27	2.67	1.18
10	1	2.50	34.96	1.33	35.62	2.23	2.13	2.33	1.09
10	3	2.00	24.54	1.95	39.81	4.83	4.50	5.17	1.15
10	7	3.13	47.98	1.76	38.68	3.20	2.71	3.00	1.11
10	30	2.43	33.47	0.95	31.83	1.94	1.92	2.04	1.06
11	1	2.55	35.91	1.39	36.11	2.93	2.79	3.07	1.10
11	3	2.45	34.01	1.30	35.31	2.26	1.93	2.13	1.10
11	7	1.92	22.81	2.04	40.32	3.39	2.92	3.58	1.23
11	30	2.62	37.44	1.31	35.45	2.07	2.00	2.22	1.11
A	30	4.67	80.10	1.83	39.15	4.79	5.17	6.00	1.16
D	30	2.53	35.51	0.90	31.31	1.63	1.62	1.84	1.14

References

APHA, 2005. (American Public Health Association) Standard methods for the examination of water and wastewater, 21st ed., *in:* Eaton, A.D., Franson, M.A.H. US EPA, APHA, American Water Works Association, and the Water Environment Federation. http://www.standardmethods.org/.

Appelo, C.A.J., Postma, D., 2005. Geochemistry: groundwater and pollution, 2nd ed. CRC Press, Taylor & Francis Group, Boca Raton, FL, USA.

Bache, B.W., Williams, E.G., 1971. Phosphate sorption index for soils. J Soil Sci 22, 289-301.

Bergstrom, W.H., Wallace, W.M., 1954. Bone as a sodium and potassium reservoir. J Clin Invest 33, 867-873.

Berna, F., Matthews, A., Weiner, S., 2004. Solubilities of bone mineral from arhcaeological sites: the recrystallization window. J Archaeol Sci 31, 867-882.

Chatterjee, S., 1985. *Postosuchus*, a new Thecodontian reptile from the Triassic of Texas and the origin of Tyrannosaurs. Philos T Roy Soc B 309, 395-460.

Child, A.M., 1995. Microbial taphonomy of archaeological bone. Stud Conserv 40, 19-30.

Cuff, A.R., Rayfield, E.J., 2013. Feeding mechanics in Spinosaurid theropods and extant crocodilians. PLoS One 8, DOI:10.1371/journal.pone.0065295.

Daniel, J.C., Chin, K., 2010. The role of bacterially mediated precipitation in the permineralization of bone. Palaios 25, 507-516.

Darke, A.K., Walbridge, M.R., 2000. Al and Fe biogeochemistry in a floodplain forest: Implications for P retention. Biogeochemistry 51, 1-32.

Dowd, S.E., Callaway, T.R., Wolcott, R.D., Sun, Y., McKeehan, T., Hagevoort, R.G., Edrington, T.S., 2008. Evaluation of the bacterial diversity in the feces of cattle using 16S rDNA bacterial tag-encoded FLX amplicon pyrosequencing (bTEFAP). BMC Microbiol 8, DOI:10.1186/1471-2180-8-125.

Elliott, J.C., 2002. Calcium phosphate biominerals. Rev Mineral Geochem 48, 427-453.

Elsey, R.M., Woodward, A.R., 2010. American alligator *Alligator mississippiensis*, in: Manolis, S.C., Stevenson, C. (Eds.), Crocodiles: status, survey, and conservation action plan, Third ed. Crocodile Specialist Group, Darwin, pp. 1-4.

Georgakoudi, I., Jacobson, B.C., Muller, M.G., Sheets, E.E., Badizadegan, K., Carr-Locke, D.L., Crum, C.P., Boone, C.W., Dasari, R.R., Van Dam, J., Feld, M.S., 2002. NAD(P)H and

collagen as in vivo quantitative fluorescent biomarkers of epithelial precancerous changes. Cancer Res 62, 682-687.

Gray, C.J., Engel, A.S., 2013. Microbial diversity and impact on carbonate geochemistry across a changing geochemical gradient in a karst aquifer. ISME J 7, 325-337.

Green, J., Kleeman, C.R., 1991. Role of bone in regulation of systemic acid-base balance. Kidney Int 39, 9-26.

Hamilton, D.L., 1999. Methods for conserving archaeological material from underwater sites. Texas A&M University, College Station, Texas.

Hammer, Ø., Harper, D.A.T., Ryan, P.D., 2001. PAST: paleontological statistics software pacakge for education and data analysis. Palaeontologia Electronica 4, 1-9.

Harrell, D.L., Wang, J.J., 2006. Fractionation and sorption of inorganic phosphorus in Louisiana calcareous soils. Soil Sci 171, 39-51.

Hubert, J.F., Panish, P.T., Chure, D.J., Prostak, K.S., 1996. Chemistry, microstructure, petrology, and diagenetic model of Jurassic dinosaur bones, Dinosaur National Monument, Utah. J Sediment Res 66, 531-547.

Jans, M.M.E., 2008. Microbial bioerosion of bone - a review, in: Wisshak, M., Tapanila, L. (Eds.), Current developments in bioerosion. Springer-Verlag, Berlin, pp. 397-413.

Jans, M.M.E., Nielsen-Marsh, C.M., Smith, C.I., Collins, M.J., Kars, H., 2004. Characterisation of microbial attack on archaeological bone. J Archaeol Sci 31, 87-95.

Keenan, S.W., 2013. Freshwater vertebrate animal metagenomics, Alligatorinae, in: Nelson, K. (Ed.), Encyclopedia of Metagenomics. Springer-Verlag Berlin Heidelberg.

Keenan, S.W., Engel, A.S., Elsey, R.M., 2013. The alligator gut microbiome and implications for archosaur symbioses. Sci Rep 3, DOI:10.1038/srep02877.

Koenig, A.E., Rogers, R.R., Trueman, C.N., 2009. Visualizing fossilization using laser ablation-inductively coupled plasma-mass spectrometry maps of trace elements in Late Cretaceous bones. Geology 37, 511-514.

Kohn, M.J., 2008. Models of diffusion-limited uptake of trace elements in fossils and rates of fossilization. Geochim Cosmochim Acta 72, 3758-3770.

Kohn, M.J., Moses, R.J., 2012. Trace element diffusivities in bone rule out simple diffusive uptake during fossilization but explain in vivo uptake and release. Proc Natl Acad Sci U S A 110, 419-424.

Kolodny, Y., Luz, B., Sander, M., Clemens, W.A., 1996. Dinosaur bones: fossils or pseudomorphs? The pitfalls of physiology reconstruction from apatitic fossils. Palaeogeogr Palaeocl 126, 161-171.

Kuo, Y.M., Harris, W.G., Munoz-Carpena, R., Rhue, R.D., Li, Y.C., 2009. Apatite control of phosphorus release to runoff from soils of phosphate mine reclamation areas. Water Air Soil Poll 202, 189-198.

Lajtha, K., Driscoll, C.T., Jarrell, W.M., Elliott, E.T., 1999. Soil phosphorus: characterization and total element analysis, in: Robertson, G.P. (Ed.), Standard Soil Methods for Long-Term Ecological Research. Oxford University Press, New York, NY, pp. 115-142.

Leikina, E., Mertts, M.V., Kuznetsova, N., Leikin, S., 2002. Type I collagen is thermally unstable at body temperature. Proc Natl Acad Sci U S A 99, 1314-1318.

Matsui, H., Kato, Y., Chikaraishi, T., Moritani, M., Ban-Tokuda, T., Wakita, M., 2010. Microbial diversity in ostrich ceca as revealed by 16S ribosomal RNA gene clone library and detection of novel Fibrobacter species. Anaerobe 16, 83-93.

Midkiff, C., Roy, A., 1995. Soil survey of Cameron Parish, Louisiana., in: Agriculture, U.D.o. (Ed.). Soil Science Service, p. 134.

Munro, L.E., Longstaffe, F.J., White, C.D., 2007. Burning and boiling of modern deer bone: effects on crystallinity and oxygen isotope composition of bioapatite phosphate. Palaeogeogr Palaeocl 249, 90-102.

Olszta, M.J., Cheng, X.G., Jee, S.S., Kumar, R., Kim, Y.Y., Kaufman, M.J., Douglas, E.P., Gower, L.B., 2007. Bone structure and formation: a new perspective. Mat Sci Eng R 58, 77-116.

Parkhurst, D.L., Appelo, C.A.J., 1999. PHREEQC (Version 2)—A computer program for speciation, batch-reaction, one-dimensional transport, and inverse geochemical calculations, USGS Water-Resources Investigations Report. USGS.

Person, A., Bocherens, H., Saliege, J.F., Paris, F., Zeitoun, V., Gerard, M., 1995. Early diagenetic evolution of bone phosphate: an X-ray diffractometry analysis. J Archaeol Sci 22, 211-221.

Pfretzschner, H.U., 2004. Fossilization of Haversian bone in aquatic environments. Cr Palevol 3, 605-616.

Pouchou, J.-L., Pichoir, F., 1991. Quantitative analysis of homogeneous or stratified microvolumes applying the model “PAP”. Electron probe quantitation, Springer US, pp. 31-75.

Pucéat, E., Reynard, B., Lécuyer, C., 2004. Can crystallinity be used to determine the degree of chemical alteration of biogenic apatites? Chem Geol 205, 83-97.

Pyle, J.M., Spear, F.S., Wark, D.A., 2002. Electron microprobe analysis of REE in apatite, monazite and xenotime: protocols and pitfalls. Rev Mineral Geochem 48, 337-362.

Raja, S., Raghunathan, R., Yu, X.Y., Lee, T.Y., Chen, J., Kommalapati, R.R., Murugesan, K., Shen, X., Qingzhong, Y., Valsaraj, K.T., Collett, J.L., 2008. Fog chemistry in the Texas-Louisiana Gulf Coast corridor. Atmos Environ 42, 2048-2061.

Reiche, I., Vignaud, C., Menu, M., 2002. The crystallinity of ancient bone and dentine: new insights by transmission electron microscopy. Archaeometry 44, 447-459.

Robertson, G.P., Sollins, P., Ellis, B.G., Lajtha, K., 1999. Exchangeable ions, pH, and cation exchange capacity, in: Robertson, G.P. (Ed.), Standard Soil Methods for Long-Term Ecological Research. Oxford University Press, New York, NY, pp. 106-114.

Schachner, E.R., Farmer, C.G., McDonald, A.T., Dodson, P., 2011. Evolution of the dinosauriform respiratory apparatus: new evidence from the postcranial axial skeleton. Anat Rec 294, 1532-1547.

Schloss, P.D., Gevers, D., Westcott, S.L., 2011. Reducing the effects of PCR amplificaiton and sequencing artifacts on 16S rRNA-based studies. PLoS One 6, DOI:10.1371/journal.pone.0027310.

Schloss, P.D., Westcott, S.L., Ryabin, T., Hall, J.R., Hartmann, M., Hollister, E.B., Lesniewski, R.A., Oakley, B.B., Parks, D.H., Robinson, C.J., Sahl, J.W., Stres, B., Thallinger, G.G., Van Horn, D.J., Weber, C.F., 2009. Introducing mothur: open-source, platform-independent, community-supported software for describing and comparing microbial communities. Appl Environ Microbiol 75, 7537-7541.

Somerville, C.C., Knight, I.T., Straube, W.L., Colwell, R.R., 1989. Simple, rapid method for direct isolation of nucleic-acids from aquatic environments. Appl Environ Microbiol 55, 548-554.

Sponheimer, M., Lee-Thorp, J.A., 1999. Alteration of enamel carbonate environments during fossilization. J Archaeol Sci 26, 143-150.

Trueman, C.N., Benton, M.J., 1997. A geochemical method to trace the taphonomic history of reworked bones in sedimentary settings. Geology 25, 263-266.

Trueman, C.N., Behrensmeyer, A.K., Potts, R., Tuross, N., 2006. High-resolution records of location and stratigraphic provenance from the rare earth element composition of fossil bones. Geochim Cosmochim Acta 70, 4343-4355.

Trueman, C.N., Privat, K., Field, J., 2008. Why do crystallinity values fail to predict the extent of diagenetic alteration of bone mineral? Palaeogeogr Palaeocl 266, 160-167.

Trueman, C.N.G., Behrensmeyer, A.K., Tuross, N., Weiner, S., 2004. Mineralogical and compositional changes in bones exposed on soil surfaces in Amboseli National Park, Kenya: diagenetic mechanisms and the role of sediment pore fluids. J Archaeol Sci 31, 721-739.

Tutken, T., Pfretzschner, H.U., Vennemann, T.W., Sun, G., Wang, Y.D., 2004. Paleobiology and skeletochronology of Jurassic dinosaurs: implications from the histology and oxygen isotope compositions of bones. Palaeogeogr Palaeocl 206, 217-238.

USGS, 2011. USGS Water Data for the Nation. http://waterdata.usgs.gov/nwis.

Voegelin, A., Kaegi, R., Frommer, J., Vantelon, D., Hug, S.J., 2010. Effect of phosphate, silicate, and Ca on Fe(III)-precipitates formed in aerated Fe(II)- and As(III)-containing water studied by X-ray absorption spectroscopy. Geochim Cosmochim Acta 74, 164-186.

Wang, Q.R., Li, Y.C., Wang, Y., 2011. Optimizing the weight loss-on-ignition methodology to quantify organic and carbonate carbon of sediments from diverse sources. Environ Monit Assess 174, 241-257.

Wang, X.J., Wang, J.P., Zhang, J., 2012. Comparisons of three methods for organic and inorganic carbon in calcareous soils of northwestern China. PLoS One 7, DOI:10.1371/journal.pone.0044334.

Weiner, S., Bar-Yosef, O., 1990. States of preservation of bones from prehistoric sites in the near-East: a survey. J Archaeol Sci 17, 187-196.

White, E.M., Hannus, L.A., 1983. Chemical weathering of bone in archaeological soils. Am Antiquity 48, 316-322.

Wright, A.L., Wang, Y., Reddy, K.R., 2008. Loss-on-ignition method to assess soil organic carbon in calcareous everglades wetlands. Commun Soil Sci Plan 39, 3074-3083.

Zhang, H.S., DiBaise, J.K., Zuccolo, A., Kudrna, D., Braidotti, M., Yu, Y.S., Parameswaran, P., Crowell, M.D., Wing, R., Rittmann, B.E., Krajmalnik-Brown, R., 2009. Human gut microbiota in obesity and after gastric bypass. Proc Natl Acad Sci U S A 106, 2365-2370.

Zhou, J.Z., Bruns, M.A., Tiedje, J.M., 1996. DNA recovery from soils of diverse composition. Appl Environ Microbiol 62, 316-322.

Chapter 4: Evaluating bone diagenesis and fossilization with X-ray absorption spectroscopy

Some of the results of this chapter are in preparation to submit for eventual publication, with a preliminary citation of: Keenan, S.W., Engel, A.S., Bovenkamp, G.L., and Roy, A., Applications of X-ray absorption spectroscopy towards evaluating bone diagenesis and fossilization.

SWK performed sample preparation, data collection, conducted data analysis, and wrote the manuscript. ASE assisted with data analysis and wrote the paper. GLB and AR assisted with data collection, data analysis, and edited the manuscript.

Abstract

The transformation of hydroxyapatite in bone to a fossil apatite mineral phase results in numerous changes to the mineral structure, composition, and lattice configuration. Despite extensive research on mineralogy to geochemistry of modern and fossil bone, our understanding of the atomic-level configuration, and the potential for depositional environments to influence the composition and bonding arrangement configuration, is lacking. Modern and fossil bones were evaluated using X-ray absorption near edge structure (XANES) spectroscopy at the Ca and P K-edges to explore the potential of synchrotron-based analyses to provide insight into the process of bone fossilization. Comparison of modern bones to Late Neogene and to Late Cretaceous fossil bones indicates that fossilized bone converges on a similar atomic-level lattice structure, despite widely varying elemental chemistry. Our results highlight the role of a stable lattice structure rather than mineral chemistry in dictating preservation of fossilized apatite phases over geologic time.

Introduction

Fossilized bones provide paleobiologists with a direct record of extinct life. Despite extensive evaluation of fossil bone major and trace element composition (e.g., Hubert et al., 1996; Trueman and Benton, 1997; Koenig et al., 2009), isotopic records from fossil bone and teeth (e.g., Kolodny et al., 1996), and structure and development histories of bone through time (e.g., Olszta et al., 2007), significant gaps still remain regarding the transformations of bone during diagenesis. Notably, in terms of our understanding of whether structural and chemical changes observed during early diagenesis are retained through geologic time. Additionally, the final structural configuration and bonding in fossil bone is also unclear. Consequently, there are uncertainties in the location(s) of ion substitutions within the lattice that may enhance preservation potential.

Bone consists of an organic (i.e. collagen, lipids) and inorganic (i.e. mineral) fraction. The mineral fraction is a nonstoichiometric apatite phase, hydroxyapatite (HAP) [$Ca_{10}(PO_4)_6(OH)_2$] or a carbonated HAP (Elliott, 2002; Olszta et al., 2007). In life, flexibility of the apatite lattice in vertebrate bone permits/enhances exchange with elements such as Ca and Na, and plays a critical role in acid-base regulation within the organism (Bergstrom and Wallace, 1954; Green and Kleeman, 1991). The dynamic changes that occur to the HAP lattice *in vivo*, which provide critical functions for the vertebrate host (Rollin-Martinet et al., 2013), also facilitate recrystallization following host death.

Once bone is removed from a living organism and deposited in the environment, the HAP lattice can potentially accommodate substitutions and replacements at all sites (e.g., Ca, PO_4^{3-}, OH^-), with ion incorporation governed by depositional system geochemical conditions, as well as lattice-specific parameters including: the ionic radius of the substituting ion, local electrostatic

repulsion, previously incorporated ions in the lattice, and charge balance within the mineral structure (Fleet and Pan, 1995; Jiang et al., 2002). Within the apatite lattice, there are two distinct calcium sites (or types) that are distinguished based on shared bonds with neighboring oxygen atoms. Calcium type I is in nine-fold coordination with oxygen from PO_4^{3-}, and Ca type II is in seven-fold coordination with oxygen from hydroxyl ions (Pan and Fleet, 2002; Trueman et al., 2008). During diagenesis, CO_3^{2-} ions are incorporated into the HAP lattice, forming a carbonated apatite phase largely at the expense of PO_4^{3-}. This can form type B carbonate associated with the type I Ca sites, whereas OH^- would form type A carbonate associated with the type II Ca sites (Sponheimer and Lee-Thorp, 1999; Trueman et al., 2008). Both Ca sites can be replaced by monovalent (Na^+), divalent (Fe^{2+}, Sr^{2+}, Mn^{2+}), trivalent (Fe^{3+}, REE^{3+}), tetravalent (U^{4+}), and hexavalent (U^{6+}) cations (Pan and Fleet, 2002). Protonation at the mineral surface of PO_4^{3-} and OH^- may open the apatite lattice to exchange with CO_3^{2-} (Rollin-Martinet et al., 2013), which may serve as a mechanism to allow for ion replacement, such as F or Cl, in place of OH^-. Replacement like this would form fluorinated apatite (FAP) [$Ca_{10}(PO_4)_6F_2$] or chlorapatite, respectively. These are the primary phases found in fossils (e.g., Hubert et al., 1996). Such chemical alterations are considered essential for long-term preservation of bone as a fossil, which can often be enriched in F, Fe, Mn, Sr, Ba, and rare earth elements by several orders of magnitude (e.g., Hubert et al., 1996).

Recrystallization of the original bioapatite affects the overall mineral structure. Significant increases in crystallite size and structural ordering can facilitate long-term crystallite stability due to the reduction in the surface area to volume ratio (e.g., Kohn, 2008; Trueman et al., 2008) and the alteration of type A to type B carbonate content in fossil bone compared to modern material affects dissolution rates (e.g., Trueman et al., 2008). Reduction in the amide to

phosphate ratio reflects the loss of organics, for which degradation and removal of the organics through abiotic (e.g., Leikina et al., 2002) and biotic processes (e.g., Pfretzschner, 2004) enhances ion transport and fluid migration (e.g., Child, 1995; Kohn, 2008), and can facilitate further diagenetic alteration to the mineral fraction.

Prior research addressing changes to bone composition and structure relied on a relatively narrow range of analytical tools, including Fourier transform infrared spectroscopy (FTIR) (e.g., Person et al., 1995; Pucéat et al., 2004; Trueman et al., 2008), and electron microprobe (EMP) analyses and X-ray diffraction (XRD) (e.g., Hubert et al., 1996). Advances in imaging, spatial resolution of chemical heterogeneities, and analytical detection limits of trace elements led to the integration of novel approaches towards evaluating bone composition, including laser ablation-inductively coupled plasma-mass spectrometry (e.g., Koenig et al., 2009), proton induced X-ray emission (Goodwin et al., 2007), X-ray absorption near edge structure (XANES) spectroscopy at the Mn K-edge (Reiche and Chalmin, 2008), and element mapping with synchrotron-based rapid scanning X-ray fluorescence (e.g., Bergmann et al., 2010). Although these approaches have furthered our understanding of diagenetic transformation in bone, there are still gaps in our understanding of the atomic-level structural configuration of fossilized bones, potential changes to inter-atomic bond distances, and the influence of trace elements in altering bond configurations.

XANES spectroscopy was applied to evaluate atomic-level bonding and electron sharing in bone as a complement to FTIR and EMP analyses. A series of modern and fossil bones from the Neogene to Late Cretaceous were compared using XANES spectroscopy at the Ca and P K-edges to explore the structural and chemical transformations that occur to bone over the course of fossilization from distinct depositional environments. To our knowledge, XANES

spectroscopy has not been widely used to evaluate bone composition (Eichert et al., 2006; Wang et al., 2008; Rajendran, 2011), despite the potential for results to provide insight into bond sharing and ion coordination with surrounding elements (Franke and Hormes, 1995; Salbu et al., 2005; Voegelin et al., 2010). This research addressed several main questions: How does diagenesis influence bond sharing and distances? To what extent does depositional environment impact resulting fossil lattice configurations? Does alteration to bond spacing at the Ca and P K-edges exhibit similar changes (i.e. are bonds shortened, lengthened, or unchanged)? We evaluated the potential for XANES spectroscopy to provide previously unrecognized atomic-level configurations of fossilized bones of varying ages to test the hypothesis that atomic-level changes are critical for preserving bone over geologic time.

Materials and methods

Beamline operating conditions

XANES spectroscopy at the P and Ca K-edges was performed at the DCM beamline of the Center for Advanced Microstructures & Devices (CAMD) (Hormes et al., 2006). During XANES analyses, the ring energy at CAMD operated at 1.3 GeV, with electron currents between 80 and 200 mA. Synchrotron radiation conditions and monochromator settings were as described previously (Engel et al., 2007). The windowless Double Crystal Monochromator (DCM) beamline, with a 13 µm-thick Kapton window separating the ring from the experimental chamber, was equipped with InSb(111) crystals. The monochromator is Lemonnier-type with design modifications made at Bonn University, Germany. For analyses, the monochromator was calibrated to 2152.8 eV (Franke and Hormes, 1995) for P K-edge XANES measurements based on the white line peak of $AlPO_4$ (Sigma-Aldrich, St. Louis, MO). Spectra were collected in

fluorescence mode under vacuum (5 torr). Absolute white line values were 2050, 2139, 2185, 2200, 2250 eV, with scan steps of 3.0, 0.2, 0.5, 1.0, and 4.0. Relative white line position values were -150, -20, 40, 100, 200, 416, 652, and 947. For Ca calibration, the pre-edge peak for CaO at 4043 eV was used (Cazorla-Amoros et al., 1993). Ca K-edge spectra were collected under partial vacuum (~200 torr) after purging the sample chamber with He to reduce attenuation of fluorescence radiation. Fluorescence measurements were made with an SII Vortex silicon drift detector. Samples were measured at least twice, and the resulting spectra reflect averaged normalized spectra.

Sample acquisition and processing

Modern alligator bones were obtained from salvaged animals through the Louisiana Department of Wildlife and Fisheries (Louisiana National Heritage Program, permit LNHP-10-009). Bones were cleaned of soft tissues by dermestid beetles, and any residual debris was gently removed with a paintbrush, followed by immersion in Milli-Q deionized water by sonication (Branson 2510) for 60 min. Bone surfaces were further cleaned and sterilized using a critical point drying method (Hamilton, 1999), starting with 70% reagent grade ethanol and ending with 100% reagent grade ethanol. Bones were dried overnight at room temperature prior to processing for XANES by grinding in a mortar and pestle. One modern bone (SWK1) was autoclaved to assess the potential for heat- and pressure-induced alteration of the mineral structure. To prevent contamination, all cleaning and manual processing (using agate mortar and pestle) was performed wearing nitrile gloves, and the mortar and pestle were cleaned using autoclaved deionized Milli-Q water followed by 100% reagent grade acetone prior to and after use. The

resulting powdered aliquots were stored in sterile microcentrifuge tubes until analysis (Sponheimer and Lee-Thorp, 1999).

A Pleistocene (~ 50 ka) mammal bone deposited in deltaic-fluvial sandstones was obtained by R. Schouten (University of Bristol, UK) from the North Sea off the coast of the Netherlands in 2008. The bone was soaked for several days in tap water to remove seawater and prevent precipitation of salts within pore spaces. After soaking, the bone was allowed to dry at room temperature prior to sampling. A 1 cm^3 chip was cut from the cortex and ground in an agate mortar and pestle following the same protocol as the modern bone sample.

Late Neogene (4.5-7.0 Ma) fossil *Alligator* sp. phalanges were collected at the Gray Fossil Site, Gray, Tennessee, USA, in 2001. Samples were obtained from the McClung Museum of Natural History and Culture, University of Tennessee, Knoxville, collections, and permission was granted to conduct destructive analyses. The bones were deposited in organic-rich lacustrine mudstone deposits within a paleosinkhole (Shunk et al., 2009).

A Late Cretaceous (Campanian, ~ 72 Ma) dinosaur (hadrosaur) femur from the Judith River Formation, Montana, USA, and an additional dinosaur femur from the Two Medicine Formation, Montana, USA, were obtained from the Museum of the Rockies, Montana State University, Bozeman, MT. The Judith River Formation sample was deposited within a fluvial system, while the Two Medicine Formation femur was preserved in overbank mudstone and siltstone deposits. All fossil bone samples were prepared for analysis after cleaning bone fragments of sediment with autoclaved deionized Milli-Q water followed by 70% ethanol.

Standards selected for P K-edge XANES included HAP (reagent grade, Sigma-Aldrich), analytical grade fluorapatite (Ward's Science, Rochester, NY), a natural mineral specimen of fluorapatite (Ward's Science), $AlPO_4$ (Sigma-Aldrich), variscite (Louisiana State University,

Department of Geology and Geophysics, Baton Rouge, LA), and strengite (Louisiana State University). Ca K-edge standards included $CaCO_3$ (research grade, Ward's Science), analytical grade $CaCO_3$ (Sigma-Aldrich), analytical grade and a natural FAP mineral specimen (Ward's), NIST HAP (Gaithersburg, MD), and selenite (Ward's Science). Analytical grade and natural specimens obtained from Ward's Science were ground using an agate mortar and pestle prior to analysis to reduce artifacts due to hydration. For analyses, dry powders were spread to a uniform thickness on Kapton tape using disposable plastic paintbrushes (verified free of Ca or P).

Determination of mineralogy, crystallinity, and geochemistry

Methods were detailed in Chapter 3.

Data processing

XANES data were normalized at 2200 and 4070 eV for P and Ca, respectively, and background corrected using Athena (Ravel and Newville, 2005), and graphed with Origin or Sigma Plot. Analysis included linear combination fitting (LCF) with Athena, incorporating normalized spectra of standards with weights set between 0 and 1, and forced to sum to 1. The program applied lines of best fit to each sample compared to a set of standards, which generated values for each sample describing how well the standard matched the sample spectra.

Results and discussion

We evaluated the potential for XANES spectroscopy to provide previously unrecognized atomic-level configurations of fossilized bones of varying ages to test the hypothesis that atomic-level changes are critical for preserving bone over geologic time. Based on EMP analyses, all

bones were composed of an apatite phase, with variable minor and trace elements (Table 4.1). Fossil bones were enriched in F, indicating that the bones were preserved as FAP. The low totals (Table 4.1) reflect the incorporation of CO_3^{2-}, which cannot be quantified using EMP analysis. Even as a fluorinated phase, the fossil bones also had variable minor and trace element concentrations (Table 4.1, C.1), which highlights ion substitution flexibility of the apatite lattice

Phosphorus K-edge spectra indicated a decrease in white line intensity (peak A, 2153 eV) with increasing degree of recrystallization over time (Fig. 4.1). Additional shifts in the post-edge shoulder B (2156 eV) were due to changes in adjacent alkaline or alkaline earth ion bonding, principally Ca or Na (e.g., Franke and Hormes, 1995). Comparative study of apatite minerals (Ingall et al., 2010) indicates the post-edge shoulder for fossils likely reflects changes to Ca bonding that may be disrupted in the apatite lattice. LCF of P K-edge spectra (LCF) suggest that all bones contained a significant amount of FAP, as well as HAP, with some trace contributions from strengite in a few samples and $AlPO_4$ in all but one sample (Table 4.1). No spectra matched patterns characteristic of the presence of variscite. These results were not in close agreement with data obtained from XRD analyses (Table 4.2), which identified the presence of Al in only one of the bones examined (Judith River Formation). Additionally, XRD data suggested the presence of Fe in the Gray Fossil Site samples, as well as the Judith River Formation fossil. Based on LCF, the Fe phase did not match the structure of variscite because Fe may have been incorporated as non-stoichiometric phases.

Despite varying geochemistry, the overall shapes of P and Ca K-edge bone spectra were similar, reflecting similar lattice configurations. Differences in atomic-level bonding were evident as subtle shifts in peak positions and intensities. Decreased white line intensity (peak A, 2153 eV) in P K-edge spectra with increasing age of fossil material (Fig. 4.1) corresponds to

decreased occupancy of the p-orbital and increased electron sharing with adjacent atoms in the HAP lattice (e.g., Frank and Hormes, 1995).

Based on the spectral analysis from the P-K edge, the expectation was that more information about Ca bonding could be resolved with XANES spectral analysis at the Ca K-edge. However, Ca K-edge spectra were more difficult to evaluate due to a paucity of studies analyzing natural minerals at the Ca K-edge (e.g., Peters et al., 2000; Laurencin et al., 2010). Some peaks and shifts in peak positions were distinct, and potentially provide insight into atomic-level Ca bonding to various oxyanions. For instance, the pre-edge peak at 4037 eV (peak A) was present in fossil bone and absent from modern samples (Fig. 4.2). The main Ca peak at 4046 eV, labeled as peak B, broadened in fully recrystallized fossil bones compared to the modern and Pleistocene samples. Additionally, the ratio of peak B and C heights increased in fossilized bone compared to modern or poorly recrystallized (i.e. Pleistocene) bone (Table 4.3). The Ca K-edge LCF (Table 4.3) results suggest that modern bone consists largely of FAP and calcite, which likely represents Ca-CO_3^{2-} bonds and not actually the mineral calcite. The substitution is likely at the Ca type I site, rather than the Ca type II site. As bone undergoes diagenesis and recrystallization, there was lower contributions of a Ca-CO_3^{2-} bond estimated from LCF. Similar to EMP and P K-edge LCF analyses, all bones contained some amount of FAP with higher amounts observed in fossil bone.

Integrating chemical and structural changes to fossil bone

Ionic and structural flexibility of the apatite lattice permits multiple substitutions. Resulting fossil compositions exhibit diverse compositions, which are dictated by site-specific geochemical, mineralogical, and hydrological conditions (Berna et al., 2004; Trueman et al.,

2004). The variability of minor and trace elements measured in the fossil bones reflects the combined effects of a dynamic mineral lattice with widely varying geochemical conditions present in natural systems. In bones preserved in a paleolake interpreted to be reducing and anoxic (e.g., Gray Fossil Site, Shunk et al., 2009); bones are enriched in the redox sensitive element Fe as Fe^{2+}.

Although interpretation of Ca K-edge spectra is limited, preliminary assessment of bone crystallinity and the Ca-O bond structure can be made. Eiden-Assmann and Viertelhaus (2000) evaluated the effects of apatite precipitation in a gelatinous matrix on mineral structure. The development of a pre-edge peak around 4037 eV was ascribed to increased degree of crystallization as the apatite phase crystallized in the organic media (Eiden-Assmann and Viertelhaus, 2000). The pre-edge peak at 4037 eV from the modern and fossil bones examined in this study, is only observed in fossilized bone. This suggests that, as bones undergo recrystallization during diagenesis, the development of a pre-edge peak at 4037 eV may be indicative of crystallinity changes. Additionally, the development of this pre-edge feature also correlates to asymmetry of bonds with adjacent oxygen atoms (Eiden-Assmann and Viertelhaus, 2000), which suggests that diagenesis affects not only bone chemistry, but also atomic-level bonding between adjacent atoms in the apatite lattice. Asymmetry of the Ca-O bonds may reflect substitutions within the apatite lattice, shifting bond angles to accommodate the incorporation of larger ions like Fe or Mn (as measured with EMP and XRD analyses) in place of Ca at either site I or II. Bond spacing and distances at the Ca K-edge of a representative set of geochemically variable fossils, despite diverse chemistries, suggests that fossils achieved a similar mineral lattice structure configuration with respect to P and/or Ca (Fig. 4.2). This suggests that fossilization may be driven by a trajectory towards a more stable structural configuration,

regardless of whether substitutions result in the incorporation of Fe, REE, CO_3^{2-}, metals, or additional ionic phases.

There was a disconnect between predicted compositions made with LCF and mineralogy quantified by XRD, particularly with respect to the identification of Fe-bearing phosphates and the close match with XANES spectra and Ca-CO_3^{2-} phases at the Ca K-edge. The incorporation of carbonate into HAP during diagenesis results in the formation of a mixed carbonated fluorapatite phase, both during early transformations and preserved in fossil material over geologic time. The convergence of bones in this study on a structure that more closely matches calcite than FAP suggests that carbonate substitution in place of phosphate complexes dominates the observed changes of near-edge structure at the Ca K-edge. Systematic changes observed in the ratio of the two peaks (B and C, Fig. 4.2), in poorly recrystallized bone, which have ratios less than 2.0, and fossilized bone, which have ratios >2.0, may be useful for assessing the relative amount of carbonate incorporated into the lattice.

Conclusions

As bone undergoes fossilization, substitutions for minor and trace elements at all sites within the apatite lattice have the potential to influence atomic-level bond spacing and orientation. A shift in Ca K-edge peaks in fossil bones likely reflects changes to the Ca-O bonds within the lattice, controlled by metal substitutions and/or the incorporation of CO_3^{2-}. Further experimental work or modeling is needed to test the contributions of metals and carbonate on Ca K-edge white line intensity and shifts. Concurrent alteration in bond spacing at the P K-edge reflects the dynamic nature of the apatite lattice during diagenesis, with occupancy at one site (i.e. the Ca site) afforded by bond shortening in another (i.e. the PO_4^{3-} site).

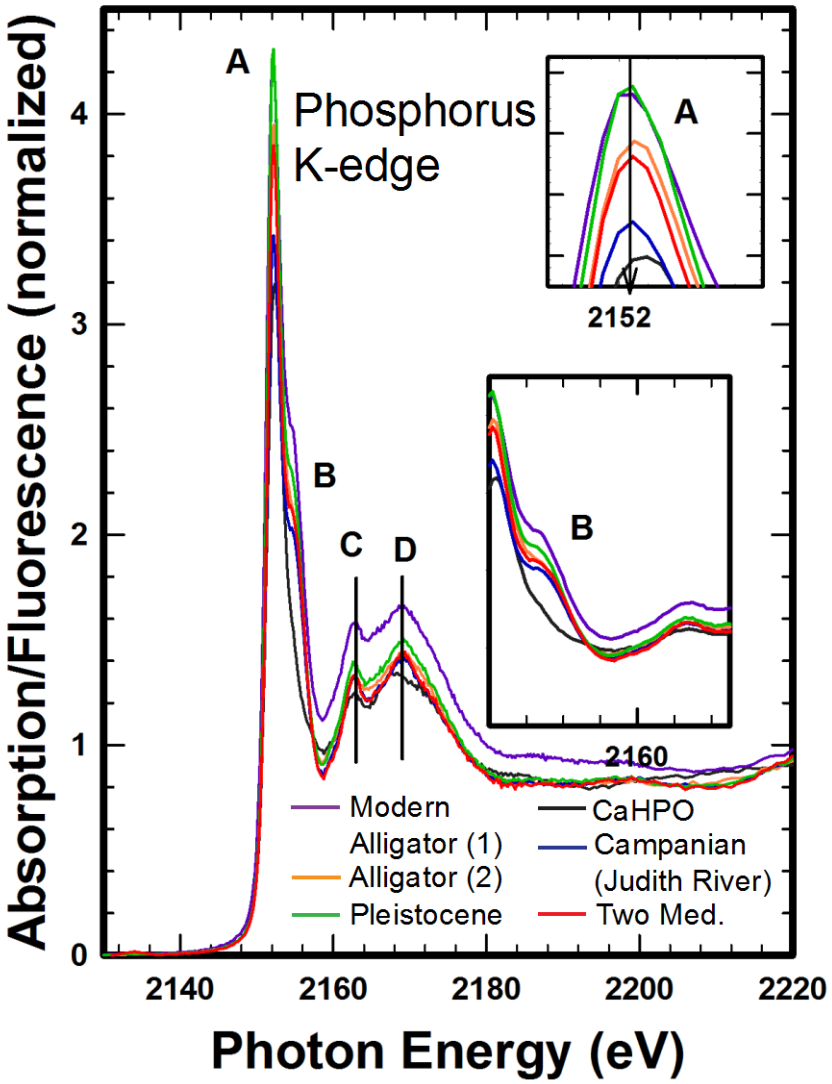

Fig. 4.1: P K-edge XANES of modern and fossil bone, and a mineral standard. As bone undergoes fossilization, there is a decrease in peak height (A). A shift in the shoulder (B) is correlated which changes to Ca occupancy.

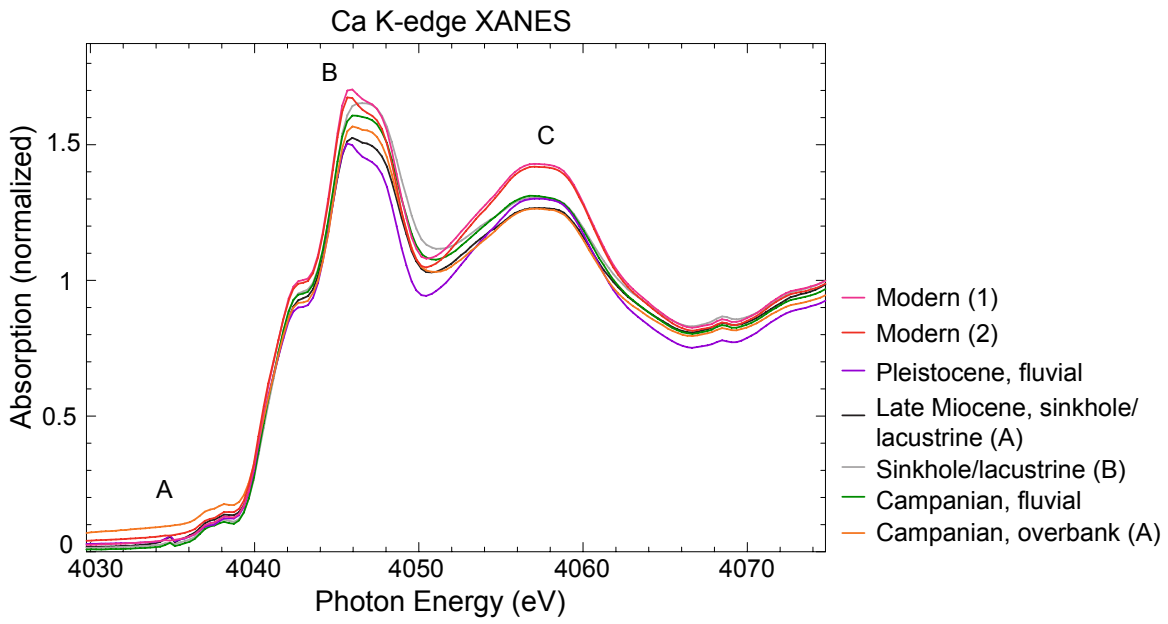

Fig. 4.2: Ca K-edge XANES for selected modern and fossil bones. Fossilized bones exhibit increased ratios of peak intensities (peaks B and C) as well as a shift in the peak position at 4046 eV. The presence of pre-edge peak A at 4035 eV was only found in fossilized bones. Samples are labelled according to depositional environment, referenced in Table 4.3 and 4.4.

Table 4.1: Major and trace element chemistry for modern and fossil bones. Values in parentheses reflect standard deviations (1σ).

			Weight % Composition														
	Age	Number of Analyses Per Specimen	P_2O_5	SiO_2	SO_2	Al_2O_3	La_2O_3	Ce_2O_3	CaO	MnO	FeO	SrO	BaO	H_2O	Na_2O	F	Cl	Total
Fluorinated apatite hand sample (Ward's)	Standard	n = 12	38.8 (10)	0.93 (22)	0.47 (32)		0.27 (7)	0.72 (15)	53.6 (3)		0.01 (1)	0.17 (2)	0.32 (37)		0.10 (4)	4.13 (15)	0.04 (3)	99.6 (8)
Analytical grade apatite (Ward's)	Standard	n = 16	40.3 (2)	0.51 (4)	0.24 (11)		0.56 (6)	0.76 (5)	53.2 (2)		0.03 (2)	0.03 (1)	0.11 (18)	0.00 (1)	0.29 (2)	3.62 (16)	0.41 (5)	100.1 (4)
Unaltered alligator vertebra	Modern	n = 12	28.8 (11)	0.02 (1)	0.48 (10)	0.00 (1)	0.02 (2)	0.01 (1)	38.2 (15)	0.00 (0)	0.00 (1)	0.02 (1)	0.02 (2)	1.09 (7)	0.76 (17)	0.07 (4)	0.46 (18)	70.0 (28)
Gray Fossil Site (1) Alligator sp. phalange	4.5 to 7 Mya	n = 52	35.0 (13)	0.01 (2)	0.06 (6)	0.23 (15)	0.09 (10)	0.10 (11)	47.8 (13)	0.06 (2)	2.40 (46)	0.05 (2)	0.17 (5)	0.55 (9)	0.23 (5)	1.99 (17)	0.03 (2)	88.6 (27)
Gray Fossil Site (2) Alligator sp. Phalange	4.5 to 7 Mya	n = 10	35.0 (2)	0.02 (1)	0.02 (1)	0.01 (1)	0.02 (1)	0.02 (2)	48.4 (4)	0.02 (1)	2.93 (24)	0.04 (2)	0.12 (2)	0.53 (8)	0.19 (3)	2.05 (17)	0.00 (0)	89.4 (5)
Hadrosaur femur, Judith River Fm., MT	~75 Mya	n = 35	34.4 (7)	0.03 (2)	0.20 (6)		0.03 (5)	0.07 (11)	50.1 (7)		0.78 (22)	0.32 (4)	0.19 (4)	0.28 (10)	0.34 (5)	2.53 (18)	0.02 (2)	89.3 (10)

Table 4.2: Linear combination fitting for P K-edge XANES spectra.

Sample	Age	Depositional Environment	$AlPO_4$	FAP (Ward's)	$CaHPO_4$	HAP	Strengite	Variscite
SWK1	modern	n/a	0	0.697	0.086	0.186	0.032	0
SWK2	modern	n/a	0.099	0.547	0.014	0.341	0	0
PLO1.2	Pleistocene	fluvial	0.062	0.491	0	0.448	0	0
GFS1A	Late Miocene	sinkhole/lacustrine	0.012	0.549	0.082	0.358	0	0
GFS1B	Late Miocene	sinkhole/lacustrine	0.046	0.646	0	0.309	0	0
JR269	Campanian	fluvial	0.038	0.802	0	0.143	0.019	0
TM728899	Campanian	overbank	0.068	0.603	0	0.329	0	0
TM810856m	Campanian	overbank	0.023	0.488	0.007	0.482	0	0

Table 4.3: X-ray diffraction data from fossil bones.

Sample	Mineralogy	Formula	Content (%)	Crystallinity
Pleistocene	Fluorapatite	$Ca_5FO_{12}P_3$	100	
	Organic phase	N, C, H, O	?	0.17
Gray Fossil Site (A)	Apatite	$Ca_5FO_{12}P_3$	74.05	
	Fluorapatite	$Ca_5FO_{12}P_3$	14.45	
	Calcium iron phosphate	$Ca_{9.333}Fe_{1.167}O_{28}P_7$	10.79	
	Calcium iron phosphide	$CaFe_2P_2$	0.71	0.24
Gray Fossil Site (B)	Fluorapatite	$Ca_5FO_{12}P_3$	91.94	
	Calcium phosphate hydroxide	$Ca_{3.29}H_{17.978}O_{18.474}P_{2.478}$	4.82	
	Calcium iron hydrogen phosphate	$Ca_9FeH_{0.9}O_{28}P_7$	3.25	0.22
Gray Fossil Site (C)	Fluorapatite	$Ca_5FO_{12}P_3$	72.24	
	Chlorapatite	$Ca_5Cl_{0.83}F_{0.17}O_{12}P_3$	18.39	
	Calcium iron phosphate hydrate	$CaFe_3P_3O_{12}H_2O$	6.08	
	Calcium iron phosphate	$Ca_{19}Fe_2O_{56}P_{14}$	3.29	0.27
Judith River Fm.	Fluorapatite	$Ca_5FO_{12}P_3$	79.10	
	Hydroxyapatite	$Ca_{4.92}H_{0.9}O_{12.87}P_3$	19.16	
	Calcium iron aluminum oxide	$Al_{0.134}Ca_2Fe_{1.866}O_5$	1.67	
	Siderite	$CFeO_3$	0.07	0.31
Two Medicine Fm.	Fluorapatite	$Ca_5FO_{12}P_3$	88.57	
	Calcite	$CaCO_3$	7.72	
	Carbonate-fluorapatite	$C_{0.03}Ca_{10.06}F_{2.03}O_{23.89}P_{5.95}$	3.71	0.45

Table 4.4: Linear combination fitting for Ca K-edge XANES spectra.

			Linear Combination Fitting						
Sample	Age	Depositional Environment	CaO	NIST CaHAP	Selenite	FAP (Ward's)	Calcite (Ward's)	Calcite (Sigma)	Peak B/C Ratio
SWK1	modern	n/a	0.032	0.015	0	0.191	0	0.762	1.79
SWK2	modern	n/a	0.020	0	0	0.288	0	0.692	1.67
PLO1.2	Pleistocene	fluvial	0	0	0	1.000	0	0	1.59
GFS1A	Late Miocene	sinkhole/lacustrine	0	0	0	0.907	0	0.093	2.11
GFS1B	Late Miocene	sinkhole/lacustrine	0	0.007	0.057	0.653	0	0.283	2.87
JR269	Campanian	fluvial	0	0	0.021	0.644	0	0.315	2.26
TM728899	Campanian	overbank	0	0	0	1.000	0	0	2.26

References

Bergstrom, W.H., Wallace, W.M., 1954. Bone as a sodium and potassium reservoir. J Clin Invest 33, 867-873.

Bergmann, U., Morton, R.W., Manning, P.L., Sellers, W.I., Farrar, S., Huntley, K.G., Wogelius, R.A., Larson, P., 2010. Archaeopteryx feathers and bone chemistry fully revealed via synchrotron imaging. Proc Natl Acad Sci U S A 107, 9060-9065.

Berna, F., Matthews, A., Weiner, S., 2004. Solubilities of bone mineral from arhcaeological sites: the recrystallization window. J Archaeol Sci 31, 867-882.

Cazorla-Amoros, D., Linaressolano, A., Delecea, C.S., Yamashita, H., Kyotani, T., Tomita, A., Nomura, M., 1993. XAFS and thermogravimetry study of the sintering of calcium supported on carbon. Energ Fuel 7, 139-145.

Child, A.M., 1995. Microbial taphonomy of archaeological bone. Stud Conserv 40, 19-30.

Eichert, D., Salome, M., Bleuet, P., Bohic, S., Susini, J., 2006. Contribution of X-ray microscopy to bone mineral studies, IPAP Series 7, 210-212.

Eiden-Assmann, S., Viertelhaus, M., 2000. In-situ XANES spectroscopy at the Ca K edge of calcium phosphate compounds, HASYLAB-Jahresbericht, 1999. HASYLAB/DESY, Hamburg, 2 pp.

Elliott, J.C., 2002. Calcium phosphate biominerals. Rev Mineral Geochem 48, 427-453.

Engel, A.S., Lichtenberg, H., Prange, A., Hormes, J., 2007. Speciation of sulfur from filamentous microbial mats from sulfidic cave springs using X-ray absorption near-edge spectroscopy. FEMS Microbiol Lett 269, 54-62.

Farlow, J.O., Argast, A., 2006. Preservation of fossil bone from the Pipe Creek Sinkhole (Late Neogene, Grant County, Indiana, U.S.A.). J Paleontol Soc Korea 22, 51-75.

Fleet, M.E., Pan, Y.M., 1995. Site preference of rare earth elements in fluorapatite. Am Mineral 80, 329-335.

Franke, R., Hormes, J., 1995. The P K-near edge absorption spectra of phosphates. Physica B 216, 85-95.

Goodwin, M.B., Grant, P.G., Bench, G., Holroyd, P.A., 2007. Elemental composition and diagenetic alteration of dinosaur bone: distinguishing micron-scale spatial and compositional heterogeneity using PIXE. Palaeogeogr Palaeocl 253, 458-476.

Green, J., Kleeman, C.R., 1991. Role of bone in regulation of systemic acid-base balance. Kidney Int 39, 9-26.

Hamilton, D.L., 1999. Methods for conserving archaeological material from underwater sites. Texas A&M University, College Station, Texas.

Hormes, J., Scott, J.D., Suller, V., 2006. Facility update: the Center of Advanced Microstructures and Devices, a status report. Synchrotron News 19, 27-30.

Hubert, J.F., Panish, P.T., Chure, D.J., Prostak, K.S., 1996. Chemistry, microstructure, petrology, and diagenetic model of Jurassic dinosaur bones, Dinosaur National Monument, Utah. J Sediment Res 66, 531-547.

Jiang, M., Terra, J., Rossi, A.M., Morales, M.A., Saitovitch, E.M.B., Ellis, D.E., 2002. Fe^{2+}/Fe^{3+} substitution in hydroxyapatite: theory and experiment. Phys Rev B 66, DOI:http://dx.doi.org/10.1103/PhysRevB.66.224107.

Koenig, A.E., Rogers, R.R., Trueman, C.N., 2009. Visualizing fossilization using laser ablation-inductively coupled plasma-mass spectrometry maps of trace elements in Late Cretaceous bones. Geology 37, 511-514.

Kohn, M.J., 2008. Models of diffusion-limited uptake of trace elements in fossils and rates of fossilization. Geochim Cosmochim Acta 72, 3758-3770.

Kolodny, Y., Luz, B., Sander, M., Clemens, W.A., 1996. Dinosaur bones: fossils or pseudomorphs? The pitfalls of physiology reconstruction from apatitic fossils. Palaeogeogr Palaeocl 126, 161-171.

Laurencin, D., Wong, A., Chrzanowski, W., Knowles, J.C., Qiu, D., Pickup, D.M., Newport, R.J., Gan, Z., Duer, M.J., Smith, M.E., 2010. Probing the calcium and sodium local environment in bones and teeth using multinuclear solid state NMR and X-ray absorption spectroscopy. Phys Chem Chem Phys 12, 1081-1091.

Leikina, E., Mertts, M.V., Kuznetsova, N., Leikin, S., 2002. Type I collagen is thermally unstable at body temperature. Proc Natl Acad Sci U S A 99, 1314-1318.

Munro, L.E., Longstaffe, F.J., White, C.D., 2007. Burning and boiling of modern deer bone: effects on crystallinity and oxygen isotope composition of bioapatite phosphate. Palaeogeogr Palaeocl 249, 90-102.

Olszta, M.J., Cheng, X.G., Jee, S.S., Kumar, R., Kim, Y.Y., Kaufman, M.J., Douglas, E.P., Gower, L.B., 2007. Bone structure and formation: a new perspective. Mat Sci Eng R 58, 77-116.

Pan, Y.M., Fleet, M.E., 2002. Compositions of the apatite-group minerals: Substitution mechanisms and controlling factors. Rev Mineral Geochem 48, 13-49.

Person, A., Bocherens, H., Saliege, J.F., Paris, F., Zeitoun, V., Gerard, M., 1995. Early diagenetic evolution of bone phosphate: an X-ray diffractometry analysis. J Archaeol Sci 22, 211-221.

Peters, F., Schwarz, K., Epple, M., 2000. The structure of bone studied with synchrotron X-ray diffraction, X-ray absorption spectroscopy and thermal analysis. Thermochim Acta 361, 131-138.

Pfretzschner, H.U., 2004. Fossilization of Haversian bone in aquatic environments. Cr Palevol 3, 605-616.

Pouchou, J.-L., Pichoir, F., 1991. Quantitative analysis of homogeneous or stratified microvolumes applying the model “PAP”. Electron probe quantitation, Springer US, pp. 31-75.

Pucéat, E., Reynard, B., Lécuyer, C., 2004. Can crystallinity be used to determine the degree of chemical alteration of biogenic apatites? Chem Geol 205, 83-97.

Pyle, J.M., Spear, F.S., Wark, D.A., 2002. Electron microprobe analysis of REE in apatite, monazite and xenotime: protocols and pitfalls. Rev Mineral Geochem 48, 337-362.

Rajendran, J., 2011. XANES and FTIR study on dried and calcined bones, Materials Science and Engineering. Masters Thesis, University of Texas at Arlington, Arlington, TX, p. 108.

Ravel, B., Newville, M., 2005. Athena, Artemis, Hephaestus: data analysis for X-ray absorption spectroscopy using Ifeffit. J Synchrotron Radiat 12, 537-541.

Reiche, I., Chalmin, E., 2008. Synchrotron radiation and cultural heritage: combined XANES/XRF study at Mn K-edge of blue, grey or black coloured palaeontological and archaeological bone material. J Anal Atom Spectrom 23, 799-806.

Rollin-Martinet, S., Navrotsky, A., Champion, E., Grossin, D., Drouet, C., 2013. Thermodynamic basis for evolution of apatite in calcified tissues. Am Mineral 98, 2037-2045.

Salbu, B., Janssens, K., Lind, O.C., Proost, K., Gijsels, L., Danesi, P.R., 2005. Oxidation states of uranium in depleted uranium particles from Kuwait. J Environ Radioact 78, 125-135.

Shunk, A.J., Driese, S.G., Dunbar, J.A., 2009a. Late Tertiary paleoclimatic interpretation from lacustrine rhythmites in the Gray Fossil Site, northeastern Tennessee, USA. J Paleolimnol 42, 11-24.

Sponheimer, M., Lee-Thorp, J.A., 1999. Alteration of enamel carbonate environments during fossilization. J Archaeol Sci 26, 143-150.

Trueman, C.N., Benton, M.J., 1997. A geochemical method to trace the taphonomic history of reworked bones in sedimentary settings. Geology 25, 263-266.

Trueman, C.N., Privat, K., Field, J., 2008. Why do crystallinity values fail to predict the extent of diagenetic alteration of bone mineral? Palaeogeogr Palaeocl 266, 160-167.

Trueman, C.N.G., Behrensmeyer, A.K., Tuross, N., Weiner, S., 2004. Mineralogical and compositional changes in bones exposed on soil surfaces in Amboseli National Park, Kenya: diagenetic mechanisms and the role of sediment pore fluids. J Archaeol Sci 31, 721-739.

Tutken, T., Pfretzschner, H.U., Vennemann, T.W., Sun, G., Wang, Y.D., 2004. Paleobiology and skeletochronology of Jurassic dinosaurs: implications from the histology and oxygen isotope compositions of bones. Palaeogeogr Palaeocl 206, 217-238.

Voegelin, A., Kaegi, R., Frommer, J., Vantelon, D., Hug, S.J., 2010. Effect of phosphate, silicate, and Ca on Fe(III)-precipitates formed in aerated Fe(II)- and As(III)-containing water studied by X-ray absorption spectroscopy. Geochim Cosmochim Acta 74, 164-186.

Wang, C., Eisa, M.H., Jin, W., Shen, H., Mi, Y., Gao, J., Zhou, Y., Yao, H., Zhao, Y., 2008. Age-related elemental change in bones. Nucl Instrum Meth B 266, 1619-1622.

Weiner, S., Bar-Yosef, O., 1990. States of preservation of bones from prehistoric sites in the near-East: a survey. J Archaeol Sci 17, 187-196.

Chapter 5: Reconstructing site diagenetic conditions from fossil bone geochemistry

Some of the results of this chapter will be submitted for publication in Palaeogeography, Palaeoclimatology, Palaeoecology, with a preliminary citation of: Keenan, S.W. and Engel, A.S., Reconstructing the site diagenetic conditions from fossil bone geochemistry.

SWK processed samples, collected data, conducted data analysis, and wrote the manuscript. ASE assisted with data analysis and wrote the manuscript.

Abstract

The preservation of vertebrate fossils requires the diagenetic transformation of bioapatite, predominantly the mineral hydroxyapatite, into a thermodynamically more stable phase. When preserved, fossil bone geochemistry and structure provides information about diagenetic conditions. Preservation of lacustrine paleoclimate records during the Cenozoic is relatively rare in North America. The Gray Fossil Site represents a succession of Late Neogene lacustrine deposits that contains a diverse biotic assemblage and a paleoclimatae record for eastern North America. To complement previous studies describing flora and fauna recovered from the site, sedimentology, and site accumulation history, the geochemistry of *Alligator* sp. phalanges was examined to provide insight into site diagenetic conditions. Electron microprobe analyses, X-ray diffraction, and Fourier-transform infrared spectroscopy, indicate that the fossils are recrystallized and enriched in F and Fe^{2+}, forming heterogeneous fluorinated and Fe-apatite phases. Bones contain evidence of bioerosion within the trabecular region, suggesting biotic utilization of collagen and organic material following deposition under suboxic to oxic conditions. The preservation of chemically zoned and laminated cortical bone reflects lines of arrested growth developed during life, and supports previous interpretations of regional

seasonality. Based on these combined analytical approaches, the diagenetic conditions preserving bone at the Gray Fossil Site were likely acidic, anoxic to suboxic, and reducing. These results highlight the utility of integrating multiple geochemical tools to reconstruct paleoenvironments to enhance understanding of bone preservation over geologic time.

Introduction

The preservation of bones as fossils is linked to a suite of physical and geochemical conditions, including pH, temperature, redox, and ionic strength, that facilitate the transformation of the organic and inorganic phases of bone, predominately bioapatite, into recrystallized and mineralized forms of apatite. Bone diagenesis is far from straight forward and varies from site to site (e.g., Zapata et al., 2006). In terrestrial systems, bones have been preserved in a range of depositional environments, including rivers (e.g., Behrensmeyer, 1988), lakes (e.g., Wallace and Wang, 2004), floodplains or wetlands (e.g., Keenan and Scannella, 2014), sinkholes (e.g., Laury, 1980), and even within speleothems in caves (e.g., Auler et al., 2006). But, distinct geochemical and diagenetic conditions, including water and sediment composition, rates of sedimentation, and depositional environment, operated in each setting to facilitate the transformation of bioapatite to fossil apatite (e.g., Trueman, 2013).

Bone is a biomineral comprised of interlayered organic material (collagen, lipids) and a mineral fraction (hydroxyapatite or HAP [$Ca_{10}(PO_4)_6(OH)_2$]). In life, the presence of collagen serves several functions for a vertebrate, including nucleation sites for HAP or sites for the formation of an amorphous precursor calcium phosphate phase that develops into non-stoichiometric HAP (Olszta et al., 2007). The intimate association of organics, predominantly type I collagen, with HAP imparts bone with characteristic strength and flexibility in life (Burr, 2002; Viguet-Carrin et al., 2006). The composition of fresh, unaltered bone generally consists of

20-30% collagen, non-collagenous proteins, and water, with the remaining 70-80% consisting of non-stoichiometric hydroxyapatite or carbonated apatite (e.g., Wopenka and Pasteris, 2005). Collagen fibers are arrayed parallel and staggered, resulting in either a series of regularly-spaced gaps or grooves between collagen molecules (Fratzl et al., 2004; Olszta et al., 2007). The spaces between collagen fibrils provide the sites for apatite mineral development, ultimately forming an inter-layered organic and mineral biomineral.

Once removed from a living organism, bone undergoes alteration via numerous and varied substitutions and replacements at potentially every site within the apatite mineral lattice largely driven by the decay and loss of collagen. Alteration results in a diverse mineral assemblage (Pan and Fleet, 2002). The replacement site(s) depends on several variables including the ionic radius of the substituting ion, charge balance within the lattice, local electrostatic repulsion, and other ions already incorporated into the lattice (Fleet and Pan, 1995; Jiang et al., 2002). Calcium occupies two distinct sites: nine-coordinated type I and seven-coordinated type II (Pan and Fleet, 2002). Type II Ca sites share a bond with oxygen from hydroxyl ions, while type I sites are associated with PO_4^{3-} (Trueman et al., 2008). During diagenesis, CO_3^{2-} ions are incorporated into the HAP lattice, forming a carbonated apatite phase. Carbonate incorporation largely occurs at the expense of PO_4^{3-}, forming type B carbonate associated with the type I Ca sites, and OH^-, forming type A carbonate associated with the type II Ca sites (Sponheimer and Lee-Thorp, 1999; Trueman et al., 2008). For metal substitutions, both Ca sites can be replaced by monovalent (Na^+), divalent (Fe^{2+}, Sr^{2+}, Mn^{2+}), trivalent (Fe^{3+}, REE^{3+}), tetravalent (U^{4+}), and hexavalent (U^{6+}) cations (Pan and Fleet, 2002). Both PO_4^{3-} and OH^- may undergo protonation at the mineral surface, providing a mechanism to open the lattice to exchanges with CO_3^{2-} (Rollin-Martinet et

al., 2013). Additionally, replacement of OH^- by F or Cl results in the formation of fluorapatite or chlorapatite, phases frequently observed in fossil bone (e.g., Hubert et al., 1996; Table C.2).

The goal of this study was to evaluate bone geochemistry using Fourier transform infrared spectroscopy (FTIR), electron microprobe analysis (EMP), and X-ray diffraction (XRD) to develop a diagenetic history for bones. Bones were obtained from the Gray Fossil Site (GFS), Gray, Tennessee, USA (Fig. 5.1), which contains plants and animals preserved in lacustrine deposits that accumulated in a paleosinkhole. Based on sediment characterization from exposures and cores (Shunk et al., 2006; Shunk et al., 2009a), and subsurface geophysical studies with high resolution gravity surveys (Whitelaw et al., 2008), the site is approximately 150 m in diameter with depths ranging from 11 to 42 m (Whitelaw et al., 2008). GFS represents one of two localities east of the Mississippi River that preserves terrestrial flora and fauna from the Late Miocene to Pliocene (~7.0-4.5 Ma). This period in Earth's recent climatic history is marked by the transition from globally high to cooler temperatures associated with extensive glaciation, during which grasses and C4 vegetation dominated much of North America (Cerling et al., 1993; Cerling et al., 1997). Few terrestrial deposits preserve information on the biotic responses (e.g., population dynamics, localized extinction or migration events) to climate change at this time, thereby making the GFS an important locality since its discovery in 2000.

Refined models of (paleo)climatic change in the region have resulted from oxygen isotope measurements from teeth (DeSantis and Wallace, 2008) and the presence of warm- and cold-adapted plant species (Wallace and Wang, 2004). These records suggest temperatures and/or precipitation did not exhibit substantial seasonal variations. Other interpretations drawn from sedimentology and facies associations suggest that there was a more varied, seasonal climate (e.g., Shunk et al., 2006; Shunk et al., 2009a). There is some evidence that the paleolake at the

sinkhole could have been oxic (e.g., Zobaa et al., 2011) or suboxic to anoxic (e.g., Shunk et al., 2009a), and that anoxia may have facilitated the preservation of plant-derived organic material.

Gray Fossil Site bone major element geochemistry, composition, and structure have not been previously investigated. Geochemical details from the bone may help constrain GFS geochemistry during early diagenesis of bone, as well as mechanisms that resulted in bone preservation. This research addressed several questions, including to what extent do bones inform site diagenetic conditions, specifically paleolake redox, and what was the accumulation history of the GFS (e.g., rapid burial vs. protracted sedimentation)? Additionally, compared to a similar paleosinkhole deposit, the Pipe Creek Sinkhole, Indiana, which spans the same geologic interval, are there any commonalities with respect to chemical changes expected in bone preserved in karst sinkhole systems?

Gray Fossil Site geology and formational history

Sinkholes and caves are widespread in the karst terrain of East Tennessee, as modern (Moore, 2006) and relict features (Zobaa et al., 2011). GFS is located within the Valley and Ridge province, characterized by northeast- to southwest-trending valleys and ridges reflecting regional structural controls (Whitelaw et al., 2008). The region is underlain by Ordovician-aged Knox Group limestone and dolomite units, which outcrop extensively from Alabama to New York, and that represent a marginal marine depositional environment (Clark et al., 2005). GFS is a paleokarst feature that represents relic weathering and paleosinkhole formation. Today, the paleosinkhole lacustrine deposits occur as topographic highs reflecting weathering of unconsolidated sediment and soluble carbonate facies that surround the paleosink deposits.

Because sinkholes and caves can serve as sediment traps, they provide an invaluable resource to evaluate climatic conditions (Shunk et al., 2009b; Worobiec and Szulc, 2010; Soriano et al., 2012) and, occasionally, surface-derived or cave-dwelling biotic communities (Laury, 1980; Lundelius, 2006). Geochemical characterization of sinkhole sediments, including stratigraphy and textural analysis (Shunk et al., 2009a), as well as isotopic analyses of sediment and mammal teeth (DeSantis and Wallace, 2008), and geophysical gravity anomaly surveys (Whitelaw et al., 2008) have provided evidence for the GFS formational history. Gravity anomaly surveys suggest at least 11 smaller sinkholes (Whitelaw et al., 2008). The largest paleosink feature likely formed from progressive collapse of underlying subsurface voids (i.e. caves), then collection of meteoric water to form a lake, followed by sediment infill (see Figure 2 from Shunk et al., 2006). The presence of angular limestone boulders mixed within, and disrupting bedding of, lacustrine deposits likely represents collapse, similar to the Pipe Creek Site, Indiana (Shunk et al., 2009b). Unlike the Mammoth Site in Hot Springs, South Dakota, there is no evidence of miring at GFS (Laury, 1980).

Rhythmite facies sediments (Shunk et al., 2006), predominantly gray to brown clay at ~ 29 m depth, transitions to laminated, organic-rich, and silty dark gray clay up section (Clark et al., 2005; Shunk et al., 2009a; Zobaa et al., 2011). Sediment mineralogy includes clay minerals interbedded with quartz, chert, feldspar, dolomite, reworked paleosol fragments, as well as minor occurrences of siderite, pyrite, gypsum, and Fe-and Mn-oxides (Shunk et al., 2006). Sediment microtextural analyses, inferred seasonal deposition, and progressive sediment infill rates have resulted in an estimate of between 0.30 and 0.74 cm material deposited per year, and that the lake may have persisted for ~ 4,500 to 11,000 years (Shunk et al., 2009a). Based on the preservation of graded and laminated sediments with pyrite and the absence of bioturbation, Shunk et al.

(2006) suggest that the paleolake bottom waters were poorly oxygenated. Some sediment intervals, the 'graded facies' of Shunk et al. (2006), contain partially oxidized organic material, which indicates that perhaps the water column was oxygenated and that the lake bottom was occasionally fully oxygenated (Zobaa et al., 2011).

Disarticulated and articulated bones of diverse terrestrial, semi-aquatic, and aquatic fauna preserved at GFS are found throughout the paleosink lacustrine deposits that have been uncovered to date. Bones are generally low density and fragile, dark brown to brownish-orange, and pore spaces do not contain secondary phases. The bones when collected are black and rapidly oxidize to a brownish color within minutes (Moore, 2004). The specimens are low density and contain no evidence of secondary infilling within pore spaces, suggesting limited recrystallization. But, to our knowledge, the composition of these bones has not been previously described. Although much of the formational history of the GFS has been resolved, there are still significant gaps in our understanding of the diagenetic conditions that facilitated bone fossilization and preservation. The high density and high diversity of vertebrate remains, with over 30 vertebrate species identified (Mead et al., 2012), provides unrivaled insight into climate, vegetation, and animal biodiversity in eastern North America during the Late Neogene. At the time, the GFS location had comparable fauna and climate to that of southern China today based on a similar fossil assemblage of plants (e.g., grape vines; Gong et al., 2010) and animals (e.g., red panda; Wallace and Wang, 2004; Wang and Wallace, 2004) compared to extant taxa.

However, uncertainty remains as to whether populations preserved at GFS reflect a local "refugia" (Wallace and Wang, 2004; DeSantis and Wallace, 2008), with animals perhaps restricted to the sinkhole region, or whether populations had greater biogeographic range than today, but lacked a fossil record, reflecting non-preservation or discoveries yet to be made. An

alternative hypothesis to the inferred seasonal lake infilling, also based on sedimentology and sediment textural analyses and stable isotope geochemistry of mammal teeth from GFS, suggests that the site experienced uniform precipitation and temperatures annually (DeSantis and Wallace, 2008). While the primary goal of this study was not to evaluate paleoclimate, *Alligator* sp. bone major- and trace-element geochemistry has the potential to inform regional conditions in the Late Tertiary during paleolake formation and infill. Modern alligators undergo seasonal growth, driven largely by ambient temperature changes leading to physiological responses including cessation of feeding and reduced physical activity (e.g., Lang, 1979). During periods of active movement, high metabolism, and feeding, modern alligators form bone, while during cooler months bone deposition rates decrease, resulting in the formation of lines of arrested growth (LAGs) (Woodward et al., 2011). These features are recognized to develop in modern (Woodward et al., 2011) as well as fossil reptilian taxa (Horner et al., 1999; Kohler et al., 2012). Therefore the presence of LAGs in GFS bones would support interpretations of a variable climate, similar to that observed today across much of the southeastern United States.

Materials and methods

Sample preparation

Fragments (n = 5; from 1.1 to 1.5 g) of *Alligator* sp. phalanges collected from GFS in 2001, shortly after the site's discovery in 2000 during highway construction (Clark et al., 2005). Fossils were held at the McClung Museum of Natural History and Culture, on the University of Tennessee, Knoxville, campus. Permission to analyze the bones to assess structure and composition, including major and selected minor element chemistry, was granted by the McClung Museum. There was no information if the bones originated from one or multiple

individuals. However, all samples were collected at the same time from a single location and stratigraphic unit at the site. Therefore, we assumed that the bones experienced similar early diagenetic conditions. Although no sediment was visible on GFS bone surfaces, bone fragments were cleaned to remove any particles or dust, then gently wiped clean with 70% reagent-grade ethanol and allowed to air dry. Two fragments were selected for thin sections and three fragments were powdered in an agate mortar and pestle. To prevent contamination, all cleaning and processing was done aseptically. Powdered bone aliquots were stored under sterile conditions until analysis.

To evaluate the extent of geochemical and structural changes that GFS alligator bones underwent compared to modern bones, as well as to compare bone composition, vertebrae from an alligator salvaged from the Rockefeller Wildlife Refuge (under the Louisiana Natural Heritage Program, permit LNHP-10-009) were included in this study. Vertebrae were treated by removing soft tissues with dermestid beetles. Any remaining organic detritus was manually removed, then rinsed in deionized (DI) water, placed into a sonicator (Branson 2510) filled with DI water for 60 min, dried using a critical drying method, starting at 70% reagent grade ethanol (Hamilton, 1999), and left to dry at 37°C for 24 hr. Bones were cut in half using a Dremel handsaw. Half of the material was powdered for FTIR and XRD, using the same protocol as for the GFS samples, and the other half of the sample was prepared for EMP analysis, as outlined below.

FTIR and XRD analyses

FTIR can assess the structure and composition of bones, particularly the amount and location of carbonate incorporation, and changes to crystallinity and crystal ordering, all of which

provides information on the conditions present during diagenesis (Sponheimer and Lee-Thorp, 1999; Trueman et al., 2004; Trueman et al., 2008). Structural and compositional data were obtained using FTIR and XRD from powdered samples at the University of Tennessee, Department of Earth & Planetary Sciences. FTIR analyses were run on an Agilent Cary 660 FTIR using a diffuse reflectance accessory. Powdered bone samples were mixed with KBr (1-5 % sample, 99-95 % KBr) and transferred to a stainless steel sample holder, according to manufacturer instructions. Each sample was measured at least five times and fresh powders mixed for each analysis. Spectra were measured with a resolution of 4 cm^{-1} and 32 scans per analysis. The resulting dataset for each sample was averaged using ResolutionsPro software, and the averaged spectra were used for data analyses. Following previously published methods, calculations were done for crystallinity (IRSF) (Weiner and Bar-Yosef, 1990), mean crystal length (nm) (Trueman et al., 2004), amide content (Am/P), organic weight % (Trueman et al., 2008), carbonate/phosphate ratio (Pucéat et al., 2004), and carbonate content (ratio of type B carbonate to the primary phosphate peak [BPI], type A carbonate to the primary phosphate peak [API], and the ratio of type B carbonate to type A carbonate [BAI]) (Sponheimer and Lee-Thorp, 1999).

X-ray diffraction (XRD) analyses of powdered bone samples (from 20 to 100 mg) were conducted on a Rigaku Ultimate IV X-ray diffractometer under 40 kV and 30 mA operating conditions with a continuous scan speed of 2° per minute. Samples were scanned from 4° to 70° 2θ with Cu Kα radiation. The same powdered samples examined with FTIR were placed onto a glass sample holder and inserted into the instrument, according to manufacturer instructions. Diffractograms were input into the Rigaku software package PDXL for peak identification, characterization of mineralogy, and calculation of mineral content (%). The crystallinity index

(CI) was calculated following the methods of Person et al. (1995) and Munro et al. (2007) using the diffractograms.

EMP analyses

Electron microprobe studies of modern and fossil bone can quantitatively assess major, minor, and, if above the detection limit, trace element composition and compositional zoning of the mineral phase(s) (Hubert et al., 1996; Tutken et al., 2004). In modern bone, approximately 30% of the bulk composition consists of organic carbon, lipids, and water. This will result in EMP totals of ~70% (Table 1). In fossilized bone, consistently low totals can also reflect the incorporation of carbonate into the mineral lattice, either structurally or as secondary carbonate phases within pore spaces. Despite low totals, however, EMP analysis is a useful approach to quantify bulk-element chemistry (Hubert et al., 1996; Tutken et al., 2004), and provides an easily accessible and relatively rapid tool to visualize elemental distributions within mineral phases.

After bone cleaning, two phalange fragments were embedded in resin (EpoThin Epoxy Resin, Buehler) under vacuum in a glass desiccation chamber to ensure complete diffusion of resin into pore spaces and to remove any air bubbles. Once set, sections were polished with progressively finer grit sizes from 240 to 600 by hand using an abrasive belt grinder (Buehler) and a MiniMet (Buehler) polisher to achieve a final uniform surface of 1 μm using MetaDi (monocrystalline diamond suspension, Buehler). Mosaic maps of the sections with reflected light were constructed to guide EMP analyses. Sections were carbon coated for EMP analysis, which was done on a Cameca SX-100 EMP at the University of Tennessee, Department of Earth & Planetary Sciences. Quantitative analyses of major (P, Ca, Na), minor (Mn, Mg, Fe, S, Si, Al), and trace (La, Ce, Cl) element chemistry and element mapping were done to visualize the

distribution of selected major elements. Prior to the start of analyses, instrument calibration and accuracy were checked by measuring known standards and re-calibrating when an element was less than 98% of the anticipated weight percent. Spot analyses under standard operating conditions (Pyle et al., 2002) (i.e. an electron beam of 10 nA and an accelerating potential of 15 kV), with 10 μm spot size, provided quantitative measures of apatite chemistry. Elements were analyzed in a fixed order under the same spectrometer conditions (Table C.1). Count times for each element ranged from 20 sec for major elements to 60 sec for minor and trace elements (Supplementary Table 1). Data were internally corrected using PAP, an approach similar to ZAF that accounts for the effects of atomic number (Z), absorption (A), and fluorescence (F), with the Cameca software PeakSight. Detection limits (3σ) for each element calculated by PeakSight ranged from ~ 150 ppm for Al to ~ 1000 ppm for F (Table C.1). Analytical precision is presented as standard deviations for each element, most of which are less than 20.

Despite appearing to be a uniform apatite composition under backscatter imaging, several elements, like Fe and Na, had standard deviations greater than 20. These high standard deviations did not correlate with low totals, which might be explained by analysis of a poorly polished area of the section or inclusion of a canal in the spot area. Element maps were constructed to visualize the potential sub-micron variation in apatite chemistry to complement spot analyses and to evaluate the potential for chemical heterogeneity of samples. Elements for element mapping were selected after examining the spot analysis data and noting that certain compounds (e.g., FeO, P_2O_5) had larger standard deviations than expected (>20), which reflected variable concentrations. Additional elements selected were Na, as NaO, because it has high mobility in living bone tissue and was expected to be mobile in an aqueous environment (Bergstrom and Wallace, 1954), and F, an element known to increase in apatite during

diagenesis. It should be noted there could have been potential biases with using EMP analysis to quantify F, as this ion can potentially be volatilized if beam current, count time, or time under vacuum are excessive (e.g., Pyle et al., 2002). Therefore, the overall trends in F concentrations are highlighted but absolute concentrations of F are likely higher in the GFS samples than in comparison samples (e.g., Pipe Creek). Several areas of cortical and trabecular bone were mapped to evaluate the variation of selected elements (Fe, P, Na, F, Ca). Maps were false colored using the Cameca software (PeakSight) to assess the changes in concentration visually, which are presented as changes to the number of counts measured by the detector. Brighter colors represent higher counts, or greater concentrations. False color element mixing also provided variations in multiple elements (e.g., P and Fe).

Comparative analyses

Comparisons of GFS bone geochemistry to the electron dispersive analysis (EDX) geochemical dataset from the Pipe Creek Sinkhole dataset (Farlow and Argast, 2006) required converting GFS bone data to weight percentages for each element according to their molar contribution for each oxide weight percent.

$$[(n * GFWx) / (GFWx_n o_{n'})] = mole\ fraction * wt.\%x_n o_{n'} = molar\ contribution$$

GFS data were also normalized to 100% on a C- and H-free basis, as implemented by Farlow and Argast (2006). Minor or trace elements (e.g. Ba, Sr, Ce, La, Cl) measured in this study by EMP analysis, but not examined by Farlow and Argast (2006), were excluded from the normalization process of the GFS dataset. These minor and trace elements contributed 0.42 wt. % to GFS bone geochemistry; excluding them to make the two datasets comparable resulted in total elemental concentrations within the standard deviation (2.7 wt. %).

Results

FTIR analyses

GFS alligator phalanges are structurally and compositionally different than modern bone (Table 5.1), which has been observed previously from other studies (e.g., Trueman et al., 2004). Mean crystal length increased from 41.5 nm in modern bone to 43.2-48.1 nm in fossil bone, which is due to increased individual crystallite size. IRSF, a measure of crystallite ordering, increased in GFS samples to 2.8 to 3.1, which indicated an overall increase in structural ordering compared to modern bone. As expected in fossil bone, organic weight % decreased from ~38% in modern alligator bone to ~16-18% in the GFS fossils. Decreased Am/P ratios also indicated a reduction in organics. GFS samples also had reduced carbonate/phosphate ratios compared to modern bone, which could have been the consequence of either an enrichment in carbonate content relative to phosphate or an overall loss of phosphate. Both the BPI and API ratios were lower than those from the unaltered bone. Lower ratios indicate the incorporation of carbonate at both Ca sites (I and II) resulting in type B and A substitutions in the apatite lattice. BAI ratios from GFS samples were depleted, likely due to higher amounts of carbonate incorporated into the B site.

XRD analyses

Powdered GFS samples were also characterized with XRD to verify mineral crystallinity and to evaluate mineralogy. GFS bones had CI values of 0.22 to 0.27, and were predominantly comprised of a fluorinated apatite phase (from 88.5 to 91.94%) (Table 5.2). Secondary phases detected included a Ca-Fe-PO_4 phase in the fossils. Because of the absence of infilling phases

within fossil bone pore spaces, the Fe was interpreted to be incorporated structurally within the apatite lattice to form a mixed Ca-Fe-PO_4 phases.

EMP analyses

Backscatter imaging of cortical and trabecular bone prior to chemical analysis with the EMP revealed numerous small (< 1 μm to 20 μm diameter) circular holes or pits and tube-like structures restricted to the trabecular region of the bone that extended several microns up to 100 μm from the bone surface inwards (Fig. 5.2A, B, C). The density and distribution of these features was non-uniform along the trabeculae. Pitting was not observed along the cortical bone margin (Fig. 5.2D).

Compared to modern bone, GFS material contained higher concentrations of Fe^{2+}, F, and lower Na (Table 3). In general, the elemental compositions of both the cortical and trabecular bone were heterogeneous. As observed from other fossils, F content increased from 0.07 wt. % in modern bone to ~ 2.00 wt. % in GFS samples. Overall total weight percent totals for modern bone were lower (~ 67-74 wt. %) than for fossil bones (~ 89 wt. %), which was expected because of the loss of organics (i.e. collagen). Spot analyses suggested a fairly uniform composition for all major and minor elements examined, with no distinct zonation, although high standard deviations (values > 20) for several elements, as oxide weight percent (e.g., FeO, P_2O_5), indicated that the samples may have had variable compositions.

The 10 μm spot size was determined to mask fine, μm-scale variations, which were identified by the element mapping. Bone composition examined by mapping selected elements (Na, Fe, P, and F) showed that the cortical region of the GFS bones, although comprised of fluorinated apatite (Fig. 5.3A), was compositional zoned at a <10 μm scale (Fig. 5.3C, E). P was relatively

uniform throughout the cortex from the P map, as P_2O_5 (Fig. 5.3B). By mixing Na, Fe, and P false color element maps, P, Na, and Fe concentrations were non-uniformly distributed throughout the cortex. There were areas with Fe enrichment within the apatite mineral, likely indicative of Fe-phosphate phases. Portions of the cortex with enriched Fe were also zones where Na was depleted, which hinted to mechanism that would incorporate Fe due to the loss of Na in the original apatite. Zones of high and low Fe content alternated, and were opposite of Na content, based on separate Fe and Na maps (Figs. 5.3C, D), and element mixing of Fe, Na, and P (Fig. 5.3E).

Several areas of the trabeculae (Figs. 5,4, 5.5) were chemically variable, as well. However, in contrast to the cortex, trabecular bone chemical variations did not appear to follow a clear zonation pattern. Fe was enriched around some osteon microstructures, but not in other areas (Fig. 5.4). Mixed element maps of an osteon within trabecular bone (Fig. 5.4B, C) showed preserved chemical variations within GFS bone. Additional element maps around a heavily pitted sections of the trabeculae revealed lower Fe and P concentrations but Na content was unaffected (Fig. 5.5 A, B, C).

Comparison of bones from the Gray Fossil Site and the Pipe Creek Sinkhole

The Pipe Creek Sinkhole (PCS), in Grant County, Indiana, preserves a Late Neogene record of terrestrial fauna and flora deposited within a paleosinkhole and lacustrine system, analogous to the interpreted depositional environment of the GFS (Shunk et al., 2009b). We compared the available bone geochemical data from PCS (Farlow and Argast, 2006) with GFS bone EMP data to assess if bones preserved in similar sinkhole depositional systems had comparable fossilization chemistry, particularly with respect to the incorporation of Fe (Table 5.4). Bones

preserved at both sites contained comparable concentrations of Ca, P, and little to no detectable Si (Table 5.4). Fossils recovered from both sites contained elevated concentrations of F, with an average of 3.51 and 2.26 wt. % observed in PCS and GFS samples, respectively. Alligator phalanges from GFS were 2 to 3 times enriched in Fe compared to PCS material. In contrast, Mn was an order of magnitude more enriched PCS samples than GFS bones (Table 5.4).

Discussion

Deciphering site geochemical conditions during early diagenesis that likely facilitated long-term preservation of bone is a formidable challenge to paleobiologists (Pate et al., 1989; Berna et al., 2004; Trueman, 2013). By combining several analytical approaches, it is possible to use the preserved bones themselves as an archive of site diagenetic conditions. The major and trace element chemistry, particularly for redox sensitive elements like Fe, inform oxygenation state of the surrounding fluids during diagenesis. Bone microstructure and morphology provide insights into physical or chemical alteration to bone post-mortem, and can be used to constrain the timing of diagenesis.

Geochemical composition of GFS bone

The first aim of this study was to evaluate the chemistry and structure of bones preserved at GFS. Quantitative data obtained with EMP through spot analyses revealed Fe and F enrichment in the GFS bones, transforming the original hydroxyapatite into a fluorinated and Fe-enriched phase. Additional support for the structural incorporation of Fe from XRD analyses indicated the formation of mixed Ca-Fe-PO_4 phases. Element mapping highlighted that diagenetic alteration to

the original HAP followed pre-existing microstructural and potentially chemical variation in the cortical bone, while alteration in the trabecular region was more heterogeneous.

In addition to chemical changes, the GFS bone has undergone recrystallization, as demonstrated by FTIR, XRD, and EMP. Both measures of GFS fossil CI were similar for all bones examined, with CI values from XRD between 0.24 and 0.27, and based on FTIR analyses, from 2.9 to 3.1. For samples examined with XRD, CI values between 0.00 and 0.15 are characterized as unaltered, while samples with values between 0.16 and 1.30, including the GFS samples, are considered altered (e.g., recrystallized) (Person et al., 1995; Munro et al., 2007). The similar crystallinity values obtained for all samples with XRD and FTIR suggest that these bones experienced similar conditions during recrystallization and diagenesis.

Bioerosion and implications for timing of diagenesis

In archaeological and paleontological studies of bone histology, the presence of pits or tunnels is invariable ascribed to the activity of microorganisms (e.g., Child, 1995; Jans et al., 2004; Jans, 2008). The circular pits and tunnels abundant within the trabeculae of GFS bone are interpreted as evidence of bioerosion (Fig. 5.1), reflecting the activity of microorganisms and/or invertebrates following burial in the sinkhole lake. The presence of borings indicates either biotic utilization of the mineral or organic fraction of the bone during diagenesis, or biotic removal of the mineral phase after fossilization. While the exact timing—either syn-diagenetic or post-recrystallization—cannot be determined, the lack of borings on the cortical surface would suggest that colonization by microorganisms or invertebrates occurred during early diagenesis and burial when organic material (e.g., collagen, lipids) were still present within the bone. If the borings were made following initial burial within the paleolake, this would suggest at least

partial oxidation of the substrate, allowing for the colonization of the bone surface. Additionally, the preferential bioerosion within the trabecular region, with larger pore sizes and a more accessible source of organic material, suggests that organic compounds rather than inorganic elements like Ca^{2+}, PO_4^{3-}, or HPO_4^{2-} were actively scavenged during early diagenesis. Soft tissues (e.g., muscle, adipose tissue, skin) likely degraded rapidly following burial (e.g., Dent et al., 2004), leaving more difficult to access organics like collagen within the trabeculae.

The preservation of bone with extensive bioerosion provides additional insight into the timing or rate of burial and diagenesis. The presence of bioerosion suggests that bone remained within the oxic to sub-oxic water-sediment interface for a protracted period of time, permitting colonization by organisms. Increased surface area as a result of bioerosion would be expected to enhance dissolution of the mineral phase, suggesting that in order for the preservation of compromised bone, subsequent removal from erosive biotic activity must have occurred relatively early during burial and diagenesis. Preservation of bone with evidence of bioerosion in the terrestrial vertebrate fossil record is rare (Trueman and Martill, 2002; Turner-Walker, 2012), and would suggest that burial and diagenesis, transforming the original hydroxyapatite into a more stable phase(s) must have occurred relatively soon following bioerosion. The interpreted seasonality of sediment input into the paleolake may have served as a mechanism to remove a shallowly-buried bone from oxic-suboxic conditions to more anoxic sediments at depth, restricting further biotic activity.

EMP analyses: retention of a biogenic signal

The application of EMP to evaluate bone geochemistry and structure not only provides information on the geochemical conditions during diagenesis reflected by the major- and trace-

element chemistry of the apatite, but may also be used to evaluate original, biogenic signatures developed during the life of the organisms. The preservation of alternating chemically zoned laminations in the cortical bone from GFS suggests that some underlying heterogeneity existed within the apatite prior to burial and diagenesis, facilitating the formation of chemically distinct laminae. The preservation of chemically distinct zones within the cortical bone therefore likely reflects LAGs developed during life. Perhaps rapid growth resulted in the deposition of apatite crystals of different size or structure, underlying physical differences that facilitated variable diagenetic alteration in the form of ion uptake and replacement. Additionally or alternatively, the original LAGs may have been chemically distinct, reflecting variations in element incorporation during periods of rapid and limited bone deposition, corresponding to a seasonally variable climate resulting in intervals of feeding or fasting. Subsequent diagenesis may have enhanced any original, biogenic chemical differences between layers of bone, preserving laminations as chemically distinct zones.

Reconstructing site diagenetic conditions

One of the goals of this research was to reconstruct potential site geochemical conditions using the geochemistry of bones preserved at the site. One important geochemical parameter that has the potential to exert significant control on apatite mineral stability is redox (Nielsen-Marsh and Hedges, 2000). In particular, for redox sensitive elements like iron, the apatite lattice can accommodate both valencies at both Ca sites (Jiang et al., 2002), and determining the valency of the incorporated iron is not straight-forward, but has the potential to inform overall site redox conditions during diagenesis. The most likely positions for Fe incorporation in the apatite lattice are the Ca sites, based on charge balance and similar ionic radii (Pan and Fleet, 2002). In a study

evaluating *in vitro* iron uptake in bone and teeth, uptake by tooth enamel maintained the valency of the solution (Bauminger et al., 1985). While the *in vitro* uptake by bone was not assessed, the results of the enamel experiments suggest that once iron is incorporated into bone, limited change in valency is expected to occur. Assuming that the majority of iron in the GFS bones exists as Fe^{2+}, the valency measured with EMP, some discussion of potential geochemical conditions during recrystallization can be developed.

Conditions would have been acidic, favoring the formation of Fe-phosphates, which are more stable under acidic conditions (Moore and Reddy, 1994). The paleolake however is located within a karst terrain; the bulk water chemistry would more than likely have been buffered to circum-neutral pH by carbonate dissolution. The acidic conditions favoring the formation and preservation of Fe-bearing phosphates may then have been localized to the sediment and pore fluids immediately surrounding the bones. The development of acidic conditions may have been enhanced through the decomposition of organic matter derived from the abundant vegetation deposited into the lake and possibly the decaying alligator itself or other decomposing vertebrates and invertebrates, releasing organic acids into sediments and pore fluids. The incorporation of iron as Fe^{2+} also suggests that conditions were reducing, preventing the oxidation of Fe^{2+} to Fe^{3+} either in solution as an Fe-oxide solid associated with the bone surface or within the apatite lattice once substituted for Ca^{2+} (Jiang et al., 2002).

Comparison to the Pipe Creek Sinkhole

Geochemical data derived from bones preserved at the Late Neogene PCS were compared with the GFS dataset to evaluate whether bones deposited in sinkhole lakes, depositional systems dominated and buffered by carbonate dissolution, undergo similar early diagenetic histories.

Some elements displayed similar patterns, particularly major elements like P and Ca. Others, like Mn and Fe are distinct between the two sites. Low Mn totals in bone recovered from GFS contrasts with an order of magnitude greater Mn incorporation in bones from PCS (Table 5.4). The opposite is true with respect to Fe, where bones from GFS are significantly more enriched in Fe compared to PCS.

While bones preserved at the two sites are chemically distinct based on trace element chemistry, bones recovered from both sites contain evidence of bioerosion in the form of numerous pits and tunnels. In contrast to GFS bones, evidence of bioerosion was observed along the cortical margin of bone from PCS (Farlow and Argast, 2006), although it is unclear from their study if Farlow and Argast (2006) evaluated the trabecular bone for evidence of bioerosion. This suggests that bottom waters or shallow sediment pore waters at both sites were, at a minimum, suboxic, allowing for microorganisms and/or invertebrates to colonize deposited bones.

Based on the presence of siderite infilling pore spaces in bone recovered from PCS, Farlow and Argast (2006) suggest the early diagenetic conditions would have been slightly alkaline with high sulfur and high iron concentrations. The formation of $FeCO_3$ at PCS rather than a Ca-Fe-PO_4 phase as observed at GFS suggests that the two paleolakes or pore fluids surrounding bones during diagenesis were geochemically distinct, particularly with respect to pH. Additionally, with an estimated length of 75 m, width of 50 m, and a depth of 11 m (Farlow et al., 2001), the volume of the PCS sinkhole lake was an order of magnitude smaller than GFS (length, width, and depth of 175, 150, and 40 m, respectively), which would potentially result in distinct circulation patterns and rates of lake turnover. Pore space within the trabecular and cortical bone of GFS samples is not infilled by secondary minerals, suggesting either porewater movement

during diagenesis, stripping any ions released during dissolution from the bones and preventing secondary mineral nucleation on exposed surfaces, or porewaters undersaturated with respect to commonly observed secondary phases (e.g., siderite), precluding mineral precipitation in voids.

Conclusions and future work

Recrystallization of bone to a thermodynamically more favorable apatite phase is a direct reflection of ambient geochemical conditions during early diagenesis. The geochemical evaluation of *Alligator* sp. bones preserved at the Gray Fossil Site using multiple analytical tools provides a window into the conditions likely present during early diagenesis and demonstrates the utility of a combined approach to examine paleoenvironments. The combined observation of bioerosion on trabecular surfaces, requiring some level of oxygen, and the incorporation of Fe into apatite suggests at least when these bones were first deposited, perhaps either directly onto the lake floor or buried within the shallow subsurface, that conditions were not completely anoxic. Once removed from the oxic to suboxic surface or shallow subsurface conditions below the water-sediment interface through burial or perhaps a seasonal change to deepwater oxygenation, the bones experienced anoxic and reducing conditions. These diagenetic conditions facilitated the incorporation of Fe^{2+} at the expense of Ca^{2+} within the apatite lattice, forming a comparatively more stable mixed Ca-Fe-PO_4 phase. Diagenetic conditions within the paleolake, at least when the alligator bones were deposited, were likely reducing, acidic, and anoxic to suboxic.

In combination with previously described palynology and sedimentology (Shunk et al., 2006; Shunk et al., 2009a; Zobaa et al., 2011), alligator bone geochemistry from GFS site supports the hypothesis that during the Late Neogene, the climate of east Tennessee was more humid and

warmer than at present. The preservation of LAGs within the alligator bones suggest that the regional climate was seasonal with annual periods of warmer and cooler conditions, and potentially periods of dry followed by monsoonal rains (Shunk et al., 2009a).

While examining a single suite of bones recovered from one horizon within the bone-rich lacustrine deposits may only provide a snap-shot of diagenetic conditions specific to preservation of those bones, there is great potential at the site to evaluate reptile and mammal bones in stratigraphic succession to investigate the evolution of the paleolake geochemistry through time. Additionally, as a way to further explore the bone diagenetic history of GFS, comparisons between site sediment geochemistry and bone geochemistry may provide insight into the source or sources of substituting elements in the apatite lattice (e.g., Fe-oxides or sulfides). Comparisons to modern sinkhole deposits with a similar seasonal climate as that inferred for the Late Neogene of east Tennessee could provide information on rates, timing, and physical and chemical processes enabling faunal accumulation and facilitating preservation as well as the controls on early diagenesis of bone diagenetic in karst sinkholes.

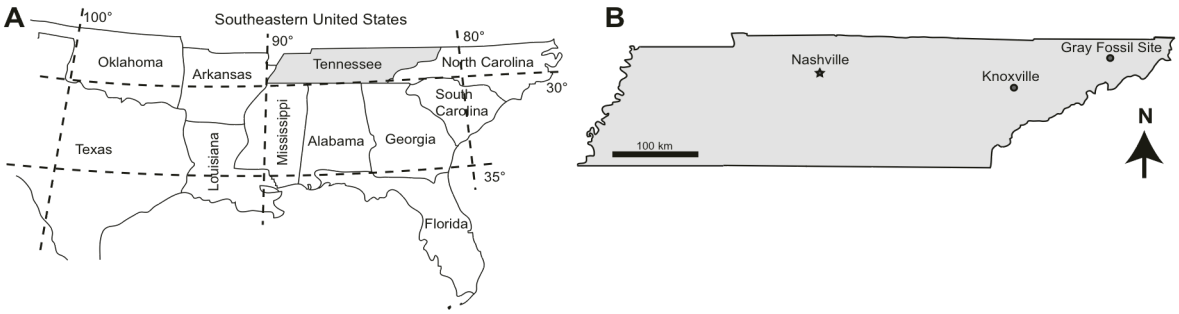

Fig. 5.1: Map of the southeastern United States and the location of the Gray Fossil Site. (A) Regional view of the southeast and the location of Tennessee. (B) The Gray Fossil Site is located in Washington County in northeastern Tennessee, approximately 150 km northeast of Knoxville.

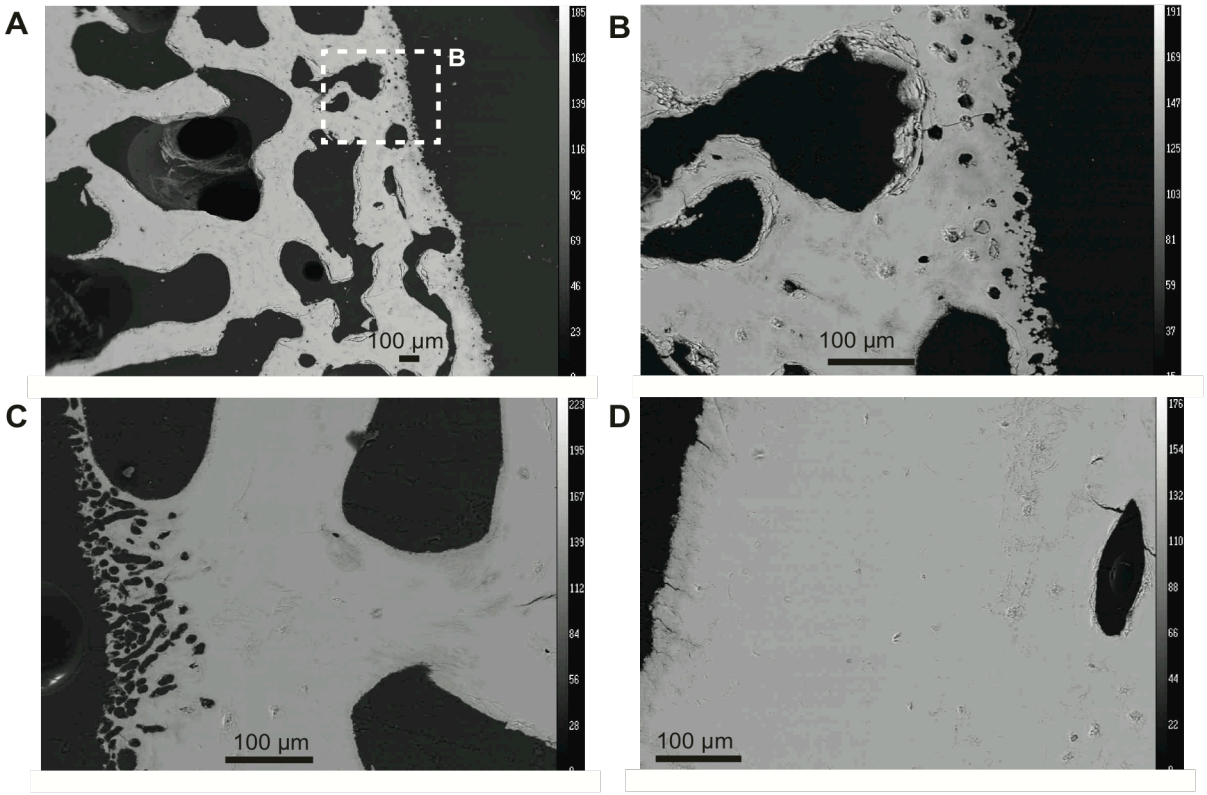

Fig. 5.2: Preferential bioerosion(?) in trabecular bone viewed with backscatter imaging with EMP. (A-C) Extensive pitting and etching was observed along the trabecular margins. Erosive morphology ranged from isolated pits to more extensive tube-like structures extending up to 100 µm into the bone. Within the trabeculae, modification was non-uniform—some portions of the trabeculae (C), namely smaller vascular canals likely not in direct contact with sediment during burial are largely unaffected by surface modifications while other portions are highly altered. (D) Cortical bone lacked bioerosion, highlighted by a representative view of cortical bone.

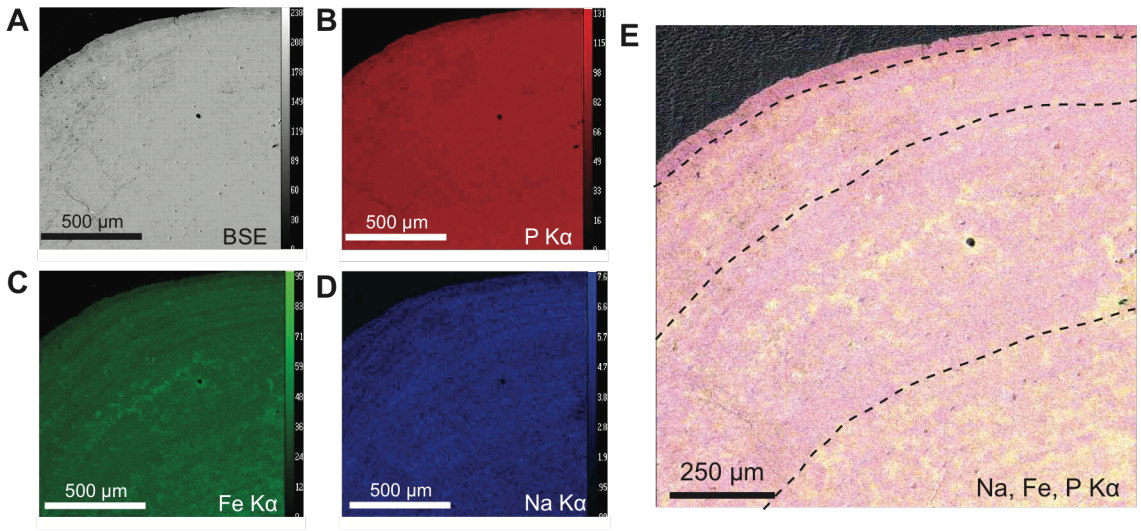

Fig. 5.3: Element maps of fossil Alligator sp. cortical bone extending from the outermost preserved surface ~1500 µm into the cortex. (A) Backscatter imaging suggests some variation in apatite composition on sub-micron scales, forming concentric laminations extending from the outer surface inwards. (B-D) Element maps of P, Fe, and Na at the Kα line reveal clear chemical heterogeneity. Fe and Na element maps highlight chemical zonation within the outer cortex on <10 µm scales. (E) Mixing P, Fe, and Na together into a single map emphasizes the variable chemistry of what appears to be a uniform apatite phase viewed under backscatter. Dashed black lines highlight several of the distinct laminations.

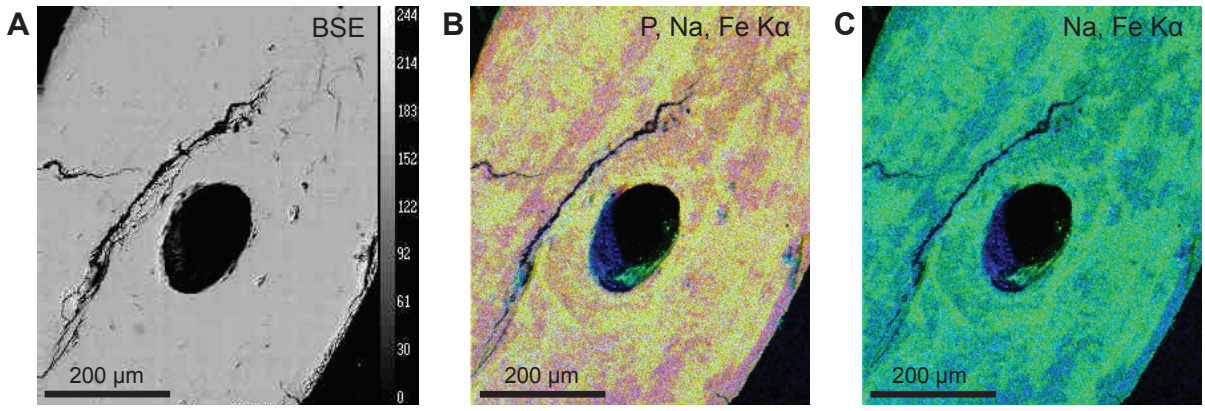

Fig. 5.4: Backscatter image and elemental maps of fossil Alligator sp. trabecular bone from the Gray Fossil Site. Brighter colors in the mixed images (B, C) reflect greater concentrations of an element with all concentrations normalized to be comparable. (A) Backscatter imaging of the trabecular region suggests a uniform apatite mineral composition, with no visible heterogeneities. (B) In contrast, element mixing of Na (blue), Fe (green), and P (red) concentrations measured at the Kα line reveals a non-uniform apatite composition. Some regions are enriched with Fe, particularly around the osteon, while other portions are less enriched. (C) Mixed maps of Fe (green) and Na (blue) also indicates a non-uniform element distribution.

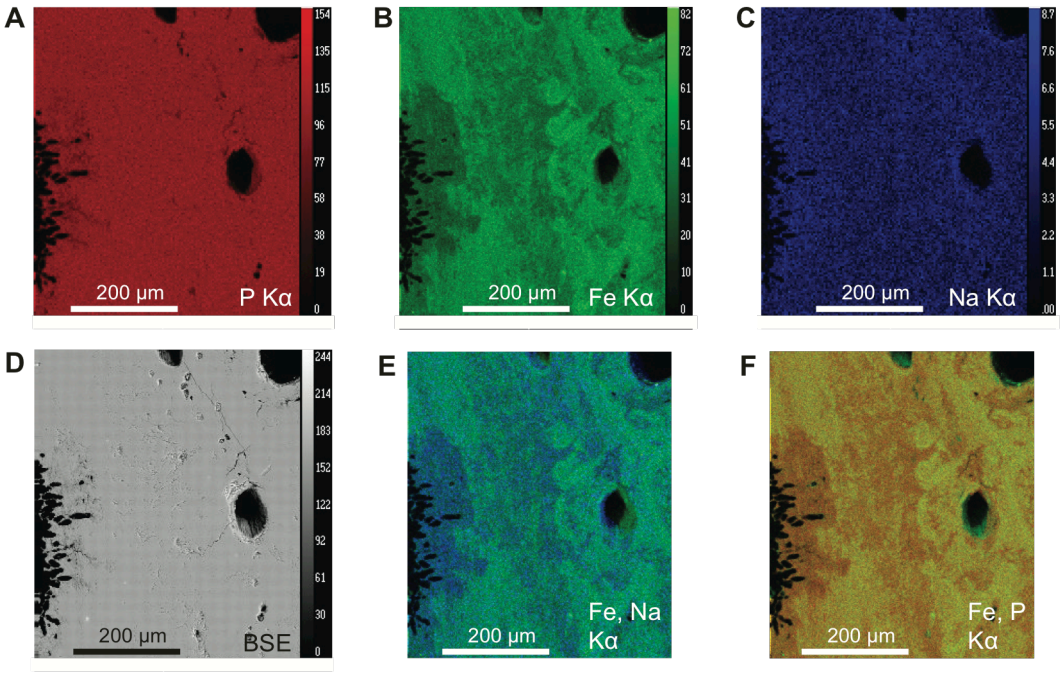

Fig. 5.5: Element maps, backscatter image, and mixed element maps for Alligator sp. trabecular bone adjacent to an extensively bioeroded(?) region. (A) P element map reveals slight depletion of bone in areas adjacent to the extensive pitting and tunneling. (B) Fe element map suggests significant Fe depletion in areas adjacent to pits and tunnels as well as other surrounding areas of the trabecular bone. (C) No observable depletion or enrichment of Na is observed adjacent to eroded bone surfaces. (D) Apatite composition appears to be largely homogenous, with some slight chemical differences adjacent to eroded surfaces. (E, F) Mixed element maps of Fe and Na, and Fe and P at the Kα line indicate a heterogenous apatite composition, with some areas comparatively enriched in Fe and others depleted. Areas adjacent to the pits and tunnels are Fe depleted, and appear to consist largely of a mixed Fe, P, Na, Ca (not presented) phase.

Table 5.1: Modern and fossil bone structural composition determined with FTIR. Ratios derived from the average spectra of 5 analyses per sample.

	Age	Crystallinity (IRSF)	Mean crystal length (nm)	Amide/ Phosphate	Weight % organic matter	Carbonate/ Phosphate	BPI	API	BAI
Modern Alligator Bone	Modern	2.813	41.469	1.600	37.638	2.378	2.130	2.522	1.184
Gray Fossil Site (A)	4.5-7.0 Mya	2.895	43.182	0.253	17.221	0.933	0.952	0.904	0.949
Gray Fossil Site (B)	4.5-7.0 Mya	2.929	43.887	0.261	17.555	0.902	0.915	0.890	0.973
Gray Fossil Site (C)	4.5-7.0 Mya	3.130	48.076	0.235	16.380	0.911	0.908	0.862	0.949

Table 5.2: Mineralogy and crystallinity determined with XRD.

Sample	Mineralogy	Formula	Content (%)	Crystallinity Index (CI)
Gray Fossil Site (A)	Apatite	$Ca_5FO_{12}P_3$	74.05	
	Fluorapatite	$Ca_5FO_{12}P_3$	14.45	
	Calcium iron phosphate	$Ca_{9.333}Fe_{1.167}O_{28}P_7$	10.79	
	Calcium iron phosphide	$CaFe_2P_2$	0.71	0.24
Gray Fossil Site (B)	Fluorapatite	$Ca_5FO_{12}P_3$	91.94	
	Calcium phosphate hydroxide	$Ca_{3.29}H_{17.978}O_{18.474}P_{2.478}$	4.82	
	Calcium iron hydrogen phosphate	$Ca_9FeH_{0.9}O_{28}P_7$	3.25	0.22
Gray Fossil Site (C)	Fluorapatite	$Ca_5FO_{12}P_3$	72.24	
	Chlorapatite	$Ca_5Cl_{0.83}F_{0.17}O_{12}P_3$	18.39	
	Calcium iron phosphate hydrate	$CaFe_3P_3O_{12}H_2O$	6.08	
	Calcium iron phosphate	$Ca_{19}Fe_2O_{56}P_{14}$	3.29	0.27

Table 5.3: Major and trace element chemistry (wt. %) of modern and Gray Fossil Site bones. Values in parentheses reflect standard deviations (1σ).

	Age	Number of Analyses Per Specimen	P_2O_5	SiO_2	SO_2	Al_2O_3	La_2O_3	Ce_2O_3	CaO	MnO	FeO	SrO	BaO	H_2O	Na_2O	F	Cl	Total
Modern Alligator	Modern	n = 12	28.8 (11)	0.02 (1)	0.48 (10)	0.00 (1)	0.02 (2)	0.01 (1)	38.2 (15)	0.00 (0)	0.00 (1)	0.02 (1)	0.02 (2)	1.09 (7)	0.76 (17)	0.07 (4)	0.46 (18)	70.0 (28)
Gray Fossil Site (D)	4.5 to 7 Mya	n = 52	35.0 (13)	0.01 (2)	0.06 (6)	0.23 (15)	0.09 (10)	0.10 (11)	47.8 (13)	0.06 (2)	2.40 (46)	0.05 (2)	0.17 (5)	0.55 (9)	0.23 (5)	1.99 (17)	0.03 (2)	88.6 (27)
Gray Fossil Site (E)	4.5 to 7 Mya	n = 10	35.0 (2)	0.02 (1)	0.02 (1)	0.01 (1)	0.02 (1)	0.02 (2)	48.4 (4)	0.02 (1)	2.93 (24)	0.04 (2)	0.12 (2)	0.53 (8)	0.19 (3)	2.05 (17)	0.00 (0)	89.4 (5)

Table 5.4: Major and trace element chemistry from the Gray Fossil Site and the Pipe Creek Sinkhole (wt. %).

		Ca	P	O	F	Na	Mg	Al	Si	S	Mn	Fe
PCS Bones	Frog limb bone (N = 7)	37.36	15.99	41.69	3.34	0	B.d.	B.d.	0	0	0.47	1.04
	Turtle shell (N = 10)	37.13	16.23	41.92	3.49	0	0	0	0	0	0.51	0.72
	Tortoise shell (N = 15)	37.84	16.19	40.91	3.81	B.d.	B.d.	0	0	0.32	0.19	0.70
	Mammal rib (N = 42)	38.02	16.17	41.21	3.41	0	0	0	0	0	0.39	0.80
GFS Bones	Alligator phalange (D) (N = 52)	38.89	17.41	38.88	2.27	0.20		0.14	0.01	0.03	0.05	2.12
	Alligator phalange (E) (N = 10)	39.01	17.26	38.71	2.25	0.16		0.01	0.01	0.01	0.02	2.57

References

Auler, A.S., Pilo, L.B., Smart, P.L., Wang, X.F., Hoffmann, D., Richards, D.A., Edwards, R.L., Neves, W.A., Cheng, H., 2006. U-series dating and taphonomy of Quaternary vertebrates from Brazilian caves. Palaeogeogr Palaeocl 240, 508-522.

Bauminger, E., Ofer, S., Gedalia, I., Horowitz, G., Mayer, I., 1985. Iron uptake by teeth and bones: a Mossbauer-effect study. Calcif Tissue Int 37, 386-389.

Behrensmeyer, A.K., 1988. Vertebrate preservation in fluvial channels. Palaeogeogr Palaeocl 63, 183-199.

Bergstrom, W.H., Wallace, W.M., 1954. Bone as a sodium and potassium reservoir. J Clin Invest 33, 867-873.

Cerling, T.E., Harris, J.M., MacFadden, B.J., Leakey, M.G., Quade, J., Eisenmann, V., Ehleringer, J.R., 1997. Global vegetation change through the Miocene/Pliocene boundary. Nature 389, 153-158.

Cerling, T.E., Wang, Y., Quade, J., 1993. Expansion of C4 ecosystems as an indicator of global ecological change in the Late Miocene. Nature 361, 344-345.

Child, A.M., 1995. Microbial taphonomy of archaeological bone. Stud Conserv 40, 19-30.

Clark, G.M., Kohl, M., Moore, H.L., Sasowsky, I.D., 2005. The Gray Fossil Site: a spectacular example in Tennessee of ancient regolith occurrences in carbonate terranes, Valley and Ridge subprovince, southern Appalachians U.S.A., in: Beck, B.F. (Ed.), Tenth Multidisciplinary Conference on Sinkholes and the Engineering and Environmental Impacts of Karst. American Society of Civil Engineers, San Antonio, Texas, pp. 82-90.

Dent, B.B., Forbes, S.L., Stuart, B.H., 2004. Review of human decomposition processes in soil. Environ Geol 45, 576-585.

DeSantis, L.R.G., Wallace, S.C., 2008. Neogene forests from the Appalachians of Tennessee, USA: geochemical evidence from fossil mammal teeth. Palaeogeogr Palaeocl 266, 59-68.

Farlow, J.O., Argast, A., 2006. Preservation of fossil bone from the Pipe Creek Sinkhole (Late Neogene, Grant County, Indiana, U.S.A.). J Paleontol Soc Korea 22, 51-75.

Farlow, J.O., Sunderman, J.A., Havens, J.J., Swinehart, A.L., Holman, J.A., Richards, R.L., Miller, N.G., Martin, R.A., Hunt, R.M., Storrs, G.W., Curry, B.B., Fluegeman, R.H., Dawson, M.R., Flint, M.E.T., 2001. The Pipe Creek Sinkhole biota, a diverse Late Tertiary continental fossil assemblage from Grant County, Indiana. Am Midl Nat 145, 367-378.

Fleet, M.E., Pan, Y.M., 1995. Site preference of rare earth elements in fluorapatite. Am Mineral 80, 329-335.

Gong, F.D., Karsai, I., Liu, Y.S., 2010. *Vitis* seeds (Vitaceae) from the late Neogene Gray Fossil Site, northeastern Tennessee, USA. Rev Palaeobot Palyno 162, 71-83.

Hamilton, D.L., 1999. Methods for conserving archaeological material from underwater sites. Texas A&M University, College Station, Texas.

Horner, J.R., de Ricqles, A., Padian, K., 1999. Variation in dinosaur skeletochronology indicators: implications for age assessment and physiology. Paleobiology 25, 295-304.

Hubert, J.F., Panish, P.T., Chure, D.J., Prostak, K.S., 1996. Chemistry, microstructure, petrology, and diagenetic model of Jurassic dinosaur bones, Dinosaur National Monument, Utah. J Sediment Res 66, 531-547.

Jans, M.M.E., 2008. Microbial bioerosion of bone - a review, in: Wisshak, M., Tapanila, L. (Eds.), Current developments in bioerosion. Springer-Verlag, Berlin, pp. 397-413.

Jans, M.M.E., Nielsen-Marsh, C.M., Smith, C.I., Collins, M.J., Kars, H., 2004. Characterisation of microbial attack on archaeological bone. J Archaeol Sci 31, 87-95.

Jiang, M., Terra, J., Rossi, A.M., Morales, M.A., Saitovitch, E.M.B., Ellis, D.E., 2002. $Fe^{2+/}Fe^{3+}$ substitution in hydroxyapatite: theory and experiment. Phys Rev B 66, DOI:http://dx.doi.org/10.1103/PhysRevB.66.224107.

Keenan, S.W., Scannella, J.B., 2014. Paleobiological implications of a *Triceratops* bonebed from the Hell Creek Formation, Garfield County, northeastern Montana, in: Hartman, J., Wilson, G., Horner, J.R., Clemens, W. (Eds.), Through the end of the Cretaceous in the type locality of the Hell Creek Formation in Montana and adjacent areas. Geol S Am S 503, 349-364.

Kohler, M., Marin-Moratalla, N., Jordana, X., Aanes, R., 2012. Seasonal bone growth and physiology in endotherms shed light on dinosaur physiology. Nature 487, 358-361.

Lang, J.W., 1979. Thermophilic response of the American alligator and the American crocodile to feeding. Copeia, 48-59.

Laury, R.L., 1980. Paleoenvironment of a Late Quaternary mammoth-bearing sinkhole deposit, Hot Springs, South Dakota. Geol Soc Am Bull 91, 465-475.

Lundelius, E.L.J., 2006. Cave site contributions to vertebrate history. Alcheringa Special Issue, 195-210.

Mead, J.I., Schubert, B.W., Wallace, S.C., Swift, S.L., 2012. Helodermatid lizard from the Mio-Pliocene oak-hickory forest of Tennessee, eastern USA, and a review of monstersaurian osteoderms. Acta Palaeontol Pol 57, 111-121.

Moore, H., 2004. The bone hunters : the discovery of Miocene fossils in Gray, Tennessee, 1st ed. University of Tennessee Press, Knoxville, p. 102.

Moore, H.L., 2006. A proactive approach to planning and designing highways in East Tennessee karst. Environ Eng Geosci 12, 147-160.

Moore, P.A., Jr., Reddy, K.R., 1994. Role of Eh and pH on phosphorus geochemistry in sediments of Lake Okeechobee, Florida. J Environ Qual 23, 955-964.

Munro, L.E., Longstaffe, F.J., White, C.D., 2007. Burning and boiling of modern deer bone: effects on crystallinity and oxygen isotope composition of bioapatite phosphate. Palaeogeogr Palaeocl 249, 90-102.

Nielsen-Marsh, C.M., Hedges, R.E.M., 2000. Patterns of diagenesis in bone I: the effects of site environments. J Archaeol Sci 27, 1139-1150.

Pan, Y.M., Fleet, M.E., 2002. Compositions of the apatite-group minerals: substitution mechanisms and controlling factors. Rev Mineral Geochem 48, 13-49.

Person, A., Bocherens, H., Saliege, J.F., Paris, F., Zeitoun, V., Gerard, M., 1995. Early diagenetic evolution of bone phosphate: an X-Ray diffractometry analysis. J Archaeol Sci 22, 211-221.

Pucéat, E., Reynard, B., Lécuyer, C., 2004. Can crystallinity be used to determine the degree of chemical alteration of biogenic apatites? Chem Geol 205, 83-97.

Pyle, J.M., Spear, F.S., Wark, D.A., 2002. Electron microprobe analysis of REE in apatite, monazite and xenotime: Protocols and pitfalls. Rev Mineral Geochem 48, 337-362.

Rollin-Martinet, S., Navrotsky, A., Champion, E., Grossin, D., Drouet, C., 2013. Thermodynamic basis for evolution of apatite in calcified tissues. Am Mineral 98, 2037-2045.

Shunk, A.J., Driese, S.G., Clark, G.M., 2006. Late Miocene to earliest Pliocene sedimentation and climate record derived from paleosinkhole fill deposits, Gray Fossil Site, northeastern Tennessee, U.S.A. Palaeogeogr Palaeocl 231, 265-278.

Shunk, A.J., Driese, S.G., Dunbar, J.A., 2009a. Late Tertiary paleoclimatic interpretation from lacustrine rhythmites in the Gray Fossil Site, northeastern Tennessee, USA. J Paleolimnol 42, 11-24.

Shunk, A.J., Driese, S.G., Farlow, J.O., Zavada, M.S., Zobaa, M.K., 2009b. Late Neogene paleoclimate and paleoenvironment reconstructions from the Pipe Creek Sinkhole, Indiana, USA. Palaeogeogr Palaeocl 274, 173-184.

Soriano, M.A., Luzon, A., Yuste, A., Pocovi, A., Perez, A., Simon, J.L., Gil, H., 2012. Quaternary alluvial sinkholes: record of environmental conditions of karst development: examples from the Ebro Basin, Spain. J Cave Karst Stud 74, 173-185.

Sponheimer, M., Lee-Thorp, J.A., 1999. Alteration of enamel carbonate environments during fossilization. J Archaeol Sci 26, 143-150.

Trueman, C.N., 2013. Chemical taphonomy of biomineralized tissues. Palaeontology 56, 475-486.

Trueman, C.N., Martill, D.M., 2002. The long-term survival of bone: the role of bioerosion. Archaeometry 44, 371-382.

Trueman, C.N., Privat, K., Field, J., 2008. Why do crystallinity values fail to predict the extent of diagenetic alteration of bone mineral? Palaeogeogr Palaeocl 266, 160-167.

Trueman, C.N.G., Behrensmeyer, A.K., Tuross, N., Weiner, S., 2004. Mineralogical and compositional changes in bones exposed on soil surfaces in Amboseli National Park, Kenya: diagenetic mechanisms and the role of sediment pore fluids. J Archaeol Sci 31, 721-739.

Turner-Walker, G., 2012. Early bioerosion in skeletal tissues: persistence through deep time. Neues Jahrb Geol P-A 265, 165-183.

Tutken, T., Pfretzschner, H.U., Vennemann, T.W., Sun, G., Wang, Y.D., 2004. Paleobiology and skeletochronology of Jurassic dinosaurs: implications from the histology and oxygen isotope compositions of bones. Palaeogeogr Palaeocl 206, 217-238.

Wallace, S.C., Wang, X.M., 2004. Two new carnivores from an unusual late Tertiary forest biota in eastern North America. Nature 431, 556-559.

Wang, X.M., Wallace, S., 2004. Two new immigrants from the Old World: the earliest and most primitive red panda (Parailurus) and a new Eurasian badger (Arctomeles) from Late Miocene/Early Pliocene Gray Fossil Site, Eastern Tennessee. J Vertebr Paleontol 24, 126A.

Weiner, S., Bar-Yosef, O., 1990. States of preservation of bones from prehistoric sites in the near-East: a survey. J Archaeol Sci 17, 187-196.

Whitelaw, J.L., Mickus, K., Whitelaw, M.J., Nave, J., 2008. High-resolution gravity study of the Gray Fossil Site. Geophysics 73, B25-B32.

Woodward, H.N., Horner, J.R., Farlow, J.O., 2011. Osteohistological evidence for determinate growth in the American alligator. J Herpetol 45, 339-342.

Worobiec, E., Szulc, J., 2010. A Middle Miocene palynoflora from sinkhole deposits from Upper Silesia, Poland and its palaeoenvironmental context. Rev Palaeobot Palyno 163, 1-10.

Zobaa, M.K., Zavada, M.S., Whitelaw, M.J., Shunk, A.J., Oboh-Lkuenobe, F.E., 2011. Palynology and palynofacies analyses of the Gray Fossil Site, eastern Tennessee: their role in understanding the basin-fill history. Palaeogeogr Palaeocl 308, 433-444.

Chapter 6: Conclusions

Portions of this chapter were published in an encyclopedia chapter. Additional content and references were added.

Keenan, S.W., 2013. Freshwater vertebrate animal metagenomics, alligatorinae, in: *The Encyclopedia of Metagenomics*, Neslon, K. (ed.), Springer-Verlag, Heidelberg.

One of the ultimate objectives of paleobiologists and biogeochemists is to use modern processes to reconstruct the past. The motivation behind this research was to address questions surrounding how bone as a living tissue is transformed into a fossil phase(s). From the processes involved in the early stages of decomposition and exposure of bone to a natural environment, to diagenetic transformations into a thermodynamically more stable mineral phase, there are significant gaps in our understanding of the process of fossilization. Even basic questions related to timing remain unanswered. For example, on what time-scale does the mineral fraction of bone exhibit changes? What is the potential for those changes to be preserved over time? Additionally, what controls does biology exert on facilitating bone degradation or preservation in environmental systems?

To address questions related to the transformations of fresh bone tissue to fossil, the American alligator, with diverse and prolific ancestral lineages based on an abundant fossil record, was selected as a model organism. Conservative morphology, diet, and niche occupation makes them ideal modern organisms to study symbiotic interactions, physiological, biochemical, and ultimately, diagenetic processes that may have occurred in the geologic past. Diet (Dethlefsen et al., 2007) and environment (McFall-Ngai, 2002) undoubtedly play a major role in shaping the observed microbiome composition in alligators, and have done so over geologic

time. The relative stability in terms of diet and habitat use in Crocodylomorpha through time is suggestive of a stable gut microbial community as well, which would have been dominated by Fusobacteria, as suggested in Chapter 2. Questions surrounding the mechanisms of bacterial acquisition and maintenance, the processes leading to the establishment of a symbiotic community, the feedback between a host cell and the resident microbiota, and the timing of these events through vertebrate evolution still remain unanswered for most taxa. Despite the numerous questions still to be addressed, insights into the co-evolution of vertebrates and microorganisms, and selective pressures that shape the resident microbiota, are gradually emerging (Zoetendal et al., 2006; Turnbaugh et al., 2007). The potential for diverse "core" assemblages, endemic to specific host taxa is high, as demonstrated for the American alligator. As the nature and extent of host-specific core assemblages are revealed, evolutionary histories of each host taxon may be recapitulated based on the observed similarities (or differences) in gut microbial composition, which is partially controlled by shared and evolved symbiotic associations. From the origin of metazoans, through hundreds of millions of years of diversification events leading to present-day crown vertebrate groups, microbial communities have been shaped not only by changes in host habitat use and diet, but by major metazoan radiation events as well. Attempting to unravel the stability of these communities over geologic time remains an unexplored avenue of research for tetrapoda as a whole. Additionally, the functional significance of Fusobacteria in Archosaurs (chickens and alligators) remains to be tested, particularly if the acquisition of the phylum is a reflection of an ancestral relationship or a secondarily acquired community with similar metabolic role(s) in physiologically distinct host taxa.

Following host death and introduction in an environment, the microbial communities previously critical to host health transition to the first line of attack and degradation of tissues.

The role of biology, particularly microorganisms, has long been held as destructive (e.g., Jans, 2008), breaking down collagen and HAP, a source of the limiting nutrient phosphorus. However, based on results from experiments presented in Chapter 3, microbial interactions with bone may act to shield the mineral phase from alteration after several weeks, contrasting with the long-held view. In bones recovered from buried alligator remains, chemical and structural alterations, including the transformation of HAP to Ca-Fe-PO_4 phases, were observed after as little as one year. Through a series of experiments designed to simulate indirect and direct colonization of bone, alteration was observed after days to weeks, periods previously not viewed as integral to bone recrystallization and diagenesis.

The process of fossilization, though long investigated by paleobiologists, is vastly understudied, particularly processes occurring during early diagenesis. Additionally, the structural composition of fossil apatite is poorly characterized. The results of Chapter 4 provide a new level of insight into the atomic-level arrangement of modern and fossil apatite lattice structure. Similar lattice bond lengths as visualized at the Ca and P K-edges demonstrate that despite variable chemistry, age, and depositional environments, fossil bones converge on a similar lattice arrangement, suggesting that structure rather than chemistry dictates preservation over geologic time.

Early diagenetic changes of bone are driven by site geochemistry. The uptake and incorporation of major and trace elements from the surrounding pore fluids and sediment into the apatite lattice provides a geochemical fingerprint of site-specific conditions during diagenesis. As a way to demonstrate the utility of a combined approach towards reconstructing site geochemistry, *Alligator* sp. phalange fragments from the Gray Fossil Site were examined in Chapter 5 to test the hypothesis that conditions facilitating preservation were reducing and

acidic. Based on major and trace element geochemistry, the bones contained a significant amount of Fe, over three orders of magnitude enriched from fresh bone and over twice as enriched as fossils of the same age preserved in an analogous depositional environment. The preservation of marked zones of bioerosion within the trabecular bone highlights the importance of rapid and early recrystallization, transforming physically compromised bone into a thermodynamically more stable, and less soluble, phase.

The processes occurring during early diagenesis are a consequence of biological, chemical, and physical activities, and dictate the ultimate preservation potential of bone over geologic time. The early diagenetic transformations of bone, from the microbial contributions to the changes that occur to bone as a biomineral, have only begun to be explored.

References

Dethlefsen, L., McFall-Ngai, M.J., Relman, D.A., 2007. An ecological and evolutionary perspective on human-microbe mutulaism and disease. Nature 449, 811-818.

Jans, M.M.E., 2008. Microbial bioerosion of bone: a review, in: Wisshak, M., Tapanila, L. (Eds.), Current developments in bioerosion. Springer-Verlag, Berlin, pp. 397-413.

McFall-Ngai, M.J., 2002. Unseen forces: The influence of bacteria on animal development. Dev Biol 242, 1-14.

Turnbaugh, P.J., Ley, R.E., Hamady, M., Fraser-Liggett, C.M., Knight, R., Gordon, J.I., 2007. The human microbiome project. Nature 449, 804-810.

Zoetendal, E.G., Vaughan, E.E., de Vos, W.M., 2006. A microbial world within us. Mol Microbiol 59, 1639-1650.

Appendix A

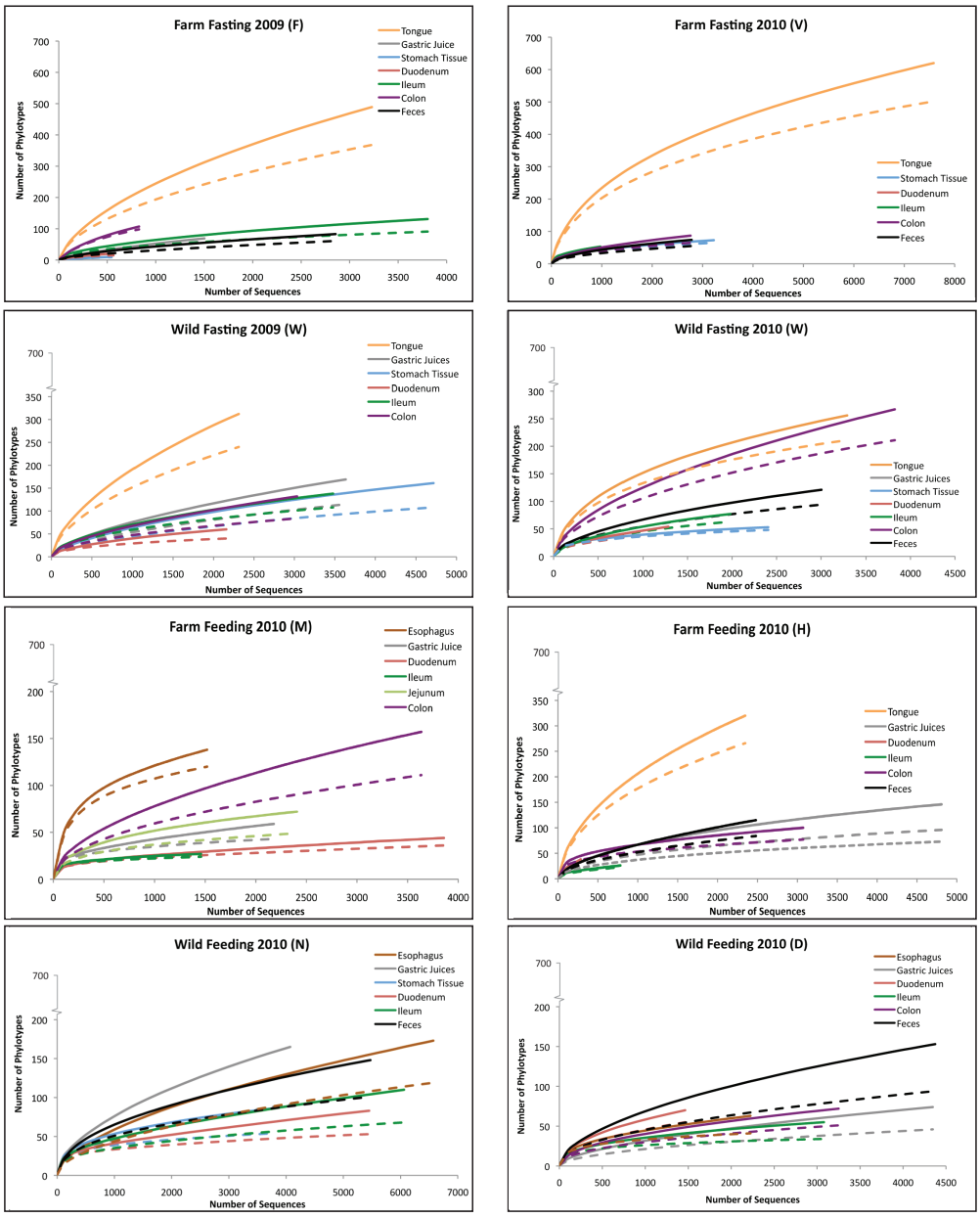

Fig. A.1: Rarefaction curves from fasting and feeding, wild and farm-raised *A. mississipiensis*. Solid lines indicate OTU (phylotype) identity at 97% and dashed lines indicate OTUs at 96%. OTU classification and clustering was performed using 96% sequence identity. Letters in parenthesis in the chart titles refer to specific animals. Colors correspond to tissue or sample type. Saturation of sampling intensity and OTU recovery has been reached for most samples. The curves for tongue bacterial reads suggest that additional sampling will increase the total number of recovered phylotypes, likely reflecting the mixed input from the environment and indigenous, resident flora in the mouth.

Fig. A.2: Shannon index of diversity and Chao estimate of bacterial richness from GI tract tissues. (A) Shannon index (α-diversity) of tissue and GI tract samples grouped as a function of individual. Samples are arranged in order of location along the GI tract from anterior to posterior, and divided into wild, farmed, spring, and winter animals. (B) Chao estimate of bacterial richness observed in GI tract samples from each individual (96% sequence identity). Error bars reflect 95% confidence intervals calculated in mothur. Richness values correspond to number of recovered phylotypes.

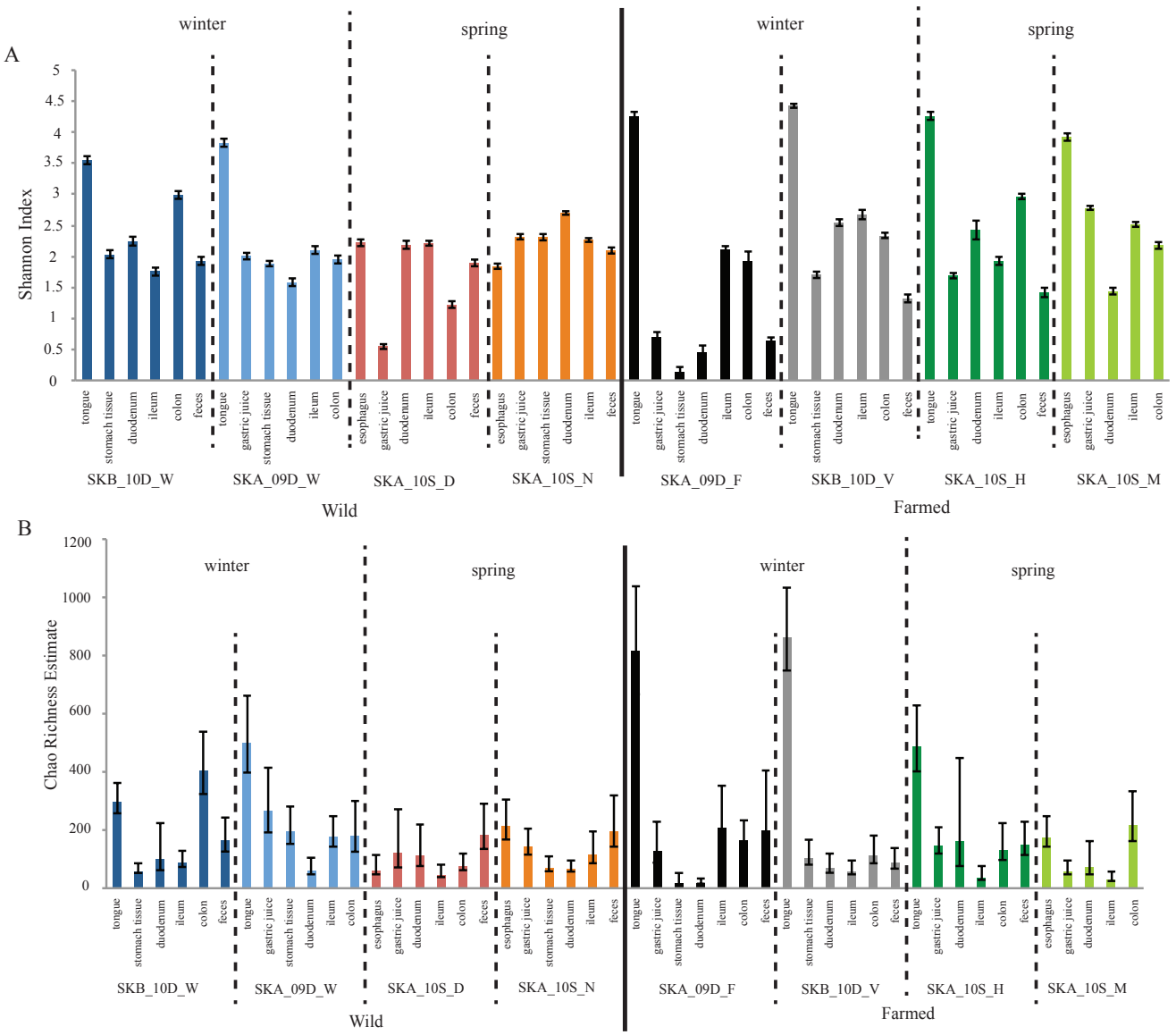
A
winter
spring
winter
spring
Shannon Index
0
0.5
1
1.5
2
2.5
3
3.5
4
4.5
5
tongue
stomach tissue
duodenum
ileum
colon
feces
tongue
gastric juice
stomach tissue
duodenum
ileum
colon
esophagus
gastric juice
duodenum
ileum
colon
feces
esophagus
gastric juice
stomach tissue
duodenum
ileum
feces
tongue
gastric juice
stomach tissue
duodenum
ileum
colon
feces
tongue
stomach tissue
duodenum
ileum
colon
feces
tongue
gastric juice
duodenum
ileum
colon
feces
esophagus
gastric juice
duodenum
ileum
colon
SKB_10D_W
SKA_09D_W
SKA_10S_D
SKA_10S_N
SKA_09D_F
SKB_10D_V
SKA_10S_H
SKA_10S_M
Wild
Farmed
B
winter
spring
winter
spring
Chao Richness Estimate
0
200
400
600
800
1000
1200
tongue
stomach tissue
duodenum
ileum
colon
feces
tongue
gastric juice
stomach tissue
duodenum
ileum
colon
esophagus
gastric juice
duodenum
ileum
colon
feces
esophagus
gastric juice
stomach tissue
duodenum
ileum
feces
tongue
gastric juice
stomach tissue
duodenum
ileum
colon
feces
tongue
stomach tissue
duodenum
ileum
colon
feces
tongue
gastric juice
duodenum
ileum
colon
feces
esophagus
gastric juice
duodenum
ileum
colon
SKB_10D_W
SKA_09D_W
SKA_10S_D
SKA_10S_N
SKA_09D_F
SKB_10D_V
SKA_10S_H
SKA_10S_M
Wild
Farmed

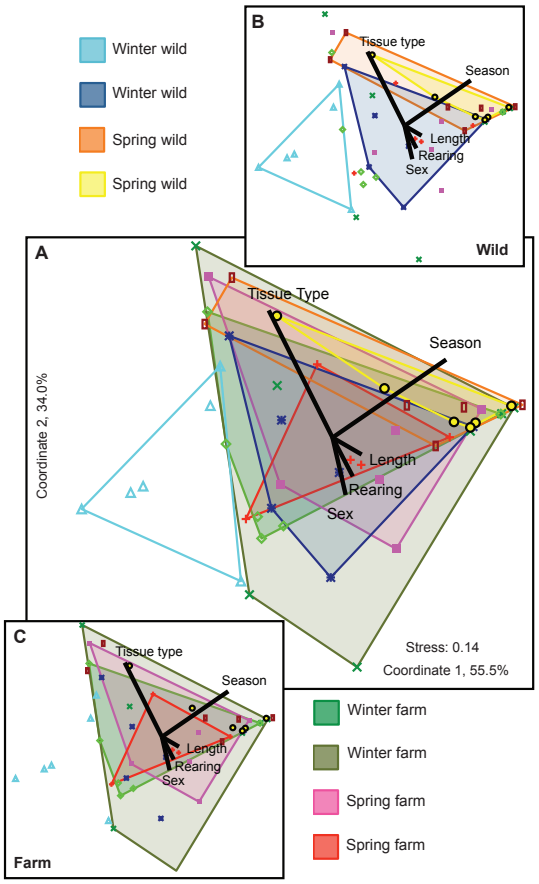

Fig. A.3: NMDS plots of class-level bacterial diversity as a function of individual and season. (A) A single NMDS plot of class-level bacterial diversity according to individual animal. Symbols that are closer to each other in NMDS space have more similar community compositions. Samples from the same animal, regardless of tissue type, are colored, revealing (A) substantial similarity among bacterial communities from almost all animals, regardless of rearing history or feeding status (season). Distinguishing data by rearing history, (B) bacterial communities from wild individuals differed from winter to spring, whereas (C) bacterial communities from farmed individuals were similar in NMDS space, regardless of season. NMDS plots were constructed from cluster analysis based on Euclidean distances of normalized log abundances and the parameters tissue (or sample) type, season (spring or winter), animal length, rearing history (Farmed or wild), and sex (male or female). Lines indicate vector overlays on NMDS ordination, indicating the direction of change for a specific parameter and strength of the variability as length of the line. Coordinates 1 and 2 account for 89% of the observed variation.

Table A.1: Normalized class-level taxonomy

Sex		Female							Female					
Length (inches)		140	Winter Farm (SKA_09_F)						166	Winter Farm (SKB_10D_V)				
			Tongue	Gastric Juice (*)	Stomach Tissue	Duodenum	Ileum	Colon	Feces	Tongue	Stomach Tissue	Duodenum	Ileum (*)	Colon	Feces
Fusobacteria	Fusobacteria		0.03	0.24	0.13	0.28	41.68	0.97	93.94	0.05	0.10	0	0	21.84	73.49
Fibrobacteres	Fibrobacteria		0	0	0	0	0	0	0	0.01	0	0	0	0	0
Chlorobi	Ignavibacteria		0	0	0	0	0	0	0	0.01	0	0	0	0	0
Nitrospira	Nitrospira		0	0	0	0	0	0	0	0	0	0	0	0	0
Armatimonadetes	Armatimonadetes		0	0	0	0	0	0	0	0	0	0	1.21	0	0
Lentispharae	Lentisphaeria		0	0	0	0	0	0	0	0.10	0	0	0	0	0
Gemmatimonadetes	Gemmatimonadetes		0	0	0	0	0	0	0	0.08	0	0	0	0	0
	Planctomycetacia		0	0	0	0	0	0	0	0.03	0	0	0	0	0
Planctomycetes	Phycisphaerae		0	0	0	0	0	0	0	0.01	0	0	0	0	0
	Cyanobacteria		0	0	0	0	0	0	0	0	0.04	0.12	0.09	0.05	0.79
Cyanobacteria	Unclassified Cyanobacteria		0	0	0	0	0	0	0	0	0	0	0	0	0
	Opitutae		0.03	0	0	0	0	0	0	0.79	0	0	0	0	0
	Verrucomicrobidae		0	0	0	0	0	0	0	0.03	0	0	0	0	0
Verrucomicrobia	Unclassified Verrucomicrobia		0	0	0	0	0	0	0	0	0	0	0	0	0
OD1	OD1		0	0	0	0	0	0	0	0	0	0	0	0	0
Deinococcus-Thermus	Deinococci		0	0	0	0	0	0	0	0.03	0	0.31	0	0	1.01
Spirochaetes	Spirochaetes		0.05	0	0	0	0	0.10	0	1.17	0	0	0	0	0
Tenericutes	Mollicutes		0.03	0	0	0	0	0	0	0	0	0	0	0	0
	Erysipelotrichia		0.03	0	0	0	0.38	0.68	0	0	0	0	0	4.39	0
	Bacilli		0.19	0.19	0	2.48	0.09	2.14	0	0.23	0	0	15.14	0.03	0
	Clostridia		1.12	96.64	91.47	79.34	18.75	9.44	1.80	2.62	91.90	7.29	0.52	7.42	0.57
Firmictues	Unclassified Firmicutes		0.16	0.28	6.72	13.50	0.02	0.19	0.03	0.25	2.75	0.25	0.35	0	0.02
TM7	TM7		1.14	0	0	0	0	0	0	0.09	0	14.71	1.38	0	0
SR1	SR1		0	0	0	0	0	0.19	0	0.07	0	0	0	0	0
Synergistes	Synergistia		0	0	0	0	0	0.39	0	0.05	0	0	0	0	0
	Actinobacterdae		2.53	0.33	0.13	0	0	0.29	0	1.19	0.59	9.74	9.78	0	0.05
	Coriobacteridae		0	0	0	0	0	0	0	0	0	0	0	0	0
	Acidimicrobidae		0	0	0	0	0	0	0	0.01	0	0	0.09	0	0
	Rubrobacteridae		0	0	0	0	0	0	0	0.02	0	0	0	0	0
Actinobacteria	Unclassified Actinobacteria		0	0	0	0	0	0	0	0	0	0	0.52	0	0
	Chlorflexi		0.24	0	0	0	0	0.10	0	0	0	0	0	0	0
	Anaerolineae		0	0	0	0	0	0	0	0.11	0	0	0	0	0
	Thermomicrobia		0	0	0	0	0	0	0	0	0	0.12	0	0	0
Chloroflexi	Unclassified Chloroflexi		0.11	0	0	0	0	0	0	0	0	0	0	0	0
	Flavobacteria		2.90	0.19	0	0.69	0	0.10	0	2.53	0.15	0.37	0.95	0.59	0.31
	Sphingobacteria		3.16	0.14	0.13	0	0	72.25	0	6.03	0.13	0.06	0	0	0.10
	Bacteroidia		8.29	0.62	0	0.28	31.22	4.38	3.31	1.28	0.06	11.21	0.26	14.74	14.64
Bacteroidetes	Unclassified Bacteroidetes		4.86	0.14	0	0	2.39	1.46	0.23	7.19	0.80	0.31	0.09	3.00	3.78
	Acidobacteria_Gp 4		0.03	0	0	0	0	0	0	0.07	0	0	9.95	0	0
	Acidobaceria_Gp3		0	0	0	0	0	0	0	0.09	0	0	0	0	0
	Acidmicrobia_Gp1		0	0	0	0	0	0	0	0	0	0	0	0	0
	Acidobacteria_Gp6		0	0	0	0	0	0	0	0.03	0	0	0	0	0
Acidobacteria	Holophagae		5.95	0	0	0	0	0	0	7.08	0	0	0	0	0
	Delta		0.08	0	0.13	0	0	0.39	0	1.56	0.02	0	0.35	0.03	0
	Alpha		2.31	0	0.13	0	0	0.10	0.03	8.01	0	0.55	0.61	0.08	0.19
	Gamma		3.14	0.43	0.13	0.41	5.28	0.97	0.61	12.73	1.76	5.94	16.96	47.00	4.64
	Beta		61.00	0.76	0.13	0.28	0	0.68	0	41.62	1.07	36.40	28.03	0.03	0.02
	Epsilon		0	0	0	0	0	0.58	0	0.13	0	10.42	10.73	0	0
Proteobacteria	Unclassified Proteobacteria		0.24	0	0.13	0	0	0	0	0.94	0.04	0.06	0.26	0.11	0
Unclassified Bacteria	Unclassified Bacteria		2.39	0.05	0.78	2.75	0.20	4.58	0.06	3.74	0.59	2.14	2.77	0.70	0.38

Normalized bacterial class-level composition. Taxonomic assignments were made in RDP at 80% sequence similarity unless otherwise indicated (*), where sequence similarity was lowered to 60%. Other taxa are phyla that constituted less than 2% of recovered reads. Additional information on host animal sex and length (cm) are also included.

Table A.1 (continued)

Male							Female					
114	Winter Wild (SKA_09_W)						180	Winter Wild (SKB_10D_W)				
	Tongue	Gastric Juice	Stomach Tissue	Duodenum	Ileum	Colon	Tongue	Stomach Tissue	Duodenum (*)	Ileum (*)	Colon	Feces
Fusobacteria	0.07	9.78	14.21	13.05	45.35	52.05	0.08	0	0	0	29.87	67.64
Fibrobacteria	0	0	0	0	0	0	0	0	0	0	0	0
Ignavibacteria	0.04	0	0	0	0	0	0	0	0.07	0	0	0
Nitrospira	0	0	0	0	0	0	0	0	0.15	0	0	0
Armatimonadetes	0	0	0	0	0	0	0.03	0	0	0	0	0
Lentisphaeria	0	0	0	0	0	0	0	0	0	0	0	0
Gemmatimonadetes	0	0	0	0	0	0	0.10	0	0	0	0	0
Planctomycetacia	0	0	0	0	0	0	0.05	0	0	0	0	0
Phycisphaerae	0	0	0	0	0	0	0.18	0	0	0	0	0
Cyanobacteria	0	0	0	0	0.05	0	0.08	0.02	0	0.35	0	0
Unclassified Cyanobacteria	0	0	0	0	0	0	0	0	0	0	0	0
Opitutae	0	0	0	0	0	0	0.37	0.52	0	0	0	0
Verrucomicrobidae	0	0	0	0	0	0	0	0	0	0	0	0
Unclassified Verrucomicrobia	0	0	0	0	0	0	0.03	0.07	0	0	0	0
OD1	0	0	0	0	0	0	0	0	0	0	0	0
Deinococci	0	0	0	0	0	0	0.21	0	0	0	0	0
Spirochaetes	0.04	0	0	0	0	0	0	0	0	47.59	0	0
Mollicutes	0	0	0	0	0	0	0	0	0	0	0	0
Erysipelotrichia	0	0	0	0	0.02	0.09	0	0	0	0	0.43	0.22
Bacilli	0.15	0	0.20	0.13	0.16	0.03	0.03	6.26	3.46	0	0.17	0.05
Clostridia	1.60	2.33	9.07	6.89	2.60	3.19	3.97	81.78	28.57	10.40	21.96	8.53
Unclassified Firmicutes	0.15	0.12	0.34	0.96	0.11	0.09	0.10	3.31	6.77	6.68	0.19	0
TM7	0.11	0	0.05	0	0.11	0	0.78	0.12	0	0.04	0	0
SR1	0.11	0	0.02	0	0.05	0	0	0	0	0	0	0
Synergistia	0	0	0	0	0	0	0	0	0	0	0	0
Actinobacterdae	0.37	0.04	0.15	0.13	0.65	0	3.45	2.41	0.88	7.61	0	0.10
Coriobacteridae	0	0	0	0	0	0.12	0	0	0	0	0.15	0
Acidimicrobidae	0	0	0	0.03	0.02	0	0	0	0	0.12	0	0.02
Rubrobacteridae	0	0	0	0	0	0	0	0	0	0.39	0	0
Unclassified Actinobacteria	0	0	0	0	0.02	0	0.08	0	0	0	0	0
Chlorflexi	0	0	0	0	0.02	0	0.31	0	2.21	0	0	0
Anaerolineae	0	0	0	0.03	0	0	0.03	0	0	0	0	0
Thermomicrobia	0	0	0	0	0	0	0	0.07	0	0	0	0
Unclassified Chloroflexi	0	0	0	0	0	0	0	0	0	0	0	0
Flavobacteria	6.73	0.12	0.09	0.13	0	0	28.85	0	0	0.23	0	0.02
Sphingobacteria	1.53	0.08	0.08	0	0.02	0	0.81	0.10	0	0.08	0	0
Bacteroidia	16.78	0.10	0.11	0.99	8.76	34.28	11.20	0.74	0	0	9.70	9.13
Unclassified Bacteroidetes	3.42	0.02	0.02	0.03	0.45	2.08	1.07	0.21	2.43	0.54	0.97	2.75
Acidobacteria_Gp 4	0.04	0	0	0	0	0	0	0	0	0	0	0
Acidobaceria_Gp3	0	0	0	0	0	0	0	0.02	0	0	0.06	0
Acidmicrobia_Gp1	0	0	0	0	0	0	0	0	0	0.39	0	0.02
Acidobacteria_Gp6	0	0	0	0	0	0	0	0	0	0	0	0
Holophagae	0.19	0	0	0	0	0	1.54	0	0	0	0	0
Delta	0	0	0	0	0	0	0.08	0.05	0.07	0	0.02	0
Alpha	0.71	0	0.09	0.07	0.14	0.06	18.46	0.12	11.12	0.23	0.04	1.54
Gamma	8.11	86.99	74.79	76.78	38.35	7.67	8.72	1.93	16.79	1.28	34.41	8.70
Beta	58.52	0.22	0.56	0.23	2.33	0.06	16.37	0.40	0.22	0	0.04	0.05
Epsilon	0	0	0	0	0.02	0	0.03	0.02	0	0	0	0.02
Unclassified Proteobacteria	0.11	0	0.05	0	0.02	0	0.60	0.05	0.07	0.04	0.02	0.82
Unclassified Bacteria	1.23	0.18	0.20	0.53	0.75	0.29	2.40	1.79	27.17	24.03	1.96	0.39

Normalized bacterial class-level composition. Taxonomic assignments were made in RDP at 80% sequence similarity unless otherwise indicated (*), where sequence similarity was lowered to 60%. Other taxa are phyla that constituted less than 2% of recovered reads. Additional information on host animal sex and length (cm) are also included.

Table A.1 (continued)

Male							Male					
132	Spring Wild (SKB_10S_D)						140	Spring Wild (SKA_10S_N)				
	Esophagus	Gastric Juice	Duodenum (*)	Ileum	Colon	Feces	Esophagus	Gastric Juice	Stomach Tissue	Duodenum (*)	Ileum (*)	Feces
Fusobacteria	9.85	0.03	1.15	19.54	74.3 0	83.23	70.30	1.93	0.43	0.20	5.05	32.09
Fibrobacteria	0	0	0	0	0	0	0	0	0	0	0	0
Ignavibacteria	0	0	0	0	0	0	0	0	0	0	0	0
Nitrospira	0	0	0	0	0	0	0	0	0	0	0	0
Armatimonadetes	0	0	0	0	0	0	0	0	0	0	0	0
Lentisphaeria	0	0	0	0	0	0	0	0	0	0	0	0
Gemmatimonadetes	0	0	0	0	0	0	0	0	0	0	0	0
Planctomycetacia	0	0	0	0	0	0	0	0	0.28	0	0	0
Phycisphaerae	0	0	0	0	0	0	0	0		0	0	0
Cyanobacteria	1.25	0	0.11	0	0	0	0.02	0.07	0.61	0	0	0.13
Unclassified Cyanobacteria	0.21	0.16	0	0	0	0	0	0	0	0	0	0
Opitutae	0	0	0	0	0	0	0	0	0	0	0	0
Verrucomicrobidae	0	0	0	0	0	0	0	0	0	0	0	0
Unclassified Verrucomicrobia	0	0	0	0	0	0	0	0	0	0	0	0
OD1	0	0	0	0	0	0	0	0	0	0	0	0
Deinococci	0	0	0	0	0	0	0	0	0	0	0	0
Spirochaetes	0	0	0	0.07	0	0	0	0	0	0	0	0
Mollicutes	0	0	0	0	0	0	0	0	0	0	0	0
Erysipelotrichia	0	0	0	0	0	0	0	0	0	0	0	0.34
Bacilli	1.00	0.02	0.69	0.02	0	0.02	0.22	0.03	1.52	7.76	1.51	0.11
Clostridia	82.48	99.58	66.90	67.64	5.90	14.86	26.74	96.20	82.92	81.57	77.16	59.88
Unclassified Firmicutes	1.43	0.11	0.86	1.41	0.19	0.08	0.21	1.04	4.94	1.28	3.66	0.40
TM7	0	0	0	0	0	0	0	0	0	0	0	0.01
SR1	0	0	0	0	0	0	0	0	0	0	0	0
Synergistia	0	0	0	0	0	0	0	0	0	0	0	0
Actinobacterdae	0	0	0.52	0	0	0	0.08	0.05	0	0	0.25	0.01
Coriobacteridae	0	0	0	0	0	0	0	0	0	0	0	0
Acidimicrobidae	0	0	0	0	0	0	0	0	0	0	0	0
Rubrobacteridae	0	0	0	0	0	0	0	0.02	0	0	0	0
Unclassified Actinobacteria	0	0	0	0	0	0	0	0	0	0	0	0
Chlorflexi	0	0	0	0	0	0	0.01	0	0	0	0	0
Anaerolineae	0	0	0	0	0	0	0	0	0	0	0	0
Thermomicrobia	0	0	0	0	0	0	0	0	0	0	0	0
Unclassified Chloroflexi	0	0	0	0	0	0	0	0	0	0	0	0
Flavobacteria	0	0	0	0	0	0	0.07	0	0	0	0	0
Sphingobacteria	0	0	0	0	0	0	0.01	0	0	0	0.01	0
Bacteroidia	0	0	0	0	0.26	0	0.02	0	0	0	0.01	0.37
Unclassified Bacteroidetes	0	0	0	0	0.02	0	0.03	0	0	0	0.30	0.06
Acidobacteria_Gp 4	0	0	0	0	0	0	0	0	0	0	0	0
Acidobaceria_Gp3	0	0	0	0	0	0	0	0	0	0	0	0
Acidmicrobia_Gp1	0	0	0	0	0	0	0	0	0	0	0	0
Acidobacteria_Gp6	0	0	0	0	0	0	0	0	0	0	0	0
Holophagae	0	0	0	0	0	0	0.67	0	0	0	0	0
Delta	0	0	0	0	0	0.02	0.02	0	0	0	0	0
Alpha	0	0	0.06	0.02	0.02	0.05	0.02	0	1.22	0	0	0.01
Gamma	2.47	0.06	4.20	10.22	19.1 3	1.68	1.10	0.38	2.75	5.40	2.37	0.08
Beta	0	0	0.29	0	0.02	0	0.14	0	0	0.34	0.29	0
Epsilon	0	0	0	0	0	0	0	0	0	0	0	0
Unclassified Proteobacteria	0	0	0.06	0	0	0	0.01	0	0.02	0	0	0
Unclassified Bacteria	1.29	0.03	25.17	1.06	0.15	0.06	0.34	0.28	5.31	3.44	9.38	6.50

Normalized bacterial class-level composition. Taxonomic assignments were made in RDP at 80% sequence similarity unless otherwise indicated (*), where sequence similarity was lowered to 60%. Other taxa are phyla that constituted less than 2% of recovered reads. Additional information on host animal sex and length (cm) are also included.

Table A.1 (continued)

	Female 131						Female 130				
	Spring Farm (SKA_10S_H)						**Spring Farm (SKA_10S_M)**				
	Tongue (*)	Gastric Juice	Duodenum	Ileum	Colon	Feces	Esophagus (*)	Gastric Juice (*)	Duodenum	Ileum	Colon
Fusobacteria	6.23	4.94	2.51	0	8.35	83.26	2.07	0	0	0	52.75
Fibrobacteria	0	0	0	0	0	0	0	0	0	0	0
Ignavibacteria	0	0	0	0	0	0	0	0	0	0	0
Nitrospira	0	0	0	0	0	0	0	0	0	0	0
Armatimonadetes	0	0	0	0	0	0	0	0	0	0	0
Lentisphaeria	0	0	0	0	0	0	0	0	0	0	0.07
Gemmatimonadetes	0	0	0	0	0	0	0	0	0	0	0
Planctomycetacia	0	0	0	0	0	0	0	0	0	0	0
Phycisphaerae	0	0	0	0	0	0	0	0	0	0	0
Cyanobacteria	0	0	0.36	0	0	0	0	0	0	0	0
Unclassified Cyanobacteria	0	0	0	0	0	0	0	0	0	0	0
Opitutae	0.08	0	0	0	0	0	0	0	0	0	0
Verrucomicrobidae	0	0.05	0	0	24.98	6.11	0	0	0	0	0.13
Unclassified Verrucomicrobia	0	0	0	0	0.03	0	0	0	0	0	0
OD1	0.04	0	0	0	0	0	0	0	0	0	0
Deinococci	0.66	0	0	0	0	0	0.11	2.07	0	0	0
Spirochaetes	2.55	0	0	0	0	0	0	0.21	0	0	0
Mollicutes	0	0	0	0	0	0	0	0	0	0	0
Erysipelotrichia	0	0.32	0	0	0.05	0.19	0	0	0	0	0.35
Bacilli	0.27	0.08	11.11	57.51	4.43	0.03	3.18	10.90	11.93	20.36	0.02
Clostridia	8.12	86.55	38.35	31.09	52.89	3.58	37.15	37.33	74.69	0.71	37.40
Unclassified Firmicutes	0.04	0.12	0	0.31	0.42	0.53	0.61	3.75	0.54	0	0.18
TM7	0.39	0	0	0	0	0	1.96	0	0	0.25	0.02
SR1	0.43	0	0	0	0	0	0.61	0	0	0	0
Synergistia	0.66	0	0	0	0	0.03	0.45	0	0	0	0
Actinobacterdae	1.43	0.05	0	0	0	0.03	27.54	0	0	26.02	0.09
Coriobacteridae	0	0	0	0	6.38	0.53	0	0	0	0	0.18
Acidimicrobidae	0	0	0	0	0	0	0	0	0	0	0
Rubrobacteridae	0	0	0	0	0	0	0	0	0	0	0
Unclassified Actinobacteria	0	0	0	0	0	0	0	0	0	0	0
Chlorflexi	0	0	0	0	0	0	0	0	0	0	0
Anaerolineae	0.15	0	0	0	0	0	0.56	0	0	0	0.02
Thermomicrobia	0	0	0	0	0	0	0	0	0	0	0
Unclassified Chloroflexi	0	0	0	0	0	0	0	0	0	0	0
Flavobacteria	9.86	0	0	0	0	0	4.75	2.18	0	4.14	0
Sphingobacteria	1.51	0	0	0.31	0	0	0.22	0.14	0	0	0
Bacteroidia	21.62	5.33	0	0	0.47	3.52	3.18	3.43	1.15	0.10	1.58
Unclassified Bacteroidetes	7.97	1.46	0	0	0.13	0.34	0.34	0.61	0.05	0.10	0.18
Acidobacteria_Gp 4	0	0	0	0	0	0	0	0	0	0	0
Acidobaceria_Gp3	0	0	0	0	0	0	0	0	0	0	0
Acidmicrobia_Gp1	0	0	0	0	0	0	0	0	0	0	0
Acidobacteria_Gp6	0	0	0	0	0	0	0	0	0	0	0
Holophagae	0.74	0	0	0	0	0	0.61	0	0	0	0
Delta	0.46	0	0	0	0.11	0.09	0.11	0	0	0	0.07
Alpha	1.93	0.03	11.47	0	0.95	0	2.29	9.47	0.32	0.51	0.18
Gamma	5.92	0	0	6.74	0.16	0.53	2.23	20.44	8.72	22.08	3.30
Beta	24.84	0	0	0	0	0	9.39	5.72	1.67	22.03	3.28
Epsilon	2.51	0	34.05	2.28	0	0	0.50	0	0.17	3.28	0
Unclassified Proteobacteria	0.50	0	1.08	0	0.13	0.28	0.11	0.29	0.02	0.20	0
Unclassified Bacteria	1.08	1.10	1.08	1.76	0.53	0.96	2.01	3.47	0.74	0.20	0.22

Normalized bacterial class-level composition. Taxonomic assignments were made in RDP at 80% sequence similarity unless otherwise indicated (*), where sequence similarity was lowered to 60%. Other taxa are phyla that constituted less than 2% of recovered reads. Additional information on host animal sex and length (cm) are also included.

Table A.2: Data processing from raw reads to OTUs

	Sample Location	Number of Seqs. (raw)	Number of Seqs. After Trimming	Potentially Chimeric	% Chimeric	Number of Seqs. (post-processing)	% Seqs. Removed	Average Seq. Length After Trimming	Unique sequences	OTUs (97% sequence identity)	OTUs (96% sequence identity)	OTU endemism (% unique to sampling loc.)
Spring wild	Esophagus	3639	2918	51	1.7	2791	23	337	2224	63	41	41.5
SKA_10S_D	Gastric Juice	7596	6407	116	1.8	6233	18	385	4346	74	46	37.0
	Duodenum	3050	1794	12	0.7	1740	43	326	1464	70	55	56.4
	Ileum	5301	4368	211	4.8	4042	24	352	3079	55	34	20.6
	Colon	5798	4855	105	2.2	4646	20	376	3250	72	51	49.0
	Feces	7723	6626	366	5.5	6232	19	397	4374	153	94	37.2
		33107	26968	143 ± 128.2	2.8 ± 1.9 %	25684	25 ± 9 %	362 ± 28.2	18737	81 ± 35.9	53 ± 21.2	41.1
Spring Wild	Esophagus	11790	9575	228	2.4	9221	22	376	6572	173	119	63.0
SKA_10S_N	Gastric Juice	7758	6302	369	5.9	5792	25	287	4072	165	91	37.4
	Stomach Tissue	9556	7498	184	2.5	6535	32	261	3772	86	54	66.7
	Duodenum	10660	8626	79	0.9	8130	24	314	5451	83	53	73.6
	Ileum	11924	9405	55	0.6	8718	27	329	6060	110	68	80.9
	Feces	10022	8304	212	2.6	7906	21	365	5473	148	101	98.0
		61710	49710	187 ± 113.6	2.5 ± 1.9 %	46302	25 ± 4 %	322 ± 44.3	31400	127 ± 39.8	81 ± 26.9	69.9
Spring Farm	Tongue	3991	2758	73	2.6	2623	34	362	2347	320	266	89.8
SKA_10S_H	Gastric Juice	8818	6844	129	1.9	6664	24	371	4808	146	96	38.5
	Duodenum	4471	2089	5	0.2	290	94	308	285	38	36	69.4
	Ileum	2755	1607	1	0.1	965	65	346	782	26	23	65.2
	Colon	4936	3963	148	3.7	3795	23	387	3073	100	77	29.9
	Feces	3981	3344	91	2.7	3238	19	403	2480	115	84	39.3
		28952	20605	74 ± 61.4	1.9 ± 1.5 %	17575	43 ± 30 %	362 ± 33.3	13775	124 ± 106.4	97 ± 87.6	63.6
Spring Farm	Esophagus	2629	1976	93	4.7	1790	32	360	1519	138	120	70.0
SKA_10S_M	Gastric Juice	4019	3212	383	11.9	2799	30	360	2178	59	43	27.9
	Duodenum	11976	8721	360	4.1	5976	50	363	3858	44	36	66.7
	Ileum	4463	2994	165	5.5	1976	56	337	1459	27	24	37.5
	Colon	6047	4994	395	7.9	4548	25	382	3635	157	111	45.9
		29134	21897	251 ± 142.8	6.3 ± 3.2 %	17089	37 ± 13 %	360 ± 14.3	12649	82 ± 52.6	63 ± 41.0	50.9

Table A.2 (continued)

	Sample Location	Number of Seqs. (raw)	Number of Seqs. After Trimming	Potentially Chimeric	% Chimeric	Number of Seqs. (post-processing)	% Seqs. Removed	Average Seq. Length After Trimming	Unique sequences	OTUs (97% sequence identity)	OTUs (96% sequence identity)	OTU endemism (% unique to sampling loc.)
Winter Wild SKA_09D_W	Tongue	5807	3298	421	12.8	2688	54	347	2312	312	240	72.5
	Gastric Juice	9203	6904	413	6.0	4926	46	325	3635	169	115	40.9
	Stomach Tissue	11504	8027	561	7.0	6552	43	333	4716	161	108	34.3
	Duodenum	5230	3690	86	2.3	3019	42	334	2158	60	40	25.0
	Ileum	8346	4919	178	3.6	4428	47	356	3478	138	108	39.8
	Colon	7205	3655	187	5.1	3416	53	380	3033	132	84	44.0
		47295	30493	307 ± 183.4	6.1 ± 3.6 %	25029	48 ± 5 %	345 ± 20.1	19332	162 ± 83.0	115 ± 66.8	50.1
Winter Wild SKB_10D_W	Tongue	7001	4208	234	5.6	3830	45	339	3293	256	211	94.8
	Stomach Tissue	8014	5732	50	0.9	4199	48	339	2406	53	48	58.3
	Duodenum	3407	2383	4	0.2	1358	60	352	1284	54	43	53.5
	Ileum	4565	3202	89	2.8	2576	44	374	1980	77	63	71.4
	Colon	6219	4924	227	4.6	4650	25	337	3823	267	211	55.0
	Feces	5870	4474	200	4.5	4150	29	356	3004	121	94	46.8
		35076	24923	134 ± 99.0	3.1 ± 2.2 %	20763	42 ± 12.8 %	349 ± 14.3	15790	138 ± 98.8	111 ± 79.0	68.1
Winter Farm SKA_09D_F	Tongue	6885	4472	552	12.3	3762	45	353	3229	489	368	89.1
	Gastric Juice	3921	2168	14	0.6	2111	46	377	1502	69	59	42.4
	Stomach Tissue	991	799	1	0.1	774	22	401	544	20	9	22.2
	Duodenum	1711	856	10	1.2	729	57	369	564	21	15	40.0
	Ileum	10979	6494	263	4.0	4523	59	366	3804	131	91	73.6
	Colon	1269	1065	9	0.8	1027	19	384	828	107	98	81.6
	Feces	8431	3589	129	3.6	3449	59	386	2855	87	61	21.3
		34187	19443	139 ± 205.9	3.3 ± 4.3 %	16375	44 ± 17 %	376 ± 15.6	13326	132 ± 162.8	100 ± 122.9	74.3
Winter Farm SKB_10D_V	Tongue	13859	11068	1123	10.1	9755	30	344	7583	620	538	95.7
	Stomach Tissue	6775	4796	66	1.4	4768	30	366	3222	73	65	52.3
	Duodenum	13624	7577	59	0.8	1632	88	326	1217	54	46	58.7
	Ileum	8068	4804	55	1.1	1156	86	330	971	53	43	48.8
	Colon	5448	4098	148	3.6	3732	31	327	2760	87	65	64.6
	Feces	6133	4463	171	3.8	4179	32	357	2782	74	55	63.6
		53907	36806	270 ± 420.6	3.5 ± 3.5 %	25222	49 ± 29 %	341 ± 16.9	18535	160 ± 225.6	129 ± 182.8	86.9

Data processing information including number of raw reads, number of chimera, and sequence information following trimming. Information on OTUs presented for both 97% and 96% sequence similarity. OTU endemism is based on Bray Curtis (β-diversity) calculations and matrices, and reflects the percentage of OTUs only recovered from that specific sample and absent from any other GI tract samples.

Table A.3: Unique OTUs (defined at 96% sequence identity) recovered from each individual as a function of tissue type

			Unique OTUs						
Rearing History	Individual	Season (individual)	Oral	Gastric Juice	Stomach Tissue	Duodenum	Ileum	Colon	Feces
Wild	SKA_09D_W	Winter(a)	185 (33.6)	90 (45.7)	102 (45.7)	49 (25.4)	126 (40.1)	46 (16.1)	-
	SKB_10D_W	Winter(b)	184 (33.4)	-	90 (41.3)	29 (15.0)	59 (18.8)	150 (52.3)	93 (32.6)
	SKA_10S_N	Spring(n)	71 (12.9)	61 (31.0)	61 (28.0)	50 (25.9)	62 (19.7)	-	90 (31.6)
	SKA_10S_D	Spring(d)	28 (5.1)	23 (11.7)	-	31 (16.1)	25 (8.0)	53 (18.5)	48 (16.8)
Farm	SKA_09D_F	Winter(f)	218 (21.1)	50 (27.1)	8 (9.8)	18 (15.8)	138 (61.6)	90 (28.3)	29 (16.6)
	SKB_10D_V	Winter(v)	428 (41.4)	-	71 (86.6)	50 (43.9)	47 (21.0)	67 (21.1)	57 (32.6)
	SKA_10S_H	Spring(h)	136 (13.1)	91 (49.5)	-	9 (7.9)	6 (2.7)	40 (12.6)	63 (36.0)
	SKA_10S_M	Spring(m)	59 (5.7)	35 (19.0)	-	31 (27.2)	24 (10.7)	66 (20.8)	-

OTUs were calculated by combining all reads recovered from wild or farm-raised individuals from each tissue type. Cluster analysis of pooled reads (e.g. wild oral) enabled evaluation of unique and shared (Appendix Table B.4) OTUs. Values in parenthesis indicate the percentage of OTUs unique based on the total number of OTUs recovered from the tissue type (unique or shared). Dashes indicate tissues for which samples were not available, and resulting cluster analyses reflect reads recovered from two or three individuals.

Table A.4: Shared OTUs from wild and farmed individuals as a function of tissue type

Rearing History	Season (W or S) and individual	Oral	Gastric Juice	Stomach Tissue	Duodenum	Ileum	Colon	Feces
Wild	Wa+Sn	4	2	2	0	2	-	-
	Wa+Sd	0	1	-	1	1	1	-
	Wa+Sn+Sd	1	1	-	3	1	-	-
	Wb+Sn	7	-	4	1	12	-	7
	Wb+Sd	0	-	-	5	1	12	10
	Wb+Sn+Sd	1	-	-	1	2	-	13
	Wa+Wb+Sn	6	-	2	0	1	-	-
	Wa+Wb+Sd	0	-	-	0	0	8	-
	Wa+Wb	45	-	6	3	3	16	-
	Sn+Sb	19	19	-	19	19	-	24
	Wa+Wb+Sn+Sd	0	-	-	1	0	-	-
Farm	Wf+Sh	20	4	-	1	0	1	9
	Wf+Sm	3	1	-	0	0	4	-
	Wf+Sh+Sm	4	0	-	0	0	2	-
	Wv+Sh	25	-	-	0	0	0	6
	Wv+Sm	5	-	-	2	2	9	-
	Wv+Sh+Sm	6	-	-	1	2	5	-
	Wf+Wv+Sh	26	-	-	0	1	1	4
	Wf+Wv+Sm	7	-	-	0	0	1	-
	Wf+Wv	49	-	3	2	2	4	7
	Sh+Sm	20	3	-	0	2	24	-
	Wf+Wv+Sh+Sm	29	-	-	0	0	4	-

Samples were divided into two broad datasets to reflect rearing history (wild and farmed), or season, specifically spring (S) and winter (W). Additional annotation reflects the labeling scheme per individual (e.g., "Wf" is the number of shared OTUs observed in the winter individual, F). Dashes indicate a comparison in shared bacterial groups was not possible due to unavailable tissues for processing. Taxonomic assignments of shared OTUs are presented in Table 2.2.

Table A.5: Shared OTU taxonomic assignment for shared reads observed in three or four individuals

Rearing History	Tissue Type	OTUs (from 3 or 4 individuals)	Taxonomic Assignment	Sequence Affinity and Accession Number	Query Coverage (%)	Max ID (%)
Wild	Oral	0				
	Gastric Juice	1	Firmicutes (*Enterobacteriaceae*)	JN420874.1	100	88
	Stomach Tissue	2	Gammaproteobacteria (*Enterobacteriales*)	JN420552.1	96	95
			Firmicutes (*Clostridiales*)	JQ248565.1	100	96
	Duodenum	1	Gammaproteobacteria (*Xanthomonadales*)	JN422443.1	100	87
	Ileum	0				
	Colon	8	Fusobacteria (*Fusobacteriaceae*)	human feces; NR_025533.1	100	91
			Bacteroidetes (*Bacteroidales*)	human and fish feces; JQ317227.1	90	100
			Fusobacteria (*Fusobacteriaceae*)*	human feces; NR_025533.1	100	90
			Gammaproteobacteria (*Enterobacteriales*)	JN422224.1	99	92
			Bacteroidetes (*Bacteroidales*)	human and fish feces; JQ317236.1	100	92
			Bacteroidetes (*Bacteroidales*)	human and fish feces; JQ317256.1	100	92
			Gammaproteobacteria (*Enterobacteriales*)	darter fish; JQ918394.1	92	100
			Bacteroidetes (*Bacteroidales*)	human and fish feces; JQ317227.1	92	93
	Feces	13	Firmicutes (*Clostridiales*)	JF733433.1	100	92
			Unknown (uncultured)	HM630230.1	92	92
			Firmicutes (*Clostridia*)	EU780407.1	97	90
			Firmicutes (*Clostridiales*)	FR745875.1	94	92
			Firmicutes (*Clostridiaceae*)	AB538430.1	100	92
			Firmicutes (*Clostridiales*)	AJ229244.1	100	93
			Firmicutes (*Clostridiaceae*)	JQ897418.1	100	93
			Firmicutes	IBD, human mucosa; EF071429.1	100	94
			Gammaproteobacteria (*Enterobacteriales*)	newborn feces; GU145917.2	100	93
			Firmicutes (*Clostridiales*)	NR_029246.1	99	94
			Unknown (Uncultured)	HQ813454.1	100	88
			Fusobacteria (*Fusobacteriaceae*)	carp intestine; AB665782.1	100	92
			Firmicutes (*Clostridiales*)	FJ764372.1	100	96

Table A.5 (continued)

Rearing History	Tissue Type	OTUs (from 3 or 4 individuals)	Taxonomic Assignment	Sequence Affinity and Accession Number	Query Coverage (%)	Max ID (%)
Farm	Oral	29	Firmicutes (*Clostridiaceae*)	AB721399.1	100	98
			Chlorobi	canine oral; JQ299696.1	91	91
			Betaproteobacteria (*Burkholderiales*)	JN421447.1	100	92
			Actinobacteria (*Actinobacteridae*)	HM210084.1	93	98
			Firmicutes (*Clostridia*)	GQ390386.1	86	97
			Bacteroidetes	GU179784.1	100	86
			Betaproteobacteria (*Burkholderiales*)	JN421447.1	100	95
			Bacteroidetes	JN809633.1	88	97
			Betaproteobacteria (*Burkholderiales*)	AB680706.1	97	89
			Bacteroidetes	JN183369.1	81	90
			Bacteroidetes (*Porphyromonadaceae*)	JX575921.1	97	100
			Alphaproteobacteria (*Rhodobacteraceae*)	AB681112.1	100	93
			Betaproteobacteria (*Burkholderiales*)	JN422726.1	100	88
			Firmicutes (*Clostridiales*)	JQ087063.1	99	92
			Betaproteobacteria	DQ451457.1	93	92
			Firmicutes (*Clostridiales*)	FP565809.1	100	100
			Firmicutes (*Clostridiales*)	FP565809.1	100	100
			Betaproteobacteria (*Burkholderiales*)	JN421447.1	100	86
			Gammaproteobacteria	JF344052.1	83	91
			Betaproteobacteria	FM253016.1	100	91
			Bacteroidetes (*Porphyromonadaceae*)	JQ815593.1	97	100
			Betaproteobacteria (*Burkholderiales*)	JN421720.1	100	85
			Fusobacteria (*Fusobacteriaceae*)	human oral; CU921109.1	100	93
			Betaproteobacteria (*Burkholderiales*)	JN421720.1	86	91
			Betaproteobacteria (*Rhodocyclales*)	JX170095.1	97	100
			Actinobacteria (*Actinobacteridae*)	GU430066.1	86	100
			Actinobacteria (*Actinobacteridae*)	GU430066.1	80	100
			Bacteroidetes (*Bacteroidales*)	HQ133063.1	98	100
			Bacteroidetes	EF221070.1	83	84
	Gastric Juice	0				
	Stomach Tissue	3	Firmicutes (*Clostridiales*)	JF815501.1	91	89
			Firmicutes (*Clostridiales*)	JQ993877.1	100	88
			Firmicutes (*Clostridiales*)	AY607195.1	94	89
	Duodenum	0				
	Ileum	0				
	Colon	4	Bacteroidetes (*Bacteroidales*)	JF413562.1	79	94
			Bacteroidetes (*Sphingobacteriales*)	FN668063.2 human feces;	96	87
			Fusobacteria (*Fusobacteriaceae*)*	NR_025533.1	100	92
			Gammaproteobacteria (*Enterobacteriales*)	JN420552.1 human and trout feces;	99	94
	Feces	4	Bacteroidetes (*Bacteroidales*)	JQ317255.1	99	94
			Bacteroidetes (*Bacteroidales*)	HM218882.1 human and fish feces;	98	84
			Bacteroidetes (*Bacteroidales*)	JQ317256.1 human and fish feces;	100	94
			Bacteroidetes (*Bacteroidales*)	JQ317227.1	100	80

Shared OTUs calculated from each tissue in wild and farm-raised individuals based on BLAST results. OTUs were classified based on BLAST results of a representative read from the OTU. Where sequences were closely aligned with other microbiome studies, sequence affinity is noted as well as accession numbers. Query coverage (%) and maximum identity (%) were optimized when assigning taxonomy to OTUs. For all reads, maximum identity values were above 85%. * represents a species of Fusobacteria, also aligned with Bacteroidetes in BLAST results.

Table A.6: Paired t-tests of significant differences in bacterial communities within each animal from class-level taxonomic assignment

Winter Farm (F)

	tongue	gastric juice	stomach tissue	duodenum	ileum	colon	feces
tongue							
gastric juice	0.002 **						
stomach tissue	0.006 **	0.710					
duodenum	0.066	0.195	0.354				
ileum	0.396	<0.001 ***	<0.001 ***	0.008 **			
colon	0.247	0.048	0.107	0.490	0.046*		
feces	0.004 **	0.845	0.860	<0.001 ***	<0.001 ***	0.074	

Winter Farm (V)

	tongue	stomach tissue	duodenum	ileum	colon	feces
tongue						
stomach tissue	<0.001 ***					
duodenum	0.751	<0.001 ***				
ileum	0.290	<0.001 ***	0.458			
colon	0.203	<0.001 ***	0.113	0.021*		
feces	<0.001 ***	0.150	<0.00 1 ***	<0.001 ***	0.021 *	

Winter Wild (09W)

	tongue	gastric juice	stomach tissue	duodenum	ileum	colon
tongue						
gastric juice	0.013*					
stomach tissue	0.122	0.341				
duodenum	0.092	0.418	0.887			
ileum	0.829	0.007**	0.079	0.058		
colon	0.909	0.018*	0.152	0.116	0.741	

Winter Wild (10W)

	tongue	stomach tissue	duodenum	ileum	colon	feces
tongue						
stomach tissue	<0.001 ***					
duodenum	0.463	<0.001 ***				
ileum	0.024*	0.004 **	0.123			
colon	0.080	<0.001 ***	0.305	0.601		
feces	<0.001 ***	0.224	0.002 **	0.096	0.029 *	

Spring Wild (D)

	esophagus	gastric juice	duodenum	ileum	colon	feces
esophagus						
gastric juice	0.199					
duodenum	0.283	0.019*				
ileum	0.263	0.017*	0.963			
colon	0.578	0.067	0.604	0.572		
feces	0.903	0.245	0.233	0.215	0.489	

Spring Wild (N)

	esophagus	stomach tissue	gastric juice	duodenum	ileum	feces
esophagus						
stomach tissue	0.079					
gastric juice	0.463	0.304				
duodenum	0.523	0.261	0.924			
ileum	0.792	0.135	0.638	0.708		
feces	0.481	0.015*	0.151	0.180	0.333	

Spring Farm (H)

	tongue	gastric juice	duodenum	ileum	colon	feces
tongue						
gastric juice	<0.001 ***					
duodenum	0.005 **	<0.001 ***				
ileum	<0.001 ***	0.046*	0.139			
colon	<0.001 ***	0.007**	0.447	0.469		
feces	<0.001 ***	0.786	0.002**	0.084	0.015*	

Spring Farm (M)

	esophagus	gastric juice	duodenum	ileum	colon
esophagus					
gastric juice	0.735				
duodenum	<0.001 ***	<0.001 ***			
ileum	0.726	0.991	<0.00 1 ***		
colon	0.025*	0.010 **	0.244	<0.001 ***	

Paired T-tests were performed in PAST. Significance values (α-value) were established at P < 0.05 (*), 0.05-0.01 (**), and P < 0.001 (***).

Table A.7: Phylum-level bacterial diversity of selected vertebrate microbiomes

				Percentage Composition of Dominant Bacterial Taxa															
	Vertebrate Host (sample location)	Source of Data	No. animals	Fusobacteria	Firmicutes	Bacteroidetes	Proteobacteria	Acidobacteria	Actinobacteria	Chloroflexi	Cyanobacteria	Deferribacteres	Fibrobacteres	Lentisphaerea	Spirochaetes	Tenericutes	Verrucomicrobia	Unclassified	Other
Reptilia	Alligator (feces)	this study	n = 9	69.6	16.7	5	2.7	0.002	0.08	0	0.1	0	0	0	0	0	4.3	1.4	0.12
	Python (fasted, pooled GI tract)	Costello et al. (2010)	n = 3	0.5	61.8	20.6	10.1	0	0.6	0	0	3.9	0	0.01	0	0	0.6	0	1.89
	Land iguana (feces)	Hong et al. (2011)	n = 16	0.6	63.9	4.2	1.4	0	1.3	0	0	0	0	0	0	0.1	0.2	26.6	1.70
	Marine iguana (feces)	Hong et al. (2011)	n = 30	0	75.1	8.2	0.6	0	0.6	0	0	0	0	0	0	0	1	14.5	0.00
	Giant tortoise (feces)	Hong et al. (2011)	n = 4	0	81.1	4.4	2	0.1	0.8	0	0.1	0	0	0	0	0	0.1	10.4	1.00
	Green iguana (feces)	Hong et al. (2011)	n = 2	0	74	10.1	3.1	0	0.1	0	0	0	0	0.1	0.6	0	1	10.1	0.90
Aves	Chicken (ceca)	Qu et al. (2008)	n = 2	9	50	33	3.5	0	1	0	0	0	0	0	0	0	2.5	0	1.00
	Chicken (ileum and cecum, conventional)	Bjerrum et al. (2006)	n = 40	0	81.08	2.78	2.16	0	0	0	9.72	0	0	0	0	0	0	0	4.26
	Chicken (ileum and cecum, organic)	Bjerrum et al. (2006)	n = 40	0	82.89	0	0	0	0	0	17.11	0	0	0	0	0	0	0	0.00
	Ostrich (ceca)	Matsui et al. (2010)	n = 3	0	68.2	25.5	0	0	0	0	0	0	0.9	0	2.7	0	0.9	0	1.80
	Turkey (feces)	Lu and Domingo (2008)	n = 31	0	89.3	0.5	4.7	0	5.5	0	0	0	0	0	0	0	0	0	0.00
Mammalia	Macaque (intestines, feces)	McKenna et al. (2008)	n = 34	0	38.8	45.4	3.5	0	0	0	0.5	0	0.6	0	7.3	1.1	0	0.8	2.00
	Human (lower intestine)	Eckburg et al. (2005)	n = 3	0	50	47	2	0	0	0	0	0	0	0	0	0	1	0	0.00
	Human (feces)	Ochman et al. (2010)	n = 2	0	63.85	8.71	13.98	0	2.37	0	0	0	0	0.00	0.00	0.03	11.05	0	0.00
	Gorilla spp. (feces)	Ochman et al. (2010)	n = 4	0.00	7.73	39.37	50.31	0.00	2.35	0.00	0	0	0.00	0.00	0.10	0.07	0.04	0	0.02
	Bonobo (feces)	Ochman et al. (2010)	n = 5	0	71.33	18.94	1.06	0.01	6.69	0.01	0	0	0.36	0.06	0.41	0.37	0.64	0	0.12
	Chimpanzee spp. (feces)	Ochman et al. (2010)	n = 14	0.01	42.30	26.43	25.69	0.01	3.96	0.00	0	0.00	0.09	0.07	0.78	0.29	0.31	0	0.05
	Pig (colon and cecum)	Pryde et al. (1999)	n = 1	0	37.70	0	0	0	0	0	1.64	0	0	0	0	0	0	60.66	0.00
	Mouse (feces, cecum and colon)	Hill et al. (2010)	n = 4	0	15.9	75.5	0	0	0	0	0	0	0	0	0	0	0.01	0.7	7.89
	Alpaca (gastric juices)	Pei et al. (2010)	n = 4	0	73.5	21.7	0	0	0	0	0	0	0	0	5	0	0	0	0.00
	Sheep (gastric juices)	Pei et al. (2010)	n = 4	0	40	43.4	0	0	13.3	0	0	0	0	0	3.3	0	0	0	0.00
	Canine (feces, low fiber)	Swanson et al. (2011)	n = 6	8.64	30.52	41.22	15.26	0	1	0.29	0.52	0	0.18	0	0.53	0	0.3	0.08	1.46
	Canine (feces, added fiber)	Swanson et al. (2011)	n = 6	7.13	34.72	40.81	13.08	0	1.01	0.31	0.47	0	0.13	0	0.49	0	0.26	0.08	1.51
	Horse (colon and cecum)	Daly et al. (2001)	n = 5	0	60.89	20.66	0.74	0	0.74	0	0	0	0	0	3.32	1.11	2.95	9.59	0.00
	Cheetah (feces)	Ley et al. (2008a)	n = 2	1.5	73.5	1.0	13.5	0	11.0	0	0	0	0	0	0	0	0	0	0.00
	Lion (feces)	Ley et al. (2008a)	n = 3	0	80.0	3.3	3.3	0	13.0	0	0	0	0	0	0	0	0	0	0.40
	Polar Bear (feces)	Ley et al. (2008a)	n = 2	23.5	51.0	1.0	24.5	0	0	0	0	0	0	0	0	0	0	0	0.00
	Black Bear (feces)	Ley et al. (2008a)	n = 2	0	97.0	0	3.0	0	0	0	0	0	0	0	0	0	0	0	0.00
Fish	Grass Carp (intestines)	Wu et al. (2012)	n = 3	3	25	5	26	0	13	0	17	0	0	0	0	0	1	1	9.00
	Zebrafish (intestines)	Roeslers et al. (2011)	n = 30	13.31	6.36	0.88	60.51	0	2.85	0.03	15.14	0	0	0	0	0	0	0	0.92

Table A.8: Non-human microbiome studies, number of individuals sampled, sample type(s), and date and location of publication

	Vertebrate Host	No. Individuals Sampled	Sample Type	Date of Publication	Journal
Reptiles	Alligator	n = 8	tongue (excised mucosa), stomach (excised mucosa), gastric contents, ileum (excised mucosa), colon (excised mucosa), feces	this study	this study
	Python	n = 3	pooled GI tract (small intestine scrapings)	2010	ISME J.
	Land iguana	n = 16	feces	2011	ISME J.
	Marine iguana	n = 30	feces	2011	ISME J.
	Giant tortoise	n = 4	feces	2011	ISME J.
	Green iguana	n = 2	feces	2011	ISME J.
Amphibians	Leopard frog	n = 7	skin (swab)	2012	ISME J.
	Chorus frog	n = 14	skin (swab)	2012	ISME J.
	Tiger salamander	n = 12	skin (swab)	2012	ISME J.
Birds	Chicken	n = 2	ceca	2008	PLoS ONE
	Chicken	n = 80	ileum, cecum	2006	Poult. Sci.
	Ostrich	n = 3	ceca	2010	Anaerobe
	Turkey	n = 31	feces	2008	J. Microbiol.
	Kakapo (New Zealand Parrot)	n = 6	choana (swab; n = 4), crop (swab; n = 3), feces (n = 6)	2012	PLoS ONE
Mammals	Macaque	n = 34	intestine, feces	2008	PLoS Pathog.
	Gorilla spp.	n = 4	feces	2010	PLoS Biol.
	Bonobo	n = 5	feces	2010	PLoS Biol.
	Chimpanzee spp.	n = 14	feces	2010	PLoS Biol.
	Chimpanzee	n = 35	feces	2012	PNAS
	Black-and-white colobus	n = 3	feces	2010	PLoS ONE
	Tephrosceles Red colobus	n = 3	feces	2010	PLoS ONE
	Red-tailed guenon	n = 3	feces	2010	PLoS ONE
	Bat (Phyllostomidae)	n = 40	distal colon (excised mucosa)	2012	Molec. Ecol.
	Bat (Emballonuridae)	n = 2	distal colon (excised mucosa)	2012	Molec. Ecol.
	Bat (Molossidae)	n = 4	distal colon (excised mucosa)	2012	Molec. Ecol.
	Bat (Mormoopidae)	n = 6	distal colon (excised mucosa)	2012	Molec. Ecol.
	Bat (Natalidae)	n = 3	distal colon (excised mucosa)	2012	Molec. Ecol.
	Bat (Noctilionidae)	n = 2	distal colon (excised mucosa)	2012	Molec. Ecol.
	Bat (Vespertilionidae)	n = 3	distal colon (excised mucosa)	2012	Molec. Ecol.
	Pig	n = 1	colon, cecum	1999	Appl. Environ. Microbiol.
	Mouse	n = 4	feces, cecum, colon	2010	Nature
	Alpaca	n = 4	gastric juice	2010	Anaerobe
	Sheep	n = 4	gastric juice	2010	Anaerobe
	Canine	n = 12	feces	2011	ISME J.
	Horse	n = 5	colon, cecum	2001	FEMS Microbiol. Ecol.
	Cheetah	n = 2	feces	2008	Science
	Lion	n = 3	feces	2008	Science
	Polar bear	n = 2	feces	2008	Science
	Black bear	n = 2	feces	2008	Science
	Grizzly bear	n = 10	feces	2011	PLoS ONE
Fish	Grass carp	n = 7	intestines	2012	PLoS ONE
	Zebrafish	n = 30	intestines	2011	ISME J.

Appendix B

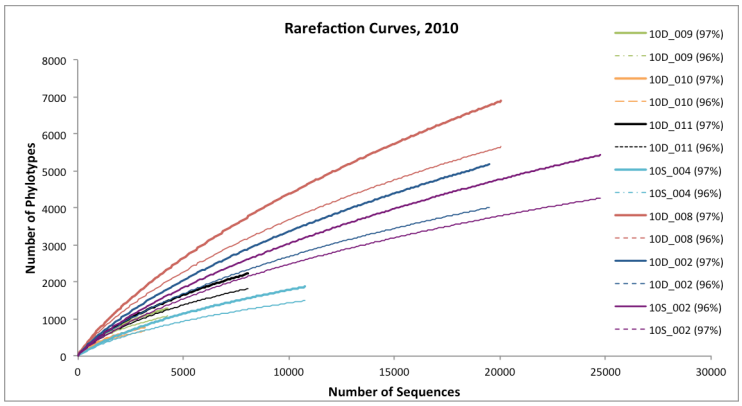

A

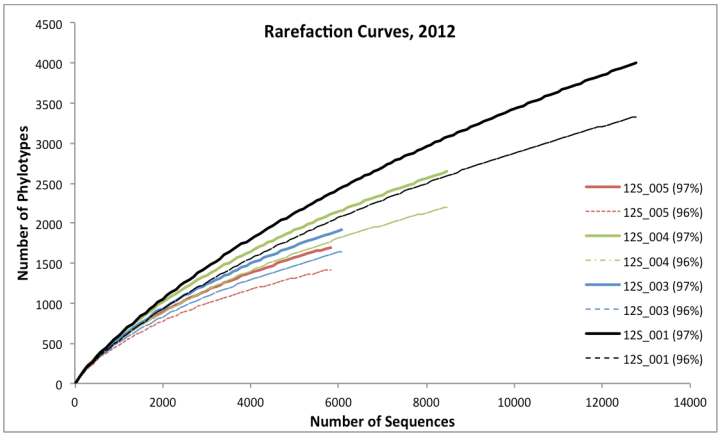

B

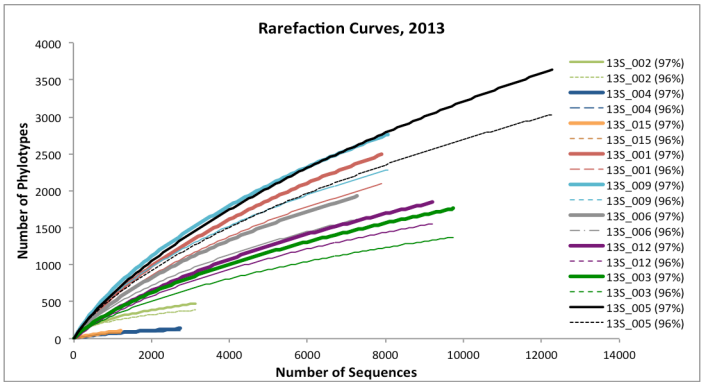

C

Fig. B.1: Rarefaction curves of wetland sediment bacterial diversity. (A-C) Curves are presented for phylotypes defined at both 97% and 96% sequence identity.

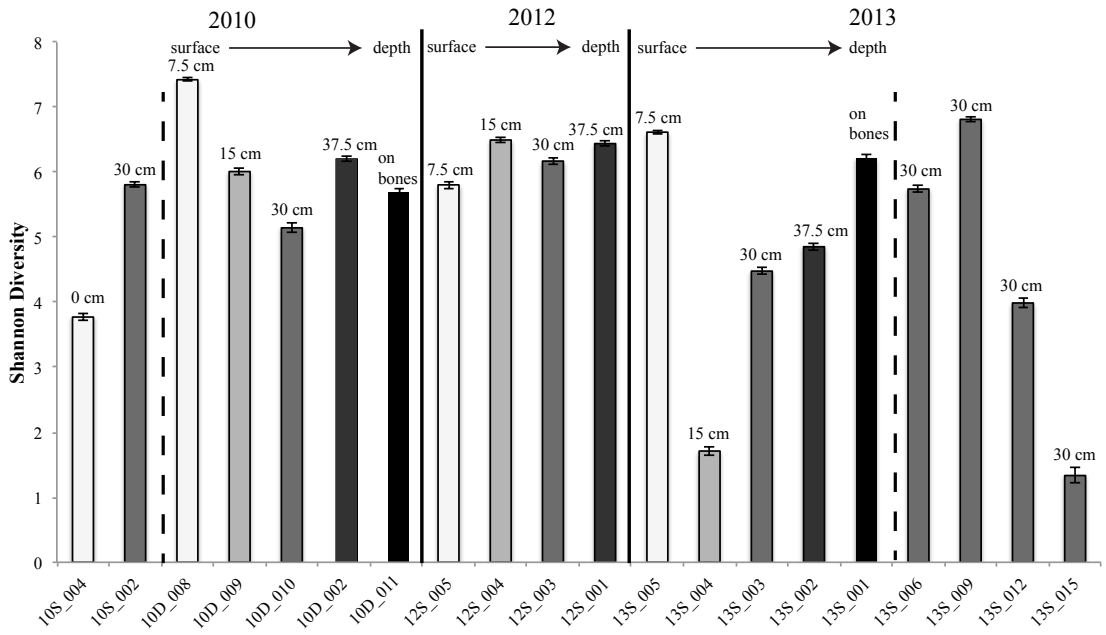

Fig. B.2: Shannon indices of bacterial diversity from wetland sediments. Samples are arranged by year and increasing depth. Bar colors also correspond to sampling depth. Index values and errors calculated using Mothur. Diversity indices from 30 cm beyond the dashed line in 2013 reflect samples collected along a linear transect at depth radiating from the burial.

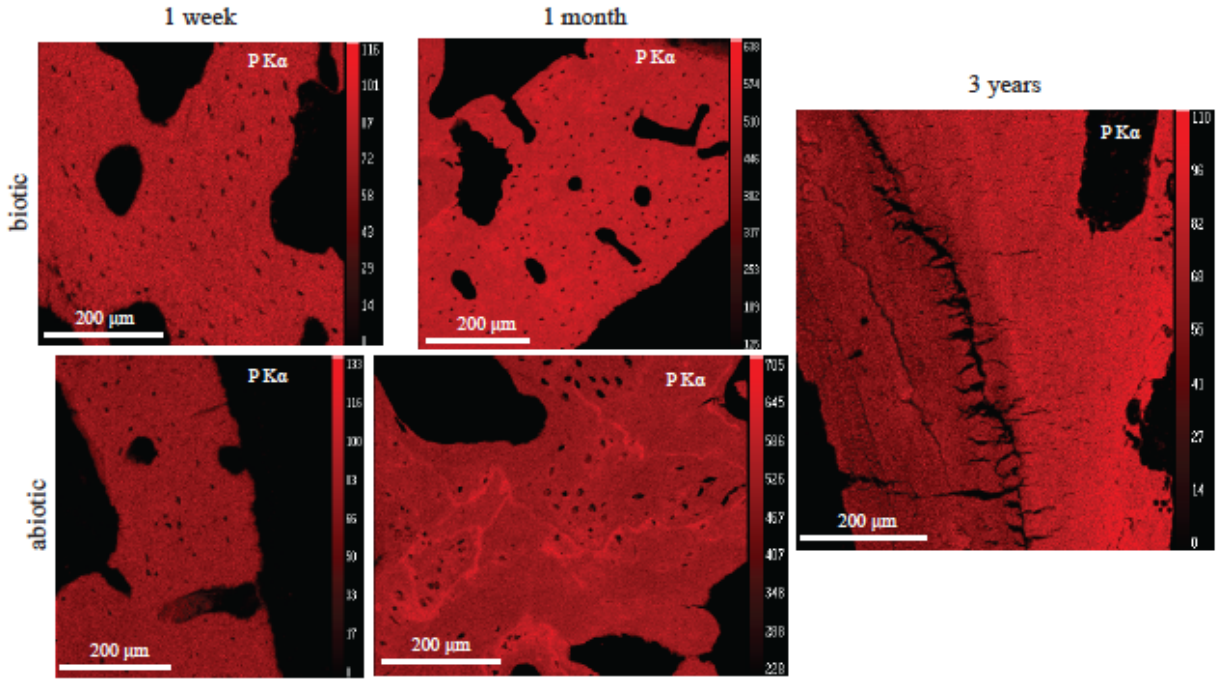

Fig. B.3: EMP X-ray maps of P concentration in abiotic and biotic treated bones at each sampling interval. Bone P concentration (brighter color indicates higher counts and higher concentrations) is similar after one week of treatment, but differs between treatments after one month. In the abiotic treatment, loss of P appears to permeate throughout the cortex.

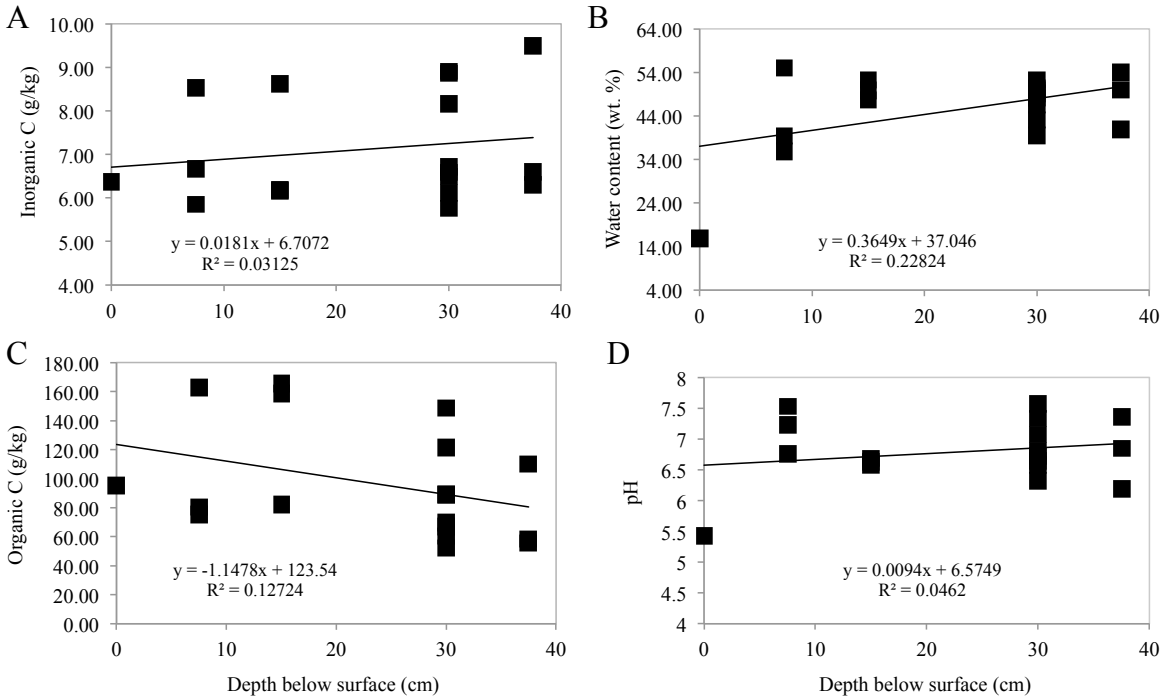

Fig. B.4: Wetland chemistry variability as a function of depth. (A-B) Inorganic carbon and water content broadly increase with depth in surface to subsurface sediments. (C) Organic carbon content decreases with increasing depth. (D) Apart from an acidic sample observed at the surface (10S_004), sediment samples ranged in pH from 6.19 to 7.57 with no clear trends as a function of depth.

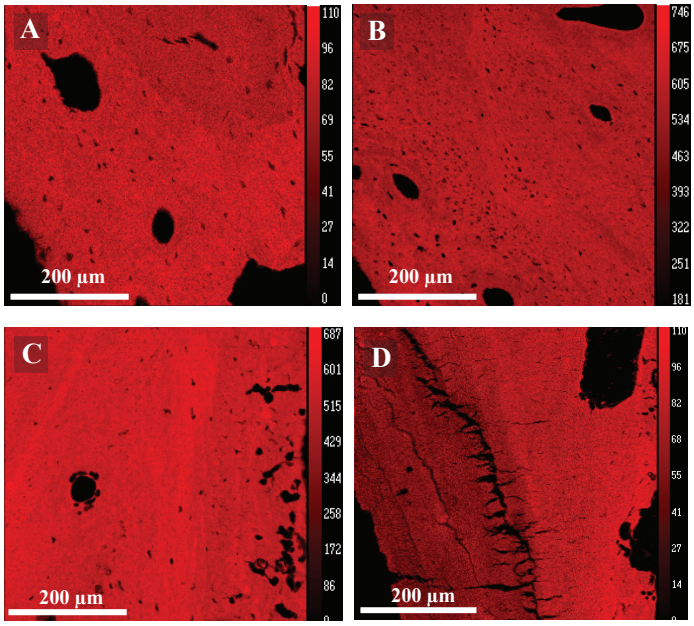

Fig. B.5: Phosphorus element maps of buried bones after three years. (A) Pre-burial, unaltered bone exhibits a broadly uniform P composition. (B) After one year, some P depletion is evident along vascular canals. (C) Further P loss occurs after 2 years of burial, particularly along bone margins in direct contact with sediment. Additionally, surface modification (pits, tunnels) are also present along the outer-most cortex. (D) Three years after burial, significant depletion of P is preserved along the outer-most cortex.

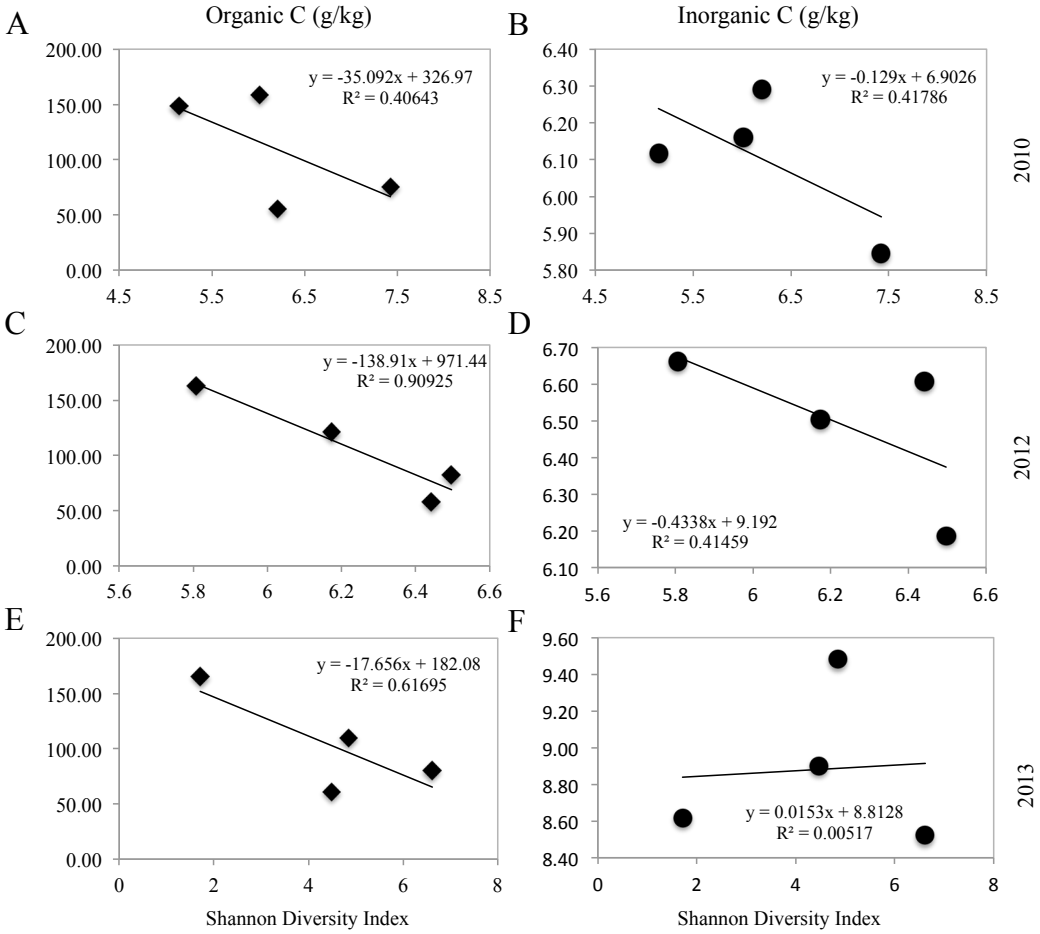

Fig. B.6: Covariance between bacterial diversity and sediment chemistry. (A-B) Both organic and inorganic carbon decrease with increasing Shannon diversity in sediments collected 8 months after burial (December 2010). (C-D) Continued co-variation between organic and inorganic carbon and bacterial diversity are observed in sediments collected in 2012. (E) After three years of burial, organic carbon content decrease is correlated with increasing bacterial diversity. (F) There are no clear trends with inorganic carbon and bacterial diversity.

Table B.1: Surface water geochemical data from Louisiana.

						mmol/L										
Source of Data	Surface Water Type	Sample Date	pH	Temp (°C)	Conductivity (mS)	TDS (mg/L	Na^+	K^+	Ca^{2+}	Mg^{2+}	Cl^-	HCO_3^-	NO_3^-	SO_4^{2-}	Fe^{2+}	O_2
USGS 294630092533500 Mermentau River at Upper Mud Lake near Grand Chenier, LA	stream	1/26/78	7.1	16	0.106	71	0.70	0.07	0.13	0.10	0.56	0.46	0.005	0.104	1.075	0.375
	stream	2/17/78	7.1	18	0.084	56	0.52	0.06	0.12	0.07	0.48	0.34	0.005	0.082	1.792	0.350
	stream	3/17/78	7.5	22	5.791	3880	47.83	2.21	1.38	6.58	62.06	1.05	0.000	2.604	1.792	0.288
	stream	4/20/78	7.5	25	13.269	8890	117.39	2.08	4.50	11.93	141.04	1.31	0.000	6.250	0.896	0.269
	stream	5/24/78	8.2	29	29.552	19800	269.57	6.41	7.75	31.69	338.50	2.13	0.161	2.604	0.538	0.247
	stream	6/21/78	7.2	32	3.015	2020	26.09	0.72	0.98	2.76	31.03	0.84	0.001	1.667	0.538	0.263
	stream	7/17/78	7.6	33	11.463	7680	104.35	2.56	0.23	11.93	118.48	1.49	0.011	6.667	1.254	0.263
	stream	9/1/78	7.4	31	1.084	726	9.13	0.26	0.43	1.03	10.72	0.85	0.000	0.604	0.358	0.225
	stream	9/13/78	7.6	31	0.982	658	8.26	0.26	0.40	0.91	9.59	1.07	0.001	0.500	0.358	0.244
	stream	11/1/78	7.7	22	18.507	12400	165.22	3.85	3.75	18.11	191.82	1.92	0.000	10.417	1.792	0.253
	stream	11/22/78	8	22	25.373	17000	226.09	6.15	5.25	25.93	259.52	2.30	0.000	15.625	0.358	0.325
	stream	12/20/78	7.8	18	1.612	1080	13.91	0.44	0.60	1.60	16.36	1.00	0.003	0.760	0.896	0.285
	stream	2/29/80	7	18	0.309	207	2.57	0.12	0.18	0.28	2.76	0.51	0.005	0.167	5.914	0.288
	stream	3/31/80	6.9	22	0.121	81	0.78	0.08	0.13	0.11	0.85	0.38	0.008	0.115	2.867	0.303
	stream	5/1/80	6.9	29	0.119	80	0.78	0.09	0.14	0.12	0.79	0.43	0.006	0.097	3.763	0.256
	stream	5/21/80	6.8	29	0.106	71	0.70	0.06	0.13	0.11	0.71	0.41	0.006	0.079	2.330	0.234
	stream	6/25/80	6.9	32	0.469	314	4.13	0.14	0.19	0.41	4.51	0.66	0.000	0.167	4.122	0.213
	stream	9/4/80	8.2	31	22.537	15100	200.00	5.38	4.75	23.46	259.52	1.57	0.000	3.438	1.075	0.259
	stream	10/30/80	7.5	27	7.507	5030	65.22	1.59	1.85	7.41	78.98	0.00	0.000	4.063	0.717	0.313
	stream	11/20/80	7.6	22	19.552	13100	169.57	3.59	4.50	20.16	211.57	0.00	0.000	8.542	1.254	0.338
	stream	12/12/80	7.4	18	2.388	1600	21.30	0.44	0.75	2.26	24.54	0.00	0.000	1.146	0.717	0.334
	stream	1/22/81	7.2	16	0.425	285	3.52	0.11	0.20	0.45	3.95	0.00	0.002	0.250	2.509	0.363
Baton Rouge, LA (Raja et al., 2008)	Fog		5	17			0.11	0.01	0.03	0.03	0.11	0.00	0.181	1.791	0.000	0
Houston, TX (Raja et al., 2008)	Fog		4.3	13			0.23	0.01	0.25	0.07	0.38	0.00	0.368	0.953	0.000	0

Table B.1 (continued): Surface water geochemical data from Louisiana.

							mmol/L									
Source of Data	Surface Water Type	Sample Date	pH	Temp (°C)	Conductivity (mS)	TDS (mg/L)	Na^+	K^+	Ca^{2+}	Mg^{2+}	Cl^-	HCO_3^-	NO_3^-	SO_4^{2-}	Fe^{2+}	O_2
USGS 07386980 Vermillion River at Perry, LA	Stream	12/8/69	6.6	14.4			3.43	0.12	0.70	0.49	3.53	2.03	0.029	0.146	0.000	0
	Stream	1/5/70	6.4	14.4			0.83	0.10	0.20	0.14	0.76	0.57	0.019	0.092	4.480	0
	Stream	2/4/70	6.1	6.1			1.00	0.06	0.22	0.06	0.93	0.46	0.002	0.092	0.000	0
	Stream	3/9/70	6.2	8.3			0.57	0.06	0.22	0.04	0.54	0.52	0.003	0.056	0.179	0
	Stream	5/7/70	6.1	22.2			0.83	0.08	0.30	0.11	0.76	0.80	0.002	0.050	1.075	0
	Stream	6/9/70	6.6	28.9			1.04	0.07	0.45	0.35	1.02	1.49	0.005	0.075	1.254	0
	Stream	7/12/70	6.4	31.7			1.13	0.08	0.50	0.12	1.04	1.31	0.002	0.079	0.000	0
	Stream	8/12/70	5.7	25.6			0.40	0.08	0.15	0.04	0.34	0.38	0.003	0.048	1.613	0
	Stream	9/13/70	6.4	28.9			1.57	0.14	0.38	0.09	1.58	0.90	0.005	0.085	1.971	0
	Stream	12/6/70	6.2	16.7			1.70	0.13	0.38	0.21	1.75	1.08	0.006	0.052	0.717	0
	Stream	3/29/71	6.3	20.6			0.91	0.08	0.35	0.13	0.85	0.90	0.006	0.075	2.151	0
	Stream	4/13/71	6.6	25			1.39	0.09	0.45	0.24	1.24	1.44	0.018	0.104	9.857	0
	Stream	5/23/71	6.5	21.7			0.70	0.08	0.18	0.12	0.62	0.56	0.031	0.056	12.366	0
	Stream	6/15/71	6.8	29.4			0.61	0.07	0.28	0.14	0.54	0.82	0.005	0.042	5.735	0
	Stream	7/13/71	6.2	28.9			1.00	0.06	0.40	0.12	0.96	0.98	0.003	0.069	8.961	0
	Stream	9/13/71	6.4	24.4			0.52	0.09	0.23	0.13	0.59	0.74	0.013	0.004	4.659	0
	Stream	10/19/71	6.7	22			1.74	0.08	0.45	0.25	1.55	1.52	0.042	0.065	0.000	0
	Stream	11/28/71	7.1	20			2.52	0.07	0.43	0.20	2.48	1.15	0.006	0.104	0.000	0
	Stream	12/27/71	6.6	12			0.96	0.09	0.33	0.16	1.07	0.75	0.002	0.067	0.000	0
	Stream	1/26/72	7.2	11			0.91	0.04	0.25	0.15	0.90	0.72	0.006	0.077	0.001	0
	Stream	3/27/72	6.9	14			0.70	0.04	0.28	0.12	0.62	0.72	0.005	0.098	0.003	0
	Stream	4/24/72	7	26			1.04	0.07	0.43	0.16	1.04	1.02	0.003	0.071	0.000	0
	Stream	5/22/72	7.4	26			0.87	0.07	0.48	0.07	0.62	1.21	0.034	0.081	0.000	0
	Stream	6/26/72	7.2	26			0.83	0.04	0.43	0.21	0.62	1.34	0.011	0.094	0.002	0
	Stream	7/24/72	7.3	27			1.22	0.03	0.45	0.23	0.85	1.61	0.011	0.046	0.002	0
	Stream	8/21/72	7.3	31			1.48	0.04	0.53	0.35	1.21	1.90	0.002	0.115	0.000	0
	Stream	10/3/72	7	27			1.30	0.08	0.53	0.21	1.13	1.61	0.003	0.092	0.000	0
	Stream	10/30/72	6.7	20			1.65	0.13	0.53	0.21	1.44	1.56	0.003	0.067	0.001	0
	Stream	11/26/72	7	16			2.96	0.08	0.65	0.19	2.71	1.77	0.044	0.167	0.000	0
	Stream	12/21/72	6.5	13			0.57	0.08	0.24	0.11	0.56	0.56	0.034	0.115	0.717	0
	Stream	1/31/73	6.9	18			1.39	0.10	1.13	0.18	1.55	2.41	0.016	0.125	0.717	0
	Stream	3/1/73	6.6	14			0.61	0.07	0.23	0.09	0.51	0.62	0.010	0.081	1.075	0
	Stream	3/29/73	6.5	17			0.61	0.07	0.30	0.13	0.54	0.82	0.008	0.069	0.000	0
	Stream	4/26/73	6.4	20			0.52	0.10	0.22	0.11	0.42	0.69	0.008	0.052	0.003	0
	Stream	5/24/73	6.5	27			0.70	0.08	0.25	0.13	0.59	0.79	0.010	0.048	0.002	0
	Stream	6/27/73	6.5	30			6.57	0.14	0.50	0.39	7.33	0.87	0.039	0.229	0.000	0

Table B.1 (continued): Surface water geochemical data from Louisiana.

							mmol/L									
Source of Data	Surface Water Type	Sample Date	pH	Temp (°C)	Conductivity (mS)	TDS (mg/L)	Na^+	K^+	Ca^{2+}	Mg^{2+}	Cl^-	HCO_3^-	NO_3^-	SO_4^{2-}	Fe^{2+}	O_2
USGS 07386980 Vermillion River at Perry, LA	Stream	7/30/73	6.5	31			0.96	0.07	0.38	0.14	0.79	1.10	0.039	0.069	0.179	0
	Stream	9/5/73	6.7	29			1.35	0.13	0.38	0.13	1.18	1.08	0.015	0.069	0.358	0
	Stream	9/18/73	6.9	29			2.78	0.19	0.55	0.21	2.48	1.56	0.052	0.115	0.358	0
	Stream	10/31/73	7	21			2.26	0.18	0.45	0.21	2.03	1.52	0.042	0.085	0.358	0
	Stream	11/27/73	7.5	17			5.30	0.24	0.88	0.49	4.80	2.97	0.089	0.104	0.358	0
	Stream	12/25/73	7.2	14.5			0.96	0.16	0.38	0.02	0.82	0.67	0.087	0.135	3.405	0
	Stream	1/24/74	7.1	9.5			2.09	0.12	0.35	0.20	2.06	0.79	0.035	0.156	0.717	0
	Stream	2/21/74	7.1	13			1.78	0.10	0.50	0.15	1.55	1.20	0.079	0.177	0.538	0
	Stream	3/31/74	7.2	18.5			0.61	0.09	0.40	0.18	0.56	1.05	0.008	0.104	1.792	0
	Stream	4/24/74	7	25			1.04	0.13	0.40	0.23	0.85	1.28	0.040	0.104	1.792	0
	Stream	5/21/74	6.9	25.5			0.57	0.10	0.33	0.16	0.48	0.92	0.013	0.083	2.151	0
	Stream	6/20/74	6.7	31			1.13	0.10	0.53	0.45	0.96	1.85	0.005	0.125	0.358	0
	Stream	7/31/74	6.8	31			1.61	0.08	0.45	0.29	1.27	1.67	0.003	0.088	0.538	0
	Stream	10/31/74	7.2	18			0.61	0.15	0.24	0.05	0.54	0.62	0.015	0.085	1.971	0
	Stream	11/28/74	7	14.5			0.91	0.10	0.35	0.16	0.73	1.02	0.000	0.146	3.405	0
	Stream	12/18/74	7	13.5			1.09	0.09	0.33	0.16	1.02	0.82	0.027	0.115	4.301	0
	Stream	1/23/75	6.7	13			1.09	0.08	0.43	0.26	1.10	1.13	0.065	0.115	6.272	0
	Stream	2/21/75	6.6	16			0.70	0.09	0.38	0.05	0.62	0.74	0.026	0.092	0.896	0
	Stream	3/20/75	6.3	18			0.74	0.10	0.25	0.13	0.68	0.72	0.035	0.069	1.792	0
	Stream	4/20/75	6.5	23			1.00	0.08	0.35	0.18	0.76	1.23	0.008	0.096	1.971	0
	Stream	5/28/75	6.6	21.5			0.87	0.11	0.35	0.17	0.73	1.07	0.010	0.083	1.613	0
	Stream	6/26/75	7.3	30			1.39	0.06	0.40	0.26	0.99	1.59	0.010	0.077	0.538	0
	Stream	7/28/75	7.1	29			1.04	0.09	0.40	0.18	0.82	1.28	0.023	0.042	1.792	0
	Stream	9/3/75	7.5	29			1.35	0.10	0.45	0.27	1.10	1.52	0.034	0.096	0.000	0
	Stream	9/21/75	6.5	25			0.48	0.13	0.22	0.08	0.48	0.59	0.016	0.054	0.717	0
	Stream	11/10/75	7.1	22.5			0.83	0.13	0.35	0.16	0.68	1.08	0.044	0.090	2.867	0
	Stream	2/1/76	6.6	10.5			0.23	0.08	0.14	0.06	0.16	0.41	0.029	0.040	1.613	0
	Stream	3/4/76	6.5	15			0.48	0.07	0.20	0.09	0.45	0.48	0.037	0.052	0.717	0

Table B.1 (continued): Surface water geochemical data from Louisiana.

Source of Data	Surface Water Type	Sample Date	pH	Temp (°C)	Conductivity (mS)	TDS (mg/L)	mmol/L									
							Na^+	K^+	Ca^{2+}	Mg^{2+}	Cl^-	HCO_3^-	NO_3^-	SO_4^{2-}	Fe^{2+}	O_2
USGS 07386980 Vermillion River at Perry, LA	Stream	3/30/76	6.6	21			0.43	0.09	0.22	0.11	0.37	0.66	0.016	0.071	1.075	0
	Stream	4/29/76	7.3	22			3.39	0.13	0.45	0.35	3.39	1.41	0.031	0.198	1.613	0
	Stream	6/21/76	7.4	28.5			0.70	0.09	0.33	0.12	0.59	0.90	0.010	0.069	0.717	0
	Stream	7/21/76	6.6	28			14.78	0.38	1.68	0.70	16.93	1.11	0.026	0.792	0.358	0
	Stream	9/1/76	6.9	29			1.57	0.10	0.50	0.32	1.41	1.67	0.013	0.135	1.075	0
	Stream	9/29/76	7.1	27			2.09	0.16	0.55	0.30	1.69	1.70	0.035	0.188	3.943	0
	Stream	10/27/76	7.6	21			1.87	0.19	0.63	0.19	1.69	1.66	0.035	0.156	0.000	0
	Stream	1/27/77	6.5	13			0.65	0.12	0.25	0.12	0.54	0.77	0.035	0.100	1.434	0
	Stream	5/11/77	6.5	24			0.38	0.08	1.63	0.09	0.37	0.52	0.035	0.058	1.792	0
	Stream	7/28/77	7	30			1.35	0.09	0.45	0.22	0.96	1.66	0.021	0.075	1.613	0
	Stream	10/26/77	6.5	24			0.78	0.16	0.30	0.26	0.65	1.00	0.008	0.067	0.000	0
	Stream	4/18/78	7.2	20			0.96	0.08	0.38	0.21	0.93	0.97	0.018	0.078	0.000	0

Table B.2: Representative RWR water geochemistry used to design synthetic wetland water

				mmol/L						
Conductivity (mS)	pH	Temp (°C)	TDS	Na^+	K^+	Ca^{2+}	Mg^{2+}	Cl^-	HCO_3^-	SO_4^{2-}
3.03	6.5	25.5	2030.1	19.81	0.49	1.22	3.71	23.84	3.45	1.71

Table B.3: EMP operating conditions, crystal assignments, detection limits, and standards.

Element	Count Time (seconds)	Spectrometer and Crystal	Electron Transition Probed	Approximate Detection Limit (ppm)	Standards
F	30	Sp1 (PCI)	Kα	1000	Fluorapatite
P	20	Sp2 (TAP)	Kα	350	Fluorapatite
Sr	60	Sp2 (TAP)	Lα	450	SrNbBa
Si	20	Sp2 (TAP)	Kα	200	Diopside
Ca	20	Sp4 (PET)	Kα	450	Fluorapatite
Cl	20	Sp4 (PET)	Kα	400	HgCl
S	30	Sp4 (PET)	Kα	350	Barite
Fe	20	Sp3 (LLIF)	Kα	550	Hematite
Ba	60	Sp4 (PET)	Lα	800	SrNbBa
Mn	40	Sp3 (LLIF)	Kα	350	Spessartine
Ce	60	Sp3 (LLIF)	Lα	890	CeO_2
La	60	Sp3 (LLIF)	Lα	890	LaB_6
Al	40	Sp2 (TAP)	Kα	150	Spinel
Na	40	Sp2 (TAP)	Kα	300	Albite

Table B.4: Pairwise analysis of significant variance in bacterial community membership as a function of year.

	10D_008	10D_009	10D_010	10D_002	
10D_008					
10D_009	F = 1.62, p = 0.35				2010
10D_010	F = 1.02, p = 0.98	F = 1.59, p = 0.36			
10D_002	F = 2.09, p = 0.15	**F = 3.39, p = 0.02**	F = 2.12, p = 0.14		

	12S_005	12S_004	12S_003	12S_001	
12S_005					
12S_004	F = 2.02, p = 0.17				2012
12S_003	F = 1.78, p = 0.26	F = 1.14, p = 0.80			
12S_001	F = 1.17, p = 0.76	F = 2.36, p = 0.10	F = 2.07, p = 0.16		

	13S_005	13S_004	13S_003	13S_002	
13S_005					
13S_004	**F = 9.87, p < 0.01**				2013
13S_003	**F = 2.84, p = 0.04**	**F = 3.47, p = 0.02**			
13S_002	F = 1.07, p = 0.90	**F = 10.5, p < 0.01**	**F = 3.04, p = 0.03**		

Table B.5: Pairwise analysis of significant variance in bacterial community membership as a function of depth.

	10D_008	12S_005	13S_005	
10D_008				
12S_005	F = 1.14, p = 0.80			7.5 cm
13S_005	F = 1.33, p = 0.57	F = 1.51, p = 0.42		

	10D_009	12S_004	13S_004	
10D_009				
12S_004	F = 1.10, p = 0.85			15 cm
13S_004	**F = 12.0, p < 0.01**	**F = 13.2, p < 0.01**		

	10D_010	12S_003	13S_003	
10D_010				
12S_003	F = 1.54, p = 40			30 cm
13S_003	F = 2.17, p = 0.13	**F = 3.34, p = 0.02**		

	10D_002	12S_001	13S_002	
10D_002				
12S_001	F = 1.58, p = 0.37			37.5 cm
13S_002	**F = 2.98, p = 0.04**	F = 1.88, p = 0.22		

Appendix C

Table C.1: EMP operating conditions, crystal assignments, detection limits, and standards.

Element	Count Time (seconds)	Spectrometer and Crystal	Electron Transition Probed	Approximate Detection Limit (ppm)	Standards
F	30	Sp1 (PCI)	Kα	1000	Fluorapatite
P	20	Sp2 (TAP)	Kα	350	Fluorapatite
Sr	60	Sp2 (TAP)	Lα	450	SrNbBa
Si	20	Sp2 (TAP)	Kα	200	Diopside
Ca	20	Sp4 (PET)	Kα	450	Fluorapatite
Cl	20	Sp4 (PET)	Kα	400	HgCl
S	30	Sp4 (PET)	Kα	350	Barite
Fe	20	Sp3 (LLIF)	Kα	550	Hematite
Ba	60	Sp4 (PET)	Lα	800	SrNbBa
Mn	40	Sp3 (LLIF)	Kα	350	Spessartine
Ce	60	Sp3 (LLIF)	Lα	890	CeO_2
La	60	Sp3 (LLIF)	Lα	890	LaB_6
Al	40	Sp2 (TAP)	Kα	150	Spinel
Na	40	Sp2 (TAP)	Kα	300	Albite

Table C.2: Selected major and trace element concentrations (wt. %) for various modern and fossil bones; below detection (B.d.).

					Major and trace element concentrations (wt. %)							
Site or Locality	Taxon	Source of Data	Age	Bone type and number of analyses (if known)	Ca	P	F	Al	Si	S	Mn	Fe
Pipe Creek Sinkhole	Frog	Farlow & Argast (2006)	Late Neogene	Limb bone (n = 7)	37.36	15.99	3.34	B.d.	0	0	0.47	1.04
	Turtle			Shell (n = 10)	37.13	16.23	3.49	0	0	0	0.51	0.72
	Tortoise			Shell (n = 15)	37.84	16.19	3.81	0	0	0.32	0.19	0.70
	Mammal			Rib (n = 42)	38.02	16.17	3.41	0	0	0	0.39	0.80
Gray Fossil Site	*Alligator* sp.	this study	Late Neogene	Phalange (B) (n = 52)	38.89	17.41	2.27	0.14	0.01	0.03	0.05	2.12
				Phalange (C) (n = 10)	39.01	17.26	2.25	0.01	0.01	0.01	0.02	2.57
South America (wild)	*Caiman*	Goodwin et al. (2007)	Modern	Femur	36.00	19.00					0.001	0.001
Prince Creek Fmn., Alaska	*Edmontosaurus*	Goodwin et al. (2007)	Maastrichtian	Femur	30.00	18.00					0.15	1.60
				Femur (Haversian canal)	19.00	16.00					1.30	18.00
	Edmontosaurus			Femur	19.46	5.76				0.05	0.08	0.62
Dinosaur Park Fmn., Canada	Hadrosauridae	Goodwin et al. (2007)	Campanian	Femur	29.0	19.00					0.36	6.00
	Hadrosauridae			Radius	32.0	20.00					0.23	0.90
	Tyrannosauridae			Phalanx	25.89	7.88				0.43	0.12	0.69
	Tyrannosauridae			Tibia	25.67	7.86				0.23	0.18	0.65
	Hadrosauridae			Radius	25.65	7.99				0.08	0.21	1.19
	Plesiosaur			Vertebra	24.59	7.98		1.08	0.11		0.23	1.23
	Crocodylia			Femur	22.94	7.12				0.15	0.12	0.71
				Femur	31.00	18.00					0.25	0.80
Hell Creek Fmn., Montana	*Tyrannosaurus*	Goodwin et al. (2007)	Maastrichtian	Rib	28.00	19.00					0.17	0.70
	Hadrosauridae			Femur	20.14	6.42		0.68	0.09	0.11	0.17	0.46
Kayenta Fmn., Arizona	*Dilophosaurus*	Goodwin et al. (2007)	Lower Jurassic	Femur	25.83	7.43				0.73	0.03	0.30
	Dilophosaurus			Tibia	20.98	64.60				0.70	0.01	0.71
				Rib	21.65	4.63				15.78	0.05	0.05

Vita

Sarah Wheeler Keenan was born in February, 1986, in New York City, New York, the first child to Sarah Frassinelli and Stephen Patrick Keenan. At the age of 3, she moved with her family to Easton, Connecticut, where her parents still reside. She attended the Hopkins Grammar School in New Haven, Connecticut, for high school. She graduated in 2004 and received the Paul W. Schueler Art Prize. Sarah moved as far away from Connecticut as possible after graduation, to the Northeast coast of Scotland where she attended the University of St. Andrews, St. Andrews, Fife, from 2004-2008, and pursued a dual Bachelors of Science degree in Geoscience and Environmental Biology. As an undergraduate, she conducted field research in Montana as part of an honors thesis titled, "Taphonomy of *Triceratops'* from the Upper Hell Creek Formation, Garfield County, Montana." She has continued to be involved in research in the Hell Creek since 2007. After graduating with honors from St. Andrews, she moved south to Bristol, England, where she received a Masters of Science in Palaeobiology from the University of Bristol (2008-2009). Her thesis was titled, "Rare Earth Elements and Rates of Fossilization in Tetrapod Bones." With optimism for a new type of culture shock, Sarah entered Louisiana State University in the Fall of 2009, where she started her doctoral research with Annette S. Engel. She transferred with Annette to the University of Tennessee, Knoxville, in the Fall of 2011. That move was undoubtedly the best thing that could have happened.